

**„U(VI) bioaccumulation by *Paenibacillus* sp. JG-TB8 and
Sulfolobus acidocaldarius;
Au(0) nanoclusters formation on the S-layer of *S. acidocaldarius***

Von der Fakultät für Chemie und Physik
der Technischen Universität Bergakademie Freiberg

genehmigte

DISSERTATION

Zur Erlangung des akademischen Grades

Doctor rerum naturalium

Dr. rer. nat.

vorgelegt

von Dipl. Biol. Thomas Reitz

geboren am 17. Mai 1981 in Bautzen

Gutachter: Prof. Dr. Michael Schlömann, TU Bergakademie Freiberg

Prof. Dr. Gert Bernhard, Helmholtz-Zentrum Dresden-Rossendorf

Tag der Verleihung: 13. Dezember 2011

INTRODUCTION	5
INTERACTIONS OF THE URANIUM WASTE PILE ISOLATE	
<i>PAENIBACILLUS</i> SP. JG-TB8 WITH U(VI) UNDER AEROBIC AND	
ANAEROBIC CONDITIONS.	19
ABSTRACT.....	20
INTRODUCTION	21
MATERIALS AND METHODS	22
Isolation, cultivation and growth conditions.....	22
Phylogenetic affiliation.....	23
Carbon and nitrogen sources utilized by <i>Paenibacillus</i> sp. JG-TB8	24
Isolation of total protein and SDS-PAGE.....	25
Heavy metal tolerance	25
Cell preparation for U(VI) treatments	26
Time-Resolved Laser-induced Fluorescence Spectroscopy (TRLFS).....	26
X-ray Absorption Spectroscopy (XAS).....	28
Transmission electron microscopy	29
Live/Dead staining.....	29
Enzymatic assay.....	30
Colorimetric determination of phosphate	30
RESULTS AND DISCUSSION	31
Phylogenetic affiliation of the cultivated <i>Bacillus</i> isolates.....	31
Morphological and physiological characterization of <i>Paenibacillus</i> sp. JG-TB8	33
Heavy metal tolerance	36
Bioaccumulation of U(VI) by JG-TB8	37
Characterization and molecular structure of the uranium complexes formed	
under aerobic conditions.....	40
TRLFS studies	40
XAS analyses	43
Microscopic analyses	47
Characterization and molecular structure of the uranium complexes formed	
under anaerobic conditions.	51
XANES studies	51
TRLFS	52
XAS studies	54
Microscopic analyses	56
Key role of the phosphatase activity in uranium complexation.....	57
CONCLUSIONS	61
SUPPLEMENTAL MATERIAL	62
INTERACTIONS OF <i>SULFOLOBUS ACIDOCALDARIUS</i> WITH URANIUM 65	
ABSTRACT.....	66
INTRODUCTION	67
EXPERIMENTAL.....	68
Archaeal strain, growth conditions, and cell preparation for the U-treatments.....	68
Tolerance to U(VI) and other heavy metals.....	68
U(VI) biosorption	69
X-ray Absorption Spectroscopy (XAS).....	69
Time-Resolved Laser-induced Fluorescence spectroscopy (TRLFS)	70

RESULTS AND DISCUSSION.....	71
Tolerance of <i>S. acidocaldarius</i> DSM 639 to U(VI) and other heavy metals	71
U(VI) biosorption.....	73
XAS studies	75
Time-resolved laser-induced fluorescence spectroscopic studies.....	77
CONCLUSIONS.....	83
 BIOSORPTION AND BIOMINERALIZATION OF U(VI) BY <i>SULFOLOBUS</i>	
<i>ACIDOCALDARIUS</i> AT MODERATE ACIDIC CONDITIONS.....	85
ABSTRACT.....	86
INTRODUCTION	87
MATERIALS AND METHODS	88
Cultivation and archaeal cell sample preparation	88
U(VI) bioaccumulation	89
X-ray Absorption Spectroscopy (XAS)	89
Fourier-Transform Infrared-Spectroscopy (FT-IR)	91
Time-Resolved Laser-induced Fluorescence Spectroscopy (TRLFS).....	91
Enzymatic assay	92
Colorimetric determination of phosphate	93
Live/Dead staining	93
Microscopic analyses	94
RESULTS AND DISCUSSION.....	95
U(VI) bioaccumulation	95
XAS.....	98
FT-IR.....	105
TRLFS.....	108
Acid phosphatase assay and determination of phosphate concentration	112
Microscopic Analyses	115
CONCLUSIONS.....	118
 COMPLEXATION OF URANIUM BY S-LAYER AND CELL GHOSTS OF	
<i>SULFOLOBUS ACIDOCALDARIUS</i>.....	121
ABSTRACT.....	122
INTRODUCTION	123
MATERIALS AND METHODS	124
Preparation of the SlaA-layer ghosts and the cell envelope ghosts	124
SDS-PAGE analysis of the SlaA-layer and the cell envelope ghosts	125
SlaA-layer stability assay.....	125
Biochemical analyses of the SlaA-layer ghosts	126
Treatments with U(VI).....	127
Time-Resolved Laser-induced Fluorescence Spectroscopy (TRLFS).....	127
X-ray Absorption Spectroscopy (XAS)	128
RESULTS AND DISCUSSION.....	129
Properties of the purified SlaA-layer ghosts and the cell envelope ghosts.....	129
U(VI) sorption by the SlaA-layer and the cell envelope ghosts	133
TRLFS studies on the U(VI) complexes formed at the SlaA-layer and the cell	
envelope ghosts	135
XAS studies	141
CONCLUSIONS.....	145

FORMATION OF MAGNETIC GOLD NANOPARTICLES USING THE SLAA-LAYER OF <i>SULFOLOBUS ACIDOCALDARIUS</i> AS A TEMPLATE.....	147
ABSTRACT.....	148
INTRODUCTION	149
MATERIAL AND METHODS	150
Gold nanoparticles preparation.....	150
Transmission-electron microscopy (TEM) and Energy Dispersive X-ray spectroscopy (EDX).....	151
X-ray Photoelectron Spectroscopy (XPS)	151
Magnetization measurements	151
RESULTS AND DISCUSSION	152
Au(III) complexation	152
Gold reduction	153
Characterization of the gold nanoparticles	154
Magnetic properties of the gold nanoparticles.....	157
CONCLUSIONS	158
OUTLOOK.....	159
LITERATURE	163

INTRODUCTION

The rapid industrial growth in the developing world has introduced many environmental pollutants as a significant factor affecting human health. One of the big challenges of the third millennium is the management of radioactive waste and the protection of humans and the environment from its chemical and radiological toxicity. Since the 1940s large quantities of anthropogenic radioactive waste were accumulated primarily due to the mining and milling of uranium ore and its subsequent processing for nuclear energy and weapon production [1]. In Eastern Germany alone, several hundreds of millions of cubic metres radioactive liabilities, in particular waste rock material and tailings, were left behind after the cessation of uranium production [2]. Up to date about 70% (September 2010) of the contaminated sites above ground were rehabilitated [3], which primarily includes a capping to prevent from direct radiation as well as from the release of radon gas or radioactive dusts. However, none of the rehabilitated sites is sealed at the bottom, allowing an accidental release of uranium from these tailings into the ground water by erosion and leaching processes at any time [4]. The aqueous phase is the only conceivable transport medium for uranium, present in soils, sediments, and other geological formations. In order to estimate the possible extent of uranium transport within the aqueous phase, it is important to predict the reactions of uranium compounds, which are dissolved or suspended in groundwater, with the surrounding inorganic and organic material. For this purpose it is essential to know the chemical and biological factors determining physicochemical uranium speciation as well as the long-term stability of the compounds and complexes which are formed under certain conditions. The most relevant chemical parameter regarding uranium mobility is the redox potential, because it predominantly determines the oxidation state of this radionuclide. Uranium can occur in the oxidation states of +3, +4, +5, and +6. However, U(III) and U(V) are very unstable at common environmental conditions and thus tetravalent and hexavalent uranium compounds are by far the most frequent in nature. U(IV) has a strong tendency to precipitate, usually in form of the oxide mineral uraninite (UO_2), whereas U(VI) generally forms soluble and thus mobile complexes. In addition to the oxidation state, the interaction mechanisms of uranium with the environment are strongly influenced by pH-dependent hydrolysis reactions, which alter its solubility and influence the sorption to inorganic particles [5]. Further, site specific parameters, that play a crucial role for the speciation of uranium in aquatic systems, are the ionic strength as well as the type and the concentration of inorganic ligands. Besides the chemical parameters, biotic factors influence uranium migration in nature as well. In

particular, the indigenous microbial community can significantly change uranium mobility. The bioavailability of this radionuclide, e.g. its ability to interact with surrounding (micro)organisms, after its release into the pore and ground water depends on its concentration and physicochemical speciation [6]. Previous studies showed reasonable evidences suggesting that UO_2^{2+} and UO_2OH^+ are the most bioavailable chemical forms of U(VI). In contrast to that, bioavailability is dramatically reduced for uranyl complexes formed with inorganic ligands (e.g. carbonates, phosphates) or with humic substances [6].

Several studies were performed exploring the microorganisms that inhabit such radionuclide-contaminated environments, by using culture-independent, molecular approaches, such as 16S rRNA gene analyses [7-11], also combined with phospholipid fatty acid (PLFA) analysis [12]. In addition, a more recent study focused in particular on the metabolically active microbial community of radionuclide-contaminated subsurface sediments from the “Oak Ridge Field Research Center” (Oak Ridge, Tennessee, USA), which was assessed by comparing RNA and DNA clone libraries [13]. The authors demonstrated that in particular several groups of heavy metal tolerant nitrate-reducers, belonging to the phyla *Proteobacteria*, *Firmicutes*, *Actinobacteria* and *Bacteroidetes*, are well adapted to such polluted environments [13]. However, a comparison of the microbial communities of different radionuclide-polluted sites suggests that the composition is site-specific and depends on geological and physicochemical parameters. Nevertheless, it was consistently demonstrated, that these environments are not hostile, but inhabited by a large variety of microbial populations.

As mentioned before, these microbial communities are able to interact with uranium and other metals in multiple ways (Fig. 1), due to the large variety regarding metabolism and cell surface structures. The latter provide a highly efficient matrix for metal complexation. Some studies demonstrated that the binding at surfaces of microbial cells is even more efficient than that at inorganic soil components, like minerals [14-16]. The high metal complexation ability of microbial cells is primarily based on two facts: the high surface-to-volume ratio and the usually large number of metal binding ligands, which are provided by the organic cell surface polymers, e.g. peptidoglycan, lipopolysaccharides, proteins, and glycolipids. These ligands primarily include negatively charged, functional groups, such as deprotonated phosphate, carboxyl, hydroxyl, amino and sulfhydryl groups. The adsorption of aqueous metal cations onto these functional groups, the so called biosorption process, is rapid, reversible and simply based on physical adsorption, ion exchange or chemical sorption of the positive charged

metal ion to the negatively charged cellular ligands. Hence, it is controlled only by the pH-dependent protonation status of the functional groups at the cell surface, and by the affinity of these functional groups for the specific aqueous metal, whereas biosorption does not depend on the cell metabolism. The abiotic nature of the biosorption process had previously been verified by similar affinities of bacterial cells and their isolated cell walls to aqueous heavy metals cations [17]. The temperature effect on the biosorption process is small compared to the other influencing factors, given that the temperature does not damage the structural components of the cells [18].

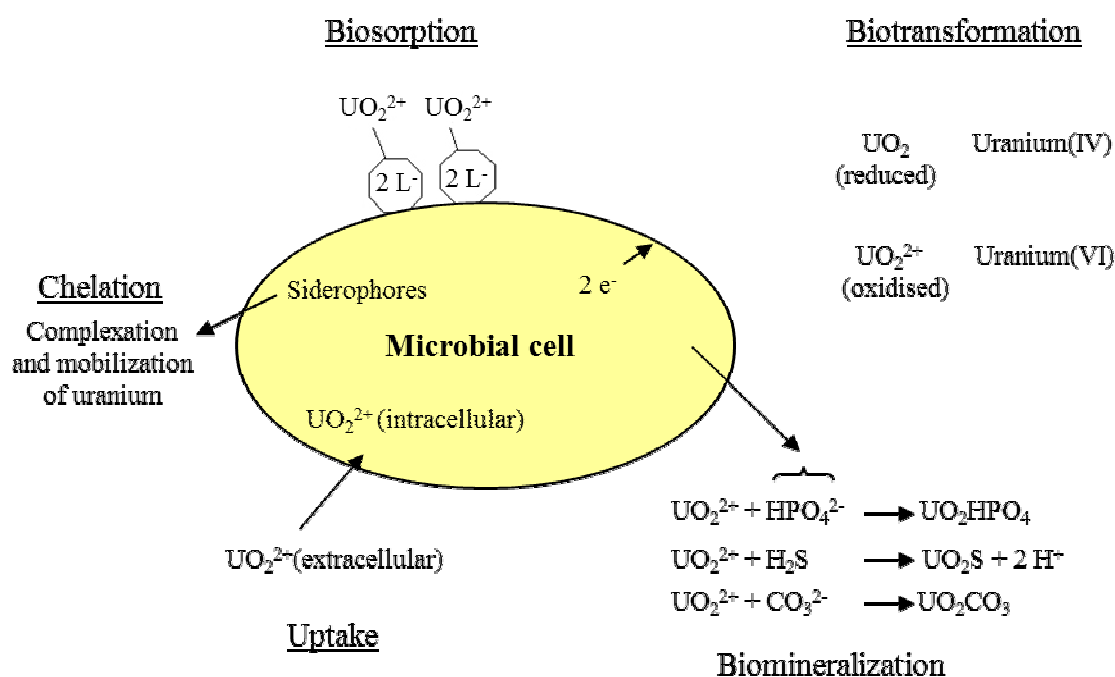


Figure 1. Important interaction mechanisms of uranium and microbial cells (after Lloyd and Macaskie [19]).

Besides the “passive” biosorption, which is exclusively based on the affinity between the biosorbent (cell structures) and sorbate (uranium), metabolism-dependent processes can also alter uranium migration behaviour. Such “active” processes can act mobilising and immobilising and involve biotransformations such as oxidation and reduction, an uptake inside the cells or a complexation by microbially generated compounds (Fig. 1). The term biotransformation, in general, includes all chemical modifications of a compound caused by the metabolic activity of organisms. In the case of uranium and other metals, it primarily involves microbial oxidation and reduction processes. The microbe-mediated uranium oxidation under aerobic conditions was demonstrated for some acidophilic microorganisms, e.g. for the archaeal species *Sulfolobus metallicus* [20] and *Metallosphaera sedula* [21] as

well as for the bacterial strain *Acidithiobacillus ferrooxidans* [22]. Under anaerobic conditions nitrate can be used, instead of oxygen, as electron acceptor as it was shown for the anaerobic U(IV) oxidation conducted by *Thiobacillus denitrificans* [23]. In contrast to that, many anaerobic microorganisms can transfer electrons under anaerobic conditions from an electron donor to U(VI) and thus reduce the radionuclide to U(IV). Suzuki and co-workers studied U(VI) reduction in a sediment sample from the inactive open pit uranium mine “Midnite”(Stevens County, WA, USA) [24]. After incubation for one month at anaerobic conditions, uranium was detected in form of U(IV) accumulates at the surface of microbial cells, bringing the authors to the conclusion that uranium was reduced by the enzymatic activity of these microorganisms [24]. Indeed, by now the reduction of U(VI) to insoluble uraninite under anaerobic conditions has been described for a large variety of bacteria [25-29]. Some strains like *Geobacter metallireductans* and *Shewanella putrefaciens* are even able to cover their whole energy demand by the electron transfer to U(VI) [30]. In addition, uranium reduction was also demonstrated at high temperatures of about 100 °C, performed by the hyperthermophilic archaeon *Pyrobaculum islandicum* [31].

Another mechanism that influences uranium transport in natural systems is the complexation of this radionuclide by inorganic and organic compounds released from microbial cells. In this regard, it is differentiated between those uranium-binding ligands which enhance solubility and mobility, and those which reduce them. The release of the latter can cause biomineralization of uranium. By definition, the term “biomineralization” includes the precipitation of insoluble mineral complexes, formed due to the release of microbial generated inorganic ligands, like phosphates, sulphides, and carbonates. A well-studied example for a corresponding mechanism is the complexation of uranium by orthophosphate and the concomitant formation of low soluble uranyl phosphates. The release of orthophosphate is attributed to the activity of various enzymes, summarized as phosphatases, which release inorganic phosphate (PO_4^{3-}) from organic phosphate compounds. Respective enzyme activities have been described for a large variety of aerobic and anaerobic bacteria as well as for some archaea [32-34]. In addition to the inorganic ligands capable for uranium complexation, microorganisms can also produce organic compounds which may alter uranium mobility. One class of corresponding compounds are humic substances (humics) which are released due to the microbial degradation of complex organic matter. They are very resistant to further biodegradation and thus accumulate within the environment [35]. Humics were separated operational, differing in acidity and chemical composition, in humin

(insoluble fraction), humic acid (soluble under alkaline conditions), and fulvic acid (soluble at all pH conditions) [36]. In particular the latter two are known to interact efficiently with uranium and, thus, can influence the migration of uranium in nature [37-43]. Humics may also be involved in U(VI) reduction by providing an electron shuttle, i.e. they serve as terminal electron acceptor in microbial respiration pathways and subsequently donate these electrons to U(VI) [44]. A similar mechanism most likely underlie the U(VI) reduction described for *Deinococcus radiodurans*, which is able to reduce U(VI) in the presence of the humic acid analogue anthraquinone-2,6-disulfonate (AQDS), whereas no uranium reduction occurred without it [45].

Other microbially generated compounds which interact highly efficient with metals are siderophores. These chelating agents are usually formed by microorganisms in the case of iron deficiency, in order to increase iron solubility due to a complexation *via* functional groups, in particular catechol and hydroxamate groups [46]. However, siderophores are usually not highly specific. Therefore they also increase solubility and thus bioavailability of other metals, heavy metals and radionuclides. A measureable enhancement of uranium mobility by the activity of microorganisms was demonstrated by the siderophores pyoverdine and desferrioxamine-B [47, 48].

Finally, microorganisms are also able to take up metals by active processes using metal transporters located in their cell walls. In the case of uranium it was speculated that it can be taken up wrongly by such transporters as a consequence of a mix up with essential metals, e.g. calcium [6, 19]. Once inside the cell, uranium may be bound to, or precipitated within intracellular structures. However, by now it is commonly assumed that the accumulation of uranium inside microbial cells is based on a passive, metabolism independent transport due to an increased permeability of the cell membrane as a result of the toxic stress [49]. Up to date, there is no concrete evidence that uranium can be taken up by microorganisms *via* active cell processes.

Some of the described interaction processes were specifically used for industrial and economic purposes. Microbial U(IV) oxidation, for example, has been used for uranium bioleaching processes, which is the transformation to and extraction of soluble U(VI) from uranium ores [50]. Because of the physicochemical conditions in such mining sites, the microorganisms that catalyse bioleaching processes are required to grow in a basically inorganic, aerobic, and highly acidic environment. For this reason, extremophilic bacteria as well as archaea were frequently detected in commercial bioleaching areas [51].

Besides mining of metals, the before described interactions were intensively studied in the last years, in particular focussing on their potential for bioremediation, i.e. decontamination, of heavy metal and radionuclide-polluted environments [52-54]. The need for developing such microbial-based clean-up procedures is mainly caused by the very high costs, the technological limitations and the lack of specificity of the currently available physicochemical approaches. In addition, the invasive physical clean-up, which involves excavation, transport and disposal of soil as well as pumping and treating of groundwater can have negative influences on biodiversity and can even increase human health risks [55]. Thus, *in situ* bioremediation approaches are advantageous, as they are expected to provide a cost-effective, more specific and environmental-friendly method for decontamination. Moreover, it was shown that the metal recovery using biological approaches is much more efficient, allowing the treatment of polluted sites with low concentrations of uranium which are not amenable to chemical approaches [56]. Among the biotechnological processes, biosorption is limited by the availability of uranium-binding sites. Moreover, insufficient specificity and stability of biosorbents turned out to cause little progress in industrial application [57]. Therefore, the potential for commercial development and application of biosorption is rather weak, and likely will be used in the future only as supporting process in remediation procedures [58]. As mentioned above the cellular uptake of uranium is also supposed to be a passive process and it is most likely based on increased cell membrane permeability of death cells and subsequent adsorption to intracellular structures. Hence, the same limits and problems, which are applied for biosorption-based remediation procedures, apply for this process as well. And even in the case, uranium would be taken up by an active microbial process, the potential of this uptake for bioremediation is strongly limited due to uranium toxicity [59].

Because of these reasons, many established and novel bioremediation procedures based on active processes, conducted by living microbial cells. As a matter of course, the applicability of corresponding industrial approaches is primarily determined by the ability of the used microorganisms to survive and maintain the desired metabolic pathways under the radiation exposition and the chemical toxicity of uranium. Therefore, the use of highly radiotolerant microbial strains is advantageous. An eligible, well-studied bacterium is *Deinococcus radiodurans* which maintain its viability in excess of 5000 Gray [60], a dose that is approximately 300 times higher than the dose which typically kills *Escherichia coli*. However, it was demonstrated by studying two bacterial strains naturally occurring in

contaminated sites, *Deinococcus radiodurans* and *Pseudomonas putida*, that uranium, as well as other actinides, are less toxic to bacteria than other heavy metals [61]. Hence, the actinide toxicity should not impede bioremediation approaches which are based on active microorganisms. The strains investigated in the present work are, for example, able to grow in the presence of uranium up to concentrations of 0.5 mM for *Paenibacillus* sp. JG-TB8 (Chapter I) and 1.1 mM for *S. acidocaldarius* (Chapter II), i.e. the strains tolerate uranium concentrations of more than 120 ppm and 260 ppm, respectively. These tolerated concentrations are higher than those of most uranium waste rock dumps and tailings, e.g. the uranium concentration of the soil sample from the “Haberlandhalde”, the natural habitat of *Paenibacillus* sp. JG-TB8, was “only” about 40 ppm. Hence, it is obvious for both strains that their growth and metabolism is in principle possible in many uranium-polluted sites.

The main focus of attention for an active microbial bioremediation of uranium-polluted sites is on two processes, uranium precipitation and U(VI) reduction. The latter has been intensively studied as it promises a high potential for uranium immobilization under reducing conditions. Microcosm experiments were performed using U(VI) polluted sediments from the inactive “Midnite mine” located in Stevens County (WA, USA) as well as soils from the “DOE NABIR field research center site” in Oak Ridge (TN, USA). In both studies a stimulation of microbial U(VI) reduction by the addition of organic substrates was demonstrated [24, 62]. In addition, field studies at the pilot-scale uranium *in situ* bioremediation field of the US Department of Energy site (Oak Ridge, TN, USA) were conducted in order to check transferability of the obtained results to natural systems [63]. Within this project, uranium immobilization was stimulated by the injection of ethanol, which in turn shifted, and stimulated activity of, the indigenous microbial community. As a consequence of that, U(VI) levels were reduced within two years from about 50 mg/L to below drinking water standard (< 30 µg/L). Biodiversity studies demonstrated a high abundance of metal reducing bacteria, e.g. *Desulfovibrio*, *Geobacter*, *Anaeromyxobacter* and *Shewanella* [63].

Another successful remediation based on bioreduction was conducted at a former uranium ore processing facility, called “Old Rifle” (CO, USA). In this case acetate was injected into the subsurface and as a consequence of that U(VI) concentrations decreased within 50 days from initial values between 0.4 and 1.4 µM to below the prescribed treatment level of 0.18 µM [12]. A combination of ¹³C-labeled acetate incorporation and subsequent DNA and PLFA analyses revealed that the uranium reduction is accompanied by a stimulation of

δ-Proteobacteria, in particular *Geobacter* species, suggesting that these bacteria are key players concerning U(VI) reduction [64].

However, the presence of oxygen as well as highly acidic pH conditions and high concentrations of nitrate can suppress U(VI) reduction as it was demonstrated in microcosm experiments using sediments from the FRC aquifer (Oak Ridge, TN, USA) [65].

An alternative strategy for bioremediation under oxygenated conditions is the immobilization of uranium due to the precipitation of hardly soluble inorganic uranium compounds. A well-known mechanism for bioprecipitation of uranium is based on the activity of non-specific phosphatases, in particular acid and alkaline phosphomonoesterases, which are commonly generated by active soil microorganisms [66]. These enzymes were expressed by a large variety of aerobic and anaerobic bacteria [34, 67, 68] and release inorganic orthophosphate from organic phosphate compounds. As a consequence of this, the released orthophosphate interacts with uranium and causes the precipitation of inorganic uranyl phosphate phases, directly at the cell surface or in the surrounding aqueous system. The applicability of this mechanism for remediation of uranium-polluted sites was previously suggested in studies on different *Pseudomonas* strains, which releases sufficient amounts of orthophosphate to cause precipitation of uranium from a low concentrated solution (0.02 mM uranium) [69]. The release of orthophosphate was stimulated within the latter work by the addition of an organic phosphate source and a simultaneous overexpression of the phosphatase gene. Moreover, Beazley and co-workers demonstrated that the hydrolyzation of organophosphate by aerobic heterotrophic bacteria can be may play an important role in bioremediation of uranium-contaminated sites [70].

It is evident, that up to date, much research was done to understand the biogeochemistry of uranium cycling in the environment and the central role of microorganisms in affecting uranium mobility. However, a deeper understanding of the behaviour of the actinides in the environment is needed to allow proper and reliable modelling, needed for disposition of nuclear waste over many thousands of years [71]. In addition, a better knowledge is necessary in order to develop new and to improve established bioremediation strategies for the contaminated sites.

Within the scope of this thesis different batch experiments were performed to study the interaction mechanisms of U(VI) with the bacterial isolate *Paenibacillus* sp. JG-TB8 and the acidothermophilic crenarchaeon *Sulfolobus acidocaldarius*, in order to determine and compare the ability of these two strains for uranium immobilization at different experimental

conditions. The present work combines wet chemistry with powerful spectroscopic and microscopic techniques, allowing profound conclusions about the uranium complexation by the studied strains.

The uranium complexation was studied within the acidic pH range, in particular at pH 2 (pH 1.5 for *S. acidocaldarius*), pH 3, pH 4.5 and pH 6. The rationale for using acidic conditions is based on both, the fact that many uranium-contaminated sites exhibit moderate acidic pH conditions (pH 4 to 6), as well as the chemistry and bioavailability of uranium. Assuming non-reducing and acidic conditions, uranium is predominantly present, in particular at pH values below 4, in form of the free uranyl ion, which is highly mobile, bioavailable and toxic (Table 1). The amount and kind of uranium species in aqueous systems, as presented in Table 1, can be estimated by several speciation methods, either assigned to analytical or computational methods [6]. The latter based on thermodynamic data which includes a system of mathematical equations that describes the metal-ligand equilibrium [72]. In this work the initial uranium speciation in the used solutions was calculated using the software package EQ3/6 [73] using equilibrium constants of the “Nuclear Energy Agency (NEA)” database [74] and uranyl hydrolysis constants of Guillaumont and co-workers [75].

Table 1. Main uranyl species present in the uranyl solutions used within this thesis.

	pH 1.5 [U]=5·10 ⁻⁴ M	pH 2 [U]=5·10 ⁻⁴ M	pH 3 [U]=5·10 ⁻⁴ M	pH 4.5 [U]=5·10 ⁻⁴ M	pH 6 [U]=5·10 ⁻⁵ M
UO ₂ ²⁺	98.8%	98.6%	98.1%	57.3%	
(UO ₂) ₂ (OH) ₂ ²⁺				26.3%	
(UO ₂) ₃ (OH) ₅ ⁺				6.3%	61.4%
(UO ₂) ₄ (OH) ₇ ⁺					12.4%
(UO ₂) ₂ CO ₃ (OH) ₃ ⁻					14.5%

Concerning the studied strains, the physiological pH optimum of *S. acidocaldarius* is between pH 2 and 3 [76], whereas that of the *Paenibacillus* species is around pH 7 (Chapter I). The latter strain was isolated from an anaerobic microbial consortium containing representatives of *Firmicutes* and yet to be cultured mesophilic *Crenarchaeota* belonging to the soil cluster 1.1b [77]. This consortium, in turn, was initially enriched from a uranyl nitrate treated (four weeks at pH 4 and under anaerobic conditions [78]) soil sample of the uranium mining waste pile “Haberland” (Saxony, Germany) which had a moderate acidic pH of around 4.5. For these reasons, it was suggested that the isolated *Paenibacillus* strain tolerates

moderate acidic pH conditions. This assumption was confirmed within this work by live/dead staining, demonstrating that a significant part of the cells remain alive after treatments with U(VI) at pH 4.5 (Chapter I). The studied *Paenibacillus* strain is a facultative anaerobic, endospore-forming bacterium, which means that the cells become metabolically active when suitable substrates for their growth are available, whereas they produce resistant endospores when their nutrients become exhausted. Because of this resistance mechanism against the changes of soil parameters, their motility, and the ability to switch their metabolism under anaerobic conditions, it can be assumed that paenibacilli play a significant role in the biogeochemical cycles of matter in natural ecosystems. Therefore, the first objective of this thesis was to study the influence of *Paenibacillus* JG-TB8 on uranium mobility in aqueous systems. The fate of uranium was determined in order to draw qualitative and quantitative conclusions about uranium biosorption, biomineralization, and bioreduction by this strain, also in the face of a potential use for bioremediation procedures. It was shown that cells of the studied strain can dramatically influence uranium migration in aqueous systems. The strain was able to accumulate U(VI) over the whole pH range studied. In contrast to the previous studies where uranium complexation was studied exclusively under aerobic or anaerobic conditions, in this work for the first time one and the same strain (*Paenibacillus* sp. JG-TB8) was investigated under both aeration conditions, in order to determine the influence of oxygen on the U/bacteria interactions. The rationale for using this strain was its ability to grow and carry out metabolism under aerobic as well as under anaerobic conditions. The latter correspond to the natural habitat of the strain, as the soil sampling point was in a depth of two metres. Dramatic morphological changes of the *Paenibacillus* cells were observed after the exposition to anaerobic conditions. In this case the cells exhibited a filamentous phenotype, i.e. they were significantly longer (some cells exhibit a length of more than 200 μm) compared to the rods grown under aerobic conditions which had a size of 3 to 6 μm . This morphological difference most likely causes the reduced uranium binding capacity observed under anaerobic conditions, due to the smaller cell surface and therefore the smaller number of U(VI) complexing ligands relating to their weight. In addition and more important, an inhibition of the indigenous phosphatase activity of the strain was observed under anaerobic conditions. As a consequence of that, uranyl phosphate mineral phases, which were precipitated under aerobic, moderate acidic conditions, were not formed under anaerobic conditions. Noteworthy the *Paenibacillus* isolate does not reduce U(VI), even not after the addition of acetate as electron donor, although acetate usually stimulates microbial U(VI)

reduction [12]. These findings are in contrast to all previous studies which were performed on bacterial uranium interactions under moderate acidic, anaerobic conditions, where either bioreduction or biomineralization of uranium was observed.

In contrast to the high number of studies dealing with the bacterial processes responsible for the binding of uranium, only little is known about the processes implicated in the complexation of this radionuclide by representatives of the second microbial domain of life, the “*Archaea*”. Archaea were shown to be present in various soil and water ecosystems and they play an important role in the global cycles of matter [79]. They differ in many aspects from bacteria and their cell walls are significantly simpler than those of bacteria [80]. Therefore another objective of this thesis was to investigate whether the structural differences between the cell surfaces from representatives of archaea and bacteria influence the binding capacity and the local coordination of uranium bound to the cells. The thermoacidophilic crenarchaeal strain *S. acidocaldarius* was chosen as a model organism for this study, as it is one of the best studied archaeon. The cell wall of *S. acidocaldarius* consists only of a proteinaceous surface layer (S-layer), called SlaA-layer, which is anchored to the cytoplasmic membrane *via* another protein, called SlaB [81] (Fig. 2). Because of the low content of negatively charged amino acids and the absence of phosphorylated sites, this S-layer seems to be ineffective in the complexation of uranium. In this case a small amount of uranium might pass through the pores of the S-layer and is complexed by the reactive groups of the cytoplasmic membrane. In contrast to that, the cells of *Paenibacillus* sp. JG-TB8 possess a more complex cell wall structure, which includes a thick layer of peptidoglycan that is rich on phosphate and carboxylic groups and represents the major metal binding component of this bacterium (Fig. 2). And indeed, the structural differences between the cell surfaces of both strains strongly influence the uranium binding ability. As expected, the binding capacity of the cells of *S. acidocaldarius* was only about one third of that measured for the cells of *Paenibacillus* sp. JG-TB8 under corresponding experimental conditions (Chapters I, II and III). Spectroscopic studies on the uranium complexes formed by *S. acidocaldarius* at highly acidic conditions (pH 1.5 and pH 3) demonstrated that uranium was mainly complexed by organic phosphate groups of the cytoplasmic membrane in a monodentate binding mode (Chapter II). This finding is in agreement to the U(VI) complexation mode at highly acidic conditions observed for the studied bacterial isolate *Paenibacillus* sp. JG-TB8 (Chapter I) as well as for other Gram-positive and Gram-negative bacteria [82-84]. These results suggest that at highly acidic conditions, i.e. pH values of 3 and below, the complexation mode of U(VI) by microbial cells is universal and independent from the microbial domain.

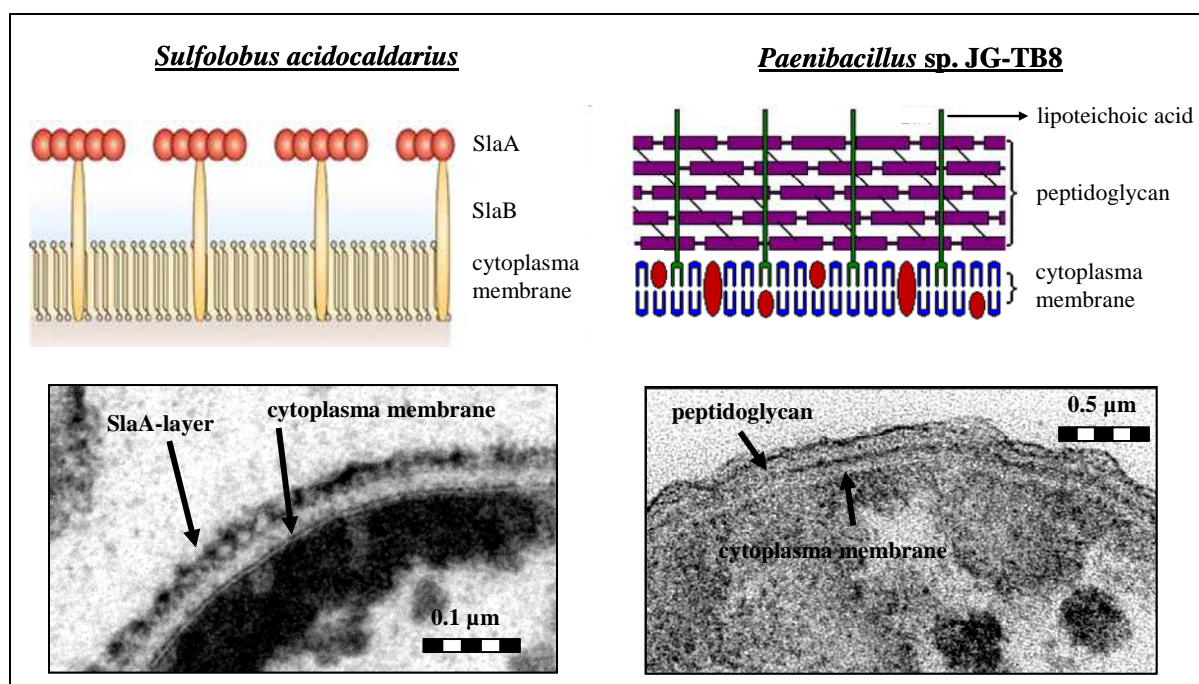


Figure 2. Comparison of the cell envelopes of *S. acidocaldarius* (schematic picture taken from [85]) and the isolated *Paenibacillus* strain (schematic picture taken from www.cehs.siu.edu).

With increasing pH an additional complexation mode at functional groups of organic origin was detected. Besides the phosphate groups of the cell membrane, deprotonated carboxylic groups are involved in the U(VI) complexation by the cells of *Sulfolobus acidocaldarius* at pH 4.5 (Chapter III). Moreover, a part of the added uranium was mineralized due to the release of orthophosphate by the cells, as a consequence of increased cytoplasmic membrane permeability and the acid phosphatase activity of the strain (Chapter III). The phosphatase activity of the strain was, however, linked neither to U(VI) biomineralization nor to orthophosphate liberation. The highest enzymatic activity was calculated at pH 3, which is reasonable, as this pH corresponds to the physiological pH optimum of the strain. However, U(VI) biomineralization does not occur at this pH. Instead, the formation of uranyl phosphate mineral phases was observed at pH 4.5 and pH 6, where the phosphatase activities were only half and a quarter of that at pH 3, respectively. A possible reason for this may be the inhibition of mineral formation at highly acidic conditions. This assumption is supported by a study of Wellmann and co-workers, who demonstrated that uranyl phosphate minerals are rather unstable at acidic pH conditions [86]. Nevertheless, according to the phosphatase activity, at least the release of orthophosphate should be highest at pH 3. Therefore another, even more likely explanation for the inhibition of U(VI) biomineralization is the very healthy population of *S. acidocaldarius* during the incubation with uranium at pH 3 (Chapter III),

which may limit the amount of degradable organophosphate, which is especially provided by a release from dead cells.

Beazley and co-workers propose that aerobic heterotrophic microorganisms that can hydrolyse organophosphate at low pH conditions may play an important role in the bioremediation of uranium-contaminated environments [70]. *S. acidocaldarius* exactly meet this criterion, as it is well-adapted to acidic conditions and, moreover, maintains its metabolism also at moderate temperatures. However, as demonstrated within this thesis, phosphate-containing organic substrates may limit the uranium biomineralization process at highly acidic conditions. Hence, for an effective immobilization of uranium by *S. acidocaldarius*, the addition of an organic phosphate source serving as substrate for the enzymatic release of orthophosphate is suggested.

The diverse U(VI) complexation by organic phosphate and carboxylate groups as well as inorganic phosphate groups, observed for the cells of *S. acidocaldarius* at pH 4.5, differs from those of the previously studied interactions of acidophilic bacteria with U(VI) where only organic phosphate groups participate in the complexation process at pH 4.5 [87]. Moreover, this finding is also in contrast to the predominant precipitation of inorganic U(VI) phosphate mineral phases observed by all neutrophilic bacteria [83, 88, 89]. Therefore, the results of the present work suggest that bacteria and archaea exploit different U(VI) complexation modes at moderate acidic pH conditions.

For a more detailed elucidation of the U(VI) complexation mechanism by the archaeal cells, the U(VI) binding by two purified cell envelope fractions of *S. acidocaldarius* (SlaA-layer ghosts and cell envelope ghosts, the latter consisting of cytoplasmic membrane covered with S-layer protein) were investigated (Chapter IV). The S-layer protein of *S. acidocaldarius*, recently called “SlaA”, possesses hexagonal (p3) symmetry and is fastened to the archaeal cells via the anchoring protein, SlaB, which is integrated into the cytoplasmic membrane [90]. A comparison of the obtained results with those about the interactions of the whole cells of *S. acidocaldarius* with U(VI) allowed differentiating the role of the outermost SlaA-layer in the uranium complexation and thus detoxification processes of this radionuclide. The comparison of the binding capacity of the two cell envelope fractions clearly revealed that the major part of the complexed U(VI) is bound to functional groups of the cytoplasmic membrane. No uranium binding at the SlaA-layer was observed at highly acidic conditions ($\text{pH} \leq 3$), and only very low amounts bound to the carboxylic groups of the SlaA-proteins at pH 4.5 and pH 6 (Chapter IV). These results demonstrate that the proteinaceous SlaA-layer of *S. acidocaldarius* does not have a protective role against uranium at highly acidic conditions

which correspond to the physiological optimum of the strain. In addition, the studies on the isolated cell envelope fractions of *S. acidocaldarius* revealed that the use of cryogenic TRLF spectroscopic techniques open up new possibilities to investigate the U(VI) complexation by organic ligands of microbial cell surfaces (Chapter IV).

Concluding the interactions with U(VI), this thesis gives new insights in the microbial complexation of U(VI), in particular regarding the influence of aeration conditions, archaeal interaction mechanisms, and the TRLF spectroscopic detection of uranium complexes.

Beside the interactions with U(VI) the SlaA-layer of *S. acidocaldarius* was also studied with regard to its potential for nanoclusters formation (Chapter V). A general feature of S-layer proteins is their ability to reassemble from their single subunits in suspension and even on solid surfaces, reproducing highly ordered regular structures [91]. Moreover S-layers can serve as a template for the formation of metal nanoparticle arrays, whether by wet chemical processes stimulating precipitation from solution or by a binding of pre-synthesized nanoparticles [92]. Therefore, S-layer proteins are a promising tool for controlled “bottom-up” fabrication of nanobiotechnological structures and devices [93]. In this work the paracrystalline S-layer of *S. acidocaldarius* (SlaA-layer) was investigated with regard to its potential to serve as a macromolecular template for the formation of gold nanoparticles. In contrast to many bacterial S-layer proteins, the studied SlaA-layer is extremely stable and can resist high temperatures, low pH, proteases, and detergents, making it interesting for the production of defined nanostructures. Moreover, the most interesting property of the SlaA-layer is the indigenous presence of two sulphur-containing cystein residues per monomer. These residues provide thiol groups, usually not present in bacterial S-layer proteins. Diluweit and co-workers demonstrated a stimulation of gold nanoparticle formation after the introduction of thiol groups into the S-layer protein of a *Bacillus sphaericus* strain [94]. This thiolization is not necessary using the SlaA-layer protein. The formed gold nanoparticles onto the SlaA-layer were irregular distributed and had a particle size between 2 and 3.5 nm. XPS analysis demonstrated that the gold clusters consisted mainly of Au(0). Most interesting feature of the formed gold nanoparticles is their magnetic behaviour most likely based on the interactions of the gold nanoparticles with the thiol groups of the SlaA-layer protein. Hence, within this thesis, the evocation of magnetism in gold nanoparticles formed on a not-modified, natural biotemplate was demonstrated for the first time, suggesting new strategies for a clean and environmental friendly production of well-defined noble metal nanoclusters.

Chapter I

Interactions of the uranium waste pile isolate *Paenibacillus* sp. JG-TB8 with U(VI) under aerobic und anaerobic conditions.

Thomas Reitz, Mohamed L. Merroun, Andre Rossberg and Sonja Selenska-Pobell

ABSTRACT

A facultative anaerobic bacterium, designated JG-TB8, was isolated from an anaerobic microbial consortium, enriched from a soil sample of a uranium mining waste pile. Phylogenetic analysis based on the 16S rRNA gene sequence revealed that JG-TB8 belongs to the genus *Paenibacillus*, and is closely related to *P. borealis*.

Studies on the uranium tolerance demonstrated that JG-TB8 grows at the presence of uranium up to a concentration of $5 \cdot 10^{-4}$ mM. Regarding the interactions with this radionuclide it was shown that the cells of the strain are able to accumulate uranium from aqueous solutions at acidic conditions (pH 2 to 6). Thereby, the speciation of the formed uranium complexes depends on both, the pH and the aeration conditions, i.e. the presence or absence of oxygen. A combination of spectroscopic (TRLFS, XAS) and microscopic (TEM/EDX) techniques revealed that at highly acidic pH conditions (pH 2 and 3), uranium was almost exclusively bound by phosphate groups of organic macromolecules, independently on the aeration conditions. At higher pH values, a part (pH 4.5) or the total amount (pH 6) of the dissolved uranium was precipitated under aerobic conditions in a meta-autunite-like uranyl phosphate mineral phase. TEM studies of the uranium-treated samples incubated under aerobic conditions demonstrated uranium accumulates on the cell surface as well as intracellularly located. In contrast to that, mineral formation was neither observed at pH 4.5 nor at pH 6 under anaerobic conditions. At these conditions carboxylate groups, in addition to phosphate groups, were involved in the uranium complexation. The absence of biomineralization under anaerobic conditions was clearly assigned to a suppression of the indigenous phosphatase activity of JG-TB8, playing the key role in hydrolyzation of the cellular polyphosphate. Resulted orthophosphate groups play a crucial role in uranium biomineralization.

Keywords: *Paenibacillus*, Uranium, Biomineralization, XAS, TRLFS, TEM, Phosphatase activity

INTRODUCTION

The biological effects of uranium strongly depend on its mobility and bioavailability, which are, in turn, determined by its speciation and physicochemical form [6]. In the environment uranium primarily occurs in the oxidation states +4 (U^{4+}) and +6 (UO_2^{2+}). In particular the free uranyl ion (UO_2^{2+}), which predominates at acidic ($< pH\ 5$) and non-reducing conditions [95], has a high mobility and biological toxicity, which is based on both, its chemical and radiological properties. The speciation of uranium in nature is affected by a variety of abiotic [96, 97] and biotic [98, 99] factors. The latter primarily include changes induced by microorganisms due to their ubiquitary and numerous occurrences in nearly all habitats on earth. The multifaceted metabolism and structures of these organisms provoke various interaction mechanisms with radionuclides and other heavy metals [19, 98]. By now several studies have demonstrated that U(VI) is complexed by the negatively charged functional groups of the cell surface in a process called biosorption [100-102]. Because of that, uranium is supposed to bound, at least to some extent, to all microbial cells. In addition, further microbial transformations which alter the mobility of this radionuclide were demonstrated for individual microorganisms. These processes include the precipitation of uranium-containing minerals (biomineralization) [88, 89, 103], as well as the formation of mostly insoluble and therefore less toxic U(IV) species (bioreduction) [30, 104]. Both microbial-mediated processes had been studied in the face of their potential use for the remediation of contaminated environments as an efficient alternative to the commonly used chemical approaches [29, 69, 105, 106].

Soil ecosystems, even those which are polluted with heavy metals or radionuclides, are inhabited by a large variety of microorganisms [8, 77, 107, 108]. The microbial community structure, in particular that of the upper soil layers, is continually subjected to changes due to continuous changes in temperature, humidity, nutrient supply and oxygen tension. Endospore forming bacteria are well adapted to such changes. They become metabolically active when suitable substrates for their growth are available, and they form spores when their nutrients become exhausted. The resistance of their spores to environmental stress allows these organisms a long-term survival under adverse conditions. Therefore endospore formation is thought to be a strategy for survival in the soil environment, wherein these bacteria are abundant [109, 110]. However, these microorganisms are ubiquitous and can also be isolated from a wide variety of other environmental samples. Until the early 1990s, all endospores forming bacterial species were classified into the genus *Bacillus*. Due to a reclassification, based on the 16S rRNA gene sequence, eleven of these species, the so called “group 3

bacilli”, were separated from this genus and classified into the new family and genus “*Paenibacillaceae*” and “*Paenibacillus*”, respectively (“paene” (lat.) = “almost”) [111]. Up to date, further proposals for novel strains have increased the number of validated *Paenibacillus* species to more than 70 [112]. They are usually facultative anaerobic, motile by means of peritrichous flagella, degrade macromolecules by extracellular enzymes, including DNA, proteins, carboxymethyl cellulose and starch [111, 113], and were recovered from several soil samples [114-120]. Because of these abilities, paenibacilli are assumed to play a significant role in the biological cycles of carbon and nitrogen. This work focuses on the interactions of U(VI) with one representative of this genus, named *Paenibacillus* sp. JG-TB8. The strain was isolated from an anaerobic microbial consortium, cultured in *Thermosphaera* medium (DSMZ medium 817) [121], and containing representatives of *Firmicutes* and of yet to be cultured mesophilic *Crenarchaeota* classified into the soil cluster 1.1b [77]. The consortium was recovered from a soil sample of the uranium mining waste pile “Haberland” (Johanngeorgenstadt, Saxony, Germany), which was treated with uranyl nitrate under anaerobic conditions for four weeks [78].

Up to date, no study was published describing the interactions of uranium with one and the same bacterial strain under two different aeration conditions. Hence, the main objective of this work was to investigate the interactions of the facultative anaerobic isolate *Paenibacillus* sp. JG-TB8 with uranium under aerobic and anaerobic conditions, in order to determine the influence of oxygen on uranium mobilization or immobilization by this strain. The second objective was to study the pH-dependency of the U/bacteria interactions in both systems.

The aim was to determine the qualitative and quantitative incidence of uranium biosorption, biomineralization, and bioreduction by cells of JG-TB8 depending on both, the presence of oxygen and the pH conditions.

MATERIALS AND METHODS

Isolation, cultivation and growth conditions

Paenibacillus sp. JG-TB8 as well as other strains belonging to the *Bacillaceae* was isolated from an anaerobic microbial consortium, additionally containing other representatives of *Firmicutes*, in particular *Clostridia*. The consortium was recovered from a uranium-treated uranium mining waste pile soil sample [77] by the following procedure: After dilution of the consortium with sterile water (1:20, 1:100, 1:500, 1:2000) 100 µl of each dilution were

spread on agar plates (1.5% agar) with 10 g/L NB (Nutrient Broth) medium (Mast group Ltd., Merseyside, UK). After incubation at 30 °C for five days, single colonies were isolated by transferring them to fresh NB medium (10 g/L, pH 7.2). The isolates were afterwards maintained in the same medium and long-term stored at -70 °C in 50% glycerol.

For production of biomass, a fermentation system (Pilot System, Applikon Biotechnology Inc., Foster City, USA) equipped with a 5 L bioreactor, a bio-controller (Model ADI 1010), and a control unit (ADI 1075) with three pneumatic pumps (acid, base, and antifoam), stirrer controller, and rotameters was used. Anaerobic growth of *Paenibacillus* sp. JG-TB8 was carried out in airtight closed two litre bottles at pH 7.2 in ATCC medium 591, usually used for the cultivation of various *Clostridium* species [121]. In both cases, the cultivation temperature was 30 °C and growth was monitored by measuring the optical density at a wavelength of 600 nm. Cell morphology was examined by phase-contrast light microscopy using Olympus BX-61 (Olympus Optical Co. GmbH, Hamburg, Germany).

Phylogenetic affiliation

Total DNA of the bacterial isolates was recovered *via* the NucleoSpin[®] Tissue Kit (Macherey-Nagel, Düren, Germany), according to the instructions of the manufacturer. The 16S rRNA gene fragments were amplified by polymerase chain reaction (PCR) using AmpliTaq Gold[®] Polymerase with the corresponding GeneAmp[®] PCR buffer II (Applied Biosystems, Foster City, CA, USA) along with the primer pair 16S_{7-27F} (5'-AAGAGTTTGATYMTGGCTCAG-3': bacteria-specific) and 16S_{1492-1513R} (5'-TACGGYTACCTTGTTACGACTT-3': universal) [122], *Escherichia coli* numbering [123]. The PCR reaction mixture (total volume was 30 µl) contained 1.6 µL of the purified DNA, 0.8 µM each of the forward and reverse primer, 125 µM each of the four deoxynucleoside triphosphates, 1.25 mM MgCl₂, and 1.5 units of the polymerase.

Amplification was performed in a thermocycler (model T3, Biometra, Göttingen, Germany) by using the following temperature profile: After an initial denaturation at 95 °C for 3 min, the 16S rRNA gene fragments were amplified by 30 amplification cycles, including a denaturation (94 °C, 60 s), an annealing (40 s) and an elongation step (72 °C, 90 s). The annealing temperature was lowered within the first five cycles from 59 to 55 °C ("touch down" PCR) to avoid nonspecific primer binding and therewith the amplification of nonspecific sequences [124].

The amplified 16S rRNA gene fragments were purified using the QuickStep[®]2 PCR Purification Kit (Edge BioSystems, MoBiTec, Göttingen, Germany) and subsequently

sequenced with the ABI PRISM[®] Big Dye[®] Terminator v1.1 Cycle Sequencing Kit (Applied Biosystems, Foster City, CA, USA), in both cases following the manufacturers' instructions. The sequencing procedure based on the chain-terminator method developed by Sanger and co-workers [125]. Partial 16S rRNA gene sequences from each PCR product were obtained by three parallel sequencing reactions using the primers 16S_{7-27F}, 16S_{1492-1513R} and 16S_{342-361F} (5'-CTACGGGAGGCAGCAGTGGG-3') [126]. The individual nucleotide sequences of these reactions were determined with an automated ABI PRISM[®] 310 Genetic Analyser (Applied Biosystems, Foster City, CA, USA). Subsequently, the three partial sequences were assembled using the software Autoassembler 2.0 (Applied Biosystems, Foster City, CA, USA). The obtained 16S rRNA gene sequences were compared with those available in public gene banks (GenBank, EMBL-European Molecular Biology Laboratory, and DDBJ-DNA Data Bank of Japan) by using the nucleotide collection of BLAST (Basic Local Alignment Search Tool) [127] of the National Center for Biotechnology Information (NCBI, Bethesda, MD, USA). The sequences were aligned with those of the closest phylogenetic relatives by using the program Clustal W v. 1.4 [128] within the BioEdit Sequence Alignment Editor v. 4.8.10. Phylogenetic trees were generated using the neighbour-joining algorithm [129], including Jukes-Cantor corrections for distance analyses, of the PHYLIP package v. 3.5c [130]. The 16S rRNA gene sequences retrieved from the bacterial isolates have been submitted to the European Nucleotide Archive (<http://www.ebi.ac.uk>) and were assigned to the accession numbers FR849913 to FR849936. (Table A in Supplemental Material).

Carbon and nitrogen sources utilized by *Paenibacillus* sp. JG-TB8

The utilization of different carbon and nitrogen sources was studied in a basal salt medium containing: 0.5 g/L K₂HPO₄, 0.5 g/L KH₂PO₄, 0.2 g/L MgSO₄ · 7 H₂O, 33 mg/L CaCl₂ · 2 H₂O, 13 mg/L ZnSO₄ · 7 H₂O, 10 mg/L FeSO₄ · 7 H₂O, 8 mg/L MnSO₄ · H₂O, 500 µg/L thiamine, and 1 µg/L biotin at pH 7.2. Stock solutions of the carbon sources (D(+)-glucose, D(-)-fructose, D(+)-maltose, D(+)-galactose, sucrose, potassium acetate, sodium pyruvate, glycerol, D-sorbitol, methanol, citric acid, L(+)-lactic acid) as well as of the nitrogen sources (urea, ammonium sulphate, ammonium nitrate, potassium nitrate, L-glutamic acid) were sterilized separately by filtration using millipore filters with a pore size of 0.22 µm and added to final concentrations of 100 mM for carbohydrates (or 20 mM for all other carbon sources) and 50 mM for the nitrogen sources just prior to inoculation. For each test medium, the bacterial cells from 1 ml of a fresh grown culture of JG-TB8 (NB medium,

aerobic conditions) were harvested by centrifugation and washed twice with 0.9% NaCl to remove residual substrates of the NB medium. Subsequently they were transferred into Erlenmeyer flasks containing 30 ml each of the test media and incubated at 30 °C on a rotary shaker (150 rpm). All experiments were run for seven days in triplicate.

Isolation of total protein and SDS-PAGE

The proteome composition of cells of JG-TB8, which were grown to the mid-exponential growth phase under aerobic and anaerobic conditions, respectively, was analysed by denaturing sodium dodecyl sulphate polyacrylamide gel electrophoresis (SDS-PAGE) according to Laemmli [131] in a Mini-PROTEAN[®] II electrophoresis cell system (Bio-Rad Laboratories, Munich, Germany). Total protein was recovered by a cell disruption at 95 °C for 30 min in SDS sample buffer [131]. After centrifugation of the samples, the supernatants were loaded on the gel. Proteins were separated on a 10% separation gel and stained with Coomassie Brilliant Blue.

Heavy metal tolerance

The tolerance of *Paenibacillus* sp. JG-TB8 to uranium and other heavy metals was studied on low phosphate agar plates [132], containing 14.3 g/l Tris, 80 mM NaCl, 20 mM KCl, 20 mM NH₄Cl, 3.25 mM (NH₄)₂SO₄, 10 mM MgCl₂, 1% peptone, and 0.5% glycerol (pH ~7.2). All components, together with 1.5% Bacto[™] agar, were added to the medium and sterilized by autoclaving for 20 min at 121 °C. Prior to solidification, sterile stock solutions of CaCl₂, thiamine, and ZnSO₄ (excluded from those agar plates used for studying zinc tolerance) were added to achieve final concentrations of 100 µM, 20 mg/L, and 2.7 mg/L, respectively. Finally, the medium was supplemented with filter-sterilized (0.22 µm nitrocellulose filters) metal salt solution. Uranium as well as cadmium, chromium, cobalt, copper, lead, nickel, and zinc were provided as nitrate salts up to final concentrations of 1 µM, 5 µM, 10 µM, 50 µM, 100 µM, 250 µM, 500 µM, 750 µM, 1 mM, 2 mM, 3 mM, 4 mM, 6 mM, 8 mM, and 10 mM. For comparison, the heavy metal tolerance of some other *Bacillaceae* strains, isolated from the mentioned microbial consortium, was studied as well. From each strain, cells were harvested in the logarithmic growth phase, washed twice with 0.9% NaCl and transferred to the different test media. All experiments were run for seven days in triplicate. Agar plates without metal and those containing 10 mM Mg(NO₃)₂, to exclude inhibition by nitrate, served as control for the growth of the strains. The minimal inhibitory concentration (MIC) was defined as the lowest concentration that completely inhibits the growth of the tested strains.

Cell preparation for U(VI) treatments

For the cells incubated under anaerobic conditions, all experimental steps described in the following sections were, except as noted otherwise, performed in a glove box under nitrogen atmosphere. All required solutions were deoxygenated by five cycles of degassing under vacuum and subsequent flushing with nitrogen.

After reaching the end of the logarithmic growth phase, i.e. at an OD_{600} of ~ 0.6 and ~ 0.35 for aerobic and anaerobic growth, respectively, the cells were harvested by centrifugation (10000 g, 15 min) and parallel portions were rinsed twice with 0.1 M $NaClO_4$ at pH 2, 3, 4.5 or 6, respectively. Subsequently, the cells were suspended in the corresponding electrolyte solution; the pH of the cell suspensions was checked and if necessary adjusted to the desired values.

U(VI) bioaccumulation studies were performed at room temperature using a biomass concentration of about $0.5 \text{ mg}_{\text{dry biomass}} \cdot \text{mL}^{-1}$. The microbial cells were incubated in triplicate on a rotary shaker with a $5 \cdot 10^{-4}$ M uranyl nitrate solution diluted in 0.1 M $NaClO_4$ (pH 2, 3 or 4.5). At pH 6 the uranium concentration was reduced to $5 \cdot 10^{-5}$ M in order to prevent the formation of uranyl hydroxide precipitates. The amount of accumulated uranium was normalized to the dry biomass, which was determined by weighting parallel samples after drying for 48 hours at 70 °C. The uranium binding capacity of the cells was determined in dependency on the incubation time and the pH of the solution. For quantification of the uranium removal the bacterial cells were removed from the solution by centrifugation and the unbound U(VI) in the supernatant was measured by inductively-coupled-plasma mass-spectroscopy using an Elan 9000 system (Perkin Elmer, Waltham, MA, USA). Control reactions without cells were treated in the same way to exclude abiotic uranium removal from the solution, due to precipitation and/or chemical sorption at the used test vials.

Time-Resolved Laser-induced Fluorescence Spectroscopy (TRLFS)

For TRLFS measurements, each about 50 mg of the cells were treated with U(VI) for 48 hours at pH 2, 3, 4.5 or 6 under aerobic as well as under anaerobic conditions. After the contact with U(VI) the cells were washed twice with 0.1 M sodium perchlorate solutions with the corresponding pH and under corresponding atmospheric conditions. In order to determine the luminescence properties of the uranium complexes formed by the cells of JG-TB8, small portions of the dried and powdered samples were put into quartz micro cuvettes. Each of the anaerobic samples was transferred immediately before the TRLFS measurement under

nitrogen atmosphere into a quartz micro cuvette, which was subsequently closed airtight. Excitation of the uranium luminescence was performed with a pulsed Nd-YAG laser (GCR 190, Spectra Physics, Santa Clara, CA, USA) coupled with an optical parametric oscillator module (MOPO-730, Spectra Physics, Santa Clara, CA, USA), which allows a tunable signal output. Thereby two pairs of beta-barium borate crystals determine the output wavelength of the system, which was tuned to 410 nm for the excitation of U(VI). The laser intensity was set to 300 μ J, to avoid any damages of the samples. The luminescence signal was measured perpendicularly to the laser beam and transmitted *via* a fiber optic cable to the detection system (HORIBA Jobin Yvon GmbH, Darmstadt, Germany), consisting of a spectrograph (model M270), an intensified charge-coupled-device camera and a data acquisition program. For time-resolved measurements a digital delay generator (DG535, Stanford Research Systems, Sunnyvale, CA, USA) was used. The central wavelength of the spectrograph and the gate time of the ICCD camera were set to 520 nm and 50 μ s, respectively. TRLF spectra were recorded between 444 and 594 nm with a resolution of 0.3 nm. The number of laser pulses for excitation (30 to 70) was adjusted depending on the amount of uranium in the samples. Before each series of measurements the background signal was measured 2 ms after the laser pulse and automatically subtracted from the spectra.

The spectrograph was calibrated using a mercury lamp with known emission lines. Deviations of the measured main emission peak from the set-point value of 507.3 nm were used for correction of the determined emission maxima. Subsequently, 101 U(VI) luminescence spectra (each calculated by averaging three single measurements) were recorded after defined delay times. For an accurate determination of the uranium luminescence lifetime(s) two series of measurements were performed for each sample. One of them was performed with a step size of the delay time of 200 ns to determine uranium species exhibiting short luminescence lifetimes. For the calculation of longer lifetimes yet a second series was recorded. The step size for this second series was set to one percent of that delay time, at which the complete U(VI) luminescence had faded away. The luminescence emission spectra were deconvoluted with the PeakFit module 4.0 of the software package Origin 7.5 (OriginLab Corporation, Northampton, MA, USA). Gaussian functions were used to describe the individual peaks and the parameters which were varied during the fitting procedure were peak wavelength, peak height and full width at half maximum. The luminescence lifetimes of the uranium complexes were calculated with exponential decay functions included in the software package.

X-ray Absorption Spectroscopy (XAS)

Portions of the dried and powdered TRLFS samples were used for XAS measurements. The samples incubated under aerobic conditions were mounted on Kapton tape as described earlier [133]. In the case of the samples incubated under anaerobic conditions, the powdered biomass was transferred into specifically designed, heat sealed, polyethylene sample holders and subsequently stored under anaerobic conditions.

The XAS measurements were performed at the ROssendorf BeamLine (ROBL) at the European Synchrotron Radiation Facility (ESRF), Grenoble, France [134]. Samples were measured at room temperature in fluorescence mode using a Si(111) double-crystal monochromator and a 13-element germanium fluorescence detector. The energy was calibrated by measuring the yttrium *K*-edge transmission spectrum of a Y foil and defining the first inflection point as 17038 eV. Depending on the amount of uranium in the cell samples, three to six U *L*_{III}-edge fluorescence spectra were recorded and averaged. Subsequently dead-time correction was applied. The region from about 45 eV below to 60 eV above the absorption edge of each scan was isolated for the X-ray Absorption Near Edge Structure (XANES) analysis. The pre-edge background was subtracted, and the absorption coefficient was normalized to equal intensity at 17230 eV so that all spectra could be plotted on the same scale.

The EXAFS oscillations were isolated from the raw, averaged data by removal of the pre-edge background, approximated by a first-order polynomial, followed by μ_0 -removal *via* spline fitting techniques and normalization using a Victoreen function. The ionization energy for the U *L*_{III}-electron, E_0 , was arbitrarily defined as 17185 eV for all averaged spectra. The EXAFS spectra were analysed according to standard procedures using the program EXAFSPAK [135]. The theoretical scattering phase and amplitude functions were calculated from structural models (Fig. 1.9) *via* the software FEFF8.2 [136]. All fits included the four-legged multiple scattering (MS) path of the uranyl group, U-O_{ax}-U-O_{ax}. The coordination number (N) of this MS path was linked to the N of the single-scattering (SS) path U-O_{ax}. The radial distance (R) and Debye-Waller factor (σ^2) of the MS path were linked at twice the R and σ^2 of the SS path U-O_{ax}, respectively [137]. During the fitting procedure, N of the U-O_{ax} SS path was held constant at two. The amplitude reduction factor was held constant at 1.0 for FEFF8.2 calculations and EXAFS fits. The shift in threshold energy, ΔE_0 , was varied as a global parameter in the fits.

Transmission electron microscopy

The cellular localization of the uranium complexes formed by *Paenibacillus* sp. JG-TB8 was performed by using Transmission Electron Microscopy (TEM) combined with Energy Dispersive X-ray spectroscopy (EDX) for elemental analyses. The TEM samples were prepared in the following way: About 5 mg of the bacterial cells were treated with 10 ml of the uranyl nitrate solutions (pH 2, 3, 4.5 or 6) for 48 hours. After that the cells were rinsed twice with 0.1 M NaClO₄, with the corresponding pH. A third washing step was performed with 0.1 M sodium cacodylate buffer (pH 7.2) followed by a prefixation with 2.5% glutardialdehyde in the same buffer. After that the samples were washed three times with 0.1 M cacodylate buffer and postfixed for 60 min at 4 °C in the dark using 1% osmium tetroxide in distilled water. The samples were dehydrated with ethanol and subsequently infiltrated in a resin (EMbed 812; Electron Microscopy Sciences, Hatfield, PA, USA). After polymerization of the resin at 60 °C, ultrathin sections (50-70 nm) of each sample were cut using a diamond knife on an Ultracut-R microtome (Leica Microsystems, Wetzlar, Germany). The ultrathin sections were mounted on copper grids and contrasted with lead citrate according to the method described by Reynolds [138]. Finally, the samples were coated with carbon. TEM observations were made using a “High Resolution Philips CM 200” transmission electron microscope at the “Centro de Instrumentación Científica” of the University of Granada (Spain) at an acceleration voltage of 200 kV. EDX analyses were performed at the same voltage using a spot size of 70 Å and a live counting time of 200 s.

Live/Dead staining

After the uranium treatments at the different experimental conditions for 48 hours, the cell suspensions were centrifuged at 4 °C and 10000 g for 10 min. After that, the cells were washed twice with 0.9% NaCl and subsequently suspended in 330 µl of the same solution. 1 µl of the staining solution, containing a mixture of two fluorescence dyes (SYTO[®] 9 and propidium iodide) (Live/Dead[®] BacLight[™] Bacterial Viability Kit L-7012, Molecular Probes, Inc., Eugene, OR, USA) was added to the samples. After incubation in the dark and on ice for 15 minutes, the samples were centrifuged once again and the supernatant containing the unbound stains was removed. Cells were suspended in 25 µl 0.9% NaCl and examined with an Olympus light microscope (Olympus Europa Holding GmbH, Hamburg, Germany) - BX-61, combined with BX-UCB (control box) and U-RFL-T (power supply for the 100 W mercury lamp) - along with the accompanying imaging software “cell^P”. Fluorescence was excited by light with wavelengths between 420 and 460 nm, using a

super-wide band filter mirror unit (U-MSWB, Olympus Europa Holding GmbH, Hamburg, Germany).

Enzymatic assay

The phosphatase activity was determined by the “Acid Phosphatase Assay Kit” from Sigma-Aldrich (Saint Louis, MO, USA). The assay is based on the enzymatic hydrolysis of *p*-nitrophenyl phosphate to *p*-nitrophenol, a chromogenic product with an absorbance maximum at 405 nm. One unit of phosphatase was defined as the amount of the enzyme that hydrolyzes 1 μmol of *p*-nitrophenyl phosphate per minute. Differently than given in the manufacturer’s instructions, *p*-nitrophenyl phosphate was dissolved in 0.1 M NaClO_4 with pH 2, 3, 4.5 or 6, respectively, according to the conditions used for the U(VI) accumulation studies. For each pH value three samples, each containing 2 mg of freshly grown cells of JG-TB8 were washed four times with 0.1 M NaClO_4 (pH 2, 3, 4.5 or 6). At each washing step, pH was controlled and if necessary readjusted to the required value. After that, the cells were suspended in 100 μl 0.1 M NaClO_4 with the corresponding pH. The cells of three more samples were killed by heating at 121 $^{\circ}\text{C}$ for 20 min and afterwards studied analogically at pH 6. 50 μl from each of the cell suspensions was transferred to 50 μl *p*-nitrophenyl phosphate solution with the same pH. Control reactions without cells were prepared to quantify the spontaneous hydrolysis of *p*-nitrophenyl phosphate. After incubation for 30 min at room temperature, the reaction was stopped by the addition of 200 μl 0.5 M NaOH. Subsequently, the cells were spun down and the supernatants of the samples were used to quantify the produced *p*-nitrophenol at 405 nm. Phosphatase activity in the different samples was calculated according to the protocol of the manufacturer.

Colorimetric determination of phosphate

Phosphate was quantified by colorimetric measurements using malachite green. This dye complexes inorganic phosphate groups in the presence of molybdate and forms a complex which can be determined at a wavelength of 660 nm [139]. The phosphate reagent containing ammonium molybdate and malachite green was prepared as described by Ekman and Jäger [140]. Eleven potassium dihydrogen phosphate solutions with concentrations ranging from 0 to 20 μM were prepared and served as a standard. For the test samples each about 5 mg of freshly grown cells were suspended in triplicate in 10 ml uranyl nitrate solutions. In addition, parallel samples without uranium were prepared. Samples were shaken for 48 hours at room

temperature. After that, the samples were centrifuged and the amount of inorganic phosphate in the supernatant was determined. For this purpose 100 μ l of the phosphate reagent was added to 100 μ l of the cell supernatants as well as to the standard solutions. Samples were incubated for 20 min at room temperature and subsequently the absorption of the complex was measured at 660 nm and quantified *via* the determined standard curve. As a control phosphate concentrations of the initial solutions were checked and corresponding values were subtracted from the concentrations determined in the supernatants of the cell samples.

RESULTS AND DISCUSSION

Phylogenetic affiliation of the cultivated *Bacillus* isolates

Isolation approaches from the described microbial consortium were limited to aerobic cultivation methods, to prevent from the growth of possibly pathogenic *Clostridia*. From the inoculated with the microbial consortium, and incubated under aerobic conditions, agar plates, 24 single colonies were obtained. The isolates were transferred to fresh medium and phylogenetic affiliated by 16S rRNA gene analyses. All retrieved sequences could be related to the order of *Bacillales* (Fig. 1.1 and Table A in Supplemental material). Within this order, eight isolates were classified into the genus *Bacillus*, closely related to strains commonly detected in various environmental samples. Individual members of this genus are known to have an anaerobic metabolism, but the majority of them exhibit a strict aerobic way of life. Therefore the latter strains might have been inactive in the anaerobic microbial consortium and their growth on agar plates during the isolation procedure under aerobic conditions is based on the germination of resistant endospores. All other 16 isolates were related to different strains of the genus *Paenibacillus*. The 16S rRNA gene of the studied in this work strain JG-TB8 shares 99.5% sequence identity with that of the bacterial isolate *Paenibacillus* sp. 436-1, recovered from a soil sample from Wisconsin (USA). In addition, JG-TB8 is closely related to *Paenibacillus borealis*, strain DSM 13188^T (=KK19^T), a nitrogen-fixing strain isolated from an acid humus, collected in Finland [114]. Besides JG-TB8, twelve more isolates could be assigned to this *Paenibacillus* cluster. Only three isolates (JG-TB3, JG-TB4, JG-TB16) were assigned to another cluster of this genus, related to *Paenibacillus amylolyticus* NRRL:NRS-290^T [141]. The closest phylogenetic relative, *Paenibacillus* sp. IDA5358, sharing 99.1%, 98.9% and 98.8% sequence identity with JG-TB3, JG-TB4 and JG-TB16, respectively, had also been recovered from an environmental soil sample [142].

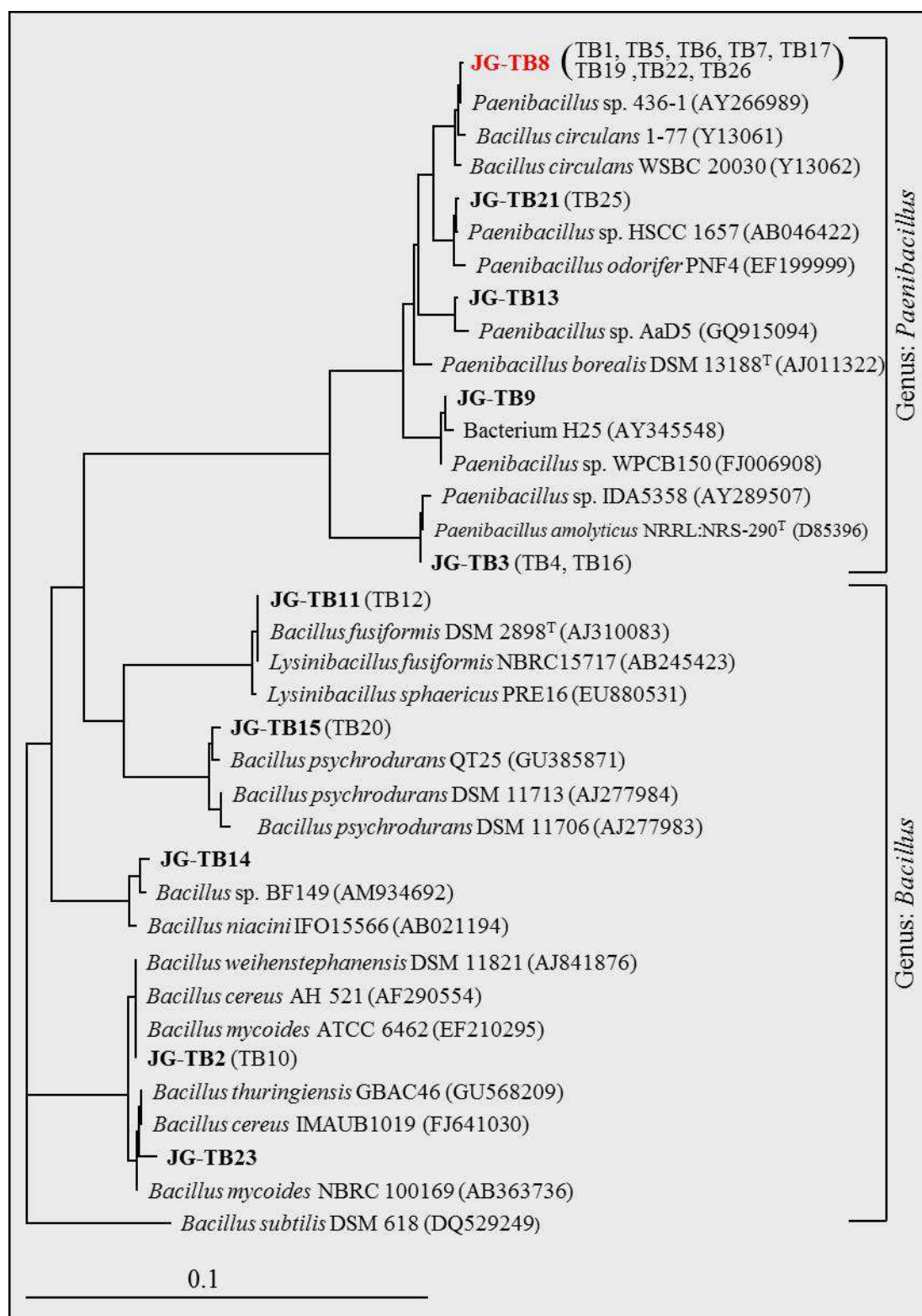


Figure 1.1. Phylogenetic dendrogram of 16S rRNA gene sequences retrieved from *Bacillus* and *Paenibacillus* isolates recovered from an anaerobic microbial consortium [77]. All isolates were classified within the order of *Bacillales*. For the sake of clarity, closely related isolates were represented by only one sequence in the phylogenetic tree, given related isolates in parentheses. The dendrogram was constructed using neighbour-joining method, based on sequence comparison of the region corresponding to the *E. coli* 16S rRNA gene positions 101 to 1477 [123] and rooted with the 16S rRNA gene sequence of *Bacillus subtilis* (defined as outgroup). The scale bar represents a 10% difference in nucleotide sequences.

Morphological and physiological characterization of *Paenibacillus* sp. JG-TB8

Growth of *Paenibacillus* sp. JG-TB8 on NB agar plates was observed after an incubation of two days at 30 °C. Single colonies were circular, usually 2 to 3 mm in diameter and had a flat to low convex appearance (Fig. 1.2). Looking at small, still-growing colonies with a 100-fold magnification, slightly irregular edges were observed at the margins of the colonies (Fig. 1.3-A). At later stages of growth, these edges disappear and the colony has an entire circular shape (Fig. 1.3-B). The colonies have a smooth and glossy surface and are initially opaque and white coloured. After longer incubations, the colour changes and they occurred beige and translucent, which is related to endospore formation and subsequent cell lysis. This was confirmed by light microscopy at a 100-fold magnification, clearly showing refracting endospores (Fig. 1.3-C).

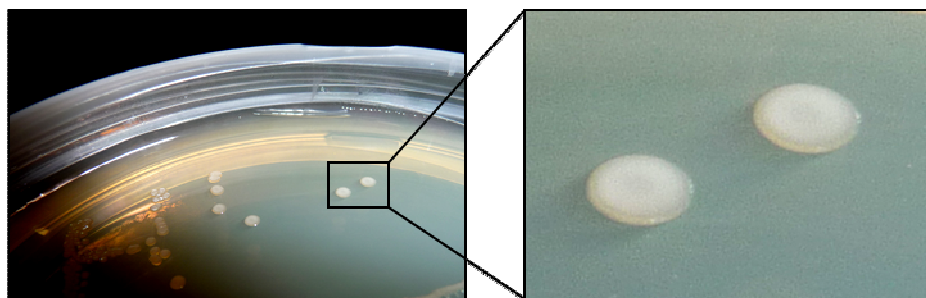


Figure 1.2. Morphology of single colonies of *Paenibacillus* sp. JG-TB8 grown for two days on nutrient broth agar plates at 30 °C.

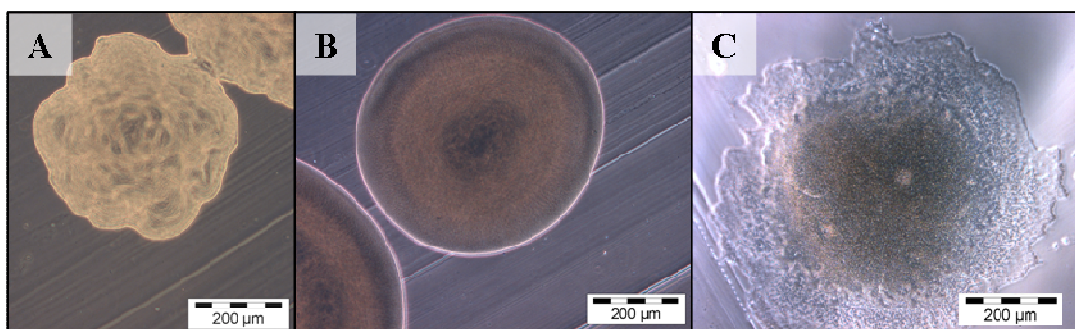


Figure 1.3. Light microscopic pictures of single colonies of *Paenibacillus* sp. JG-TB8 taken at 100-fold magnification after an incubation for 7 hours (A), 24 hours (B) and 3 days (C) at 30 °C on nutrient broth agar plates

The cells of JG-TB8 are motile and rod-shaped exhibiting a length of 3 to 6 μm and a width of 0.7 to 1 μm . (Fig. 1.4-A1). In later stages of cultivation, in particular when growing on agar plates, the production of endospores was observed (Fig. 1.4-A2, B2). The spores exhibit an ellipsoidal to rectangular form with a size of about 1 x 2 μm , and are located terminal in swelled sporangia, producing the typical club-shaped form of paenibacilli. (Fig. 1.4-A2, B2).

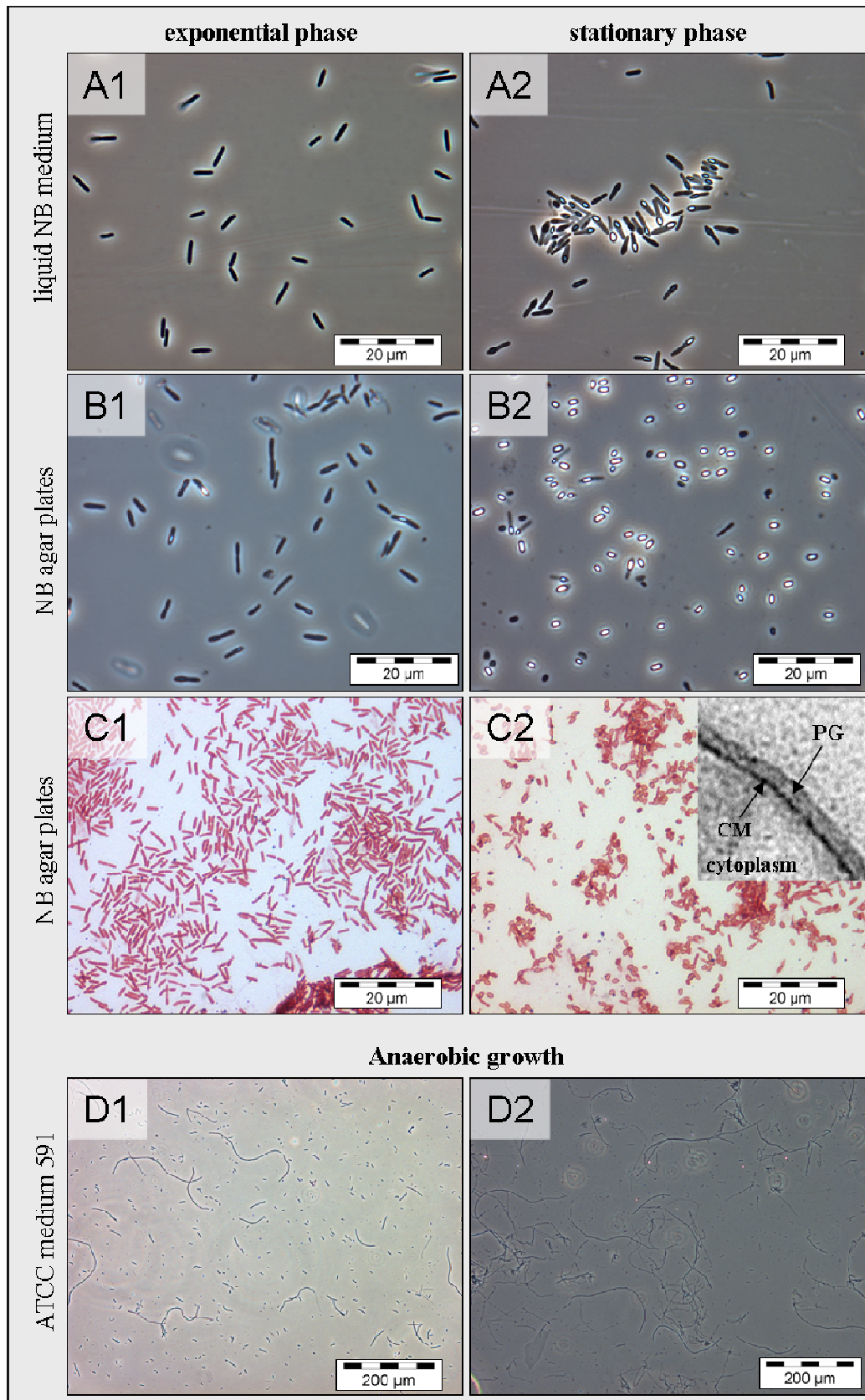


Figure 1.4: Light microscopic pictures of *Paenibacillus* sp. JG-TB8 grown for 12 hours in liquid NB medium (A1), on NB agar plates (B1) and under anaerobic conditions in ATCC medium 591 (D1) and 48 h (A2, B2, D2). In addition, the pictures show Gram-stained samples of fresh grown (C1) and old cells (C2) of this strain and a TEM picture of the Gram-positive cell envelope structure of JG-TB8, consisting of cytoplasmic membrane (CM) and peptidoglycan (PG).

The isolate JG-TB8 was also able to grow in the absence of oxygen and therewith identified as a facultative anaerobic strain. However, anaerobic growth of JG-TB8 was not observed on agar plates. In addition, no formation of endospores was observed under anaerobic conditions even after long incubation times. In addition, many cells of JG-TB8 grown at anaerobic conditions were significantly longer (some cells even had a length of more than 200 μm) and exhibit a filamentous phenotype (Fig. 1.4-D1, D2). Similar observations were already made for *ftsH* null mutants of *Bacillus subtilis* [143]. Interestingly, further studies on the anaerobic growth of *B. subtilis* indicated that the same protein, *ftsH*, is essentially required for the fermentation process [144]. The observed morphological differences in the case of JG-TB8 might be based on the expression of a corresponding protein.

Besides the morphology, also significant changes in the protein synthesis were observed comparing the cells grown under anaerobic conditions with those grown under aerobic conditions (Fig. 1.5). This finding can be explained by the adaption of the cell metabolism to the respective aeration conditions, as it was demonstrated for some enzymes of *Bacillus subtilis*, for example [145, 146]. The individual protein bands (Fig. 1.5) were not further investigated in this work.

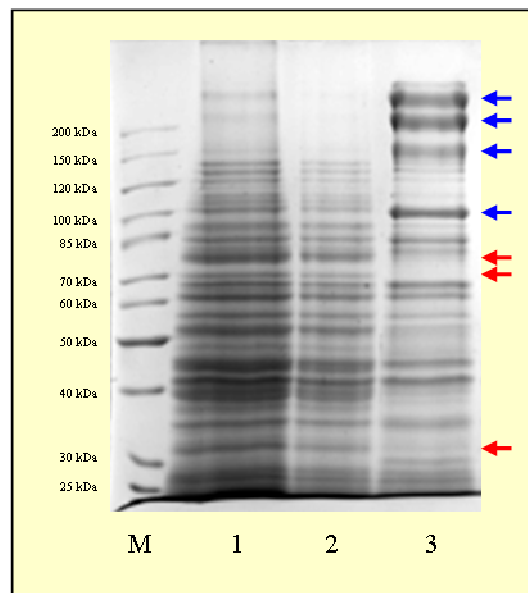


Figure 1.5. SDS-PAGE protein gel stained with Coomassie Brilliant, showing the proteome of JG-TB8 grown under anaerobic conditions (lanes 1 and 2) and under aerobic conditions (lane 3). For the estimation of molecular protein weights, a protein marker (M) was used (Pageruler™ SM0661 (Fermentas GmbH, Sankt Leon-Rot, Germany)). Arrows indicate bands, which represent proteins that were obviously significantly more (blue) or less (red) expressed under aerobic conditions.

The cells of JG-TB8 stained Gram-negative at all stages of cultivation (Fig. 1.4-C1, C2), although no apparent outer membrane structure was observed in the cell wall structure by TEM analysis (Fig. 1.4-C2), which was more like that of Gram-positive bacteria, an observation which was already made for other members of the genus *Paenibacillus* [115].

Growth in liquid NB medium was observed up to a temperature of 40 °C and in the pH range from 5.2 to 8.8, with optima around 30 °C and pH 7.5, respectively.

Carbon sources utilized by the JG-TB8 were glucose, fructose, maltose, galactose, sucrose and glycerol, which is in accordance with utilization pattern of the close phylogenetic relative *Paenibacillus borealis* DSM 13188^T, as well as with those of several other *Paenibacillus* [114] and *Bacillus* species [147]. No growth was observed in the presence of sodium pyruvate, potassium acetate, methanol, sorbitol, citric acid, or lactic acid as carbon source. From the tested nitrogen sources, potassium nitrate, ammonium nitrate, ammonium sulphate and urea were utilized by the strain whereas the addition of glutamic acid (which could be both, carbon and nitrogen source) failed to enable growth of JG-TB8.

Heavy metal tolerance

The mineral medium used for heavy metal tolerance tests contains only very low amounts of phosphate in order to prevent inorganic metal complexation by phosphate ions.

Growth of strain JG-TB8 was observed up to a uranium concentration of 0.5 mM. The MIC of uranium was determined with 0.75 mM. Other heavy metals (cadmium, cobalt, lead, zinc) inhibited the growth even at lower concentrations (Table 1.1), whereas copper, chromium and nickel were tolerated by the strain in higher amounts.

Table 1.1. Minimal inhibitory concentration (in mM) of different heavy metals for the growth of selected bacterial isolates. For each heavy metal, the lowest (red) and highest (green) value of the determined MICs is highlighted.

	UO ₂ ²⁺	Cd ²⁺	Co ²⁺	Cr ³⁺	Cu ²⁺	Ni ²⁺	Pb ²⁺	Zn ²⁺
Genus <i>Paenibacillus</i>								
JG-TB8	0.75	0.05	0.25	4.0	1.0	2.0	0.5	0.25
JG-TB3	1.0	0.1	0.1	4.0	3.0	1.0	0.5	0.25
JG-TB9	0.25	0.05	0.25	2.0	0.75	0.05	0.25	0.1
JG-TB13	0.5	0.05	0.5	3.0	0.25	0.1	0.25	0.1
JG-TB21	0.25	0.05	0.1	1.0	0.75	0.05	0.1	0.1
Genus <i>Bacillus</i>								
JG-TB2	6.0	0.75	2.0	6.0	3.0	3.0	0.75	2.0
JG-TB11	2.0	0.05	0.5	6.0	3.0	2.0	0.5	0.5
JG-TB14	3.0	0.001	0.25	6.0	3.0	1.0	0.25	0.1
JG-TB15	0.5	0.5	0.25	2.0	4.0	3.0	0.5	0.25
JG-TB23	2.0	0.5	0.25	2.0	4.0	3.0	0.5	0.25

A comparison of the determined MICs with those of some other bacterial isolates indicates that, the isolates classified into the genus *Paenibacillus*, in general, exhibit a lower tolerance to the tested heavy metals than the *Bacillus* isolates (Table 1.1). We did not further investigations on this observation. However, a possible explanation for this might be the different cell envelope structures. *Bacilli* are usually covered with a thick layer of peptidoglycan, whereas that of *Paenibacillus* species is often thinner, causing the variable Gram behaviour of the latter. Hence, the lower thickness of the cell wall might reduce uranium tolerance. Moreover, another explanation for the results can be assumed, which is based on the presence of a proteinaceous surface layer (S-layer). S-layers cover numerous *Bacillus* strains [91] and can effectively bind metals and therewith protect the cells from metal toxicity. Surface layers were, for example, described for different strains of *B. thuringiensis* [148, 149]. The isolate JG-TB2, which tolerates, among the tested strains, the highest concentrations of all heavy metals (beside copper) is closely related *B. thuringiensis* species (Fig. 1.1 and Table A in Supplemental material). Another strain *B. sphaericus* JG-A12, which was also investigated in our laboratory, possesses a metal accumulating surface layer which could be removed from the cell after its saturation with heavy metals [150]. In the case of JG-TB8 we could not identify a corresponding layer on the cell surface. Therefore it is also possible, that the presence or absence of such a S-layer have an influence on heavy metal tolerance.

Bioaccumulation of U(VI) by JG-TB8

In order to investigate the influence of the *Paenibacillus* isolate JG-TB8 on the migration behaviour of uranium in nature, U(VI) bioaccumulation studies were performed. Thereby we focussed on the bioaccumulation at highly acidic pH conditions (pH 2 and pH 3), where U(VI) is present almost exclusively in form of the highly toxic, because motile and bioavailable, uranyl ion. In addition, the U(VI) bioaccumulation at moderate acidic conditions (pH 4.5 and 6) was studied, which are typical for many uranium-contaminated sites [151].

In a first approach we investigated the U(VI) bioaccumulation kinetics at a pH of 4.5 under aerobic conditions. As evident from Figure 1.6 (top), U(VI) was removed very fast from the aqueous uranium solution and bound to the cells of JG-TB8. Saturation of the binding sites was already reached after an incubation of about 30 minutes. This rapid complexation of uranium is a typical feature of the so called biosorption process [19], which describes a metabolism-independent sorption of radionuclides and other heavy metals to biomass. The

process is based on the complexation of metals by organic ligands exhibiting negatively charged functional groups, including phosphate, carboxylic, or hydroxylic residues [152].

The U(VI) binding capacity of the cells at the studied experimental conditions was determined to be (65 ± 4) mg/g_{dry biomass}. The results demonstrate, that in accordance with former kinetic studies, an incubation time of one or two hours is suitable for determining the amount of uranium bound to the cells *via* biosorption processes.

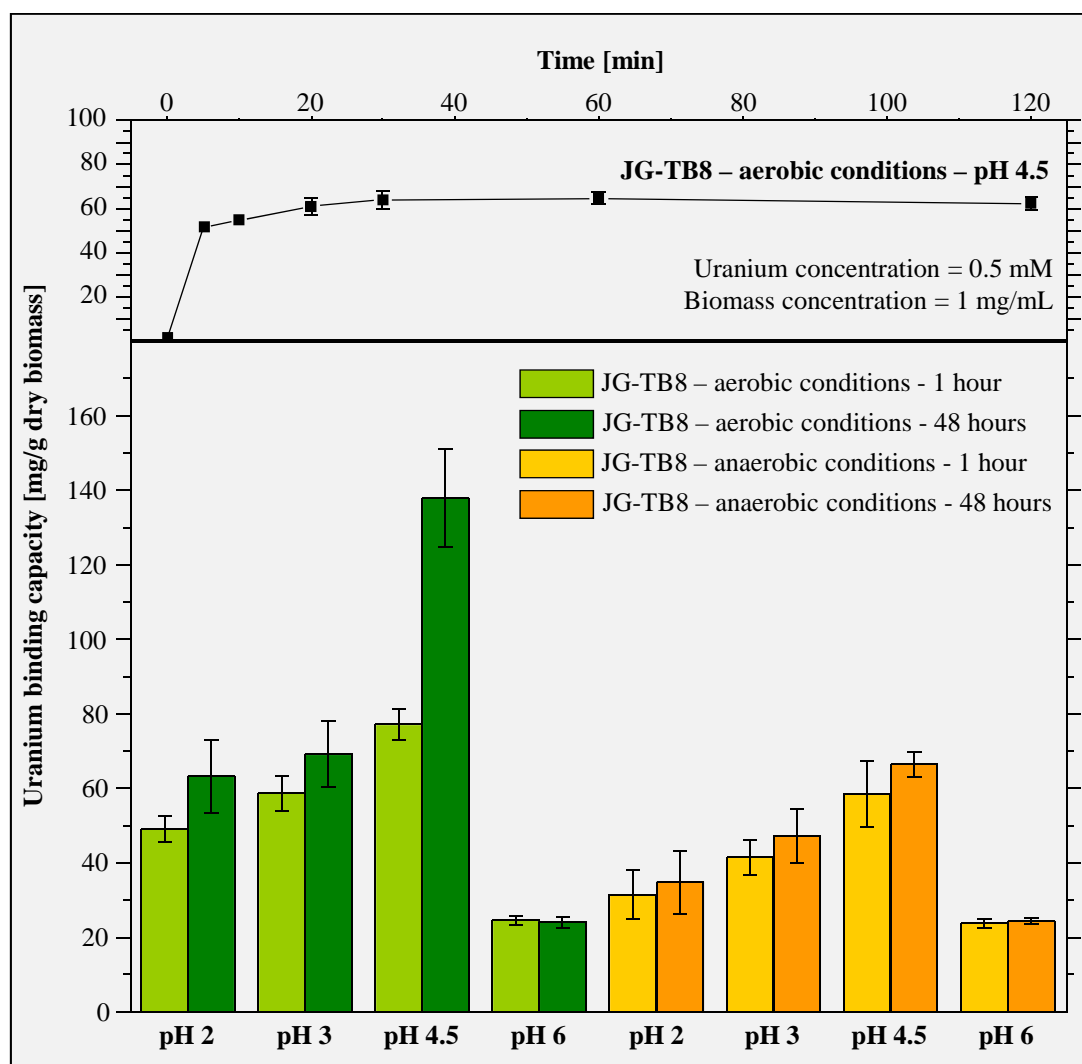


Figure 1.6. Sorption kinetics of U(VI) on the cells of JG-TB8 at pH 4.5 (top) [153] and uranium binding capacity calculated for the cells depending on different incubation times, the presence of oxygen, and the pH value (bottom). In contrast to the sorption kinetics (top), the biomass concentration used for determination of the binding capacity was in each case (0.5 ± 0.05) mg/mL.

Therefore we calculated the binding capacity for the cells after an incubation for one hour under aerobic or anaerobic conditions at pH values of 2, 3, 4.5 and 6. (Table 1.2 and Fig. 1.6, bottom). Noteworthy, the biomass concentration in this and all further experiments was 0.5 mg/mL, instead of 1 mg/mL used in the initial kinetic study. This change increases the

amount of uranium bound by the cells, by reducing cell agglomerations as demonstrated before for other microbial strains [133, 154].

Table 1.2. U(VI) binding capacity calculated for the cells of JG-TB8 in dependency of pH conditions, presence of oxygen and incubation time.

Experimental conditions	U(VI) binding capacity [mg/g _{dry biomass}]	
	1 hour	48 hours
JG-TB8 – pH 2.0 – aerobic conditions	49.1 ± 3.6	63.2 ± 9.8
JG-TB8 – pH 3.0 – aerobic conditions	58.7 ± 4.7	69.1 ± 8.8
JG-TB8 – pH 4.5 – aerobic conditions	77.1 ± 4.2	138 ± 13
JG-TB8 – pH 6.0 – aerobic conditions	24.6 ± 1.3	24.0 ± 1.4
JG-TB8 – pH 2.0 – anaerobic conditions	31.5 ± 6.6	34.8 ± 8.5
JG-TB8 – pH 3.0 – anaerobic conditions	41.5 ± 4.7	47.3 ± 7.3
JG-TB8 – pH 4.5 – anaerobic conditions	58.6 ± 9.0	66.4 ± 3.4
JG-TB8 – pH 6.0 – anaerobic conditions	23.8 ± 1.1	24.4 ± 0.8

The results, presented in Figure 1.6 (bottom) and Table 1.2, demonstrate that the binding capacity, under aerobic as well as under anaerobic conditions, is pH dependent and increases with increasing pH values (up to pH 4.5). The binding capacity at pH 6 is not suitable for comparison or interpretation, as it was limited to about 24 mg/g_{dry biomass}, due to the lower U(VI) concentration used, in order to avoid the formation and precipitation of poorly soluble uranyl hydroxide species. Nevertheless, the increasing binding capacity at higher pH values can be explained by a uranium complexation at additional deprotonated and therefore binding-capable functional groups at the cell surface. In particular carboxylic groups might be involved in the uranium complexation at increased pH values, as it was demonstrated by Fowle and co-workers, who studied the U(VI) adsorption onto cells of *Bacillus subtilis* [155]. The calculated binding capacities are well in line with those determined in studies using comparable experimental conditions. For instance it was shown, that *Chryseomonas* sp. accumulates about 60 mg uranium per g of dry biomass at pH 4 [156]. Studies on *Bacillus sphaericus* ATCC 14577 and *Pseudomonas fluorescence* ATCC 55241 revealed uranium binding capacities of 70 mg/g_{dry biomass} (at pH 4.5) and 92 mg/g_{dry biomass} (at pH 5), respectively. The efficient uranium binding by these organisms is attributed to the large number of uranium-binding ligands on their multilayer cell wall structure [157]. For instance, the cells of *Paenibacillus* sp. JG-TB8 possess a complex Gram-positive cell wall structure, which includes a layer of peptidoglycan that is rich on phosphate and carboxylic groups and represents the major metal binding component of this bacterium.

Comparing the binding capacity of the cells grown and incubated under aerobic conditions with those grown and incubated under anaerobic conditions, the uranium binding capacity of the latter is 25 to 35% lower. This is most likely due to the larger cell size observed under anaerobic conditions, as bigger cells provide a smaller cell surface compared to their weight and therefore a significant smaller number of U(VI) complexing ligands.

After an incubation of 48 h the binding capacity of the cells in the samples incubated under aerobic conditions at pH 2 and 3, as well as those incubated under anaerobic conditions, did not increase significantly. However, in contrast to that, the U(VI) complexation increased about to twice in the sample incubated at pH 4.5 under aerobic conditions, which indicates that a second process is implicated which is much slower, like a uranium biomineralization or an uptake inside the cell due to the stress caused by the non-optimal pH conditions which increase the cell wall permeability.

Characterization and molecular structure of the uranium complexes formed under aerobic conditions.

TRLFS studies

In order to investigate the U(VI) binding ligands at the bacterial cell surface, time-resolved laser-induced fluorescence spectroscopy was used. The recorded spectra of the cell samples incubated at the different pH values are presented in Figure 1.7. The corresponding peak maxima, calculated from peak fitting procedures are summarized in Table 1.3.

It is obvious from the data that the samples incubated at pH 2 and pH 3 do not differ from each other. The recorded spectra from both samples are well in line with each other and exhibit main absorption maxima at around 497.5, 519, and 542.5 nm. Comparing these spectroscopic data with those of other U(VI) complexes, the best agreement was found with those complexes formed at phosphate groups of organic molecules, e.g. fructose(6)phosphate [158] and adenosine monophosphate [159]. In addition, very similar TRLFS results were obtained from studies investigating the U(VI) complexation at single bacterial cell wall compounds, e.g. glycerol-1-phosphate [160] as well as *o*-phosphoethanolamine ($\text{NH}_3\text{CH}_2\text{CH}_2\text{OPO}_3^-$) and 1,2-dimyristoyl-sn-glycero-3-phosphate (DMGP) [161] that represent the polar head and the apolar tail of phospholipids. The latter are the major component of all cell membranes. The important role of phosphate groups as ligands for the uranium complexation at highly acidic conditions was already demonstrated for several other bacterial as well as archaeal strains [84, 133, 162].

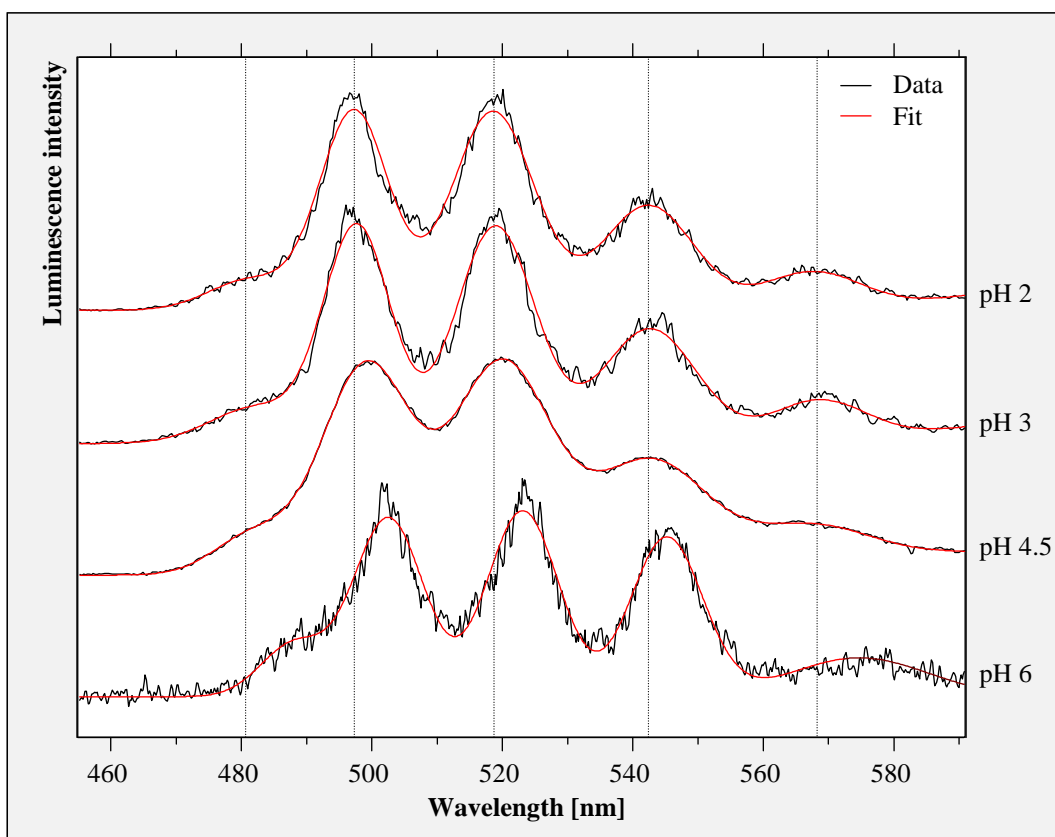


Figure 1.7. U(VI) luminescence spectra recorded from the uranium complexes formed at different pH values after 48 hours by the cells of *Paenibacillus* sp. JG-TB8 under aerobic conditions. For comparison, dotted lines indicate the luminescence emission maxima calculated for the sample incubated at pH 2.

Time-resolved analyses revealed in both samples a bi-exponential luminescence decay (Table 1.4). The calculated luminescence lifetimes were $(2.71 \pm 0.58) \mu\text{s}$ and $(26.7 \pm 4.4) \mu\text{s}$ from the sample incubated at pH 2.

For the sample incubated at pH 3 highly similar luminescence lifetimes of $(2.59 \pm 0.25) \mu\text{s}$ and $(26.3 \pm 3.8) \mu\text{s}$ were calculated. Due to the presence of two uranyl species in both samples we performed peak fits of luminescence spectra recorded after different delay times. However, we did not observe any significant changes of the absorption bands. Therefore it is obvious that the samples incubated at pH 2 and pH 3 do not differ from each other and that in both samples the same two uranyl phosphate complexes were formed by/at the cells of the investigated *Paenibacillus* strain.

The luminescence spectrum of the U(VI) complexes formed at pH 4.5 exhibit differences compared to those of the before discussed samples (Fig. 1.7). The absorption peaks of the spectrum are less separated and as a consequence of this slightly shifted absorption maxima were calculated (Table 1.3).

Table 1.3. U(VI) luminescence emission maxima of the uranium complexes formed by *Paenibacillus* sp. JG-TB8. For comparison the U(VI) luminescence emission maxima of some model compounds, as well as those of the complexes formed by other microbial strains are presented for comparison.

Sample	Luminescence emission maxima ^a					Lifetime(s) (μs)	
UO ₂ ²⁺ (pH 2)	473.0	489.4	510.8	534.3	559.7	1.98 ± 0.11	
Aerobic conditions							
U(VI) + JG-TB8 - pH 2.0	480.8	497.2	518.7	542.3	568.0	Table 1.4	
U(VI) + JG-TB8 - pH 3.0	481.1	497.7	519.0	542.5	569.0	Table 1.4	
U(VI) + JG-TB8 - pH 4.5	481.7	499.1	519.9	542.6	567.8	Table 1.4	
U(VI) + JG-TB8 - pH 6.0	488.1	502.5	523.1	545.2	574.0	Table 1.4	
Anaerobic conditions							
U(VI) + JG-TB8 - pH 2.0	482.3	497.2	518.8	542.6	568.6	Table 1.6	
U(VI) + JG-TB8 - pH 3.0	481.3	497.3	518.6	541.6	568.3	Table 1.6	
U(VI) + JG-TB8 - pH 4.5	467.5	480.9	497.1	518.1	541.1	565.3	Table 1.6
U(VI) + JG-TB8 - pH 6.0	468.2	481.0	497.2	518.3	541.2	564.9	Table 1.6
Uranyl phosphoryl complexes							
UO ₂ -fructose(6)phosphate [158]	478.9	497.1	519.0	543.3	568.9	0.13 ± 0.05	
UO ₂ -AMP [159]		497	519	542	569	n.d.	
UO ₂ -glycerol-1-phosphate [160]		497.2	519.0	543.3	568.9	0.15 ± 0.03	
UO ₂ -DMGP [161]	481.5	497.4	519.3	542.4	567.5	1.0; 20	
UO ₂ -[NH ₃ CH ₂ CH ₂ OPO ₃] ⁺ [161]	483	498.0	518.4	541.3	565.9	3.1 ± 0.6	
Lipopolysaccharide complexes							
R-O-PO ₃ -UO ₂ [163]	481.5	498.1	519.6	542.9	567.5	1.2 ± 0.4	
Microbial cells							
<i>Bacillus sphaericus</i> [154]		498	519	542	569	n.d.	
<i>B. sphaericus</i> (decomposed) [154]		502	524	548	574	n.d.	
<i>S. acidocaldarius</i> , pH 1.5 [133]	483.6	498.3	520.3	543.6	569.3	0.36, 2.8, 36	
<i>S. acidocaldarius</i> , pH 6 [164]	488.0	502.6	523.1	545.4	574.2	3.97 ± 0.76	
Uranyl phosphate minerals							
Saleeite [165]	489.0	501.1	522.1	545.7	570.9	2.3 ± 0.2	
meta-autunite [165]	491.3	501.8	522.9	546.9	572.2	0.74 ± 0.1	
Uranyl carboxylate complexes							
Uranyl acetate [166]	462.9	494.6	514.3	535.9			
(R-COO) ₂ -UO ₂ [167]	466.0	481.6	498.1	518.0	539.0	566.0	0.7; 7.3

^a Main luminescence emission bands were pointed out by bold letters

In addition, time-resolved analysis of this sample demonstrates a third, significant longer luminescence lifetime of about 120 μs . However this third species was obviously not responsible for the changes in the shape of the spectrum since the peak maxima of this long-living species, which could be isolated from the two other species very easily by analyzing the data after a delay time of 150 μs , correspond very well to those of the first two species.

Table 1.4. Calculated luminescence lifetimes of the U(VI) complexes formed by the cells of *Paenibacillus* sp. JG-TB8 under aerobic conditions.

	pH 2	pH 3	pH 4.5	pH 6
Lifetime 1 (τ_1)	$2.71 \pm 0.58 \mu\text{s}$	$2.59 \pm 0.25 \mu\text{s}$	$2.58 \pm 0.50 \mu\text{s}$	
Lifetime 2 (τ_2)	$26.7 \pm 4.4 \mu\text{s}$	$26.3 \pm 3.8 \mu\text{s}$	$29.6 \pm 3.0 \mu\text{s}$	
Lifetime 3 (τ_3)			$120 \pm 5 \mu\text{s}$	
Lifetime 4 (τ_4)				$3.05 \pm 0.24 \mu\text{s}$

The U(VI) luminescence spectrum recorded from the sample incubated at pH 6 was significantly shifted to higher wavelengths (Fig. 1.7). The main absorption maxima were shifted to 502.5, 523.1, and 545.2 nm. In this sample the luminescence decay could be described using a simple mono-exponential decay function, which indicates the presence of only one luminescent uranyl species with a luminescence lifetime of $(3.05 \pm 0.24) \mu\text{s}$. Similar luminescence properties are known for different natural and synthesized uranyl phosphate minerals (Table 1.3). Moreover, highly similar TRLFS data were obtained from uranyl phosphate mineral phases formed by the acidothermophilic crenarchaeon *Sulfolobus acidocaldarius* [164] as well as decomposed cells of *Bacillus sphaericus* [154] (Table 1.3). The high similarity of the luminescence lifetimes of U(VI) complexes built at organic (τ_1) and inorganic (τ_4) phosphates exclude a separation of these two lifetimes from each other in the sample incubated at pH 4.5. However, the presence of both, organic and inorganic uranyl phosphate species in the sample incubated at pH 4.5 is indicated by the low separated emission peaks.

XAS analyses

In order to obtain information regarding the structure of the formed uranium complexes at molecular scale, XAS measurements were performed. The described XAS sample preparation was based on soft desiccation. The method was developed several years ago by Merroun and

co-workers [162] in order to avoid uncontrolled biological processes, that can influence the fate of uranium, in the cell samples during transportation and possible storage on the way from the laboratory to the X-ray beamline. Such processes could be cell lysis resulting in pH changes, release of enzymes or even development of non-prokaryotic infections (fungal, for instance). One additional advantage of the used sample preparation procedure is that one and the same sample can be analysed many times by using different methods. The latter is of great importance for analyses of complex systems, as the samples investigated in this study. It is important to stress that this preparation method does not change the structural parameters of the formed uranium complexes [133, 162].

In order to check whether a part of the added uranium was reduced to U(IV), the XANES region, located around the absorption edge, of the recorded spectra was analysed. The results clearly demonstrate that the bound uranium still existed in the oxidation state +6 and was not reduced (data not shown).

The isolated U L_{III} -edge k^3 -weighted EXAFS spectra along with the calculated FTs are shown in Figure 1.8. In addition, the spectra of uranyl-fructose(6)phosphate, as representative of organic, and meta-autunite, as representative of inorganic uranyl phosphate complexes were presented for comparison. In agreement with the TRLFS studies, the spectra recorded from the samples incubated at pH 2 and pH 3 look like each other and show a high similarity to that of the model compound uranyl-fructose(6)phosphate. In contrast to that, the spectrum recorded from the sample incubated at pH 6 corresponds very well to that of meta-autunite. The latter exhibits a typical shoulder at $k = 4 \text{ \AA}^{-1}$ (Fig. 1.8) which results from the multiple scattering path of two times two equatorial oxygen atoms, which are located opposite to each other. As suggested by the TRLFS studies, the EXAFS spectrum of the sample incubated at pH 4.5 looks like a mixture of the two discussed complexation types. The structural parameters of the formed U(VI) complexes were obtained by an EXAFS shell fit. The results are presented in Table 1.5 and the corresponding fits are illustrated in Figure 1.8. All fits include a shell of two axial oxygen atoms at a radial distance of 1.77 to 1.79 Å, represented by the most prominent FT peak at around $R + \Delta \sim 1.3 \text{ \AA}$. The in each spectra second peak of the FTs ($R + \Delta \sim 1.8 \text{ \AA}$) is related to the backscattering contribution of the equatorial oxygen atoms. The origin of the peak/shoulder at around $R + \Delta \sim 2.3 \text{ \AA}$ is still not understood. This peak could be fitted with carbon atoms in a bidentate binding mode. However, this peak was also detected in carbon free systems as it is discussed in Chapter III. The MS path of the axial oxygen atoms, as well as the SS and MS of the phosphate atoms are visible in the FTs in the

region between $R + \Delta = 2.8$ and 3.4 Å. The structural parameters obtained by shell fitting procedures of the spectra recorded from the samples incubated at highly acidic conditions (pH 2 and 3) demonstrate an equatorial oxygen shell at a radial distance of 2.35 Å which is typical for a fivefold coordinated uranyl ion. The radial distance of the phosphorous shell at 3.62 Å indicates a monodentate binding of uranyl to phosphate groups.

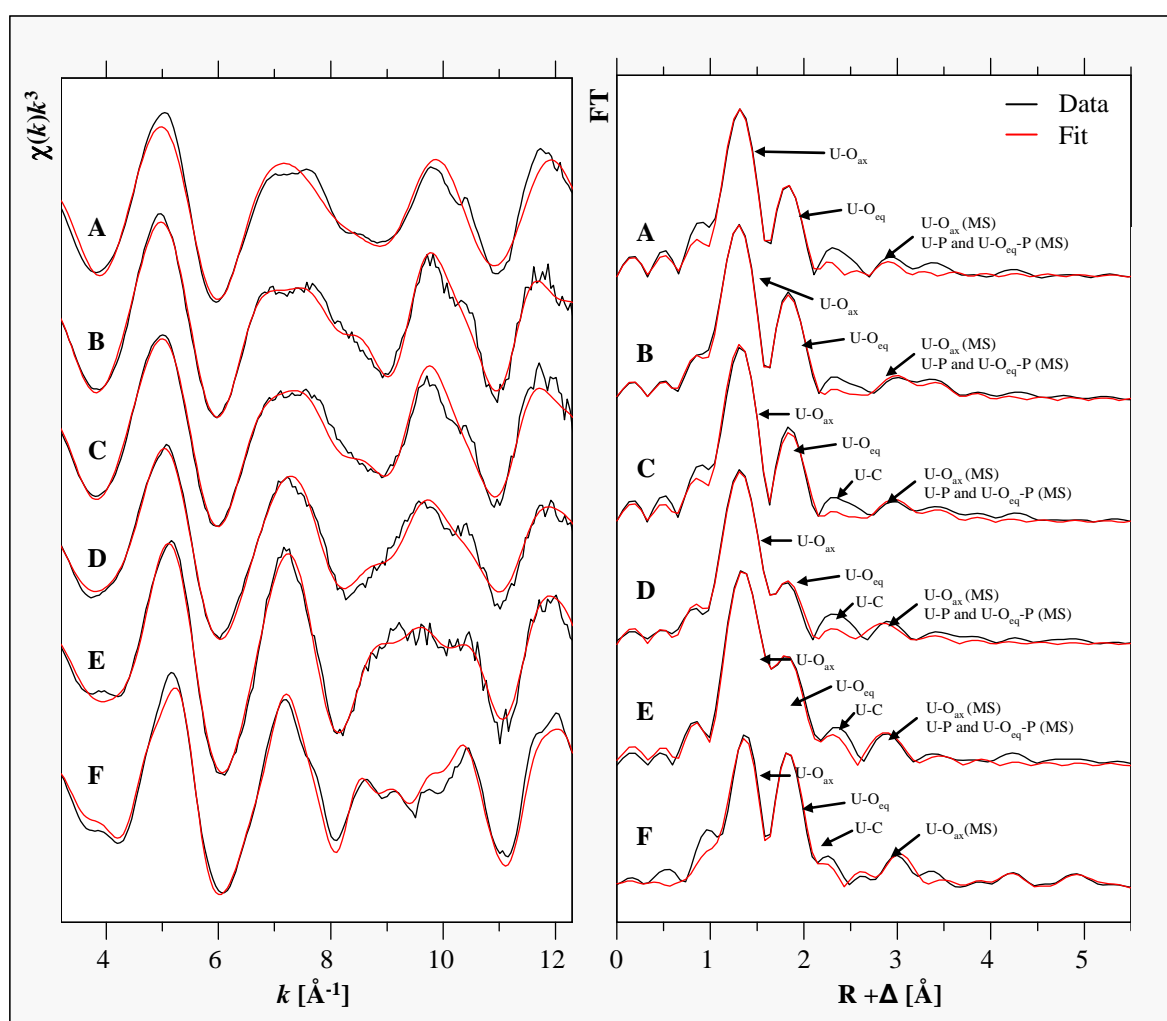


Figure 1.8. U L_{III} -edge k^3 -weighted EXAFS spectra (left) and the corresponding Fourier Transforms (right) ($3.1 \text{ Å}^{-1} < k < 12.4 \text{ Å}^{-1}$) of the uranium complexes formed by *Paenibacillus* sp. JG-TB8 at pH 2 (B), pH 3 (C), pH 4.5 (D), and pH 6 (E) under aerobic conditions. For comparison, the spectra of two model compounds, namely uranyl-fructose(6)phosphate (A) and meta-autunite (F) are illustrated as well.

At pH 6 the calculated radial distance of the equatorial oxygen plane (2.27 Å) is lower compared to the distance calculated for the samples incubated at the highly acidic conditions which suggest an only fourfold coordinated uranyl unit [168]. In accordance to that, we calculated four equatorial oxygen atoms and, moreover, an almost identical number of phosphorous atoms at a radial distance of 3.60 Å. This clearly demonstrate that uranium is

complexed in the way illustrated in Figure 1.9 (left model), which is typical for uranyl phosphate minerals.

Table 1.5. Structural parameters of the uranium complexes formed by the cells of *Paenibacillus* sp. JG-TB8 under aerobic conditions.

Sample	Shell	N ^a	R (Å) ^b	σ^2 (Å ²) ^c	ΔE_0 (eV)
UO ₂ -fructose(6)phosphate pH 5.5 [158]	U-O _{ax}	2.0 ^d	1.77(1)	0.001(1)	0.1(7)
	U-O _{eq1}	4.8(5)	2.30(1)	0.020(4)	
pH 2	U-O _{ax}	2.0 ^d	1.77(1)	0.0024(1)	2.4(3)
	U-O _{ax} (MS)	2.0 ^d	3.54 ^e	0.0048 ^e	
	U-O _{eq}	3.8(2)	2.35(1)	0.0065(4)	
	U-P	2.7(3)	3.62(1)	0.0037(7)	
	U-O-P (MS)	5.4 ^f	3.76(1)	0.0037 ^f	
pH 3	U-O _{ax}	2.0 ^d	1.78(1)	0.0021(1)	3.4(4)
	U-O _{ax} (MS)	2.0 ^d	3.56 ^e	0.0042 ^e	
	U-O _{eq}	3.3(2)	2.35(1)	0.0074(7)	
	U-P	1.8(4)	3.62(1)	0.004(1)	
	U-O-P (MS)	3.6 ^f	3.76(2)	0.004 ^f	
pH 4.5	U-O _{ax}	2.0 ^d	1.77(1)	0.0025(1)	-1.0(6)
	U-O _{ax} (MS)	2.0 ^d	3.54 ^e	0.005 ^e	
	U-O _{eq}	4.2(3)	2.27(1)	0.0103(8)	
	U-P	4.0(3)	3.59(1)	0.008 ^d	
	U-O-P (MS)	8.0 ^f	3.72(1)	0.008 ^f	
pH 6	U-O _{ax}	2.0 ^d	1.79(1)	0.0016(1)	2.7(4)
	U-O _{ax} (MS)	2.0 ^d	3.58 ^e	0.0032 ^e	
	U-O _{eq}	3.9(2)	2.27(1)	0.0037(3)	
	U-P	4.4(4)	3.60(1)	0.006(1)	
	U-O-P (MS)	8.8 ^f	3.72(2)	0.006 ^f	
meta-autunite [169]	U-O _{ax}	2.2(1)	1.76	0.0045	-11.0
	U-O _{eq}	3.9(2)	2.29	0.0026	
	U-P	2.3(3)	3.60	0.008 ^d	

Standard deviations as estimated by EXAFSPAK are given in parenthesis

^a Errors in coordination numbers are $\pm 25\%$

^b Errors in distance are ± 0.02 Å

^c Debye-Waller factor

^d Parameter fixed for calculation

^e Radial distance (R) and Debye-Waller factor (σ^2) linked twice to R and σ^2 of the of the U-O_{ax} path

^f Coordination number linked twice and Debye-Waller factor once to the N and σ^2 of the U-P path

The high Debye-Waller factor calculated for the equatorial oxygen shell from the complexes formed at pH 4.5 indicates a structural inhomogeneity. This could be explained by a mixture of complexes, exhibiting on the one hand a fivefold coordinated uranyl unit, bound to organic phosphate groups, and on the other hand uranium atoms which are included in a mineral phase complexed by four phosphate ligands. However, the low radial distance of the U-O_{eq} shell suggests that most of the uranium present in this sample exist in the uranyl phosphate mineral form. This finding is in contrast to the TRLFS results, where organic uranyl complexes were detected predominantly. However, it is well known that a complexation of

U(VI) by phosphate groups of organic molecules strongly enhances the uranyl luminescence. Because the EXAFS oscillations only depend on the type and number of surrounding atoms, this method is much more meaningful regarding the amounts of the different complexes.

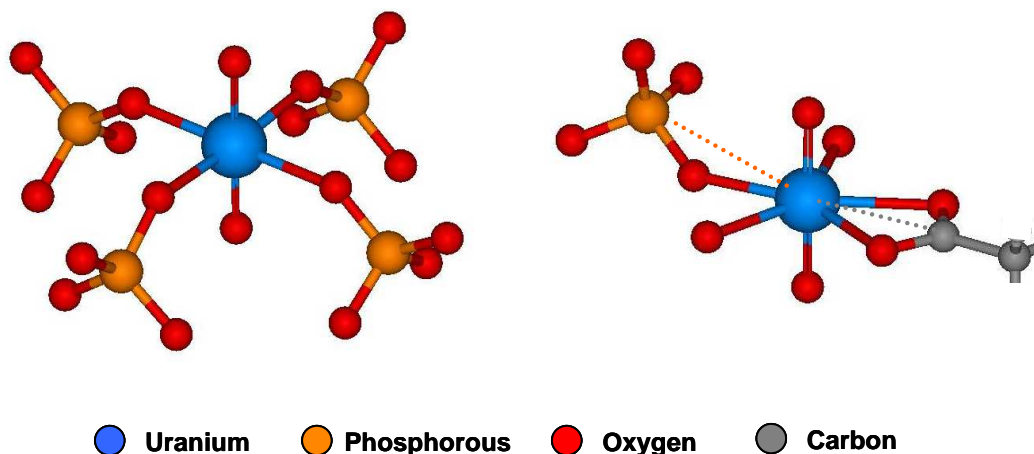


Figure 1.9. Structural models used for the fitting procedure of the EXAFS spectra obtained from the uranium complexes build by the cells of *Paenibacillus* sp. JG-TB8. The left model created from the crystal structure of meta-autunite was used for the fitting procedure of the sample incubated at pH 6 under aerobic conditions. The right model contains fragments of meta-autunite (monodentate coordination at phosphate groups) as well as uranyl triacetate (bidentate coordination to carboxylic groups) and was used for the fitting procedures of all other samples.

Microscopic analyses

Live/Dead staining was used to determine the proportion of viable and dead cells after the treatment with uranium. The staining procedure based on a mixture of two fluorescing nucleic acid stains with different membrane permeation characteristics. The green-fluorescing SYTO[®] 9 detects all cells, whereas the red-fluorescing propidium iodide can only pass through compromised or damaged cell membranes, causing a reduction of the SYTO[®] 9 fluorescence when both dyes are present.

Thus, dead cells stain red whereas intact cells occurred green. Representative microscopic pictures of each sample are presented in Figure 1.10. At pH 6 more than 90% of the cells were alive (Fig. 1.10-G) whereas the fraction of the living cells decreases with decreasing pH due to the increasing distance from the preferred pH conditions of the strain. Hence, at pH 4.5 (Fig. 1.10-E) and pH 3 (Fig. 1.10-C) only about 50% and 5% of the cells were viable, respectively. At pH 2 (Fig. 1.10-A) all cells stained red and, in addition, they were significantly shorter, indicating a strong damage of the cell wall structures and/or a cell fragmentation. Control samples without uranium exhibit no significant differences, indicating that the cell damage and cell death is caused predominantly by the acidic pH conditions. This assumption is supported by the performed uranium tolerance tests (Table 1.1), which

demonstrated that JG-TB8 grows at a uranium concentration of 0.5 mM on solid media. Hence, JG-TB8 may also tolerate corresponding concentration in aqueous solutions.

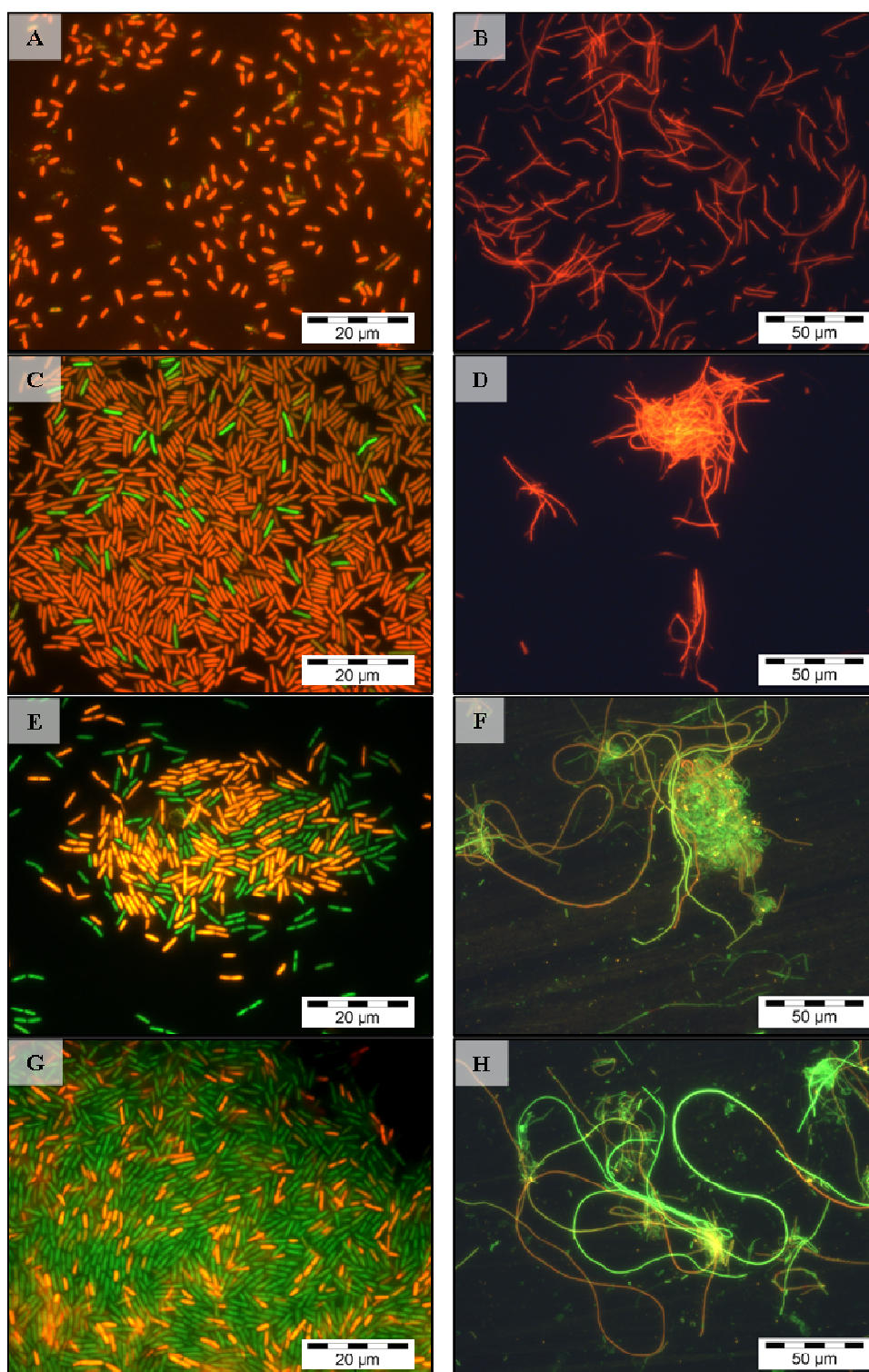


Figure 1.10. Microscopic pictures of *Paenibacillus* sp. JG-TB8, stained with the Live/Dead Kit after the treatment with uranium under aerobic (left) and anaerobic (right) conditions at pH 2 (A, B), pH 3 (C, D) pH 4.5 (E, F) and pH 6 (G, H) for 48 hours. Pictures were taken in fluorescence mode using a fluorescence mirror unit (U-MSWB; Olympus Europa Holding GmbH, Hamburg, Germany) with excitation wavelengths between 420 and 460 nm.

To localize the uranium complexes in the bacterial cell samples transmission electron microscopy combined with EDX was used. No uranium was detected in the samples incubated at pH 2 and pH 6. However it was possible to detect some high-contrasting accumulates in the sample incubated at pH 3. These accumulates contained small amounts of uranium and were localized at the cell wall of some individual cells (Fig. 1.11). Moreover, in the sample incubated at pH 4.5 a huge amount of electron-dense uranium accumulates recognizable as high contrasting spots were detected. Uranium was located at the cell surface as well as intracellular in a form of needle-like fibrils, bound to cell compounds or in polyphosphate granules (Fig. 1.11). A corresponding intracellular uranium accumulation in polyphosphatic granules was also demonstrated for *Pseudomonas aeruginosa* [89]. Such intracellular uranium deposits were exclusively detected in apparently empty cells, which is reasonable as the big uranyl ion cannot enter intact cells [170]. That indicates that the formation of these uranium deposits is a consequence of increased cell permeability after cell death.

EDX analyses demonstrated that the studied accumulates contained different amounts of uranium (U). Besides that, typical energy-lines for phosphorous (P) and oxygen (O) were observed, confirming the spectroscopic results and therewith the formation of uranyl phosphate complexes (Fig. 1.11). The peaks for C, Cu, Os, Pb, and Cl are a result of the sample preparation and the copper grid used to support the ultra-thin cell sections. The presence of silicon results from the oil in the diffusion pump of the column of the used TEM system.

The reason for the failed localization of uranium at pH 6 might result from the low amount of uranium in this sample. Another reason might be the low number of cells exhibiting damaged cell wall structures (Fig. 1.10G), those cells, which were the predominant uranium accumulating cells in the TEM sample of the cells incubated at pH 4.5. However, both facts could not explain the failed detection of uranium at pH 2, because the binding capacity of the cells is almost identical to that at pH 3 (Fig. 1.3) and all cells exhibit destroyed cell envelopes (Fig. 1.10A). A possible reason explaining this is the detection limit of this method. Bigger uranium accumulates can be detected easily, due to their high-contrasting properties. However, equally distributed uranium, e.g. those bound to the negatively charged functional groups at the cell surface is not visualizable with this method.

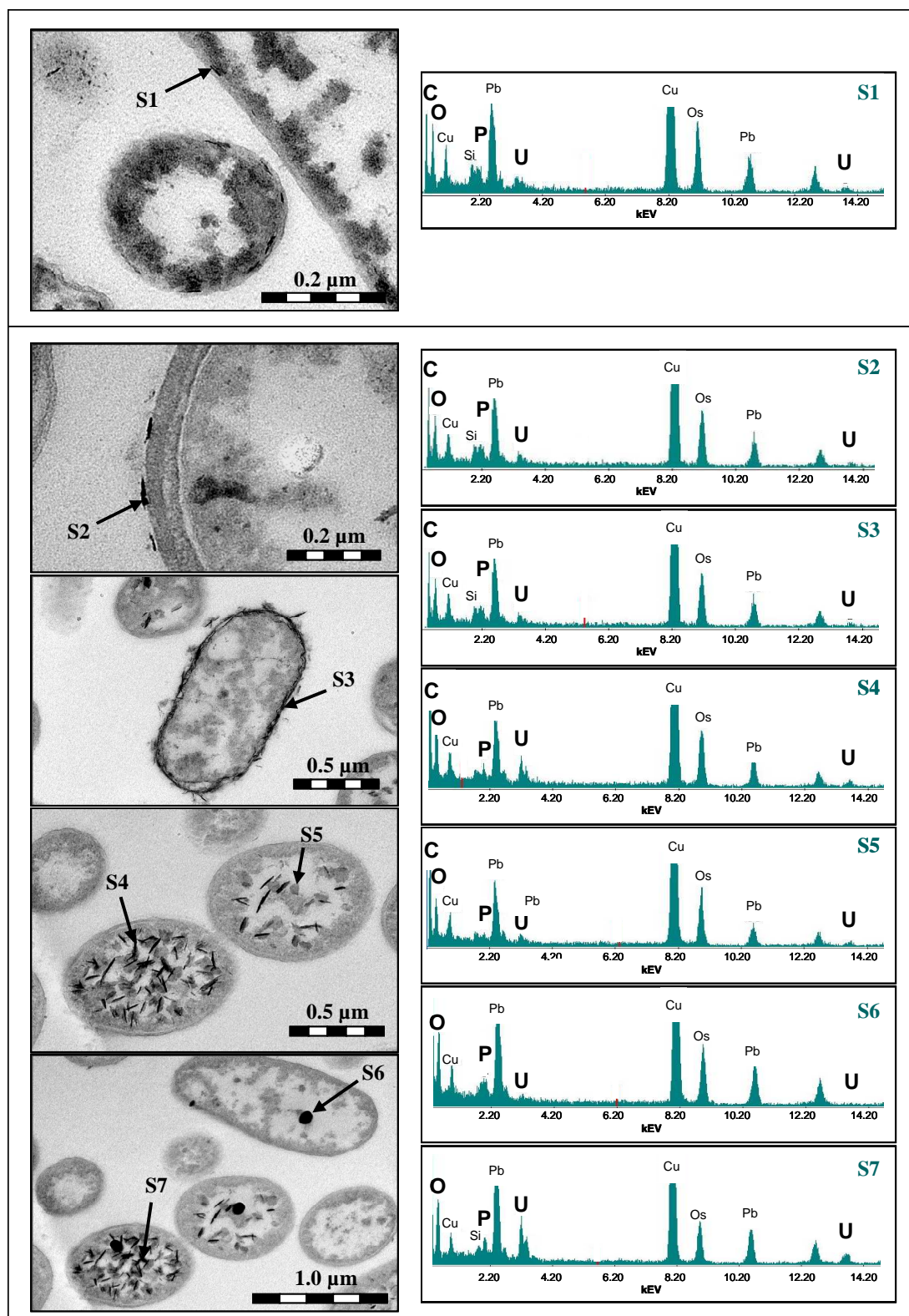


Figure 1.11. Transmission electron micrograph of uranium accumulates deposited by the cells of *Paenibacillus* sp. JG-TB8 (left) and energy-dispersive X-ray spectra (right) of the points marked with arrowheads. U(VI) was localized at pH 3 exclusively at the cell surface (S1). At pH 4.5 U(VI) was localized at the cell surface as well (S2, S3). In addition, intracellular uranium was detected in form of needle-like accumulates (S4, S7) or bound to undetermined cell compounds (S5), and in polyphosphate granules (S6).

Characterization and molecular structure of the uranium complexes formed under anaerobic conditions.

XANES studies

The ability of the studied *Paenibacillus* strain to reduce the added U(VI) to the environmental less-mobile oxidation state +4 was checked by using XANES analyses. To improve the conditions for uranium reduction, parallel U/*Paenibacillus* samples, containing uranyl acetate instead of uranium nitrate, were prepared, in order to avoid a suppression of the U(VI) reduction in favour of the energetically advantageous nitrate reduction. In addition, sodium acetate was added to these parallel samples which served as potential electron donor. The XANES spectra recorded from the four cell samples treated with uranyl nitrate at pH 2, 3, 4.5 and 6, as well as those obtained from the described parallel samples are presented in Figure 1.12.

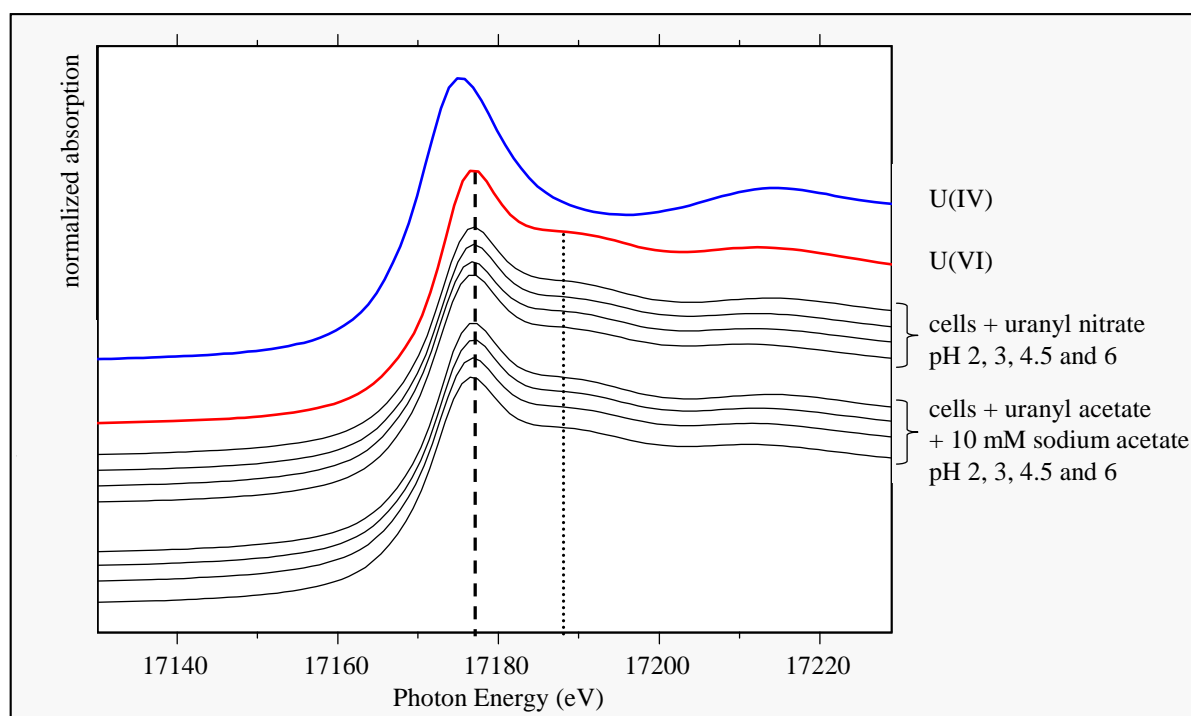


Figure 1.12. Uranium L_{III} -edge XANES spectra recorded from the uranium complexes formed by *Paenibacillus* sp. JG-TB8 at pH 2, 3, 4.5 and 6 after the addition of uranyl nitrate or uranyl acetate. In addition, the XANES spectra of two solutions, which serve as reference samples for the uranium oxidation states, one of U(VI) and another one of U(IV), each at a concentration of $4 \cdot 10^{-2}$ M in 1 M $HClO_4$, are shown in the figure. The dashed and the dotted line represent the position of the absorption edge of U(VI) and of the XANES peak resulting from the multiple scattering contribution of the axial oxygen atoms of U(VI), respectively.

The results demonstrate that uranium was not reduced in any of the samples. The presence of U(VI) was clearly confirmed due to the following observations: The absorption edges of all spectra occurred at a photon energy which is typical for U(VI) (Fig. 1.12, dashed line) and all

spectra feature the multiple scattering contribution of the two axial oxygen atoms of U(VI), represented by a XANES peak around 17188 eV (Fig. 1.12, dotted line). In addition, U(VI) reduction was also not observed in a sample incubated at an almost neutral, favourable for this strain, pH value of 7.2 (not shown). These findings demonstrate that the investigated *Paenibacillus* isolate JG-TB8 is not able to reduce uranium at the studied conditions, most likely due to the use of a unsuitable electron donor. Anyway, our experiments exclude the acidic pH as the sole inhibiting factor for the enzymatic U(VI) reduction.

TRLFS

TRLF spectroscopic analyses of the bacterial cell samples, grown and treated with U(VI) under anaerobic conditions, revealed no significant shifting of the main luminescence maxima with increasing pH values, as it was observed in those samples incubated under aerobic conditions (Fig. 1.13).

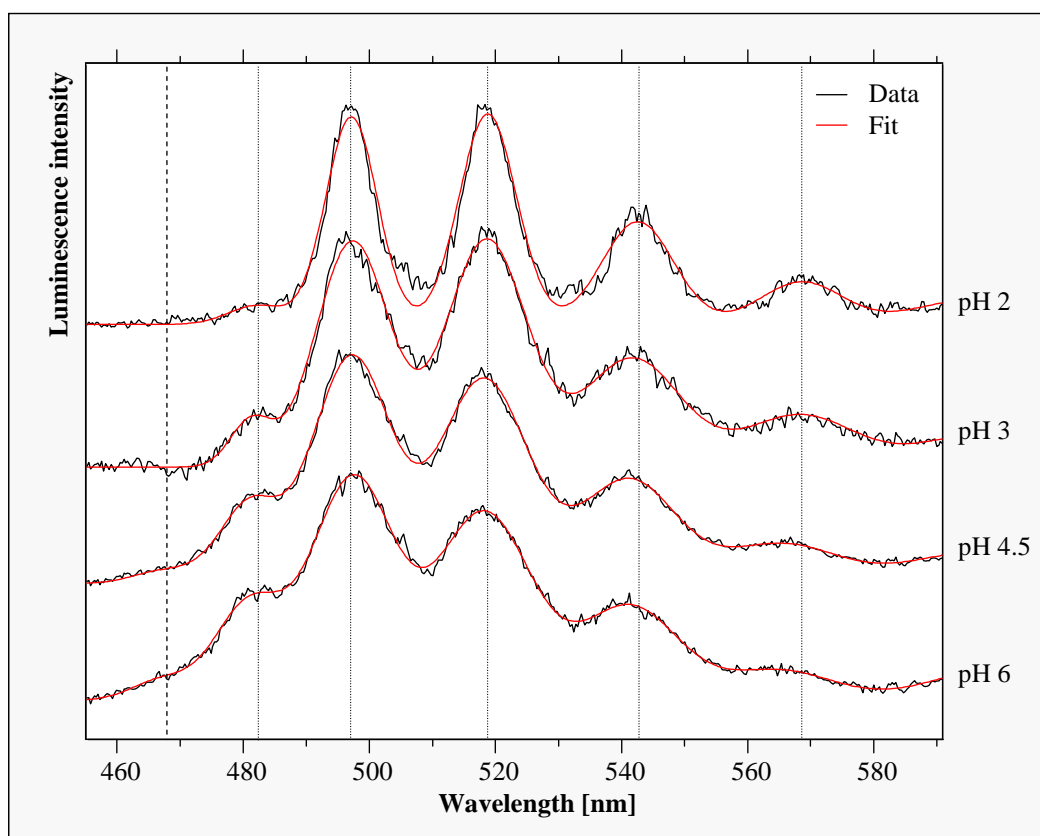


Figure 1.13. U(VI) luminescence spectra recorded from the uranium complexes formed at different pH values after 48 hours by the cells of *Paenibacillus* sp. JG-TB8 under anaerobic conditions. For comparison, dotted lines indicate the luminescence emission maxima calculated for the sample incubated at pH 2. The dashed line represents the position of the luminescence emission maxima exclusively detected at pH 4.5 and pH 6.

At all pH conditions studied, the main peak maxima were located around 497.2, 518.5, and 542 nm (Table 1.3) and therewith correspond well to those of the samples incubated under aerobic conditions at highly acidic pH values (pH 2 and 3). Lifetime analyses demonstrated two or three luminescent uranium species in the studied samples, respectively. In all samples a uranium species with a luminescence lifetime of about 3 μ s was detected (Table 1.6) which is well in line with the lifetime (τ_1 of Table 1.4) calculated from the samples incubated under aerobic conditions.

Table 1.6. Calculated luminescence lifetimes of the U(VI) complexes formed by the cells of *Paenibacillus* sp. JG-TB8 under anaerobic conditions.

	pH 2	pH 3	pH 4.5	pH 6
Lifetime 1 (τ_1)	$3.32 \pm 0.87 \mu\text{s}$	$3.62 \pm 0.45 \mu\text{s}$	$2.70 \pm 0.39 \mu\text{s}$	$2.99 \pm 0.24 \mu\text{s}$
Lifetime 2 (τ_2)	$33.4 \pm 4.0 \mu\text{s}$	$32.7 \pm 3.2 \mu\text{s}$	$36.6 \pm 4.5 \mu\text{s}$	$40.4 \pm 3.8 \mu\text{s}$
Lifetime 3 (τ_3)			$7.82 \pm 1.25 \mu\text{s}$	$9.21 \pm 1.09 \mu\text{s}$

In addition a significant longer luminescence lifetime was calculated in all samples as it was also the case in the aerobic samples. However, the lifetimes calculated for this second U(VI) species was somewhat longer than those calculated for the long-living species in the samples incubated under aerobic conditions. From the samples incubated at pH 4.5 and pH 6 a third luminescence lifetime of $(7.8 \pm 1.3) \mu\text{s}$ and $(9.2 \pm 1.1) \mu\text{s}$ was calculated, respectively. Interestingly, an additional luminescence peak located around 468 nm was observed in these two samples (Figure 1.13, Table 1.3). This luminescence peak can be related to U(VI) complexes formed at carboxylic groups. Such complexes are known to show only low luminescence intensity at room temperature. However, recent studies demonstrated that U(VI) complexes formed at carboxylic groups of peptidoglycan, the major cell wall compound of the studied bacterium, show luminescence properties at room temperature [167]. In order to prevent the formation of highly luminescent uranyl phosphate complexes the authors of the mentioned study used an isolated phosphate-free peptidoglycan. This approach allowed the authors to measure the luminescence of the formed uranyl carboxylic complexes at room temperature. Because of the similar luminescence emission maxima of the studied in this approach uranyl carboxylate complexes and those of uranyl phosphate complexes it is obvious that in case of the parallel existence of both, the luminescence of the uranyl carboxylate complexes can easily be masked by the strong luminescent uranyl phosphate complexes. However, as uranyl phosphate complexes are known to show no

luminescence properties below 470 nm, the presence of uranyl carboxylate complexes was confirmed by the emission maxima at around 468 nm. The calculated in this study lifetimes of the formed uranyl carboxylate complexes are in line with that of the 1:1 uranyl carboxylate complex studied recently [171]. Moreover, comparable results which suggested the formation of uranyl carboxylate complexes were obtained by spectroscopic studies of the U(VI) complexes formed at the cells of the acidothermophilic crenarchaeon *Sulfolobus acidocaldarius* [164] (Table 1.3).

XAS studies

The isolated U L_{III} -edge k^3 -weighted EXAFS spectra and the corresponding FTs of the U(VI) complexes formed by the cells of *Paenibacillus* sp. JG-TB8, along with the best fits are illustrated in Figure 1.14. For comparison, the spectra recorded from the model compounds uranyl-fructose(6)phosphate [158] and an 1:2 uranyl succinate complex [171] are presented as well.

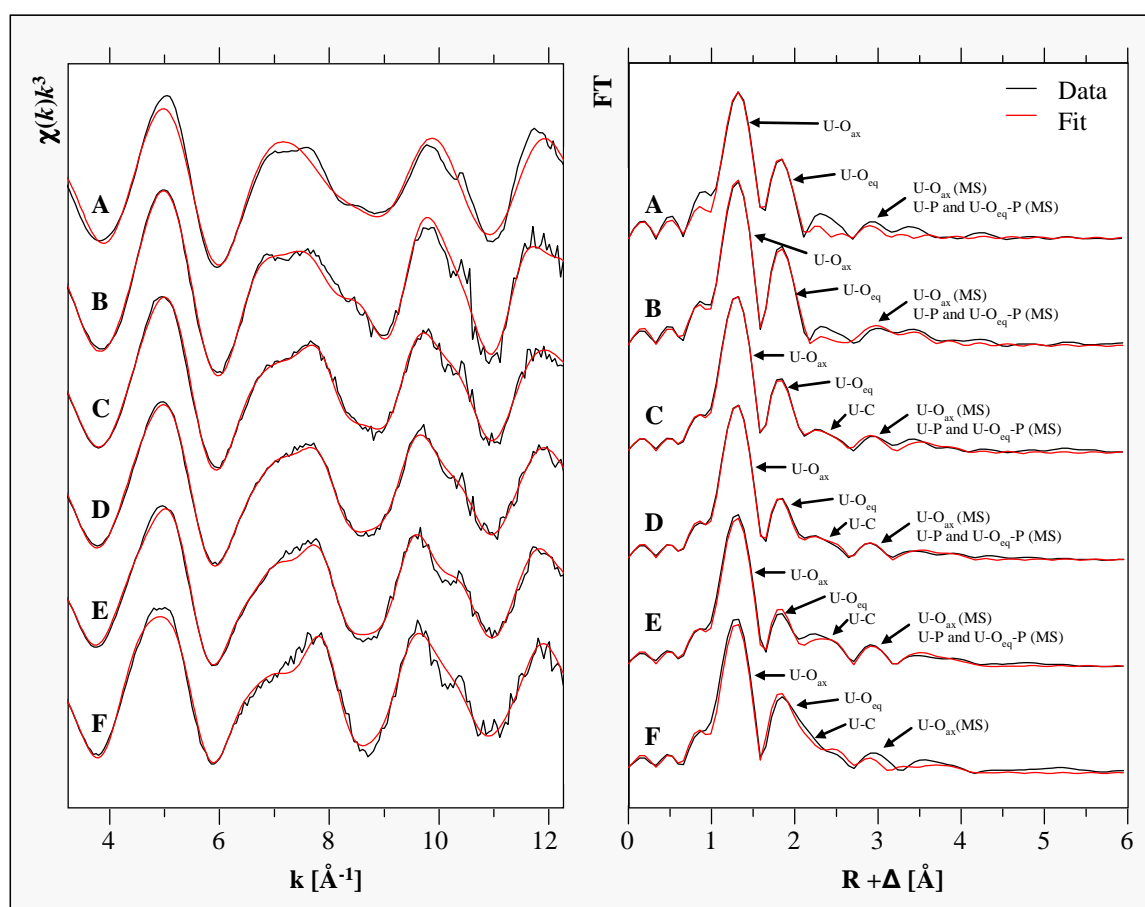


Figure 1.14. U L_{III} -edge k^3 -weighted EXAFS spectra (left) and the corresponding Fourier Transforms (right) ($3.1 \text{ \AA}^{-1} < k < 12.4 \text{ \AA}^{-1}$) of the uranium complexes formed by *Paenibacillus* sp. JG-TB8 at pH 2 (B), pH 3 (C), pH 4.5 (D), and pH 6 (E) under anaerobic conditions. For comparison, the spectra of two model compounds, namely uranyl-fructose(6)phosphate (A) and uranyl disuccinate (F) are illustrated as well.

The structural data which underlies each of the fits are summarized in Table 1.7. In accordance to the EXAFS data obtained from the uranium complexes formed by the studied strain under aerobic conditions, the spectrum recorded from the U(VI)/*Paenibacillus* sample incubated under anaerobic conditions at pH 2 originates from organic uranyl phosphate complexes. The fitting procedure revealed radial distances for the equatorial oxygen and phosphate atoms of 2.35 Å and 3.62 Å, respectively (Table 1.7).

Table 1.7. Structural parameters of the uranium complexes formed by the cells of *Paenibacillus* sp. JG-TB8 under anaerobic conditions.

Sample	Shell	N ^a	R (Å) ^b	σ ² (Å ²) ^c	ΔE ₀ (eV)
UO ₂ -fructose(6)phosphate pH 5.5 [158]	U-O _{ax}	2.0 ^d	1.77(1)	0.001(1)	0.1(7)
	U-O _{eq1}	4.8(5)	2.30(1)	0.020(4)	
pH 2	U-O _{ax}	2.0 ^d	1.77(1)	0.0018(1)	2.4(3)
	U-O _{ax} (MS)	2.0 ^d	3.54 ^e	0.0036 ^e	
	U-O _{eq}	4.0(2)	2.35(1)	0.0068(5)	
	U-P	3.1(4)	3.62(1)	0.0044(8)	
	U-O-P (MS)	6.2 ^f	3.76(1)	0.0044 ^f	
pH 3	U-O _{ax}	2.0 ^d	1.76(1)	0.0021(1)	1.6(4)
	U-O _{ax} (MS)	2.0 ^d	3.52 ^e	0.0042 ^e	
	U-O _{eq}	4.7(3)	2.36(1)	0.0126(9)	
	U-P	3.2(3)	3.61(1)	0.0056(9)	
	U-O-P (MS)	6.4 ^f	3.75(1)	0.0056 ^f	
pH 4.5	U-O _{ax}	2.0 ^d	1.77(1)	0.0022(1)	0.1(4)
	U-O _{ax} (MS)	2.0 ^d	3.54 ^e	0.0044 ^e	
	U-O _{eq}	6.5(5)	2.36(1)	0.021(1)	
	U-P	2.6(3)	3.61(1)	0.008(1)	
	U-O-P (MS)	5.2 ^f	3.74(1)	0.008 ^f	
	U-C ₁	1.9(1)	2.88(1)	0.0038 ^d	
	U-C ₂	1.9 ^g	4.35(1)	0.0038 ^d	
pH 6	U-O _{ax}	2.0 ^d	1.77(1)	0.0023(1)	0.8(3)
	U-O _{ax} (MS)	2.0 ^d	3.54 ^e	0.0046 ^e	
	U-O _{eq}	5.7(9)	2.38(1)	0.022(1)	
	U-P	2.1(3)	3.61(1)	0.004(1)	
	U-O-P (MS)	4.2 ^f	3.73(1)	0.004 ^f	
	U-C ₁	2.8(1)	2.89(1)	0.0038 ^d	
	U-C ₂	2.8 ^g	4.37(1)	0.0038 ^d	
Uranyl disuccinate [171]	U-O _{ax}	2.0 ^d	1.77(1)	0.0021(1)	3.5(5)
	U-O _{ax} (MS)	2.0 ^d	3.54 ^e	0.0042 ^e	
	U-O _{eq}	4.4(5)	2.44(1)	0.009(1)	
	U-C ₁	2.3(3)	2.90(1)	0.0038 ^d	
	U-C ₂	2.3 ^g	4.37(2)	0.0038 ^d	

Standard deviations as estimated by EXAFSPAK are given in parenthesis

^a Errors in coordination numbers are ± 25%

^b Errors in distance are ± 0.02 Å

^c Debye-Waller factor

^d Parameter fixed for calculation

^e Radial distance (R) and Debye-Waller factor (σ²) linked twice to R and σ² of the of the U-O_{ax} path

^f Coordination number linked twice and Debye-Waller factor once to the N and σ² of the U-P path

^g Coordination number (N) linked to the N of U-C₁ path

These structural parameters are well in line with those calculated for the organic uranyl phosphate complexes formed by the strain under aerobic conditions at pH 2 and pH 3 (Table 1.5). However, in contrast to the aerobic conditions, we observed differences between the samples incubated at pH 2 and pH 3 under anaerobic conditions.

At pH 3 a high Debye-Waller factor of $\sim 0.013 \text{ \AA}^2$ (compared to 0.007 \AA^2 at pH 2) was calculated for the equatorial oxygen shell suggesting a structural disorder within this shell. At pH 4.5 ($\sigma^2 = 0.021 \text{ \AA}^2$) and pH 6 ($\sigma^2 = 0.022 \text{ \AA}^2$) the Debye-Waller factor of the U-O_{eq} shell was even higher than at pH 3. Concomitant, the radial distance of the U-O_{eq} shell increases with increasing pH values from 2.35 \AA (pH 2) up to 2.38 \AA (pH 6). This indicates the enhanced formation of uranyl complexes with longer U-O_{eq} bond distances at higher pH values. According to the literature, the most likely complexation mode at these conditions, featuring significant longer U-O_{eq} bond lengths, is a bidentate U(VI) complexation at carboxylic groups of organic matter. Hence, the high Debye Waller factor can be explained by a coexistence of uranyl complexes where the uranyl ion is monodentately bound to phosphate groups (averaged U-O_{eq} bond distance = 2.35 \AA) and bidentately bound to carboxylic groups (averaged U-O_{eq} bond distance = 2.47 \AA) (Fig. 1.9, right model). With respect to the extremely high Debye-Waller factors of the U-O_{eq} shell, two shells of carbon atoms (C₁ and C₂) were included in the shell fitting procedures of the samples incubated at pH 4.5 and 6. It is obvious from the EXAFS parameters, that no mineral phases were formed by the cells under anaerobic conditions.

The exclusive binding of U(VI) at organic functional groups under anaerobic and moderate acidic pH conditions is in contrast to all studies which were performed on bacterial uranium interactions under anaerobic conditions, in which uranium was either reduced to U(IV) [25-27] or precipitated as U(VI) phosphate minerals [172, 173].

Microscopic analyses

In analogy to the experiments performed under aerobic conditions we used TEM in order to localize the uranium complexes formed by *Paenibacillus* sp. JG-TB8 under anaerobic conditions. Although significant amounts of uranium were bound by the cells at the different pH values (Fig. 1.6), we were not able to detect uranium in the samples (Fig. 1.15). In analogy to the sample incubated under aerobic conditions at pH 2, the best explanation for the failed detection is a homogenous distribution of uranium-binding ligands at the cell surface. This assumption agrees with the spectroscopic results. In contrast to the cells incubated at

aerobic conditions, U(VI) complexation occurred exclusively by organic phosphate and carboxylate groups.

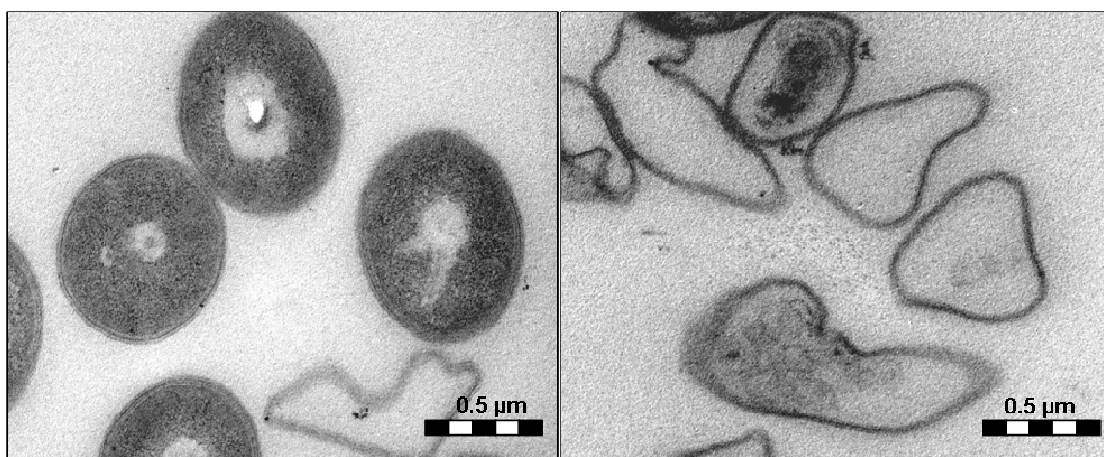


Figure 1.15. Transmission electron micrographs of ultra-thin sections of *Paenibacillus* sp. JG-TB8 after the incubation with U(VI). Besides intact cells (left), a significant amount of empty cell envelopes was found (right). Uranium accumulates were not detected in any of the samples.

Investigation of the cell viability showed results similar to that obtained under aerobic conditions, regarding the pH dependent increase of the proportion of dead cells at decreasing pH (Fig. 1.10). However, the samples incubated at pH 4.5 and 6 differ not that much from each other as it was detected in the aerobic samples. In both samples most of the cells stained green, demonstrating intact cell wall structures. In particular, almost all of cells which had a normal length of about 5 μm were alive in these two samples. The only difference which was observed was a high agglomeration of the cells at pH 4.5, which was not observed at pH 6. This agglomeration might be a protection mechanism against the unfavourable pH conditions. The same observation was made in the sample incubated at pH 3. However, all cells in this sample stained red, indicating the absence of viable cells in this sample. At pH 2 all cells were dead as well, but without showing the agglomeration effect observed at pH 3 and pH 4.5. A possible explanation for that might be that the extremely low acidic pH inhibits any cellular stress response mechanisms.

Key role of the phosphatase activity in uranium complexation

The observed formation of uranyl phosphate mineral phases by microbial cells has been described in several previous studies [67, 70, 84, 164, 174]. In most cases the release of orthophosphate, which is involved in the uranium precipitation, was attributed to the activity of various phosphatases, which release inorganic orthophosphate from organic phosphate

compounds. Corresponding enzyme activities had been described for a large variety of aerobic and anaerobic bacteria as well as archaea [32-34, 68]. It was demonstrated that at the presence of an organic phosphate source a bacterial phosphatase, which was overexpressed in *Pseudomonas* strains, could release sufficient amounts of orthophosphate to precipitate uranium even from low concentrated ($c_{\text{uranium}} = 0.02 \text{ mM}$) solutions [69]. Moreover, it was recently postulated, that the hydrolyzation of organophosphate by aerobic heterotrophic bacteria may play an important role in bioremediation of uranium-contaminated sites [70]. Therefore we checked the phosphatase activity of the cells at the different conditions studied. The phosphatase activity of the strain JG-TB8 in dependency on the pH value and the aeration conditions is shown in Figure 1.16 and Table 1.8.

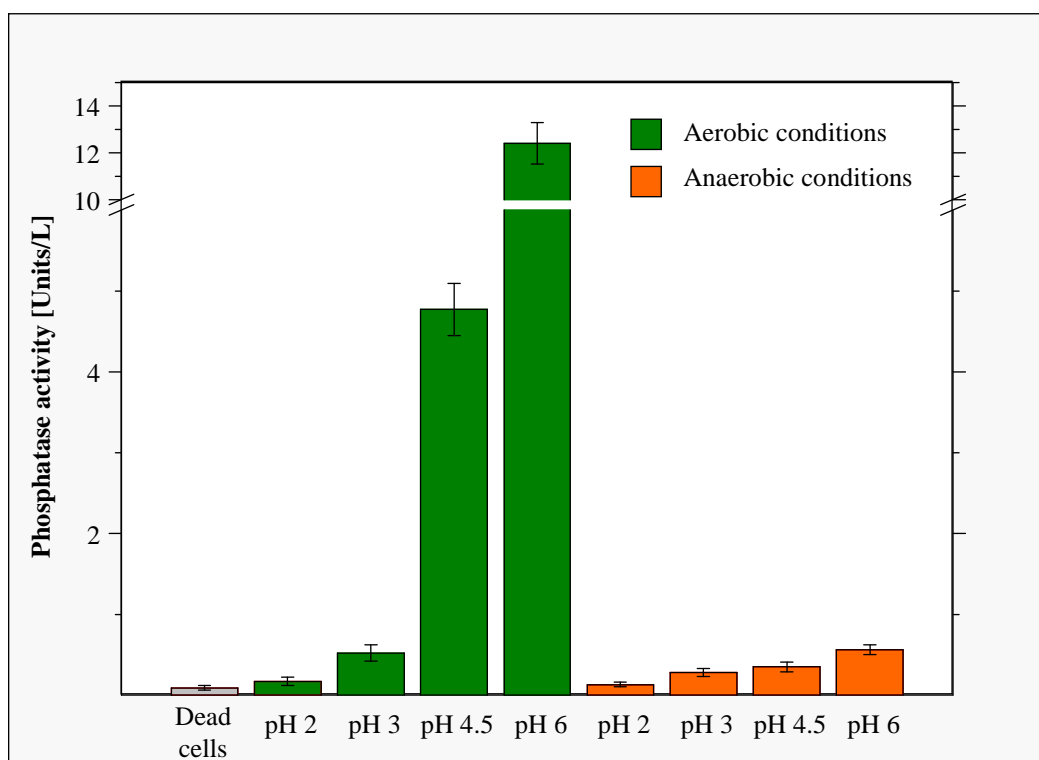


Figure 1.16. Acid phosphatase activity of cells of *Paenibacillus* sp. JG-TB8 at different pH values and in dependency on the aeration conditions.

Under aerobic as well as under anaerobic conditions the phosphatase activity increases with increasing pH. As expected, the highest activity was calculated in both cases for the samples incubated at pH 6, most probably because this pH is the closest to the growth optimum of the strain. However, the phosphatase activity was significantly reduced in the absence of oxygen. This finding is in contrast to former studies using isolated enzymes (acid and alkaline phosphatases), where the specific enzyme activity did not change significantly [175].

Moreover the phosphatase activity of the Gram-negative bacterium *E. coli* is even dramatically enhanced after a shifting from aerobic to anaerobic conditions [32]. Interestingly a reduction of the phosphatase activity of ResE, a regulatory protein for respiration processes, under anaerobic conditions was suggested by Nakano and Zuber for the Gram-positive bacterium *Bacillus subtilis* [146]. This might imply corresponding inhibition effects on dephosphorylation processes in the anaerobically growing representatives of *Bacillales*, such as *Paenibacillus* species.

Table 1.8. Phosphatase activity calculated for cells of *Paenibacillus* sp. JG-TB8 incubated at different pH values and atmospheric conditions

pH	Phosphatase activity [Units/L]	
	Aerobic	Anaerobic
2	0.17 ± 0.05	0.13 ± 0.03
3	0.52 ± 0.1	0.28 ± 0.05
4.5	4.77 ± 0.32	0.35 ± 0.06
6	12.4 ± 0.9	0.56 ± 0.06
Dead cells (pH 6)	0.09 ± 0.03	

At pH 6 the phosphatase activity under aerobic conditions is more than 20 times higher than that under anaerobic conditions. This finding should dramatically influence the release of orthophosphate from the cells. To confirm this we determined the amount of orthophosphate in the supernatants of the cell samples after an incubation for 48 h in 0.1 M NaClO₄ (pH 2, 3, 4.5 or 6) with and without the addition of uranyl nitrate. The results are presented in Figure 1.17 and Table 1.9. As expected from the phosphatase activity studies, we observed significant differences in orthophosphate production. The amount of orthophosphate depends on the pH value as well, but much more on the presence of oxygen. Under anaerobic conditions only very low concentrations of orthophosphate (<5 µM) were determined. At pH 6 the amount was somewhat higher (~16 µM). In contrast to that, the orthophosphate concentration in the aerobic samples, exhibiting a high phosphatase activity, was about 150 µM (pH 4.5) and 350 µM (pH 6), respectively. At highly acidic conditions the orthophosphate concentration was also low in the aerobic samples, which is again in good agreement with the phosphatase activity studies.

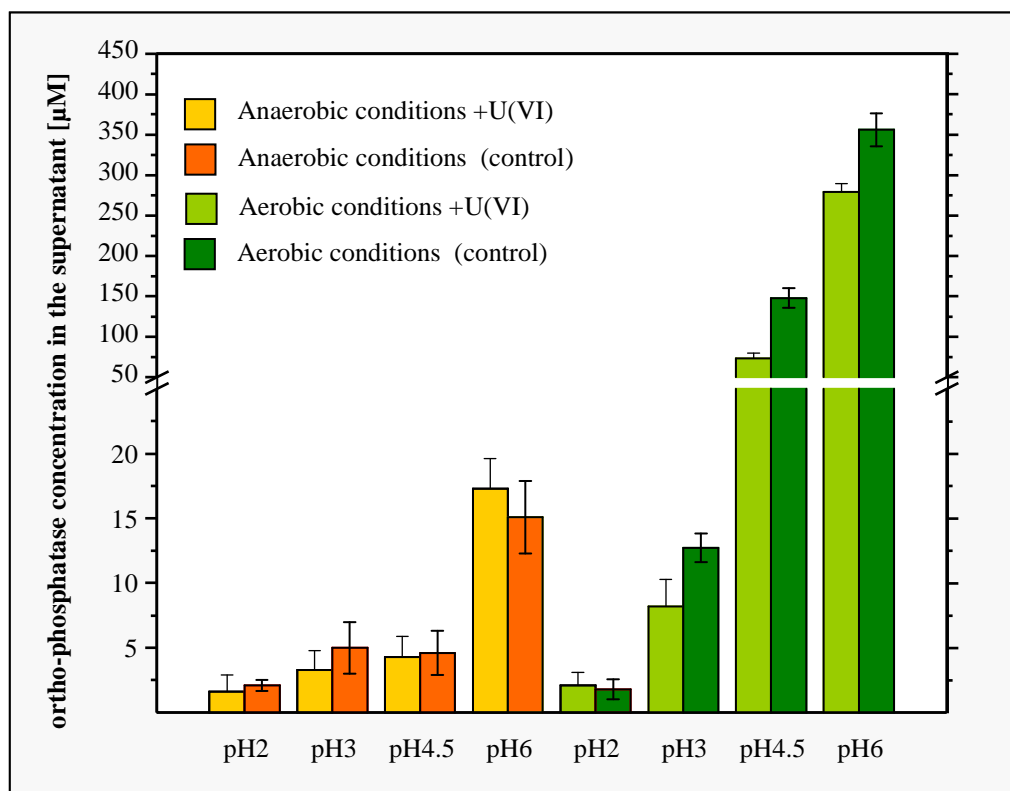


Figure 1.17: Amount of orthophosphate in the supernatant of cells of *Paenibacillus* sp. JG-TB8 after an incubation of 48 hours in dependency on pH, the aeration conditions and the presence of uranium.

Table 1.9. Concentration of orthophosphate in the supernatant of cell samples of *Paenibacillus* sp. JG-TB8 incubated at different pH values and atmospheric conditions.

pH	Concentration of orthophosphate in the supernatant [μM] (aerob)		Concentration of orthophosphate in the supernatant [μM] (anaerob)	
	Control	U treated	U treated	Control
2	2.1 ± 1.0	1.8 ± 0.8	1.6 ± 1.3	2.1 ± 0.4
3	8.2 ± 2.1	12.7 ± 1.1	3.3 ± 1.3	5.0 ± 2.0
4.5	73.4 ± 6.8	148 ± 12	4.3 ± 1.6	4.6 ± 1.7
6	279 ± 10	356 ± 21	17.3 ± 2.3	15.1 ± 2.8

We observed no differences between the uranium-treated and untreated cell samples under anaerobic conditions as well as at highly acidic aerobic conditions within the experimental errors. In contrast to that, the uranium-treated and untreated samples incubated at pH 4.5 and pH 6 differed significantly from each other. Phosphate concentration in the supernatant of the uranium-treated samples was in both cases about 75 μM lower than those of the control sample. This removal of phosphate from the supernatant confirmed the precipitation of inorganic uranyl phosphate complexes at both pH values. The fact that at both pH values about 75 μM phosphate was bound to uranium confirmed that at pH 6 (initial uranium

concentration was 50 μM) the uranium was completely, and at pH 4.5 (initial uranium concentration was 500 μM) partly, complexed *via* inorganic phosphates. Nevertheless, the rapid uranium complexation at both pH values (Fig. 1.6) suggests an initial U(VI) binding at functional groups at the cell surface, which subsequently serve as nucleation sites for metal precipitation. A corresponding mechanism was also suggested by studying the radionuclide accumulation processes of *Citrobacter* sp. [176].

CONCLUSIONS

The present study demonstrates that the interaction mechanisms of uranium with the strain *Paenibacillus* sp. JG-TB8 depend on the aeration conditions. Moreover, it confirms the important role of phosphatases in the biomineralization process of uranium. Because of the dramatic inhibition of the respective enzymatic activity under anaerobic conditions in the cells of JG-TB8, uranyl phosphate mineral phases were not precipitated at these conditions. In contrast to that, JG-TB8 was able to precipitate significant amounts of uranyl phosphate mineral phases under moderate acidic and aerobic conditions, without supplying any organic phosphate sources. This indicates that *Paenibacillus* strains, indigenous for uranium-contaminated sites, may have a crucial role in the detoxification process of uranium in the environment.

SUPPLEMENTAL MATERIAL

Table A: Affiliation of the isolated bacterial strains based on 16S rRNA gene sequence analyses.

Isolate	Closest phylogenetic relative (EMBL No.)	BLAST % similarity ⁽¹⁾	Accession number
<i>Bacillaceae</i>			
JG-TB1	<i>Paenibacillus</i> sp. 436-1 (AY266989)	99.3	FR849913
	<i>Bacillus circulans</i> 1-77 (Y13061)	99.2	
	<i>Paenibacillus borealis</i> DSM 13188 ^T (AB073364)	97.5	
JG-TB2	<i>Bacillus weihenstephanensis</i> DSM 11821 (AJ841876)	100	FR849914
	<i>Bacillus mycoides</i> ATCC 6462 (EF210295)	100	
	<i>Bacillus cereus</i> AH 521 (AF290554)	100	
	<i>Bacillus thuringiensis</i> strain IIBC-T63 001 (EF210299)	100	
JG-TB3	<i>Paenibacillus</i> sp. IDA5358 (AY289507)	99.1	FR849915
	<i>Paenibacillus amylolyticus</i> NRRL:NRS-290 ^T (D85396)	98.8	
JG-TB4	<i>Paenibacillus</i> sp. IDA5358 (AY289507)	98.9	FR849916
	<i>Paenibacillus amylolyticus</i> NRRL:NRS-290 ^T (D85396)	98.7	
JG-TB5	<i>Paenibacillus</i> sp. 436-1 (AY266989)	99.6	FR849917
	<i>Bacillus circulans</i> WSBC 20030 (Y13062)	99.5	
	<i>Paenibacillus borealis</i> DSM 13188 ^T (AB073364)	97.5	
JG-TB6	<i>Paenibacillus</i> sp. 436-1 (AY266989)	99.3	FR849918
	<i>Bacillus circulans</i> WSBC 20030 (Y13062)	99.4	
	<i>Paenibacillus borealis</i> DSM 13188 ^T (AB073364)	97.2	
JG-TB7	<i>Paenibacillus</i> sp. 61724 (AF227827)	99.6	FR849919
	<i>Bacillus circulans</i> 1-77 (Y13061)	99.6	
	<i>Paenibacillus borealis</i> DSM 13188 ^T (AB073364)	97.4	
JG-TB8	<i>Paenibacillus</i> sp. 436-1 (AY266989)	99.5	FR849920
	<i>Bacillus circulans</i> WSBC 20030 (Y13062)	99.6	
	<i>Paenibacillus borealis</i> DSM 13188 ^T	97.5	
JG-TB9	<i>Paenibacillus</i> sp. WPCB150 (FJ006908)	99.5	FR849921
	<i>Bacterium</i> H25 (AY345548)	99.5	
	<i>Paenibacillus borealis</i> DSM 13188 ^T (AB073364)	98.6	
JG-TB10	<i>Bacillus weihenstephanensis</i> DSM11821 (AJ841876)	100	FR849922
	<i>Bacillus mycoides</i> ATCC 6462 (EF210295)	100	
	<i>Bacillus cereus</i> AH 521 (AF290554)	100	
	<i>Bacillus thuringiensis</i> strain IIBC-T63 001 (EF210299)	100	
JG-TB11	<i>Lysinibacillus fusiformis</i> NBRC15717 (AB245423)	99.9	FR849923
	<i>Bacillus fusiformis</i> DSM 2898 ^T (AJ310083)	99.9	
	<i>Lysinibacillus sphaericus</i> PRE16 (EU880531)	99.7	
JG-TB12	<i>Lysinibacillus fusiformis</i> NBRC15717 (AB245423)	100	FR849924
	<i>Bacillus fusiformis</i> DSM 2898 ^T (AJ310083)	99.9	
	<i>Lysinibacillus sphaericus</i> PRE16 (EU880531)	99.7	
JG-TB13	<i>Paenibacillus</i> sp. AaD5 (GQ915094)	99.5	FR849925
	<i>Paenibacillus borealis</i> DSM 13188 ^T (AB073364)	97.0	
	<i>Bacillus circulans</i> WSBC 20030 (Y13062)	98.1	
JG-TB14	<i>Bacillus</i> sp. BF149 (AM934692)	99.6	FR849926
	<i>Bacillus niacini</i> IFO15566 (AB021194)	99.3	
JG-TB15	<i>Bacillus psychrodurans</i> QT25 (GU385871)	99.1	FR849927
	<i>Bacillus psychrodurans</i> DSM 11713 (AJ277984)	98.9	

⁽¹⁾ Similarity is calculated from those parts of the gene which were considered for BLAST analyses

Table A (continued): Affiliation of the isolated bacterial strains based on 16S rRNA gene sequence analyses.

Isolate	Closest phylogenetic relative (EMBL No.)	BLAST % similarity ⁽¹⁾	Accession number
JG-TB16	<i>Paenibacillus</i> sp. IDA5358 (AY289507)	98.8	FR849928
	<i>Paenibacillus amylolyticus</i> NRRL:NRS-290 ^T (D85396)	98.6	
JG-TB17	<i>Paenibacillus</i> sp. 436-1 (AY266989)	99.8	FR849929
	<i>Bacillus circulans</i> 1-77 (Y13061)	99.7	
	<i>Paenibacillus borealis</i> DSM 13188 ^T (AB073364)	97.6	
JG-TB19	<i>Paenibacillus</i> sp. 436-1 (AY266989)	99.6	FR849930
	<i>Bacillus circulans</i> 1-77 (Y13061)	99.5	
	<i>Paenibacillus borealis</i> DSM 13188 ^T (AB073364)	97.3	
JG-TB20	<i>Bacillus psychrodurans</i> DSM 11713 (AJ277984)	99.7	FR849931
	<i>Bacillus psychrodurans</i> DSM 11706 (AJ277983)	99.5	
JG-TB21	<i>Paenibacillus</i> sp. HSCC 1657 (AB046422)	99.6	FR849932
	<i>Paenibacillus odorifer</i> PNF4 (EF199999)	99.3	
	<i>Bacillus circulans</i> 1-77 (Y13061)	98.6	
	<i>Paenibacillus borealis</i> DSM 13188 ^T (AB073364)	97.5	
JG-TB22	<i>Paenibacillus</i> sp. 61724 (AF227827)	99.5	FR849933
	<i>Bacillus circulans</i> WSBC 20030 (Y13062)	99.5	
	<i>Paenibacillus borealis</i> DSM 13188 ^T (AB073364)	97.6	
JG-TB23	<i>Bacillus thuringiensis</i> GBAC46 (GU568209)	99.8	FR849934
	<i>Bacillus cereus</i> IMAUB1019 (FJ641030)	99.8	
	<i>Bacillus mycoides</i> NBRC 100169 (AB363736)	99.7	
JG-TB25	<i>Paenibacillus</i> sp. HSCC 1657 (AB046422)	99.7	FR849935
	<i>Paenibacillus odorifer</i> PNF4 (EF199999)	99.2	
	<i>Bacillus circulans</i> WSBC 20030 (Y13062)	98.5	
	<i>Paenibacillus borealis</i> DSM 13188 ^T (AB073364)	97.5	
JG-TB26	<i>Paenibacillus</i> sp. 436-1 (AY266989)	99.5	FR849936
	<i>Bacillus circulans</i> WSBC 20030 (Y13062)	99.6	
	<i>Paenibacillus borealis</i> DSM 13188 ^T (AB073364)	97.6	

⁽¹⁾ Similarity is calculated from those parts of the gene which were considered for BLAST analyses

Chapter II

Interactions of *Sulfolobus acidocaldarius* with uranium

Published in:

Thomas Reitz, Mohamed L. Merroun, Andre Rossberg and Sonja Selenska-Pobell

Radiochimica acta **98**, 249-257 (2010)

ABSTRACT

Interactions of the acidothermophilic archaeon *Sulfolobus acidocaldarius* DSM 639 with U(VI) were studied by using a combination of batch experiments, X-ray absorption spectroscopy (XAS), and time-resolved laser-induced fluorescence spectroscopy (TRLFS). We demonstrated that at pH 2 this archaeal strain possesses a low tolerance to U(VI) and that its growth is limited to a uranium concentration below 1.1 mM. At similarly highly acidic conditions (pH 1.5 and 3.0), covering the physiological pH growth optimum of *S. acidocaldarius*, at which U(VI) is soluble and highly toxic, rapid accumulation of the radionuclide by the cells of the strain occurred. About half of the uranium binding capacity was reached by the strain after an incubation of five minutes and nearly total saturation of the binding sites was achieved after 30 minutes. Both, EXAFS- and TRLF-spectroscopic analyses showed that the accumulated U(VI) was complexed mainly through organic phosphate groups. The EXAFS measurements revealed that U(VI) is coordinated to the organic phosphate ligands of the archaeal cells in a monodentate binding mode with an average U-P bond distance of 3.60 ± 0.02 Å.

INTRODUCTION

Environments with increased uranium (U) concentrations such as U mining and processing sites are of a serious public concern due to the considerable chemical and radiological toxicity (depending on ^{235}U enrichment) of this actinide. The mobility and toxicity of U in these environments are strongly influenced by a complex of geochemical and biotic factors [19, 78]. Microorganisms present in such habitats can influence the migration behaviour of U by both, direct enzymatic processes such as oxidation [22, 23] and reduction [30, 177] as well as by indirect processes such as biosorption [83, 178], passive uptake [82, 178, 179], and biomineralization *via* bacteria-secreted ligands [70, 84, 89]. Most of the studies on microbial interactions with U were focused so far on bacteria and only a few cases of such interactions with representatives of the third domain of life, *Archaea*, are published [31, 178]. Archaea were shown to be present in various soil and water ecosystems and they play an important role in the global cycles of matter [79]. They differ in many aspects from bacteria and their cell walls are significantly simpler than those of bacteria [80]. For example, the cell wall of *S. acidocaldarius*, studied in this work, consists only of a membrane-anchored proteinaceous surface layer (S-layer), which is glycosylated [80, 180]. The typical structures of the bacterial cell walls known to bind uranium, like the outer-membrane lipopolysaccharide layers rich on phospholipids and short peptides (Gram-negative bacteria), or the thick multiple peptidoglycan layer, consisting of sugar derivatives, a particular small group of amino acids, and containing also secondary polymers such as teichoic acid (Gram-positive bacteria) [157] are missing in this crenarchaeon.

The knowledge about the interaction mechanisms of archaea with uranium is rather limited. It was found that the hyperthermophilic crenarchaeon *Pyrobaculum islandicum* is able to reduce U(VI) to under anaerobic conditions at 100 °C [31]. This high temperature is, however, not relevant for the uranium mining and processing wastes. Francis and co-workers [178] demonstrated that the halophilic euryarchaeon *Halobacterium halobium* accumulates high amounts of U(VI) as dense extracellular uranyl phosphate deposits. This halophilic extremophile is, however, restricted to grow only in hypersaline environments and it is not relevant for the natural habitats contaminated with uranium. The studied in this work thermoacidophilic crenarchaeon *S. acidocaldarius* DSM 639 was originally isolated from geothermal springs [76] and it grows optimally at 79 °C and at pH between 2 and 3. Representatives of this species are, however, rather adaptive and they were found in a range of different habitats. Their presence was demonstrated, for instance, also at moderate temperatures in heavy metal-contaminated acidic soils [181] and in self-heating acidic coal

piles as well [182]. *S. acidocaldarius* is a facultative autotrophic organism which is involved in sulphur oxidation and bioleaching of pyrite at temperature and pH optima of 65 °C and 1.5, respectively [183]. It was demonstrated that cultures of this organism do not change dramatically their cell size or DNA content when the temperature is changed from 79 °C to room temperature and that they “conserve” their ability to continue their growth when returned to the optimal temperature [184].

The robustness and the ubiquitous distribution of *Sulfolobus acidocaldarius* in heavy metal-contaminated soils and mining piles lays in the rationale of this work which represents the first effort to study the role of archaea on U(VI) behaviour in uranium mining wastes.

EXPERIMENTAL

Archaeal strain, growth conditions, and cell preparation for the U-treatments

S. acidocaldarius DSM 639 was purchased from the “Deutsche Sammlung von Mikroorganismen und Zellkulturen” (DSMZ), Braunschweig, Germany. The strain was grown at 70 °C under heterotrophic conditions in Allen’s mineral salt medium [185] supplemented with 0.1% Bacto™ tryptone and 0.005% Bacto™ yeast extract (Becton, Dickinson and Company, Sparks, USA) and adjusted to a pH of 2.5. The archaeal cells were harvested at the end of the exponential growth phase ($OD_{600} \sim 0.45$), by centrifugation for 15 min at room temperature and 10000 g. Two parallel portions of the collected biomass were rinsed twice with 0.1 M solution of the background electrolyte ($NaClO_4$) with pH of 1.5 or 3.0. Afterwards the cells were suspended in the corresponding electrolyte solution; the pH of the cell suspensions was checked and if necessary adjusted to the required value. Before the addition of uranium, the biomass was pelleted *via* centrifugation and then suspended in 0.5 mM $UO_2(NO_3)_2$ diluted in 0.1 M $NaClO_4$ solutions with the corresponding pH (1.5 or 3.0).

Tolerance to U(VI) and other heavy metals

For determination of the tolerance of *S. acidocaldarius* DSM 639 to U(VI) the strain was grown in a modified Allen’s mineral salt medium [185], where the pH was decreased to 2.0 and KH_2PO_4 of the medium was replaced by 500 mg/L KCl to avoid formation of insoluble uranyl phosphate complexes. Yeast extract was omitted as well in order to prevent the complexation of U(VI) by undefined organic matter. Uranium was added as uranyl nitrate.

The tolerance of the studied strain to Cd, Co, Cr, Cu, Ni, Pb, and Zn was studied at the same conditions and compared to that of U(VI). The mentioned heavy metals were added to the medium as nitrate salts. As a control for the influence of nitrate on the archaeal growth magnesium nitrate was used. All experiments were run for seven days in triplicate and the cell growth was monitored microscopically and also by measuring the optical density at 600 nm. The minimal inhibitory concentration (MIC), which defines the lowest concentration that completely inhibits the growth of the strain, was determined for each metal studied.

U(VI) biosorption

The biosorption experiments were performed in two parallel series at pH 1.5 and 3.0. For this, different amounts of *S. acidocaldarius* DSM 639 biomass (between 1 and 55 mg) equilibrated to pH 1.5 or 3.0 in 0.1 M NaClO₄ as described above, were incubated in triplicate for 48 hours on a rotary shaker with 10 ml of a 0.5 mM uranyl nitrate solution diluted in 0.1 M NaClO₄ and possessing the corresponding pH. At these conditions almost 99% of the total uranium is represented by the soluble uranyl ion species. The amount of the accumulated uranium was normalized to the dry biomass, determined by weighting identically prepared samples after drying for 48 hours at 70 °C. Kinetic studies were performed also in triplicate, using a biomass concentration of (0.5 ± 0.05) g/L. After defined incubation periods at room temperature the cells were removed from the uranium solution by centrifugation and the unbound U(VI) in the supernatant was measured by inductively-coupled-plasma mass-spectroscopy (ICP-MS) using an Elan 9000 system (Perkin Elmer, USA). Control samples without cells were treated in the same way to exclude abiotic uranium removal from the solution, due to precipitation and/or chemical sorption at the used test vials.

X-ray Absorption Spectroscopy (XAS)

For XAS measurements, 50 mg of the cells were contacted for 48 hours with U(VI) in an analogous way as those used in the sorption studies. After the contact with U(VI) the cells were washed twice with 0.1 M NaClO₄ at pH 1.5 or 3.0, respectively. Subsequently they were dried for three days at 35 °C in a vacuum oven (Model VT 6025, Heraeus-Instruments Vacutherm, Germany). Afterwards the samples were powdered and mounted on a Kapton tape. Six layers of sample-covered tape were stuck on top of each other and subsequently wrapped.

Uranium *L*_{III}-edge X-ray absorption spectra were collected at the Rossendorf beamline at the European Synchrotron Radiation Facility (ESRF), Grenoble (France) [134] using a Si(111)

double-crystal monochromator, and Si-coated mirrors for focusing and rejection of higher harmonics. The data were collected in fluorescence mode using a 13-element germanium detector. Six to eight spectra of each sample were recorded. The energy was calibrated by measuring the yttrium (Y) *K*-edge transmission spectrum of an Y foil and defining the first inflection point as 17038 eV. Subsequently, dead-time correction was applied. The region from about 45 eV below to 60 eV above the absorption edge of each scan was isolated for the X-ray near edge structure (XANES) analysis. The EXAFS oscillations were isolated from the raw, averaged data by removal of the pre-edge background, approximated by a first-order polynomial, followed by μ_0 -removal *via* spline fitting techniques and normalisation using a Victoreen function. The ionisation energy for U L_{III} -electron, E_0 , was arbitrarily defined as 17185 eV for all averaged spectra. The EXAFS spectra were analysed according to standard procedures using the program EXAFSPAK [135]. The theoretical scattering phase and amplitude functions used in data analysis were calculated using FEFF8.2 [136] and using the crystal structure of meta-autunite, $\text{Ca}(\text{UO}_2\text{PO}_4)_2 \cdot 6 \text{H}_2\text{O}$ [186]. All fits included the four-legged multiple scattering (MS) path of the uranyl group, $\text{U-O}_{\text{ax}}\text{-U-O}_{\text{ax}}$. The coordination number (N) of this MS path was linked to N of the single-scattering (SS) path U-O_{ax} . The radial distance (R) and Debye-Waller factor (σ^2) of the MS path were linked at twice the R and σ^2 of the SS path U-O_{ax} , respectively [137]. During the fitting procedure, N of the U-O_{ax} SS path was held constant at two. The amplitude reduction factor was held constant at 1.0 for FEFF8.2 calculation and EXAFS fits. The shift in threshold energy, ΔE_0 , was varied as a global parameter in the fits.

Time-Resolved Laser-induced Fluorescence spectroscopy (TRLFS)

For the TRLFS-measurements of the U(VI) complexes built by the cells of the studied archaeal strain small portions of the powdered XAS samples were used. Additionally U(VI) treated and subsequently washed archaeal cells were suspended in NaClO_4 (pH 1.5 or 3) and used for U(VI) luminescence measurements in solution. The samples were placed in a quartz micro cuvette and TRLFS measurements were performed at room temperature by using home assembled equipment [187]. The uranium luminescence was excited by a pulsed Nd-YAG laser (GCR 190, Spectra Physics, USA) coupled with an optical parametric oscillator module (MOPO-730, Spectra Physics, USA) tuned to an output wavelength of 410 nm and a relatively low intensity of about 300 μJ to avoid damages of the samples. The luminescence signal was measured perpendicularly to the laser beam and transmitted *via* a fibre optic cable

to the ICCD detection system, consisting of a triple-grating spectrograph (M1235, EG&G, USA) equipped with an intensified charge-coupled-device detector and a data acquisition program. U(VI) spectra were recorded between wavelengths of 444 nm and 594 nm. The central wavelength of the spectrograph was set to 520 nm and the gate width was 5 μ s. Before each series of measurements the background luminescence was measured 2 Ms after the laser pulse and automatically subtracted from the spectra.

After excitation of the samples by 50 (pH 3.0) and 80 (pH 1.5) laser pulses, respectively, depending on the amount of uranium in the samples, three luminescence spectra were recorded. For each series of measurement 101 single spectra were recorded. For an accurate determination of the uranium luminescence lifetime(s) two series of measurements were performed for each sample. One of them was performed with a step size of 200 ns to determine uranium species exhibiting short luminescence lifetimes. For the determination of longer luminescence lifetimes another series was recorded. To calculate the step size of the delay time for this second series, we determine the delay time, at which the complete U(VI) luminescence had faded away. One percent of that delay time was calculated and set as step size for the second measurement. The obtained luminescence data were processed by using Origin 7.5 (OriginLab Corporation, Northampton, MA, USA) including the PeakFit module 4.0.

RESULTS AND DISCUSSION

Tolerance of *S. acidocaldarius* DSM 639 to U(VI) and other heavy metals

The strain *S. acidocaldarius* DSM 639 was able to grow in presence of U(VI) up to a uranium concentration of 1.1 mM. The MIC of uranium for the strain was determined to be 1.25 mM uranium (Table 2.1). The MICs for Ni (0.5 mM) as well as for Cr and Cu (1 mM for both metals) were slightly lower, while those for Zn and Cd were substantially higher (2 and 5 mM, correspondingly). However, Co and Pb, inhibited the cell growth at very low concentrations with MICs of 0.05 and 0.03 mM, respectively.

As evident from the data summarized in Table 2.1, the MICs for Cd, Cu and Ni are comparable to the already published values [188, 189]. However, some of the MICs found in the literature differ significantly between each other and also from our results, e.g. the MICs for Co, Pb and Zn. In the quoted papers, however, *S. acidocaldarius* DSM 639 was cultivated under conditions which differed from those used in our work. The pH was slightly higher (between 3.0 and 3.3) and the temperature for growth in one of the cases was 78 °C [189]

instead of 70 °C; in both cases KH_2PO_4 was not replaced by KCl in the mineral growth medium, and different carbon sources than those used in our work were added: 0.2% tryptone [188] or 0.1% yeast extract and 0.2% sucrose [189]. Miller and co-workers [189] have studied two additional *S. acidocaldarius* strains which showed up to 10 times different tolerances to Zn, Co, and Ni. These results indicate that the heavy-metal tolerance of *S. acidocaldarius* depends on the experimental conditions, such as pH, growth temperature, ionic strength and the composition of the growth medium, and that it may be even strain-specific.

Table 2.1. Minimal inhibitory concentration of tested heavy metals for the growth of *S. acidocaldarius* DSM 639.

Heavy metal	Tolerated concentration (mM)	MIC (mM)	MIC (mM) [188]	MIC (mM) [189]
UO_2^{2+}	1.1	1.25	-	-
Cd^{2+}	3.0	5.0	2.0	10
Co^{2+}	0.03	0.05	^a	1.0
Cr^{3+}	0.9	1.0	-	-
Cu^{2+}	0.9	1.0	5.0	1.0
Ni^{2+}	0.4	0.5	0.6	0.1
Pb^{2+}	0.01	0.03	1.6	-
Zn^{2+}	1.5	2.0	50	10
Mg^{2+}	10	-	-	100

^a MIC not defined (no significant inhibition by Co^{2+} detected)

- not measured

The tolerance of *S. acidocaldarius* DSM 639 to the heavy metals tested in our work, decreased in the order $\text{Cd} > \text{Zn} > \text{U} > \text{Cr/Cu} > \text{Ni} > \text{Co} > \text{Pb}$. Miller and co-workers [189] suggested that the toxicity of heavy metals on this strain might exclusively result from the strength of the metal binding and therefore it should follow the order of the Irving-Williams series [190]. In that case uranium should be most toxic to the cells, as the free uranyl ion forms most stable complexes among the tested metals [191]. Our data, in particular the higher tolerance to U(VI) than to nickel, cobalt, and lead refute this claim and indicates inherent mechanisms for the interaction of the tested individual metals with the strain.

The U(VI) tolerance of *S. acidocaldarius* is significantly lower than those described for representatives of acidophilic bacteria; for instance, the MICs determined for some strains of *Acidithiobacillus ferrooxidans* were up to 9 mM U(VI) [192]. The low tolerance of *S. acidocaldarius* to Cu was earlier attributed to the lower amount of inorganic polyphosphate in its cells in comparison to many other microorganisms [193]. It was demonstrated that in bacteria the detoxification of most bivalent cations, up taken in poisonous concentrations

inside the cells, goes through complexation by the polyphosphate bodies and cleavage of phosphate-metal complexes, which then efflux outside the cells [194, 195]. The here observed low tolerance of *S. acidocaldarius* DSM 639 to Co^{2+} , Ni^{2+} , and Pb^{2+} along with those to Cu^{2+} , is likely due to the low intrinsic amount of polyphosphate bodies in the strain. A different mechanism of bacterial tolerance to uranium was published by Renninger and co-workers [89]. The authors demonstrated that in the case of *Pseudomonas aeruginosa* orthophosphate residues, released from the cells, are involved in the complexation of U(VI) from the uranium hydroxides, adsorbed initially on the cell surface [89]. Because the secreted orthophosphate may originate not only from the polyphosphate bodies of the cells it is not excluded that the tolerance to U may be higher than those to some bivalent cations. These results indicate that the mechanisms underlying microbial interactions with U(VI) differ significantly from those responsible for detoxification of bivalent cations.

The higher tolerance of *S. acidocaldarius* DSM 639 to U(VI) than to the bivalent cations Cu, Co, Ni and Pb might be explained by the different interaction mechanisms of its cells with these two groups of elements. Studies in our laboratory on the interaction of *S. acidocaldarius* DSM 639 with U(VI) at pH values of 4.5 and 6.0, which are above the physiological optimum of the strain, clearly demonstrated extracellular precipitation of inorganic uranyl phosphate phases (Chapter III) [164].

U(VI) biosorption

The U(VI) binding capacity of *S. acidocaldarius* DSM 639 at the studied acidic conditions is presented in Figure 2.1. As evident from the results presented in the figure the amount of uranium accumulated by the strain strongly depends on the biomass concentration. The negative correlation between these two parameters is explained by the occurrence of agglomeration of the microbial cells at higher biomass concentrations which reduces the cell surface contacting with U(VI) that results in decreasing the number of the uranium-binding ligands. The agglomeration process at high cell densities was confirmed by microscopic analyses (not shown). The optimal binding of U(VI) was achieved at biomass concentrations between 0.25 g/L and 0.5 g/L.

For kinetic studies we used a biomass concentration of (0.5 ± 0.05) g/L. The analyses demonstrated a rapid complexation of uranium by the cells (Fig. 2.1), which is a typical feature of the biosorption process at functional groups on the cell surface [19]. About half of the binding capacity was already reached after an incubation of five minutes and after 30 minutes nearly total saturation of the binding sites was reached. Considering the data as

due to a biosorption process by the functional groups at the cell surface, which mainly takes place within the first minutes to an hour of incubation, the cells of *S. acidocaldarius* adsorbed between 15 and 17 mg uranium per gram dry biomass within the first hour of incubation at pH 1.5 and 3.0, respectively (Fig. 2.2). The binding capacity of the cells after an incubation of 120 hours was determined to be nearly identical – 18 mg U/g_{dry biomass} and 22 mg/g_{dry biomass} at pH 1.5 and 3.0, respectively.

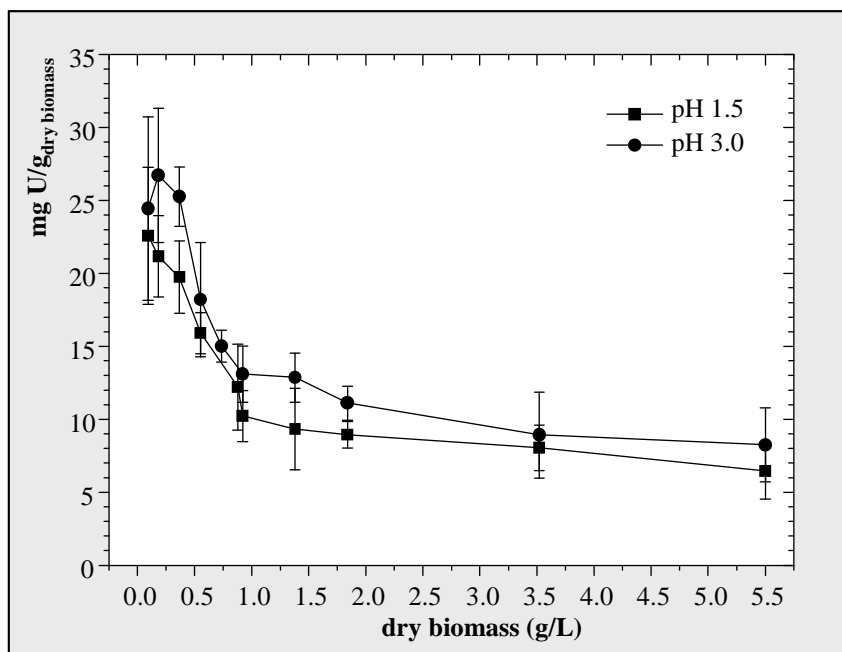


Figure 2.1. U(VI) accumulation by the cells of *S. acidocaldarius* DSM 639 after 48 hours at pH values of 1.5 and 3.0 as a function of biomass concentration; $[U]_{\text{init}} = 0.5$ mM.

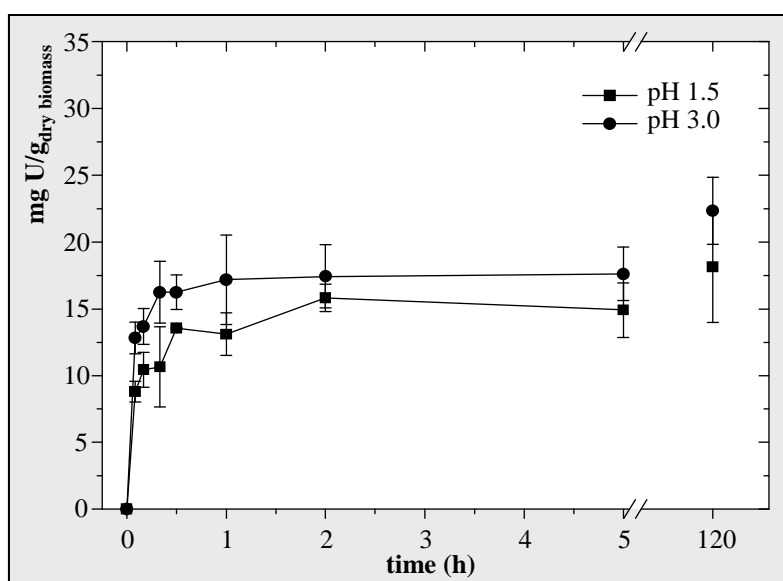


Figure 2.2. Kinetics of the U(VI) accumulation by the cells of *S. acidocaldarius* DSM 639 at pH 1.5 and 3.0 (biomass concentration = 0.5 ± 0.05 g/L and $[U]_{\text{init}} = 0.5$ mM).

A comparison of the determined U(VI) binding capacity of *S. acidocaldarius* DSM 639 to those obtained for bacteria is difficult because of the differences of the experimental parameters, such as pH, uranium and biomass concentrations, and ionic strength, which influence the binding capacity. However, considering all these parameters, it is obvious that most bacterial strains possess significantly higher binding capacities than the cells of the studied here archaeon. Hu and co-workers [196] demonstrated that *Pseudomonas aeruginosa* CSU possesses a capacity to bind about 100 mg U/g dry biomass at pH 2.4 within the first minutes of the treatment with uranyl nitrate. Another *Pseudomonas* strain was shown to accumulate about 60 mg U/g dry biomass at pH 3.5 within one hour [102]. The high uranium binding capacity of bacteria is attributed to their complex cell wall structures, which are rich on uranium-binding ligands [157]. The only cell wall component of *S. acidocaldarius* is its cytoplasmic membrane-anchored proteinaceous surface layer (S-layer) [80, 180]. Because of the low content of negatively charged amino acids (1.2 mol% aspartate and 1.8 mol% glutamate) and especially because of the absence of phosphorylated sites, this glycoprotein should be almost ineffective in uranium complexation at the studied acidic conditions. As demonstrated earlier, uranium can pass through the pores of the S-layer lattices and can be complexed by the reactive groups of the underlying biopolymers [150]. As in the case of *S. acidocaldarius* no outer membrane or peptidoglycan compounds are present, the cytoplasmic membrane is the only source offering phosphate, carboxyl, amine, or hydroxyl groups for U(VI) complexation and protection of the cells from poisoning.

XAS studies

XANES analyses of the uranium in the investigated samples showed a peak at 17,188 eV (data not shown) which can be assigned to U(VI) [137]. This finding indicates that the U(VI) added to the samples was not reduced to U(IV).

The measured U L_{III} -edge k^3 -weighted EXAFS spectra of the uranium-treated cell samples and their corresponding Fourier transforms (FT) are shown in Figure 2.3, along with the best fits. The EXAFS spectrum of one relevant model compound containing organic phosphate (UO₂-fructose(6)phosphate) is shown in the figure as well [158]. The structural parameters obtained from the fitting procedure are summarised in Table 2.2. The results indicate that at both conditions studied (pH 1.5 and 3.0) the adsorbed U(VI) has the common linear trans-dioxo structure: two axial oxygen atoms at a distance of about 1.77 to 1.78 Å (FT peak at $R+\Delta \sim 1.3$ Å), and an equatorial oxygen shell at 2.30 to 2.35 Å (FT peak at $R+\Delta \sim 1.8$ Å).

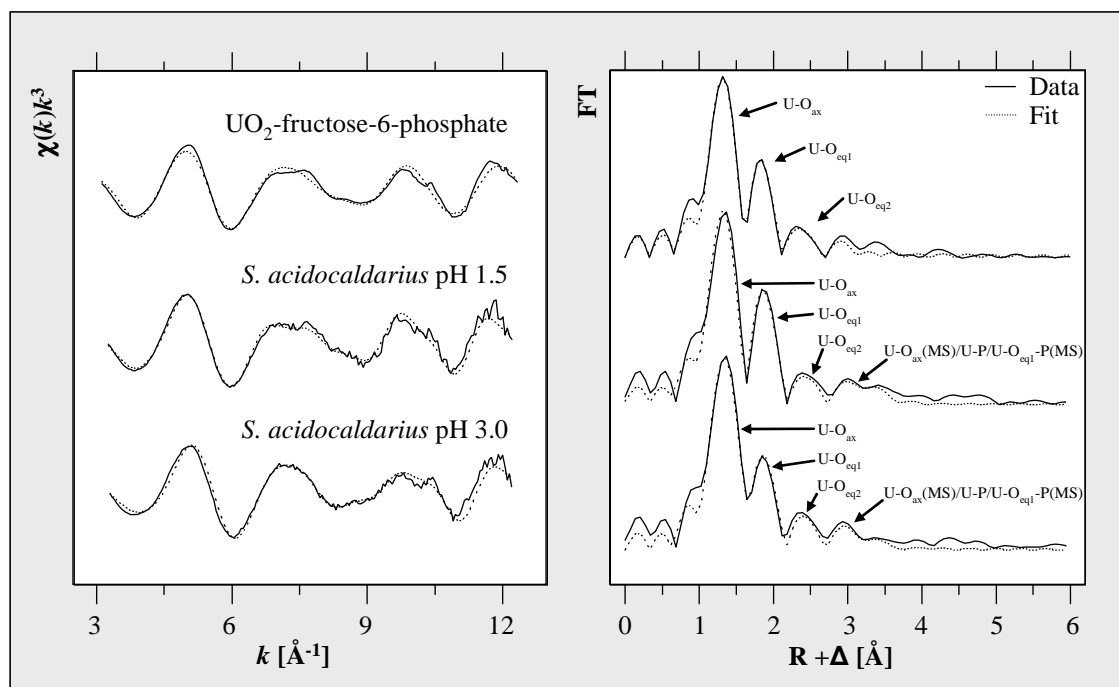


Figure 2.3. U L_{III} -edge k^3 -weighted EXAFS spectra (left) and the corresponding Fourier transforms (right) of the uranium complexes formed by *S. acidocaldarius* DSM 639 at pH values of 1.5 and 3.0 and of the model compound UO_2 -fructose(6)phosphate [158].

The FT peak, which appears at $R+\Delta \sim 3 \text{ \AA}$ consists of the contribution of the $U-O_{ax}$ multiple scattering path and the back-scattering of phosphorus atoms. This distance is typical for a monodentate coordination of U(VI) by phosphate [169]. The phosphate groups implicated in the coordination of U(VI) at the studied acidic condition (pH 1.5 and 3.0) seems to have predominantly organic origin since the EXAFS spectra shown in Figure 2.3 share a high similarity with the spectrum of UO_2 -fructose(6)phosphate [158].

In both samples, the addition of a shell of one oxygen scatter at a distance of $R = 2.86$ or 2.88 \AA ($U-O_{eq2}$) improve significantly the fit. Such a distance between uranium and oxygen atoms is not related to direct bonding but they are interpreted in several systems as scattering contributions from neighboring ligand shells known as “short contacts” in crystallography [82, 84].

The structural parameters of the U(VI) complexes formed by *S. acidocaldarius* at pH 1.5 and 3 are similar to those formed at corresponding pH conditions by different bacterial strains belonging to the Gram-positive [84] and Gram negative [82] bacteria. These structural similarities indicated that at highly acidic conditions (pH ranging between 1.5 and 3) the local coordination of U complexes formed by the microbial cells is universal and independent from microbial domain. In all cases, studied at these acidic pH values, U(VI) was coordinated in a monodentate binding mode with an average U-P bond distance of about 3.60 \AA . Because at

these conditions the carboxylic groups exist mainly in the protonated form [155], their interactions with U(VI) are excluded.

Table 2.2. Structural parameters of the uranium complexes formed by the cells of *S. acidocaldarius* DSM 639.

Sample	Shell	N ^a	R [Å] ^b	σ^2 [Å ²] ^c	ΔE_0 (eV)
pH 1.5	U-O _{ax}	2.0 ^d	1.77(1)	0.0022(2)	-12.0(6)
	U-O _{eq1}	3.9(3)	2.35(1)	0.0066(7)	
	U-O _{eq2}	1.2(2)	2.87(1)	0.0038 ^d	
	U-P	4.6(5)	3.62(1)	0.0080 ^d	
	U-O _{eq1} -P (MS)	9.2 ^e	3.74 ^f	0.0080 ^d	
pH 3.0	U-O _{ax}	2.0 ^d	1.78(1)	0.0023(2)	-13.4(7)
	U-O _{eq1}	4.1(4)	2.30(1)	0.0047(5)	
	U-O _{eq2}	1.2(2)	2.86(1)	0.0038 ^d	
	U-P	3.3(6)	3.59(2)	0.0080 ^d	
	U-O _{eq1} -P (MS)	6.6 ^e	3.70 ^f	0.0080 ^d	
UO ₂ -fructose(6)P [158]	U-O _{ax}	2.0 ^d	1.77(1)	0.0013(10)	0.1(7)
	U-O _{eq1}	4.8(5)	2.30(1)	0.020(4)	
	U-O _{eq2}	1.3(2)	2.88(1)	0.0040 ^d	

Standard deviations as estimated by EXAFSPAK are given in brackets

^a Errors in coordination numbers are $\pm 25\%$

^b Errors in distance are ± 0.02 Å

^c Debye-Waller factor

^d Parameter fixed for calculation

^e Coordination number (N) linked twice to the N of the U-P path.

^f Radial distance (R) linked to R of the U-P path, according to the model of m-autunite.

Time-resolved laser-induced fluorescence spectroscopic studies

In order to verify the results obtained by EXAFS, parallel samples of the *S. acidocaldarius* DSM 639 cells treated with U(VI) were analysed by a complementary and very sensitive method allowing discrimination between different ligands implicated in the uranium binding, namely TRLF-spectroscopy. The TRLFS analysis of the samples treated with uranium demonstrated three strong and almost identical emission bands at 498.3, 520.3 and 543.6 nm (pH 1.5) and at 498.7, 520.0 and 543.6 nm (pH 3.0) (Fig. 2.4 and Table 2.3). The red shift of about 10 nm in the emission bands compared to those of the free uranyl ion (Fig. 2.4 and Table 2.3), which is the predominant (> 99%) uranium species in the added uranium solutions (Table 1), indicates that the added U(VI) was complexed by the archaeal cells. As evident from the data presented in Table 2.3 the luminescence emission maxima of the uranium complexes formed at pH 1.5 and 3.0 correspond well to those determined from the complexation of U(VI) by various organic phosphate compounds such as sugar phosphates [169], phospholipids [161] as well as lipopolysaccharides [163]. In addition, similar emission

maxima were also found in the TRLFS studies of the uranium complexes build by the acidophilic bacterial strain *A. ferrooxidans* [159].

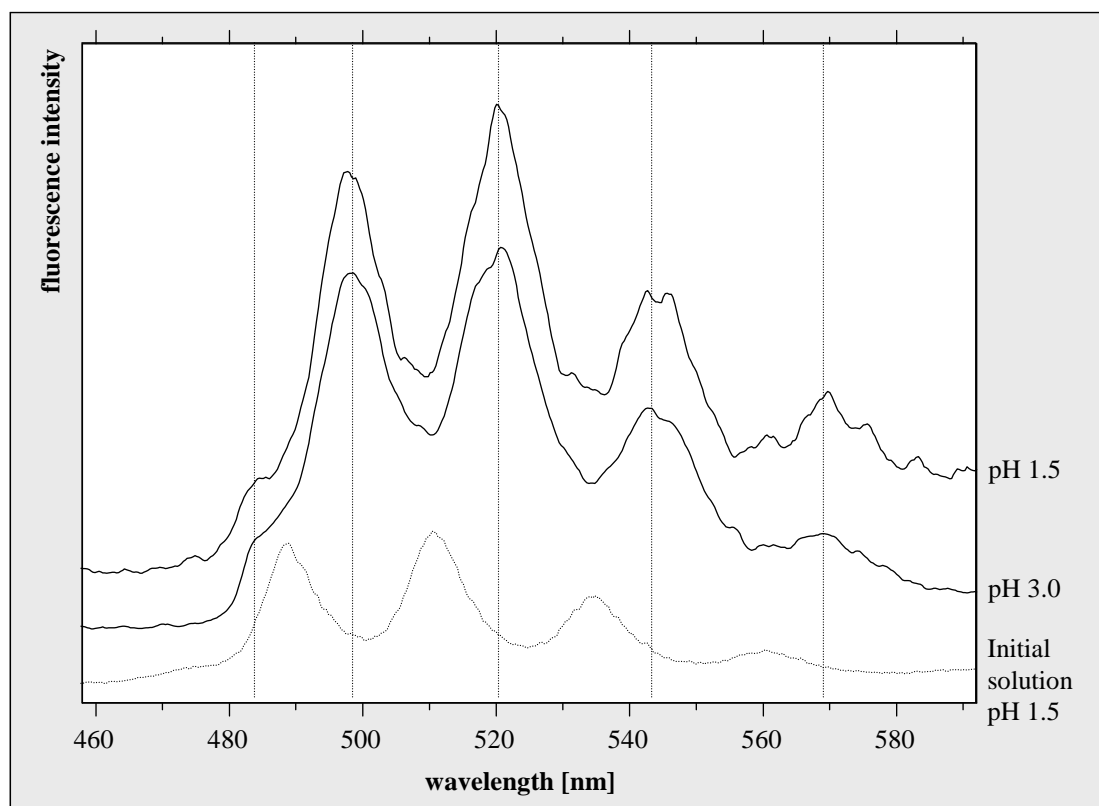


Figure 2.4. Luminescence spectra of the uranium complexes built by *S. acidocaldarius* DSM 639 at pH 1.5 and 3.0.

Besides the position of the emission maxima the decay of the luminescence was used to distinguish the uranyl species present in the treated cell samples. The luminescence lifetimes were determined by using the function $I(t) = I_0 + \sum I_i * \exp(-t/\tau_i)$ where I_0 is the background signal, measured after a delay time of 2 ms, I_i the signal factors of the uranium compounds, τ_i the corresponding luminescence lifetime and t the delay time. The time-resolved studies of the initial uranium solutions revealed in both solutions a mono-exponential luminescence decay. The determined lifetimes were $1.92 \pm 0.12 \mu\text{s}$ and $2.01 \pm 0.19 \mu\text{s}$ at pH 1.5 and 3.0, respectively, which are in accordance with the luminescence lifetime of the free uranyl ion, determined in former studies [165, 197]. Lifetime analyses of both cell samples, incubated at pH 1.5 and 3.0, demonstrated a tri-exponential decay of the uranium luminescence indicating a mixture of three different luminescent uranium species, respectively (Table 2.4).

Table 2.3. Main U(VI) luminescence emission maxima of the uranium complexes build by *S. acidocaldarius* DSM 639 and those of some model compounds, as well as U-Bacteria complexes for comparison.

Sample	Main luminescence emission maxima ^a			Lifetime(s) (μs)
UO ₂ ²⁺ (Initial solution, pH 1.5)	489.5	511.0	534.3	1.92 ± 0.12
U(VI) + <i>S. acidocaldarius</i> pH 1.5	498.3	520.3	543.6	Table 2.4
U(VI) + <i>S. acidocaldarius</i> pH 3.0	498.7	520.0	543.6	Table 2.4
Uranyl phosphoryl complexes				
UO ₂ -DMGP [161]	497.4	519.3	542.4	1.0 ± 0.1; 20 ± 2
UO ₂ -fructose(6)phosphate [158]	497.1	519.0	543.3	0.13 ± 0.05
UO ₂ -AMP [192]	497	519	542	n.d.
Lipopolysaccharide complexes [163]				
R-O-PO ₃ H-UO ₂ ⁺	497.2	518.9	542.4	8.3 ± 0.6
R-O-PO ₃ -UO ₂	498.1	519.6	542.9	1.2 ± 0.4
[R-O-PO ₃] ₂ -UO ₂ ²⁻	499.7	521.0	544.3	13.3 ± 1.4
Bacteria [159, 198]				
<i>Acidithiobacillus ferrooxidans</i> ATCC 33020	496.3	517.5	541.6	45 ± 4 3.9 ± 0.4

^a Error of emission bands is ± 0.5 nm**Table 2.4.** Calculated U(VI) luminescence lifetimes.

	pH 1.5	pH 3.0
Species 1 (τ ₁)	0.36 ± 0.05 μs	0.55 ± 0.04 μs
Species 2 (τ ₂)	2.80 ± 0.21 μs	3.79 ± 0.40 μs
Species 3 (τ ₃)	35.3 ± 9.7 μs	35.9 ± 4.6 μs

The calculated lifetimes of the uranium luminescence in these samples indicate one very short lifetime of 0.36 and 0.55 μs, a second lifetime of 2.8 and 3.8 μs at pH 1.5 and 3.0, respectively, and a third notably longer lifetime of about 35 μs. However, fitting procedures of the emission maxima after different delay times demonstrated no shift of the luminescence bands, indicating a high structural similarity of the formed complexes.

The short lifetimes of 0.36 μs and 0.55 μs calculated for the two samples (pH 1.5 and 3.0) indicate a quenching of the uranyl luminescence by an intra-molecular energy transfer from the radionuclide to low laying electronic states of the binding ligands exhibiting polyelectrolyte and aromatic structures [198]. Comparable short lifetimes were found for the

complexation of U(VI) with organic phosphate ligands (Table 2.3) [163, 169]. The second lifetime of about 3 μ s agrees well with the luminescence lifetimes calculated earlier in our laboratory for the organic phosphate complexes build by acidophilic strains of the bacterial species *A. ferrooxidans* and *Thiomonas cuprina* [198]. Several years later significantly higher luminescence lifetimes of about 25 or 45 μ s were measured for the organic uranyl phosphate complexed formed by the strains of *A. ferrooxidans* [159]. These lifetimes correspond to the here measured lifetime of 35 μ s. The formerly measured lifetimes of the organic uranyl phosphate complexes, formed by the same bacterial strains of *A. ferrooxidans*, differed by a factor of ten between the two mentioned studies [159, 198]. It is interesting that in the present work the TRLF analyses of the uranium complexes, build by the archaeal strain *S. acidocaldarius* DSM 639 revealed both, the uranyl phosphate species with the short and those with the long lifetime in the same sample. The occurrence of different lifetimes in the two former studies, was attributed to the significant differences in the experimental conditions as for instance, the concentration of the HClO₄ solution and the amounts of the biomass treated [159]. Indeed, a comparison of the respective experimental set-up most likely explains the different results found in the two previous studies [159, 198] and also in this study. In contrast to the above mentioned two studies [159, 198], NaClO₄ instead of HClO₄ was used in the treatments with U(VI). However, the most relevant difference might be the ratio of uranium to biomass, which differs significantly between these three studies: 0.5 mM U/0.1 g dry biomass/L [159], 0.05 mM U/0.27 g dry biomass/L [198] and 0.5 mM/0.5 g dry biomass/L (this work). Thus Merroun and co-workers [159] used 5 times more uranium related to the biomass as in our study, whereas Panak and co-workers [198] used about 5 times less uranium related to the biomass concentration. As found by Koban and Bernhard [161] the occurrence of different lifetimes can be explained by the formation of uranyl complexes with different metal-to-ligand ratio, as it was demonstrated for the 1:1 and 1:2 uranyl-lipopolysaccharide complexes (Table 2.3) [163]. According to this, the U(VI) luminescence lifetimes found in the three studies [159, 198], this work] can be explained by the formation of two organic uranyl phosphate species, differing in the number of phosphate groups coordinated to the U(VI) ion. The data suggest that the formation of these two complexes strongly depends on the ratio of uranium to the biomass. At low U:biomass ratio preferentially uranyl phosphate complexes exhibiting a lifetime of about 3 μ s are build [198] whereas at higher U:biomass ratios formation of the long-living (25 to 45 μ s) complexes is

advanced as well (this study). At further increased ratios the long-living complexes are built exclusively [159].

To proof that the drying procedure involved in the preparation of the samples did not change the speciation of the formed uranium complexes, we also performed TRLF spectroscopic analyses of the uranium-treated cells in solution. The luminescence spectra recorded after selected delay times from the sample incubated at pH 3.0, representative for both samples, is presented in figure 2.5. In contrast to the solid samples, we observed a significant red shift of the luminescence emission maxima with increasing the delay time in the liquid samples. This observation can be explained by desorbed uranium, which was weakly bound to the cell surface functional groups. The released uranyl ions are highly luminescent and as above mentioned they exhibit emission maxima which are located at about 10 nm lower wavelengths than those of the uranium complexes build by the archaeal cells (Fig. 2.4 and Table 2.3).

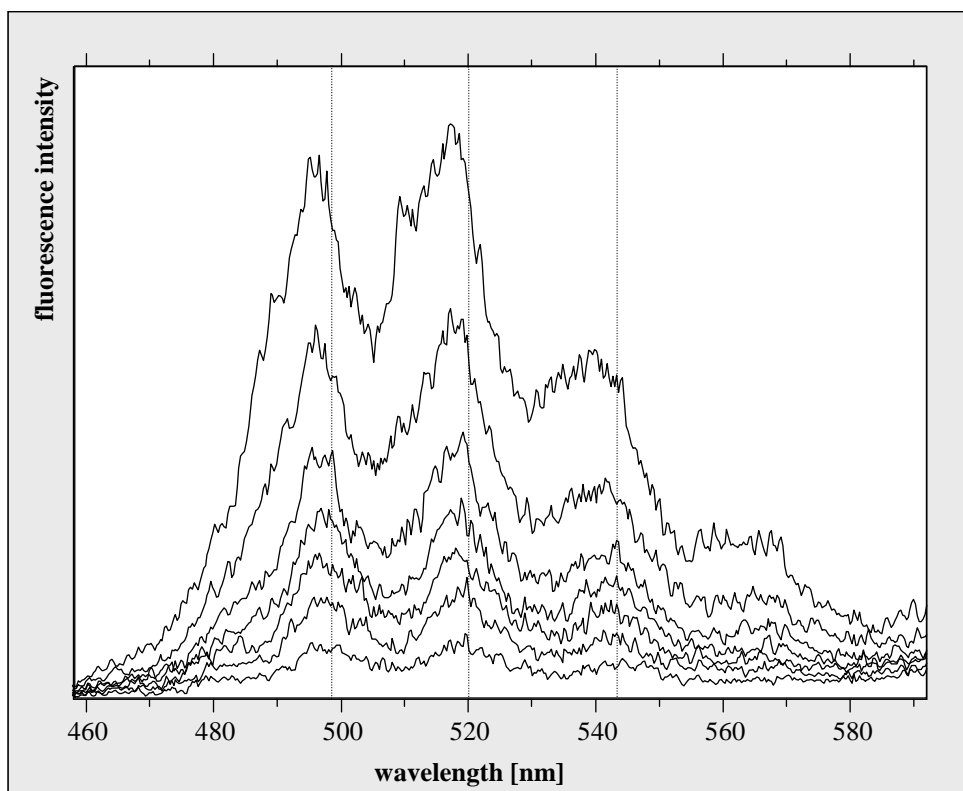


Figure 2.5. U(VI) luminescence spectra recorded after different delay times (0.1 μ s, 3 μ s, 6 μ s, 9 μ s, 12 μ s, 15 μ s, 25 μ s – from top to the bottom) from cell suspensions of *S. acidocaldarius* DSM 639, treated with U(VI) at pH 3.0. Dotted lines indicate the position of the luminescence emission maxima calculated from the corresponding solid sample for comparison.

The overlapping luminescence of the formed uranium complexes and the released uranyl ions causes a shift of the emission maxima to lower wave length and therewith hindered a proper

determination of the luminescence emission maxima of the formed uranium complexes in the solutions. Because the free uranyl ion has a luminescence lifetime of about 2 μs its influence on the total luminescence spectrum decreases with increasing delay times. For this reason it was possible to measure accurately the luminescence emission maxima of the complexes exhibiting long luminescence lifetimes (Fig. 2.5 and Table 2.5).

Table 2.5. U(VI) luminescence emission maxima determined after different delay times from cell suspensions of *S. acidocaldarius* DSM 639, treated with U(VI) at pH 3.0.

Delay time	Main luminescence emission maxima [nm]		
0.1 μs	495.0	515.6	539.5
2.0 μs	495.4	516.3	539.3
6.0 μs	496.6	517.8	541.7
9.0 μs	497.8	518.9	541.7
12 μs	498.0	519.2	542.0
15 μs	498.2	519.1	541.8
25 μs	498.5	519.5	542.4
Solid sample	498.7	520.0	543.6

Time-resolved analyses of the liquid samples demonstrated very similar luminescence lifetimes compared to those of the solid cell samples. The calculated luminescence lifetimes were $0.22 \pm 0.09 \mu\text{s}$, $4.43 \pm 0.98 \mu\text{s}$ and $32.3 \pm 4.0 \mu\text{s}$ at pH 1.5 and $0.24 \pm 0.09 \mu\text{s}$, $5.75 \pm 0.85 \mu\text{s}$ and $36.3 \pm 1.4 \mu\text{s}$ at pH 3.0, respectively. Additionally we found lifetimes of $2.02 \pm 0.28 \mu\text{s}$ and $2.13 \pm 0.23 \mu\text{s}$ in the samples incubated at pH 1.5 and pH 3.0, respectively, which were assigned to the free uranyl ion.

The detection of three different U(VI) luminescence lifetimes in the liquid as well as in the solid samples and the position of the main luminescence emission bands after longer delay times in the liquid samples, strongly suggests that the speciation of the uranium complexes in the solid cell samples is identical to that in solution. Therefore we assume that the use of solid samples is advantageous as it enables a better determination of the luminescence emission maxima of short-living complexes by avoiding the interfering luminescence of the free uranyl ion.

CONCLUSIONS

In this work interactions of U(VI) with the acidothermophilic archaeon *Sulfolobus acidocaldarius* DSM 639 were studied at pH values of 1.5 and 3.0 which are in the range of the physiological optimum of the strain. Our results demonstrate that the strain possesses a rather low tolerance to U(VI) in comparison to the so far studied acidophilic bacteria. The strain is able to accumulate limited amounts of uranium of up to 18 mg U/g dry biomass and 22 mg U/g dry biomass at pH 1.5 and 3.0, respectively. Both, EXAFS and TRLF spectroscopic analyses demonstrate that the complexation of U(VI) by the cells of the archaeon *S. acidocaldarius* DSM 639 at both studied pH values occurs *via* organic phosphate groups.

Chapter III

Biosorption and biomineralization of U(VI) by *Sulfolobus acidocaldarius* at moderate acidic conditions.

Thomas Reitz, Mohamed L. Merroun, Bo Li, Harald Foerstendorf,
Andre Rossberg, Robin Steudtner and Sonja Selenska-Pobell

Published in extract in:

Bioaccumulation of U(VI) by *Sulfolobus acidocaldarius* at moderate acidic conditions.

Thomas Reitz, Mohamed L. Merroun, Andre Rossberg, Robin Steudtner
and Sonja Selenska-Pobell

Radiochimica acta **99**, 543-553 (2011)

ABSTRACT

Microorganisms, along with the abiotic physicochemical factors, strongly influence migration of uranium in nature. In contrast to the well-investigated interactions of bacteria with uranium, the influence of archaea on the natural behaviour of this radionuclide is still not well-studied. In this work the interactions of the acidothermophilic archaeon *Sulfolobus acidocaldarius* with U(VI) at pH 4.5 and 6 were investigated. We demonstrated that at these pH values, U(VI) is rapidly complexed by the archaeal cells. A combination of XAS, FT-IR and TRLFS revealed that at pH 4.5 mainly organic phosphate and carboxylic groups are involved in the U(VI) complexation. These results are in contrast to those published for most bacteria which at this pH usually precipitate U(VI) in inorganic uranyl phosphate phases. As demonstrated by TEM, only a minor part of the added U(VI) is biomineralized extracellularly in the case of the archaeon studied in this work. Most of the U(VI) accumulates were localized in a form of intracellular deposits which were associated with the inner side of the cytoplasmic membrane. The formation of these deposits is attributed to an uncontrolled uptake of U(VI) as a result of the increased cell membrane permeability, most likely caused by the stress of the non-optimal pH and uranium toxicity. Observed differences in U(VI) bioaccumulation between the studied archaeon and bacteria can be explained by the significant differences in their cell wall structures as well as by their different physiological characteristics. After the treatment of the archaeal cells with U(VI) at pH 6, however, a formation of uranyl phosphate mineral phases, as in the case of most bacteria, was observed. Our results demonstrate that at moderate acidic conditions *S. acidocaldarius* immobilizes U(VI) via biosorption and biomineralization processes.

INTRODUCTION

The secure final storage of uranium-containing, radioactive wastes remaining from mining and milling activities, as well as from nuclear energy production is the goal of many international research programs. In particular the consequences resulting from potential release of this highly toxic radioactive heavy metal into the environment are under detailed investigation. For the development of effective remediation strategies of contaminated sites as well as for reliable risk assessment for future repositories, consolidated knowledge about the behaviour of uranium in the environment is necessary. Besides the interactions with inorganic components such as minerals and rocks, microorganisms have been shown to play an important role in the migration behaviour of this radionuclide [19, 98]. A large number of studies were performed to investigate the processes involved in the uranium accumulation by bacterial cells, which mainly involves biosorption [100-102], bioreduction [104], and biomineralization [88, 89]. Moreover, the speciation of the formed uranium complexes and their structural parameters at molecular scale have been determined [83, 84, 154, 199, 200]. However, little is known about the mechanisms of the uranium accumulation and the structural parameters of the uranium complexes formed by representatives of the second microbial domain of life, the “*Archaea*”. Archaea have been shown to be present in various soil and water ecosystems, and they play an important role in the global cycles of matter [79]. They differ in many aspects from bacteria and their cell walls are significantly simpler than those of bacteria. For example, the cell wall of the thermoacidophilic archaeon *Sulfolobus acidocaldarius*, the strain investigated in this work, consists only of two proteins [201], the outermost surface layer (S-layer), called “SlaA”, and the integrated into the cytoplasmic membrane, anchoring protein, called “SlaB” [81]. No additional cell wall structures, like peptidoglycan or lipopolysaccharide layers cover the cells, in contrast to bacteria. Hence, differences in the interaction mechanisms with uranium can be expected. The knowledge about the interaction mechanisms of archaea with uranium is limited to only a few studies. For instance, it was shown, that the hyperthermophilic archaeon *Pyrobaculum islandicum* has the ability to reduce U(VI) to poorly soluble U(IV) [31]. Furthermore, the halophilic archaeon *Halobacterium halobium* accumulates high amounts of this radionuclide *via* a U(VI) complexation by phosphate groups at the cell surface [178]. Recently, we have demonstrated the U(VI) complexation *via* organic phosphate groups by *S. acidocaldarius* under highly acidic conditions between pH 1.5 and 3, which cover the physiological growth optimum of this organism [133]. In the present study, the influence on uranium exerted by this acidophilic archaeon is investigated at moderate acidic pH values of 4.5 and 6, relevant

for many metal-polluted environments where the presence of *Sulfolobales* already had been demonstrated [181, 182].

Thermoacidophilic organisms belonging to the genus *Sulfolobus*, which were originally isolated from geothermal springs, are globally distributed in nature [76]. The growth of thermophilic *Sulfolobus* species close to a future repository is feasible because of the heat released by the decay of the radioactive waste, which will increase the temperature of the surrounding engineered barriers and host rocks. Thermal-mechanical models indicated that the temperature in the immediate vicinity of a repository will increase up to more than 100 °C within the first 100 years [202, 203]. This heating will favour the growth and multiplication of thermophilic microorganisms. As a result of their growth the pH of the local environment may be reduced due to the production of H₂SO₄ [182]. The latter will ensure optimal growth conditions for these organisms. Hence they may play an important role in the immediate vicinity of a repository and they are relevant for risk assessment of final storage for radioactive wastes. Moreover, *Sulfolobus* strains were also shown to resist moderate temperatures without any negative consequences and rapidly start growing at higher temperatures, favourable for this archaeal strain [184].

The objective of the present work was to investigate the interactions of the archaeal strain *S. acidocaldarius* DSM 639 with uranium at moderate acidic pH values and to elucidate the possible role of archaea in the biomineralization of this radionuclide. For this purpose we used a combination of wet chemistry, microscopic and spectroscopic methods.

MATERIALS AND METHODS

Cultivation and archaeal cell sample preparation

S. acidocaldarius DSM 639 was purchased from the “German Collection of Microorganisms and Cell Cultures” (DSMZ, Braunschweig, Germany) and cultivated under heterotrophic conditions in a mineral salt medium [185] supplemented with 0.1% Bacto™ tryptone and 0.005% Bacto™ yeast extract. Due to the formation of insoluble precipitates, which might have an undesired influence on further analyses, we desist from the addition of FeCl₃ with no detrimental effect on the growth of the strain. The pH of the medium was adjusted to 2.5 and the cultivation temperature was 70 °C. Growth was monitored by measuring the optical density at a wavelength of 600 nm. After reaching the end of the logarithmic growth phase (OD₆₀₀ ~ 0.45), the microbial cells were harvested by centrifugation (10000 g, room

temperature, 15 min) and parallel portions were rinsed twice with 0.1 M solutions of the background electrolyte (NaClO_4 or NaCl) with the appropriate desired pH. Afterwards the cells were suspended in the corresponding electrolyte solution; the pH of the cell suspensions was checked and if necessary adjusted to the desired values. After removing the washing solution, uranium ($\text{UO}_2(\text{NO}_3)_2$ or UO_2Cl_2) was added, diluted in a 0.1 M solution of the background electrolyte with the corresponding pH.

U(VI) bioaccumulation

For bioaccumulation studies different amounts of the cells (1 to 55 mg dry biomass) were incubated in triplicate for 48 hours on a rotary shaker with 10 ml of a $5 \cdot 10^{-4}$ M uranyl nitrate solution diluted in 0.1 M NaClO_4 (pH 4.5). At pH 6 the uranium concentration was reduced to $5 \cdot 10^{-5}$ M to prevent the formation of uranyl hydroxide precipitates. For a better comparison the amount of accumulated uranium was normalized to the dry biomass, which was determined by weighting parallel samples after drying for 48 hours at 70 °C. Kinetic studies were also performed in triplicate, using a biomass concentration of (0.5 ± 0.05) g/L. After defined incubation periods at room temperature the cells were removed from the uranium solution by centrifugation and the unbound U(VI) in the supernatant was measured by inductively-coupled-plasma mass-spectroscopy using an Elan 9000 system (PerkinElmer, Waltham, MA, USA). Control reactions without cells were treated in the same way to exclude abiotic uranium removal from the solution, due to precipitation and/or chemical sorption at the used test vials.

X-ray Absorption Spectroscopy (XAS)

For XAS measurements, 50 mg of the cells were treated with U(VI) for 48 hours in a similar way to those used for the uranium accumulation studies. After the contact with U(VI) the cells were washed twice with 0.1 M NaClO_4 at pH 4.5 or 6, respectively. Subsequently they were dried for three days at 35 °C in a vacuum oven (Vacutherm VT 6025, Heraeus-Instruments, Hanau, Germany). After that the samples were powdered and mounted on Kapton tape. Six layers of sample-covered tape were stuck on the top of each other and subsequently shrink-wrapped. The described sample preparation based on soft desiccation, which does not influence the structural parameters of the formed uranium complexes, was developed several years ago by Merroun and co-workers [162] in order to avoid uncontrolled biological processes, that can influence the fate of uranium, in the cell samples during transportation and possible storage on the way from the laboratory to the X-ray beamline.

Such processes could involve, for example, cell lysis resulting in pH changes, release of enzymes or even development of non-prokaryotic infections (fungal, for instance). One additional advantage of the used sample preparation procedure is that one and the same sample can be analysed many times by using different methods. The latter is of great importance for analyses of complex systems, as the samples investigated in this study.

The XAS measurements were performed at the Rossendorf Beamline (ROBL) at the European Synchrotron Radiation Facility (ESRF), Grenoble, France [134]. Samples were measured at room temperature in fluorescence mode using a Si(111) double-crystal monochromator and a 13-element germanium fluorescence detector. The energy was calibrated by measuring the yttrium *K*-edge transmission spectrum of an Y foil and defining the first inflection point as 17038 eV. Six (pH 4.5) and eight (pH 6) U *L*_{III}-edge fluorescence spectra were recorded and averaged, respectively. Subsequently dead-time correction was applied. The region from about 45 eV below to 60 eV above the absorption edge of each scan was isolated for the X-ray Absorption Near Edge Structure (XANES) analysis. The pre-edge background was subtracted, and the absorption coefficient was normalized to equal intensity at 17230 eV so that all spectra could be plotted on the same scale.

The EXAFS oscillations were isolated from the raw, averaged data by removal of the pre-edge background, approximated by a first-order polynomial, followed by μ_0 -removal *via* spline fitting techniques and normalization using a Victoreen function. The ionization energy for the U *L*_{III}-electron, E_0 , was arbitrarily defined as 17185 eV for all averaged spectra. The EXAFS spectra were analysed according to standard procedures using the program EXAFSPAK [135]. The theoretical scattering phase and amplitude functions were calculated from models *via* the software FEFF8.2 [136]. All fits included the four-legged multiple scattering (MS) path of the uranyl group, U-O_{ax}-U-O_{ax}. The coordination number (N) of this MS path was linked to the N of the single-scattering (SS) path U-O_{ax}. The radial distance (R) and Debye-Waller factor (σ^2) of the MS path were linked at twice the R and σ^2 of the SS path U-O_{ax}, respectively [137]. During the fitting procedure, N of the U-O_{ax} SS path was held constant at two. The amplitude reduction factor was held constant at 1.0 for FEFF8.2 calculations and EXAFS fits. The shift in threshold energy, ΔE_0 , was varied as a global parameter in the fits. The level of significance for selected scattering paths was calculated using the F-Test [204].

Fourier-Transform Infrared-Spectroscopy (FT-IR)

For IR measurements sodium chloride was used as background electrolyte instead of sodium perchlorate, and uranyl nitrate was replaced by uranyl chloride to avoid the vibration bands arising from perchlorate and nitrate groups. The sample preparation was performed analogously to that for XAS measurements. In addition, parallel cell samples were incubated at highly acidic conditions (pH 1.5 and pH 3) with and without the addition of uranium (0.5 mM). Roughly 10 mg of the dried U(VI)-treated and untreated cell samples were mixed with 300 mg potassium bromide, grounded in a high-frequency vibration mill (Perkin Elmer, Waltham, MA, USA) and pressed to a translucent tablet at a pressure of 10 Torr under vacuum. Spectra were recorded in a frequency range from 4000 cm^{-1} to 600 cm^{-1} with a spectral resolution of 4 cm^{-1} using a Vertex 80v vacuum FT-IR spectrometer (Bruker Optics, Ettlingen, Germany). A background spectrum (evacuated spectrometer without sample) was subtracted automatically from the acquired spectra. Sixty-four scans were averaged for each sample. Spectra recording and data evaluation were performed using the software package Opus 6.0 (Bruker Optics, Ettlingen, Germany).

Time-Resolved Laser-induced Fluorescence Spectroscopy (TRLFS)

Small portions of the powdered XAS samples were used for luminescence measurements of the uranium complexed with the cells of the studied archaeal strain. The samples were placed in a quartz micro cuvette and TRLF spectroscopic measurements were performed at room temperature by using home-built equipment. From the sample incubated at pH 4.5, TRLF spectra were recorded between 444 and 594 nm using a Nd-YAG laser system (Spectra Physics, Santa Clara, CA, USA) [187] with an intensity of 0.3 mJ. The central wavelength of the spectrograph was set to 520 nm and the gate width of the ICCD camera was 5 μs (complete detection system: HORIBA Jobin Yvon GmbH, Darmstadt, Germany). For time-resolved measurements a digital delay generator (DG535, Stanford Research Systems, Sunnyvale, CA, USA) was used. Before each series of measurements the background signal was measured 2 μs after the laser pulse and afterwards automatically subtracted from each spectrum.

For the sample treated at pH 6, which had a lower uranium concentration, the luminescence of the uranium complexes was measured with a Nd-YAG laser system (Inlite II, Continuum Electro-Optics Inc., Santa Clara, CA, USA), with an excitation wavelength of 266 nm and a significant higher intensity of 1.35 mJ. The central wavelength of the spectrograph (Acton Research 1236 OMA 500 mm, Princeton Instruments, Acton, MA, USA) and the gate width

of the ICCD camera (Roper Scientific, Princeton Instruments, Stuttgart, Germany) of this laser system were 507.3 nm and 20 μ s, respectively. TRLF spectra were recorded between 421 and 600 nm.

The spectrographs of both systems were calibrated using a mercury lamp with known emission lines. Luminescence was excited in both samples by 50 laser pulses. Subsequently, 101 U(VI) luminescence spectra (each calculated by averaging three single measurements) were recorded after defined delay times. For an accurate determination of the luminescence lifetime(s) of the uranium complexes two series of measurements were performed for each sample. One of them was performed with a step size of the delay time of 200 ns to determine uranium species exhibiting short luminescence lifetimes. For the calculation of longer lifetimes yet a second series was recorded with delay times of 5 μ s and 0.5 μ s for the samples incubated at pH 4.5 and 6, respectively. The obtained luminescence data were processed by using Origin 7.5 (OriginLab Corporation, Northampton, MA, USA) including the PeakFit module 4.0.

Enzymatic assay

The activity of the acid phosphatase (APase) was determined by the “Acid Phosphatase Assay Kit” from Sigma-Aldrich (Saint Louis, USA). The assay is based on the enzymatic hydrolysis of *p*-nitrophenyl phosphate to *p*-nitrophenol, a chromogenic product with an absorbance maximum at 405 nm. One unit of APase was defined as the amount of the enzyme that hydrolyzes 1 μ mol of *p*-nitrophenyl phosphate per minute. Deviant from the manufacturer’s instructions, *p*-nitrophenyl phosphate was dissolved in 0.1 M NaClO₄ and pH of the solutions was brought to 4.5 or 6, respectively. In addition, a *p*-nitrophenyl phosphate solution with pH 3 was prepared to measure the enzymatic activity at the physiological pH optimum of the investigated strain. For each pH value three samples, each containing 2 mg of freshly grown cells of *S. acidocaldarius* were washed four times with 0.1 M NaClO₄ (pH 3, 4.5 or 6). At each washing step pH was controlled and if necessary readjusted to the required values. After that, the cells were suspended in 100 μ l 0.1 M NaClO₄ with the corresponding pH. The cells of three more samples were killed by heating at 121°C for 20 min and afterwards studied analogically at pH 3. 50 μ l from each of the cell suspensions was transferred to 50 μ l *p*-nitrophenyl phosphate solution with the same pH. Control reactions without cells were prepared to quantify and later take account of the spontaneous hydrolysis of *p*-nitrophenyl phosphate at the different pH values. After incubation for 30 min at room

temperature, the reaction was stopped by the addition of 200 μ l 0.5 M NaOH. Subsequently the cells were spun down and the supernatants of the samples were used to quantify the produced *p*-nitrophenol at 405 nm. APase activity in the different samples was calculated according to the protocol of the manufacturer.

Colorimetric determination of phosphate

Phosphate was quantified by colorimetric measurements using malachite green. This dye complexes inorganic phosphate groups in the presence of molybdate and forms a complex which can be determined at a wavelength of 660 nm [139]. The phosphate reagent containing ammonium molybdate and malachite green was prepared as described by Ekman and Jäger [140]. Eleven potassium dihydrogen phosphate solutions (0 - 20 μ M) were prepared and served as a standard. For the test about 5 mg of freshly grown cells of *S. acidocaldarius* were suspended in triplicate in 10 ml uranyl nitrate solution. In addition, parallel samples without uranium were prepared. Samples were shaken for 48 hours at room temperature. After that the samples were centrifuged and the amount of inorganic phosphate in the supernatant was determined. For this purpose 100 μ l of the phosphate reagent was added to 100 μ l of the cell supernatants as well as to the standard solutions. Samples were incubated for 20 min at room temperature and subsequently the absorption of the complex was measured at 660 nm and quantified *via* the determined standard curve. As a control, phosphate concentrations of the initial solutions were checked and corresponding values were subtracted from the concentrations determined in the supernatants of the cell samples.

Live/Dead staining

After the uranium treatments at pH 3, 4.5 and 6 for 48 hours, the archaeal cell suspensions were centrifuged at 4 °C and 10000 g for 10 min. After that, the cells were washed twice with 0.9% NaCl and subsequently suspended in 330 μ l of the same solution. 1 μ l of the staining solution, containing a mixture of two fluorescence dyes (SYTO[®] 9 and propidium iodide) (Live/Dead[®] BacLight[™] Bacterial Viability Kit L-7012, Molecular Probes, Inc., Eugene, OR, USA) was added to the samples. After incubation in the dark and on ice for 15 min, the samples were centrifuged once again and the supernatant containing the unbound stains was removed. Cells were suspended in 25 μ l 0.9% NaCl and examined with an Olympus light microscope (Olympus Europa Holding GmbH, Hamburg, Germany) - BX-61, combined with BX-UCB (control box) and U-RFL-T (power supply for the 100 W mercury lamp) - along with the accompanying imaging software “cell[^]P”. Fluorescence was excited by light with

wavelengths between 420 and 460 nm, using a super-wide band filter mirror unit (U-MSWB, Olympus Europa Holding GmbH, Hamburg, Germany).

Microscopic analyses

The mineral formation in the samples of *S. acidocaldarius* treated with U(VI) was studied by using a motorized epifluorescence microscope (Olympus BX-61; Olympus Optical Co. GmbH, Hamburg, Germany). Digital pictures of the samples, treated for 48 hours with uranyl nitrate solutions (pH 4.5 and 6) and subsequently washed with 0.1 M NaClO₄, were taken in phase contrast mode. Luminescence of the uranium minerals was excited using a fluorescence mirror unit (U-MNU2; Olympus Optical Co. GmbH, Hamburg, Germany) with excitation wavelengths between 360 and 370 nm.

In addition, the cellular localization of the uranium accumulated by the cells was performed by using Transmission Electron Microscopy (TEM) combined with Energy-dispersive X-ray spectroscopy (EDX) at the “Centro de Instrumentación Científica” of the University of Granada (Spain). For this analysis, each about 5 mg of the cells were treated with 10 ml uranyl nitrate solution (pH 4.5). After incubation for 48 hours the archaeal cells were rinsed twice with 0.1 M NaClO₄, with the corresponding pH. A third washing step was performed with 0.1 M sodium cacodylate buffer (pH 5.2) followed by a prefixation with 2.5% glutardialdehyde in the same buffer. After that, the samples were washed three times with 0.1 M cacodylate buffer and postfixed for 60 min at 4 °C in the dark using 1% osmium tetroxide in distilled water. The samples were dehydrated with ethanol and subsequently infiltrated in a resin (EMbed 812; Electron Microscopy Sciences, Hatfield, PA, USA). After polymerization of the resin at 60 °C, ultrathin sections (50-70 nm) were cut using a diamond knife on an Ultracut-R microtome (Leica Microsystems, Wetzlar, Germany). The ultrathin sections were mounted on copper grids and contrasted with lead citrate according to the method described by Reynolds [138]. Parallel TEM samples were prepared which were not contrasted with lead citrate. Finally all samples were coated with carbon. TEM observations were made using a “High Resolution Philips CM 200” transmission electron microscope at an acceleration voltage of 200 kV. EDX analyses, which provide elemental information, were performed at the same voltage using a spot size of 7 nm and a live-counting time of 200 s.

RESULTS AND DISCUSSION

U(VI) bioaccumulation

The studies on the bioaccumulation of uranium showed that the cells of *S. acidocaldarius* accumulate significant amounts of this radionuclide from the acidic solutions. As evident from Figure 3.1 the amount of uranium bound to the cells strongly depends on the biomass concentration. The negative correlation between these two parameters can be explained by the agglomeration of the microbial cells, which reduces the surface contacting with U(VI). This was confirmed by microscopic analyses (not shown). For kinetic studies we used a biomass concentration of (0.5 ± 0.05) g/L. The analyses demonstrated a rapid complexation of uranium by the cells (Fig. 3.2), which is a typical feature of the biosorption process at functional groups on the cell surface [19].

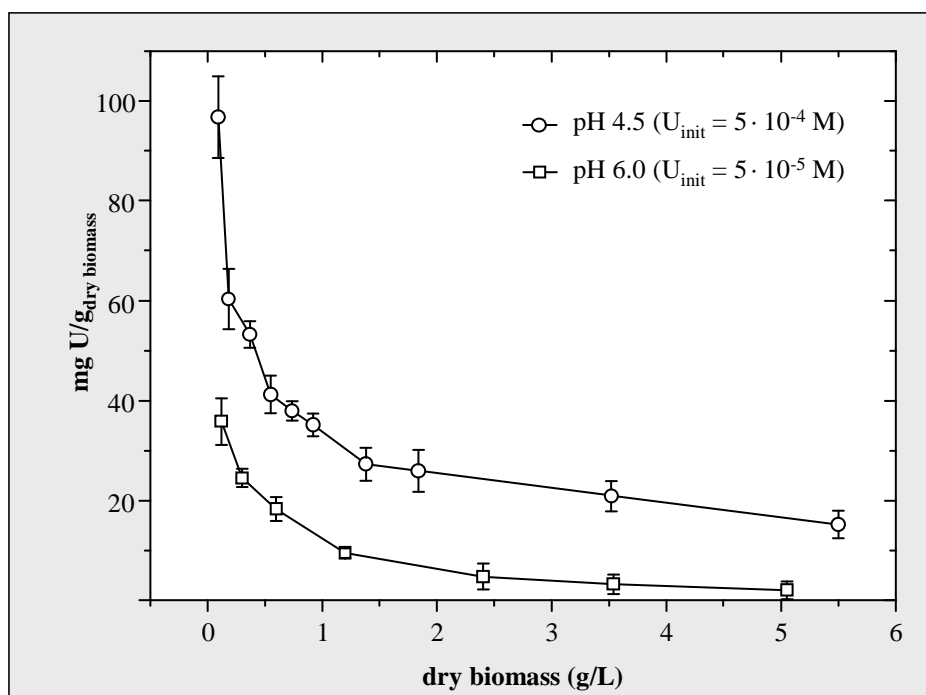


Figure 3.1. U(VI) accumulation by the cells of *S. acidocaldarius* after 48 hours at pH 4.5 and 6 as a function of biomass concentration.

Already after an incubation of five minutes significant amounts of U(VI) (7.6 ± 2.2) and (10.8 ± 0.7) mg U/g dry biomass were bound by the cells at pH 4.5 and pH 6, respectively (Fig. 3.2). Also the binding capacity is stable for some hours at both pH values (Fig. 3.3), a significant increase was observed after longer incubations at pH 4.5. The binding capacity of the cells after an incubation of 48 hours at this pH was determined to be (41.3 ± 3.4) mg/g_{dry biomass}. This value is about twice as high as those U(VI) binding capacities determined in our laboratory for the strain under highly acidic conditions [133]. The binding

capacity after 48 hours at pH 6 was calculated to be (26.1 ± 1.5) mg U/g_{dry biomass}. However, it was limited to this value, due to the lower U(VI) concentration used in this sample.

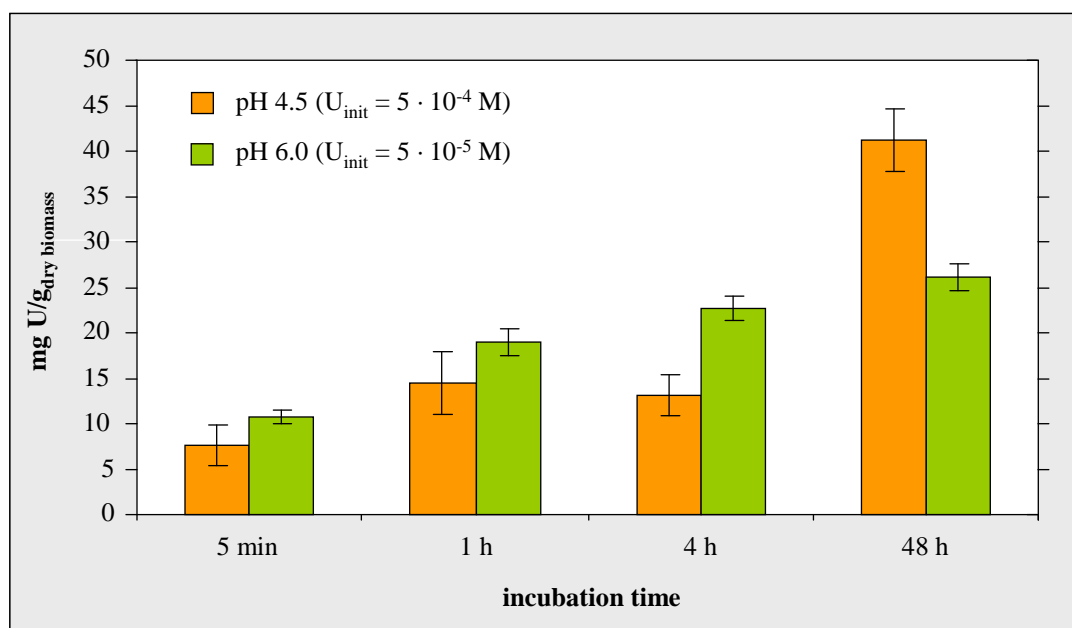


Figure 3.2. U(VI) accumulation by the cells of *S. acidocaldarius* at pH 4.5 and 6 as a function of time (biomass concentration = 0.5 ± 0.05 g/L).

Limiting the data to the biosorption process at binding-capable functional groups at the cell surface, which mainly takes place within the first minutes to hours of incubation, the cells of *S. acidocaldarius* adsorb about (14.6 ± 3.5) mg uranium per gram dry biomass within one hour of incubation at pH 4.5 (Fig. 3.2). This value is well in line with the results of U(VI) sorption studies performed with the strain at highly acidic conditions [133]. The amount of uranium bound to the cells at pH 6 within one hour is higher (~ 19 mg U/g_{dry biomass}) compared to the binding capacity at pH 4.5, which is most likely due to the uranium complexation at additional deprotonated and therefore binding-capable functional groups at the cell surface. In particular carboxylic groups provided by the negatively charged amino acids of the S-layer protein might be involved in the uranium complexation at increased pH values. This assumption is supported by titration studies of the cell surface of *Bacillus subtilis*, demonstrating a pK_a value of about 4.8 for the carboxylic groups [205]. Further studies of uranyl surface complexes on this strain pointed out that the reversible adsorption of UO_2^{2+} onto deprotonated carboxylic groups is the only mechanism that can reasonably explain an increase of U(VI) adsorption by increasing the pH in the range between, 2.5 and 5 [155].

The capability of U(VI) biosorption demonstrated for the cells of the archaeal strain *S. acidocaldarius* is significantly lower than those determined for the cells of bacteria at

corresponding pH values. For instance, it was demonstrated that *Chryseomonas* sp. accumulates about 60 mg U/g_{dry biomass} from a uranyl nitrate solution ($U_{init} \sim 0.42$ mM, pH 4) within one hour [156]. Studies on *Bacillus sphaericus* ATCC 14577 revealed amounts of more than 70 mg uranium which were adsorbed at the cell surface per gram of dry biomass ($U_{init} = 0.14$ mM, pH 4.5, biomass concentration = 0.5 g/L) [154]. An even higher binding capacity were determined for *Pseudomonas fluorescence* ATCC 55241 (92 mg U/g_{dry biomass}) within an incubation of two hours at pH 5 ($U_{init} = 0.125$ mM) [178].

The high uranium binding capacity of bacteria is attributed to the large number of uranium-binding ligands of their multilayer cell wall structure [157]. In contrast to that, the only cell wall component of *S. acidocaldarius* is its cytoplasm membrane-anchored surface layer (S-layer) [180]. Because of the low content of negatively charged amino acids (1.2 mol% aspartate and 1.8 mol% glutamate) and especially because of the absence of phosphorylated sites, this glycoprotein should be almost ineffective in uranium complexation. Interestingly, Francis and co-workers [178] demonstrated an unusually high uranium binding capability for the neutrophilic haloarchaeon *Halobacterium halobium* (114 mg U/g_{dry biomass}) at pH 5, although its cell wall is also limited to a glycosylated S-layer protein. However, in contrast to that of *S. acidocaldarius*, this S-layer is enriched in carboxylic amino acid residues [180]. According to Francis and co-workers [178] these negatively charged amino acids support proper protein folding in the high salt conditions at which the strain is living. Besides that, the high amount of negatively charged amino acids, should be also involved in the initial binding of U(VI) by the S-layer of *H. halobium*, because they represent the main binding sites for U(VI) at the studied pH of 5. The final U(VI) accumulation in the strain was, however, in a form of deep uranyl phosphate deposits onto the cytoplasm membrane [178]. Another reason for the low uranium binding capability of *S. acidocaldarius*, along with the low content of negatively charged amino acids of its S-layer, might be the significantly lower amount of polyphosphate granules in its cells in comparison to many other microorganisms [193]. The role of these granules in supplying effective uranium-binding orthophosphate ligands was demonstrated by Renninger and co-workers [89].

The significant increase of the binding capacity after the longer incubation of 48 h at pH 4.5, which was not detected in the studies at highly acidic conditions [133], indicated that uranium was in this case accumulated by more than one process: a rapid biosorption at the cell surface and additional slower processes, which occur at the later stages of the cell treatments.

XAS

The X-ray absorption spectra recorded from the uranium complexes formed by *S. acidocaldarius* at pH 4.5 and 6, as well as the corresponding first derivatives of the spectra are illustrated in Figure 3.3. For comparison, the X-ray absorption spectra recorded from two reference solutions are presented as well. The stock solution of U(VI) was prepared by dissolving sodium diuranate in 7 M HClO₄. Part of this solution was reduced electrochemically to U(IV) at a mercury pool cathode. The uranium oxidation state in the solutions was confirmed by UV/Vis spectroscopy (not shown). The spectra obtained from the investigated cell samples showed a peak at 17188 eV (dashed line in Fig. 3.3) which is assigned to the contribution of the multiple scattering of the two axial oxygen atoms of U(VI) [137]. In addition, the maximum of the first derivatives and the intensity maximum of the absorption edge, i.e. the white line, were observed in both samples at positions characteristic for U(VI) (compare the dotted lines in Fig. 3.3). These findings show that the added U(VI) was not reduced in the samples to U(IV).

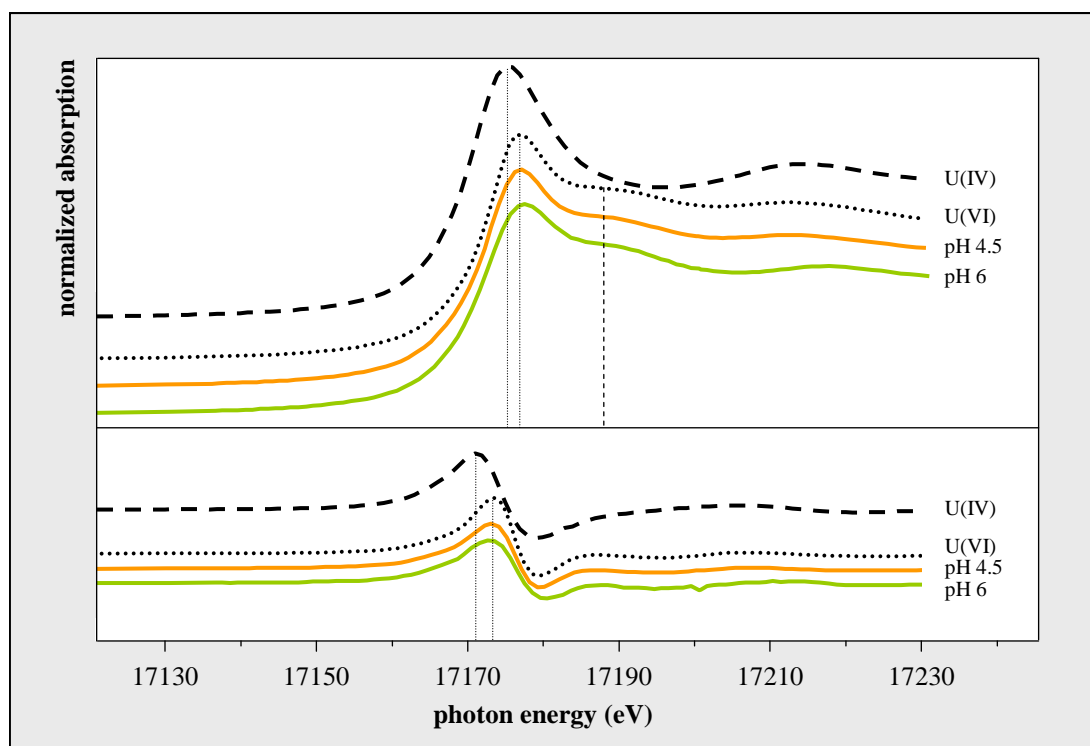


Figure 3.3. Uranium L_{III} -edge X-ray absorption spectra (top) and their first derivatives (bottom) recorded from the uranium complexes formed by *S. acidocaldarius* at pH 4.5 (orange) and pH 6 (green). The X-ray absorption spectra of the reference solutions of U(VI) and U(IV), each at a concentration of $4 \cdot 10^{-2}$ M in 1 M HClO₄, are shown in the figure as well. All spectra were normalized to an equal intensity at 17230 eV. The peak marked by the dashed line is assigned the multiple scattering contributions of the axial oxygen atoms of U(VI) and the dotted lines represent the peak maxima of the X-ray absorption spectra of U(IV) and U(VI) as well as those of their first derivatives.

The isolated U L_{III} -edge k^3 -weighted EXAFS spectra and their corresponding Fourier Transforms (FTs) of the uranium-treated cell samples, along with the best calculated fits are illustrated in Figure 3.4. In addition, the spectra of two relevant model compounds, UO_2 -fructose(6)phosphate (organic uranyl phosphate) and meta-autunite (inorganic uranyl phosphate) are given for comparison.

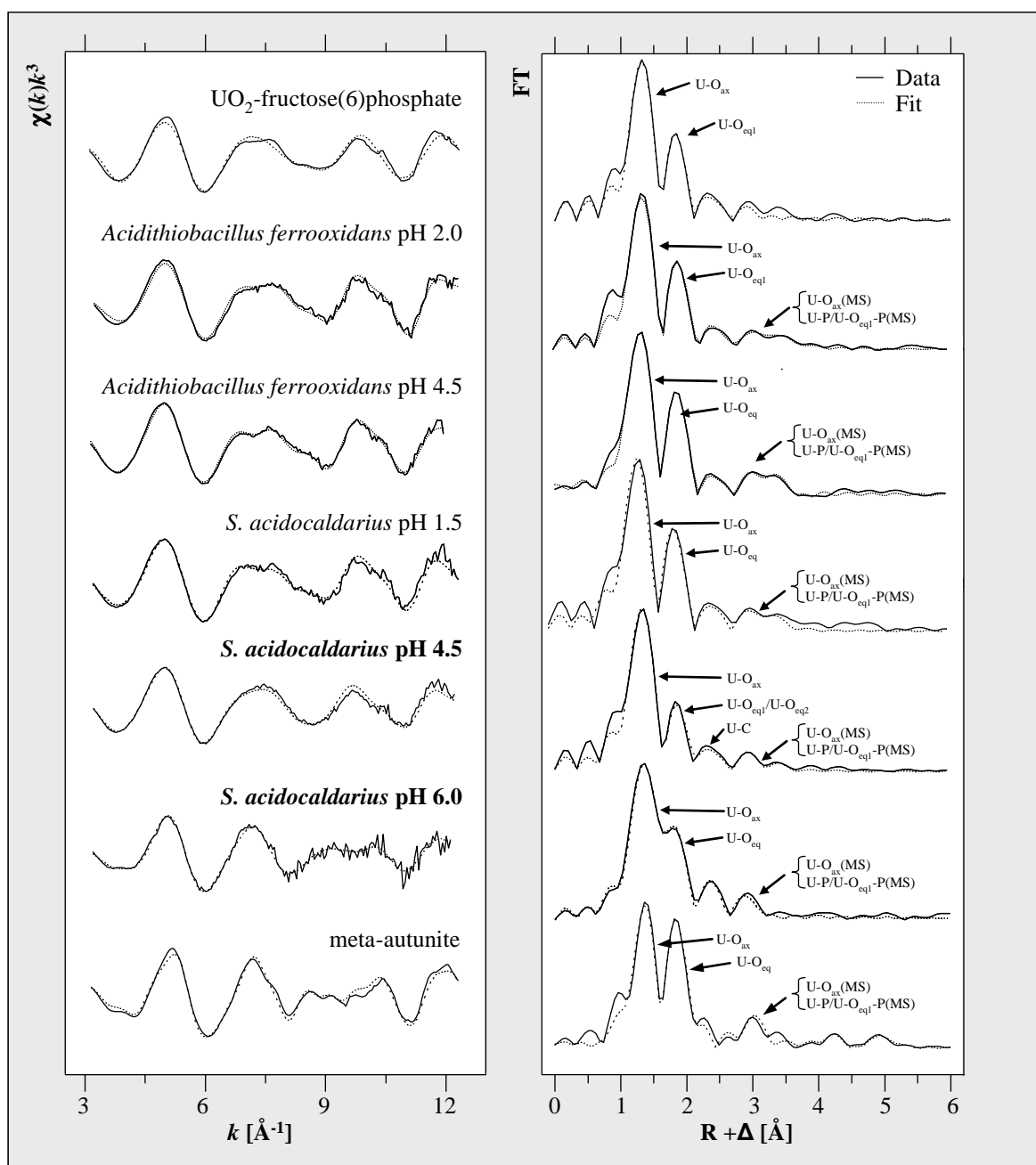


Figure 3.4. Uranium L_{III} -edge k^3 -weighted EXAFS spectra (left) and the corresponding Fourier Transforms (right) of the uranium complexes formed by *S. acidocaldarius* at pH 4.5 and 6 and those of the model compounds UO_2 -fructose(6)phosphate [158] and meta-autunite [169]. The spectra of the uranium complexes formed by *S. acidocaldarius* at pH 1.5 [133] and those formed by the acidophilic bacterial strain *A. ferrooxidans* at pH 2 [162] and pH 4.5 [87] are shown as well.

For the sample incubated with uranium at pH 6, quantitative fit results were obtained using theoretical phase and amplitude functions calculated with the FEFF8.2 code from the crystal structure of meta-autunite $\text{Ca}(\text{UO}_2)_2(\text{PO}_4)_2 \cdot 6 \text{H}_2\text{O}$ [186]. The EXAFS spectrum of the sample incubated at pH 4.5 was fitted using the model described by Merroun and co-workers [150]. This model contains fragments of two molecules: meta-autunite and uranyl triacetate. The structural parameters obtained from the fitting procedures are summarized in Table 3.1. The Fourier-transformed EXAFS data of the sample incubated at pH 4.5 showed FT peaks at radial distances of $R+\Delta \sim 1.3 \text{ \AA}$ and $R+\Delta \sim 1.8 \text{ \AA}$ representing the shells of two axial (U-O_{ax}) and of about five ($N_{\text{Oeq}} = 5.0 \pm 0.6$) equatorial (U-O_{eq}) oxygen atoms at radial distances of 1.78 \AA and 2.35 \AA , respectively (the data of the shell fit with only one U-O_{eq} shell are not presented in Table 3.1). However, the large Debye-Waller factor of 0.016 \AA^2 for the U-O_{eq} shell (not shown) indicated the existence of more than one type of oxygen atoms in the equatorial plane. Hence, the U-O_{eq} shell was split in two components: the first U-O_{eq} shell (U-O_{eq1}) at distance of 2.33 \AA and the second one (U-O_{eq2}) at a somewhat longer distance of 2.50 \AA . These two shells are not represented as separate peaks in the FT since their distances span a R range which is not large enough to be discerned as individual peaks in the EXAFS spectrum, for which $\Delta k = 9.3 \text{ \AA}^{-1}$ in accordance with $\Delta R \geq \pi/(2\Delta k)$.

During the fitting procedure the coordination numbers of the two equatorial oxygen shells were linked to each other and stabilized to a total number of five, as it was calculated by the shell fit with only one U-O_{eq} shell. The U-O_{eq1} bond distance corresponds to the previously reported values for oxygen atoms of organic phosphate groups bound to uranyl in a monodentate binding mode in the case of *Acidithiobacillus ferrooxidans* [87, 162]. The high similarity of the EXAFS spectra obtained from the uranyl complexes formed by this acidophilic bacterium to that of UO_2 -fructose(6)phosphate (Fig. 3.4), allowed the authors to conclude that uranium was bound exclusively by organic phosphate groups [162]. Corresponding complexes were also exclusively found in the samples of *S. acidocaldarius* treated with U(VI) at highly acidic conditions (Fig. 3.4, Chapter II) [133]. Assuming the presence of corresponding complexes also in the here studied sample incubated at pH 4.5, we introduce a shell of phosphorous atoms in the shell fit (Table 3.1). The radial distance obtained for this shell was 3.61 \AA , which is characteristic for the proposed monodentate U(VI) complexation mode [169] and well in line with those radial distances calculated for the U-P shells of the uranium complexes formed by *S. acidocaldarius* at highly acidic conditions.

Table 3.1. Structural parameters of the uranium complexes formed by the cells of *S. acidocaldarius* at pH 4.5 and 6, as well as those of the two model compounds UO₂-fructose(6)phosphate and meta-autunite.

Sample	Shell	N ^a	R (Å) ^b	σ ² (Å ²) ^c	ΔE ₀ (eV)
UO ₂ -fructose(6)phosphate pH 5.5 [160]	U-O _{ax}	2.0 ^d	1.77(1)	0.001(1)	0.1(7)
	U-O _{eq1}	4.8(5)	2.30(1)	0.020(4)	
pH 4.5	U-O _{ax}	2.0 ^d	1.78(1)	0.0026(1)	3.7(7)
	U-O _{ax} (MS)	2.0 ^d	3.56 ^e	0.0052 ^e	
	U-O _{eq1}	3(1)	2.33(2)	0.008(3)	
	U-O _{eq2}	2 ^f	2.50(5)	0.010(2)	
	U-C	1.8(4)	2.91(1)	0.0038 ^d	
	U-P	1.1(5)	3.61(4)	0.0080 ^d	
	U-O _{eq1} -P (MS)	2.2 ^g	3.71 ^h	0.0080 ^d	
pH 6	U-O _{ax}	2.0 ^d	1.77(1)	0.0030(2)	-2.6(9)
	U-O _{ax} (MS)	2.0 ^d	3.54 ^e	0.0060 ^e	
	U-O _{eq}	4.3(3)	2.25(1)	0.0053(6)	
	U-P	2.8(7)	3.57(2)	0.0080 ^d	
	U-O _{eq1} -P (MS)	5.6 ^g	3.66 ^h	0.0080 ^d	
meta-autunite [169]	U-O _{ax}	2.2(1)	1.76	0.0045	-11.0
	U-O _{eq}	3.9(2)	2.29	0.0026	
	U-P	2.3(3)	3.60	0.008 ^d	

Standard deviations as estimated by EXAFSPAK are given in parenthesis

^a Error in coordination number is ± 25%

^b Error in distance is ± 0.02 Å

^c Debye-Waller factor

^d Parameter fixed for calculation

^e Radial distance (R) and Debye-Waller factor (σ²) linked twice to R and σ² of the of the U-O_{ax} path

^f Coordination number (N) linked to the N of U-O_{eq1} path (N_{U-Oeq1}+N_{U-Oeq2}=5)

^g Coordination number (N) linked twice to the N of the U-P path

^h Radial distance (R) linked to R of the U-P path, according to the used structural model

However, as shown in Figure 3.4, the EXAFS spectrum of the *S. acidocaldarius* cells treated with uranium at pH 4.5 differs from the above mentioned spectra of *A. ferrooxidans* at pH 2 and 4.5 as well as that of *S. acidocaldarius* at pH 1.5. This indicates that at this pH not only a monodentate binding of U(VI) to organic phosphate groups occurred. The EXAFS parameters of the sample incubated at pH 4.5 are rather complex and suggest, in combination with other methods two additional U(VI) complexation modes. As demonstrated by TEM and FT-IR (see below) a small amount of the added U(VI) was precipitated in inorganic uranyl phosphate phases. Moreover and to a higher extent, carboxylic groups of organic molecules at the cell surface are involved in the uranium complexation at this pH (see TRIFS section). In accordance, the calculated longer equatorial oxygen bond length of 2.50 Å, is in line with previously reported values (2.45 to 2.51 Å) for the radial distance of carbon atoms bound to U(VI) in a bidentate binding mode [150, 206]. Consequently, the part of the EXAFS spectrum, corresponding to the FT peak at R+Δ ~2.3 Å (radial distance of 2.91 Å) was fitted with the scattering contribution of carbon atoms which were bidentately bound to uranium.

However, a shell related to bidentate-coordinated carbon atoms should be fitted only after thoughtful consideration, since the addition of a corresponding shell also improves EXAFS fits, where a corresponding complexation is improbable [158, 207], and even in carbon free systems like uranyl hydrate (see the residual in the brownish part of Fig. 3.5). For the latter, the reduced error (χ^2) calculated by EXAFSPAK decreases from 0.196 to 0.177 by adding such a simulated U-“C” shell (Table 3.2). The radial distance ($R = 2.92 \text{ \AA}$) of this false U-“C” shell in uranyl hydrate is very similar to that calculated for the U-C shell of the U(VI) complexes built by *S. acidocaldarius* at pH 4.5. Although the coordination number of the U-C path, calculated for the U(VI)/*S. acidocaldarius* sample, is higher ($N = 1.8$) than that of the false U-“C” shell in uranyl hydrate ($N = 1.2$), this difference is not significant enough to confirm by itself the presence of the U-C shell in the studied sample.

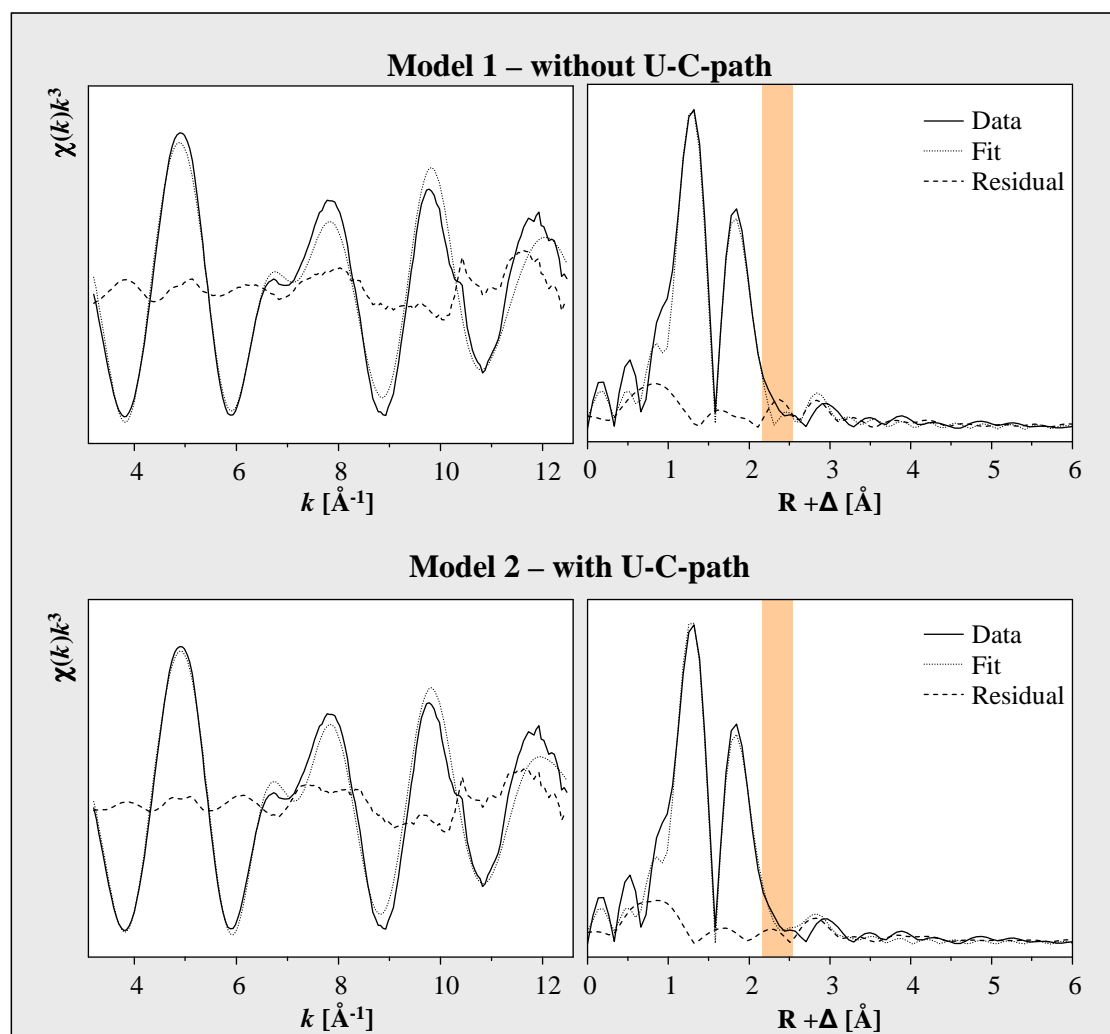


Figure 3.5. Uranium L_{III} -edge k^3 -weighted EXAFS spectra (left) and the corresponding Fourier Transforms (right) of uranyl hydrate. Shell fit was performed with the software EXAFSPAK, without (model 1) and with (model 2) the addition of a U-C shell, related to bidentate coordinated carbon atoms with a radial distance of $\sim 2.9 \text{ \AA}$ ($R + \Delta \sim 2.3 \text{ \AA}$, highlighted in brownish).

Table 3.2. Structural parameters of uranyl hydrate obtained by fitting procedures, performed using Fourier-filtered data ($R = 0.6$ to 3.4 \AA) with (model 2) and without (model 1) the consideration of a U-C shell.

Sample	Shell	N^a	$R (\text{\AA})^b$	$\sigma^2 (\text{\AA}^2)^c$	$\Delta E_0 (\text{eV})$	χ^2
model 1 (without U-C shell)	U-O _{ax}	2.0 ^d	1.76(1)	0.0021(1)	3.0(4)	0.196
	U-O _{ax} (MS)	2.0 ^d	3.52 ^e	0.0042 ^e		
	U-O _{eq1}	4.7(3)	2.41(1)	0.0072(5)		
model 2 (with U-C shell)	U-O _{ax}	2.0 ^d	1.76(1)	0.0021(1)	2.7(4)	0.177
	U-O _{ax} (MS)	2.0 ^d	3.52 ^e	0.0042 ^e		
	U-O _{eq1}	4.6(2)	2.40(1)	0.0070(5)		
	U-C	1.2(3)	2.91(1)	0.0038 ^d		

Standard deviations as estimated by EXAFSPAK are given in parenthesis

^a Error in coordination number is $\pm 25\%$

^b Error in distance is $\pm 0.02 \text{ \AA}$

^c Debye-Waller factor

^d Parameter fixed for calculation

^e Radial distance (R) and Debye-Waller factor (σ^2) linked twice to R and σ^2 of the of the U-O_{ax} path

In order to decide whether the consideration of a U-C shell in this sample is reasonable, we performed the so called “F-test” according to Michalowicz and co-workers [204]. This statistical test can be used for the comparison of two different EXAFS fitting models and evaluating the more likely of them. The EXAFS signal between 3.18 and 12.48 \AA^{-1} was Fourier-filtered in the R -range from 0.6 to 3.4 \AA and subsequently back-transformed. Shell fit was applied for model 1 (without U-C path) and model 2 (with U-C path) on the back-transformed EXAFS signal (Fig. 3.5).

The U-C shell, relevant for the F-test, has the highest backscattering amplitude at lower k -values, as it is commonly observed for light backscattering atoms. Therefore we performed the shell fitting for model 1 and model 2 with a k^1 -weighting. The fitted structural parameter for these shell fits agree with those obtained for a k^3 -weighting in the limits of the errors in determination of coordination numbers (20%) and radial distances (0.02 \AA) (compare Tables 3.1 and 3.3). For the given k - and R -interval the number of independent parameters is $N_{\text{ind}} = 2 \cdot \Delta k \cdot \Delta R / \pi = 16$ [204]. For model 1 (without U-C path) ten parameters were fitted, while for model 2 (with U-C path) two additional parameters were included in the fit (N_{Carbon} and R_{Carbon}) (Table 3.3). With the number of the fitted parameters the degrees of freedom were calculated for both models ($v_1 = 6$, $v_2 = 4$). Basing on the reduced standard deviations of the two shell fits ($\Delta\chi^2_{v_1} = 7.076 \cdot 10^{-4}$ and $\Delta\chi^2_{v_2} = 2.953 \cdot 10^{-4}$) a F-value of $F = 2.79$ was calculated [204]. According to these parameters the probability that model 2 is better than model 1 is $P = P(F, v_1, v_1 - v_2) = P(2.79, 6, 2)$, i.e. 86%. Hence, model 2 (with U-C path) is, with a score of 86%, the more conceivable model. Although the value of 86% is not absolutely decisive, we introduced the C backscattering contribution in the shell fit, mainly

because this is in accordance with our TRLS results (see below), which clearly demonstrate that in the sample incubated at pH 4.5 U(VI) was complexed by the carboxylic groups of the studied archaeal cells. Additional arguments supporting the consideration of the C-backscattering contribution in the shell fit of the studied sample can be found in the literature. As already mentioned, Fowle and co-workers [155] have demonstrated that at pH 4.5 most of the carboxylic groups of microbial cell walls exist in their deprotonated form and are implicated in U(VI) complexation. In addition, Rossberg and Scheinost [208], studying U(VI) interactions with acetic acid, demonstrated by using EXAFS that U(VI) complexation by deprotonated carboxylic groups occurs even at pH values below 4.

The presented results about the U(VI) complexation by *S. acidocaldarius* at pH 4.5 are in contrast to the previously observed pH-independent complexation of U(VI) solely *via* organic phosphate groups by the acidophilic bacterium *A. ferrooxidans* in the range from pH 2 to 4.5 (Fig. 3.4) [87, 162]. In addition, the results differ also from those obtained from neutrophilic bacteria, which at this pH immobilizes U(VI) predominantly in meta-autunite-like mineral phases [70, 83, 199, 200].

Table 3.3. Structural parameters of the uranium complexes formed by the cells of *S. acidocaldarius* at pH 4.5. Fitting procedure was performed using Fourier-filtered data ($R = 0.6$ to 3.4 Å) with (model 2) and without (model 1) the consideration of a U-C shell.

Sample	Shell	N ^a	R (Å) ^b	σ^2 (Å ²) ^c	ΔE_0 (eV)	$\Delta\chi^2_v$
model 1 (without U-C shell)	U-O _{ax}	2.0 ^d	1.78(1)	0.0026(3)	3.8(7)	$7.076 \cdot 10^{-4}$
	U-O _{ax} (MS)	2.0 ^d	3.56 ^e	0.0052 ^e		
	U-O _{eq1}	2.5(8)	2.32(1)	0.007(4)		
	U-O _{eq2}	2.5 ^f	2.48(2)	0.010(4)		
	U-P	1.3(5)	3.59(4)	0.0080 ^d		
	U-O _{eq1} -P (MS)	2.6 ^g	3.69 ^h	0.0080 ^d		
model 2 (with U-C shell)	U-O _{ax}	2.0 ^d	1.78(1)	0.0025(2)	2.2(5)	$2.953 \cdot 10^{-4}$
	U-O _{ax} (MS)	2.0 ^d	3.56 ^e	0.0050 ^e		
	U-O _{eq1}	3(1)	2.32(1)	0.009(3)		
	U-O _{eq2}	2 ^f	2.49(6)	0.014(7)		
	U-C	1.9(3)	2.92(1)	0.0038 ^d		
	U-P	0.8(3)	3.62(4)	0.0080 ^d		
	U-O _{eq1} -P (MS)	1.6 ^g	3.72 ^h	0.0080 ^d		

Standard deviations as estimated by EXAFSPAK are given in parenthesis

^a Error in coordination number is $\pm 20\%$

^b Error in distance is ± 0.02 Å

^c Debye-Waller factor

^d Parameter fixed for calculation

^e Radial distance (R) and Debye-Waller factor (σ^2) linked twice to R and σ^2 of the of the U-O_{ax} path

^f Coordination number (N) linked to the N of U-O_{eq1} path ($N_{U-O_{eq1}} + N_{U-O_{eq2}} = 5$)

^g Coordination number linked twice to the N of the U-P path

^h Radial distance (R) linked to R of the U-P path, according to the used structural model

The EXAFS spectrum of the uranium complexes formed by the cells treated at pH 6 differs significantly from all above discussed spectra. This spectrum has a high similarity to that measured from the inorganic uranyl phosphate mineral, meta-autunite [169, 209]. The structural parameters obtained for the uranium complexes formed at pH 6 confirmed this result (Table 3.1), e.g. the coordination number of the U-O_{eq} is nearly four and the radial distances of the U-O_{eq1} (2.25 Å) and U-P shells (3.57 Å) are, in analogy to those of meta-autunite, significantly shorter than those calculated for the organic phosphate complexes (Table 3.1). Therefore it is obvious that at this pH most of the added uranium was complexed by inorganic phosphate groups. This finding suggested the precipitation of poorly soluble uranyl phosphate complexes. We suggest that the inorganic phosphate groups were released by the cells of *S. acidocaldarius*, as a result of the pH stress. Interestingly, the FT peak at about R+Δ ~2.3 Å (bond distance of 2.85 Å) was also found in the sample treated at pH 6 and the addition of a shell of about one carbon atom at this bond distance improves significantly the fit (not shown). However, as above mentioned this alone does not prove the bidentate complexation of U(VI) *via* carbon atoms. And although the carboxylic groups, which are present at the cell surface and other cell compounds, are deprotonated at pH 6, the obtained EXAFS parameters (short U-O_{eq1} bond distance of 2.25 Å, in combination with a low Debye-Waller factor) as well as the results of the TRLF spectroscopic studies (see below) are inconsistent with the presence of uranyl carboxylate complexes in this sample and strongly designate that in this case uranium is exclusively bound *via* inorganic phosphate and precipitated in a form of meta-autunite-like mineral phases.

FT-IR

The FT-IR spectra of the uranium-treated samples, those of the control samples without U(VI), as well as the corresponding difference spectra are illustrated in Figure 3.6 in the range from 1800 cm⁻¹ to 800 cm⁻¹.

All recorded spectra exhibit common absorbance features, which occur independently of the pH and the presence of uranium. The first two, most prominent bands located at around 1655 cm⁻¹ and 1570 cm⁻¹ are characteristic for the amide I and amide II bands of the proteins, respectively [210]. They represent the ν(C=O) stretching mode (amide I) and a combination of the δ(N-H) bending mode as well as the ν(C-N) stretching mode (amide II) arising from peptide bonds. The absorption band located at 1453 cm⁻¹ can be assigned to the bending modes of CH₂ and CH₃ groups [211]. The band around 1235 cm⁻¹ probably attributes to the

$\nu_{\text{as}}(\text{P=O})$ mode of phosphate groups [212]. However, contributions from the (N-H) deformation mode of the amide group (amide III mode) are also expected in this region [213]. The IR range between 950 cm^{-1} and 1150 cm^{-1} can be attributed to various vibration modes arising from functional groups like phosphate and sulphate, as well as from sugar rings [159, 210-212, 214]. These groups and compounds are characteristic for various cellular components, and constitute potential binding sites for uranium or other metals.

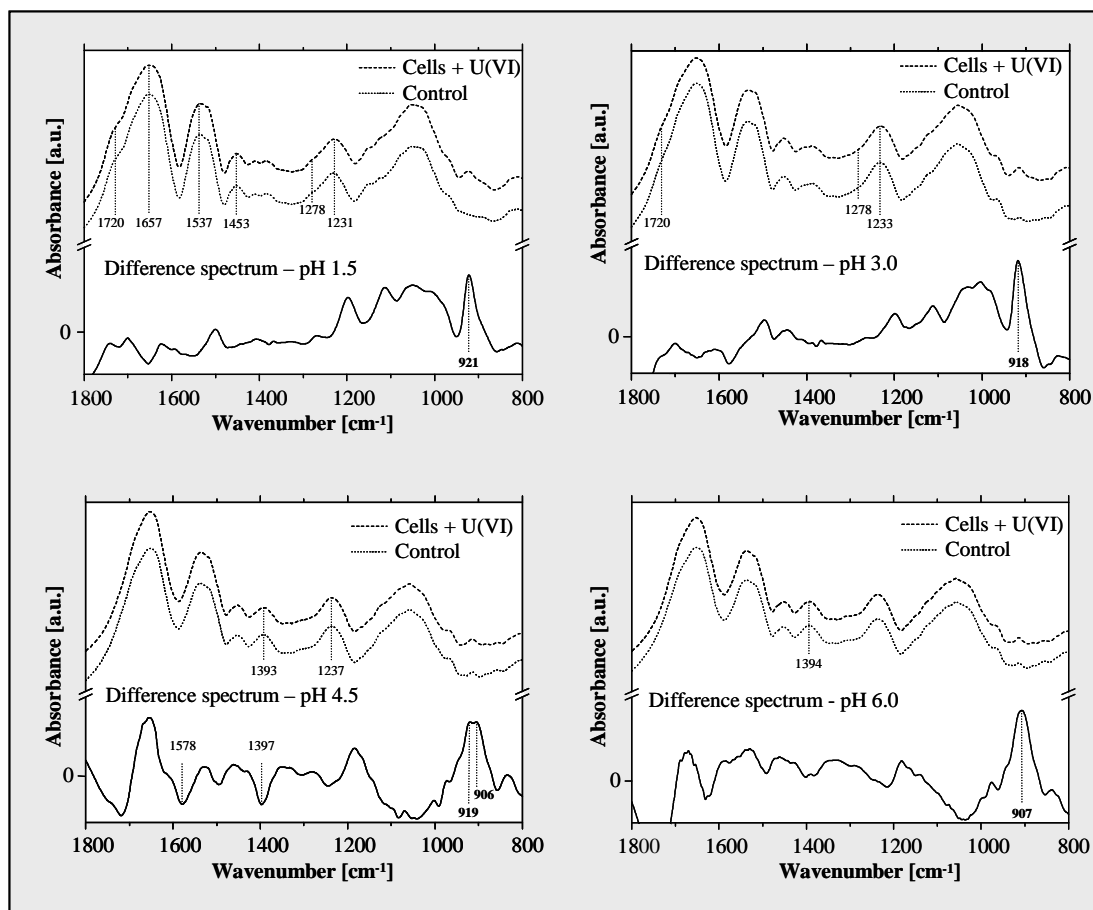


Figure 3.6. FT-IR spectra obtained from the uranium-treated and untreated cells of *S. acidocaldarius* at different pH values and the difference spectra calculated from the spectra of the U(VI) treated cells minus the corresponding spectra of untreated cells ($[\text{U}]_{\text{init}} = 5 \cdot 10^{-4}\text{ M}$, beside at pH 6: $[\text{U}]_{\text{init}} = 5 \cdot 10^{-5}\text{ M}$).

The bands at 1720 cm^{-1} and 1278 cm^{-1} , which are only present as shoulders in the spectra recorded at low pH arises from the $\nu(\text{C=O})$ and $\delta(\text{C-O-H})$ vibration modes of protonated carboxylic groups, respectively [215]. The disappearance of these shoulders with increasing pH, and the simultaneous appearance of a band around 1394 cm^{-1} , assigned to the $\nu_{\text{s}}(\text{COO}^-)$ mode, indicates the change of the protonation state of the carboxylic groups. [212]. The expected band of the $\nu_{\text{as}}(\text{COO}^-)$ mode (1550 to 1600 cm^{-1}) is hidden under the amide II bands.

To clearly determine the chemical groups which are involved in the uranium complexation, difference spectra between the uranium-treated cells and the control samples were calculated. In all samples, the band of the asymmetric stretching vibration $\nu_3(\text{U-O})$ of the uranyl ion is shifted to lower wavenumbers, compared to that of the unbound uranyl ion [216], confirming the complexation of the uranium by the cells. Under strong acidic conditions (pH 1.5 and pH 3), the absorption maximum is located at around 920 cm^{-1} whereas at pH 4.5 the band is split into two bands showing up at 919 and 906 cm^{-1} . At pH 6, a single band showing an absorption maximum at 907 cm^{-1} is observed.

The frequency of the $\nu_3(\text{UO}_2)$ mode correlates with the molecular environment of the uranyl unit. It is commonly known that an increasing number of electronegative ligands in the equatorial plane of the uranyl unit generates an increasing bathochromic shift of the $\nu_3(\text{UO}_2)$ absorption band compared to the fully hydrated ion [217]. Infrared spectra of uranyl(VI) minerals containing relatively strong electronegative ligands and a manifold coordination to the uranyl unit, such as carbonate, generally show strongly shifted absorption bands of the $\nu_3(\text{UO}_2)$ mode [217]. Consequently, the observed bathochromic shift of the uranyl band in the spectra at pH 4.5 (split band) and pH 6 obviously indicates an enhanced complexation of the uranyl ions. According to the results from XAS experiments, the enhancement of the U(VI) complexation, which occurred at pH 6, can be explained by a biomineralization of this radionuclide in a form of uranyl phosphate phases. These inorganic phases are obviously present also in the sample treated at pH 4.5, in addition to the complexes formed at highly acidic conditions (see the split peak in Fig. 3.6). The presence of different uranyl phosphate complexes in the samples is verified by the difference spectra which show a significantly different band pattern in the spectral region of the phosphate groups between 1250 and 950 cm^{-1} at pH values ≥ 4.5 , compared to that at highly acidic conditions. At pH 1.5 and 3 enhanced absorptions were detected in this FT-IR region (Fig. 3.6). The latter is in accordance to the difference spectra of the organic uranium phosphate complexes formed by three eco-types of the acidophilic bacterial strain *Acidithiobacillus ferrooxidans* [159]. In contrast to this, the difference spectra obtained from the samples incubated at pH 4.5 and pH 6 showed reduced absorptions in this region, representing great changes of the origin of the phosphate groups. The spectral changes observed by infrared spectroscopy at pH ≥ 4.5 indicate that a formation of uranyl phosphate mineral phases occurs.

Moreover, the data suggests the involvement of carboxylate groups in the uranium complexation at pH 4.5 due to two significant minima at 1397 cm^{-1} and 1578 cm^{-1} in the

difference spectra calculated for pH 4.5. Corresponding minima, which are very close to the absorption bands of the symmetric double stretching and the antisymmetric stretching modes of carboxylate groups, respectively, were not or only very weakly observed in the difference spectra of all other samples. From the reduction of these vibration modes due to the addition of uranium, the assumed involvement of deprotonated carboxylic groups in the uranium complexation at pH 4.5 is supported.

TRLFS

Another powerful and very sensitive method which allows distinguishing between different functional groups implicated in the uranium binding is TRLF spectroscopy. Besides the high sensitivity, a big advantage of this method is the possibility to identify and distinguish single uranium species in a multi-component system, like microbial cells. In Figure 3.7 the luminescence emission spectra of the U(VI) complexes formed by the cells of *S. acidocaldarius* at pH 4.5 and pH 6, respectively, are shown. The corresponding peak maxima are summarized in Table 3.4.

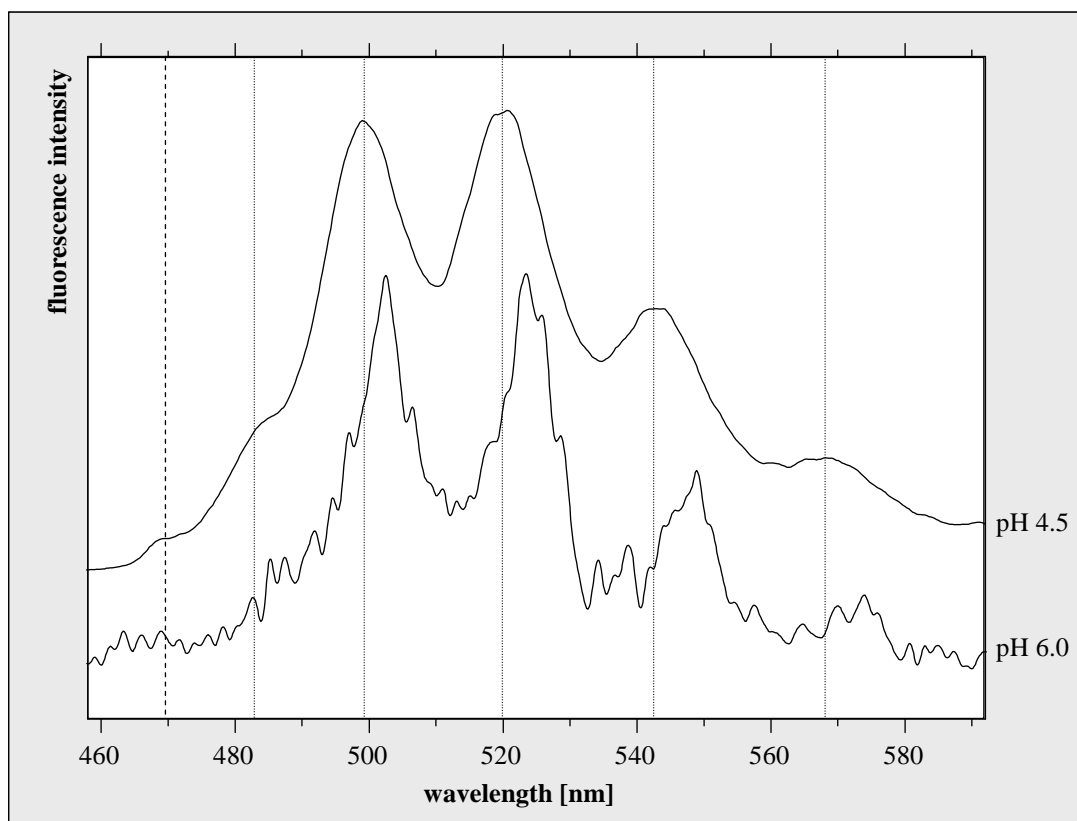


Figure 3.7. Luminescence spectra of the uranium complexes formed by *S. acidocaldarius* at pH 4.5 and 6. For a better comparison the position of the calculated peak maxima of the sample incubated at pH 4.5 are pointed out by dotted lines. The dashed line indicates the position of the luminescence peak exclusively detected in the sample incubated at pH 4.5.

Table 3.4. Luminescence emission maxima of the uranium complexes formed by *S. acidocaldarius* at pH 4.5 and 6 as well as those of some model compounds and uranium complexes formed by bacteria.

Sample	Luminescence emission maxima ^{a,b}					Lifetime(s) (μ s)
UO ₂ ²⁺ (pH 1.5)	473.1	489.5	511.0	534.3	559.6	1.92 \pm 0.12
U(VI) + <i>S. acidocaldarius</i> pH 4.5	469.8	482.9	499.2	520.0	542.7	568.0 0.71 \pm 0.03 4.08 \pm 0.72 10.8 \pm 1.4 39.7 \pm 5.9
U(VI) + <i>S. acidocaldarius</i> pH 6	488.0	502.6	523.1	545.4	574.2	3.97 \pm 0.76
Organic uranyl phosphate complexes						
UO ₂ -fructose(6)phosphate [158]	478.9	497.1	519.0	543.3	568.9	0.13 \pm 0.05
UO ₂ -DMGP [161]	481.5	497.4	519.3	542.4	567.5	1.0; 20
UO ₂ -[NH ₃ CH ₂ CH ₂ OPO ₃] ⁺ [161]	483	498.0	518.4	541.3	565.9	3.1 \pm 0.6
UO ₂ -AMP [159]		497	519	542	569	n.d.
Uranyl lipopolysaccharide complex						
R-O-PO ₃ -UO ₂ [163]	481.5	498.1	519.6	542.9	567.5	1.2 \pm 0.4
Bacteria [154]						
<i>Bacillus sphaericus</i>		498	519	542	569	n.d.
<i>Bacillus sphaericus</i> (decomposed cells)		502	524	548	574	n.d.
Uranyl phosphate minerals						
saleeite [165]	489.0	501.1	522.1	545.7	570.9	2.3 \pm 0.2
meta-autunite [165]	491.3	501.8	522.9	546.9	572.2	0.74 \pm 0.1
Uranyl carboxylate complexes						
(R-COO) ₂ -UO ₂ [167]	466.0	481.6	498.1	518.0	539	566 0.7 \pm 0.1
R-COO-UO ₂ ⁺ [167]						7.3 \pm 1.4

^a Main luminescence emission bands were pointed out by bold letters^b Error of emission bands is \pm 0.5 nm

As evident from these results the recorded spectra exhibit a significant bathochromic shift of more than ten nanometres in comparison to the luminescence spectrum of the aqueous uranyl ion (Table 3.4). The main luminescence emission maxima of the formed uranium complexes at pH 4.5 correspond well to those determined for the complexation of U(VI) by phosphate groups of various organic model compounds, such as phospholipids [161], lipopolysaccharides [163] and sugar phosphates [158]. Highly similar luminescence emission maxima were also found in comparable cell samples of *S. acidocaldarius* incubated at lower pH values of pH 1.5 and 3 [133]. In addition, the emission maxima are well in line with those obtained from TRLFS studies of the uranium complexes produced by the bacterial strain *Bacillus sphaericus* [154]. The authors of the two latter studies demonstrated that the added

uranium was predominantly bound by organic phosphate groups [133, 154]. However, in the case of the here studied sample incubated at pH 4.5, the spectrum also exhibits a distinct luminescence peak at 469.8 nm, which cannot be assigned to uranyl phosphate complexes. A similar peak at about 466 nm was recently detected in luminescence spectra of uranyl carboxylate species formed at phosphate-free peptidoglycan [167]. Hence, the detected emission maximum may rather be assigned to uranyl carboxylate complexes.

The U(VI) luminescence properties of the sample incubated at pH 6 differ significantly from those of the sample incubated at pH 4.5. The resulting luminescence emission maxima exhibit an additional bathochromic shift of 3 to 6 nm in comparison to the spectra of the cell sample incubated at pH 4.5. In agreement with the XAS and FT-IR studies the emission maxima correspond well to those of meta-autunite (Table 3.4) as well as other uranyl phosphate minerals [165]. Almost similar emission maxima were also obtained from decomposed cells of *Bacillus sphaericus* (Table 3.4) [154]. In accordance to our results the authors of the latter study assumed that the corresponding luminescence spectrum arises from inorganic uranyl phosphate complexes ($\text{UO}_2(\text{H}_2\text{PO}_4)_2$), formed due to the liberation of inorganic monophosphate from the decomposed cells of this bacterial strain [154].

Besides the position of the emission maxima the decay of the luminescence was used to distinguish between the different uranyl species present in the archaeal cell samples. The luminescence lifetimes were determined by using the function $I(t) = I_0 + \sum I_i * \exp(-t/\tau_i)$ where I_0 is the background signal, measured after a delay time of 2 ms, I_i the signal factors of the uranium compounds, τ_i the corresponding luminescence lifetime and t the delay time.

The lifetime analysis of the sample incubated at pH 4.5 revealed four luminescence lifetimes, which were determined to be $\tau_1 = (0.71 \pm 0.03) \mu\text{s}$, $\tau_2 = (4.08 \pm 0.72) \mu\text{s}$, $\tau_3 = (10.8 \pm 1.4) \mu\text{s}$ and $\tau_4 = (39.7 \pm 5.9) \mu\text{s}$. However, we could not detect a significant shift of the luminescence emission maxima depending on the delay time. With regard to the calculated errors, two of the calculated lifetimes (τ_2 , τ_4) are well in line with those determined in studies performed in our laboratory on uranium accumulation by *S. acidocaldarius* at pH values around the physiological optimum of this strain (pH 1.5 and 3) [133]. Due to the formation of corresponding uranium complexes also at highly acidic conditions and the consistent emission maxima, the lifetimes τ_2 and τ_4 were assigned to organic uranyl phosphate complexes, which differ in their metal-to-ligand ratio and/or in the binding of U(VI) to deprotonated or protonated phosphate groups as discussed earlier [133]. The lifetime of $(4.08 \pm 0.72) \mu\text{s}$ agrees also well to the luminescence lifetimes calculated for the organic phosphate

complexes formed by the acidophilic bacterial strains *A. ferrooxidans* and *Thiomonas cuprina* [198]. Further studies on one of these strains (*A. ferrooxidans* ATCC 33020) revealed a significantly longer lifetime of about 45 μs [159], which is very similar to the longest luminescence lifetime τ_4 of $(39.7 \pm 5.9) \mu\text{s}$ found in this study.

The uranium species exhibiting luminescence lifetimes of $\tau_1 = (0.71 \pm 0.03) \mu\text{s}$ and $\tau_3 = (10.8 \pm 1.4) \mu\text{s}$ were almost identical to those of the recently investigated uranyl carboxylate complexes formed at phosphate-free peptidoglycan [167]. Therefore these lifetimes were assigned to uranyl carboxylate complexes causing the luminescence emission maximum at 469.8 nm. A short luminescence lifetime, comparable to τ_1 , was also calculated from parallel samples incubated under highly acidic conditions (Chapter II). In the latter case, this short lifetime was assigned to uranyl phosphate complexes, suggesting that τ_1 had also arisen from corresponding complexes. However, a bi-exponential decay with similar lifetimes to τ_1 and τ_3 was also observed for the U(VI) luminescence between 465 and 470 nm. This finding strongly supports the assumption that τ_1 and τ_3 arose from uranyl carboxylate complexes, as this region of the spectrum is exclusively determined by the luminescence of the first emission band, which is characteristic for these complexes. Besides this first emission band, the remaining spectrum of the uranyl carboxylate complexes is masked by the highly luminescent uranyl phosphate complexes.

For the uranyl complexes formed at pH 6 only one lifetime of $(3.97 \pm 0.76) \mu\text{s}$ was calculated, which we therefore clearly attribute to the formed uranyl phosphate mineral phases. The lifetime agrees well to those obtained from TRLFs studies of various uranyl phosphate minerals (Table 3.4) [165]. However, it is also very similar to one of the lifetimes calculated from the sample incubated at pH 4.5 ($\tau_2 = 4.08 \pm 0.72 \mu\text{s}$). As mentioned above, a very similar lifetime was also calculated from parallel cell samples incubated at lower pH values where the presence of corresponding uranyl phosphate mineral phases was excluded [133]. This suggests the formation of organic (at highly acidic conditions) and inorganic (pH 6) uranyl phosphate species with similar luminescence lifetimes. With regard to this finding as well as to the XAS and FT-IR results, it is obvious that at pH 4.5 the calculated lifetime of $\tau_2 = (4.08 \pm 0.72) \mu\text{s}$ is most likely the result of the decay of these two different uranyl phosphate species. Hence, the TRLFs results demonstrate that at pH 4.5 at least four, but rather five different uranyl complexes were formed; three different uranyl phosphate and two uranyl carboxylate complexes.

In contrast to this, the TRLFS studies confirmed the exclusive formation of inorganic uranyl phosphate mineral phases at pH 6. Even though this method is outstanding due to its high sensitivity, we could not detect any organic uranyl compounds at this pH. This finding, combined with the fast removal of uranium from the solution observed at pH 6 (Fig. 3.2), suggests that at this pH uranium was initially bound to the functional groups of the cell surface biopolymers and after longer incubations complexed by inorganic phosphate groups which seems to possess a higher complexing capability than the organic ligands. A similar process was recently shown for *P. aeruginosa* [89]. In this case uranium was initially adsorbed to the cells of this bacterial strain in the form of uranyl hydroxides. However, after a longer incubation uranium was predominantly complexed by orthophosphate liberated by the cells. Our results obtained by a combination of EXAFS-, FT-IR-, and TRLF- spectroscopic analyses confirm the very high affinity of U(VI) to microbially-generated orthophosphate.

Acid phosphatase assay and determination of phosphate concentration

To clarify the origin of the inorganic phosphate groups which are responsible for the uranium complexation, we used an enzymatic assay. It is well-known that inorganic phosphate groups were liberated at acidic conditions by the activity of various enzymes summarized as acid phosphatases (APases) [218]. A corresponding enzyme had also been purified from *S. acidocaldarius* [33]. The authors of the latter study demonstrated that the isolated acid phosphatase of *S. acidocaldarius* possesses pH and temperature optima of 5 and 70 °C, respectively [33]. At moderate temperatures of 30 °C the enzyme has a significantly lower but detectable activity, which is about 10% of that at 70 °C. In contrast to this study, we used intact cells of *S. acidocaldarius* for determining the APase activity at room temperature. The obtained APase activities at the studied pH values (pH 3, 4.5 and 6) are presented in Figure 3.8.

As evident from the figure, the considerably highest activity was calculated for the sample incubated at pH 3, which equates to the physiological optimum of the strain. The reduced APase activity at pH 4.5 is most likely a result of the stress due to the non-optimal pH conditions. The latter assumption was supported by Live/Dead staining which demonstrated an increased rate of cell death (Fig. 3.9). At pH 6, in addition, the enzyme by itself is inhibited and possesses a lower activity [33].

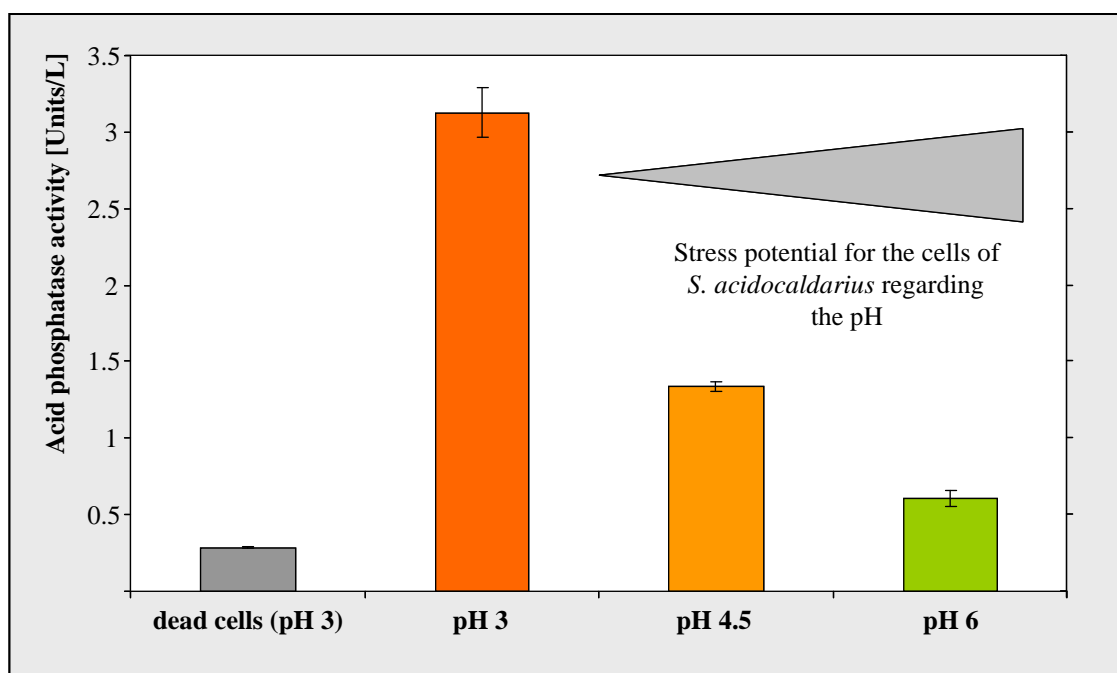


Figure 3.8. Acid phosphatase activity of *S. acidocaldarius* at different pH values. Heat-killed cells were used as a control to calculate the abiotic conversion of *p*-nitrophenyl phosphate.

We also determined the amount of orthophosphate in the supernatants of the cell samples after incubation for 48 hours in 0.1 M NaClO₄ (pH 3, 4.5 or 6) with and without the addition of uranyl nitrate (Fig. 3.10). As expected from the APase activity studies, we observed a significant release of orthophosphate from the cells into the supernatant at pH 3. The higher amounts of phosphate in the control samples incubated at pH 4.5 and 6, compared to that incubated at pH 3, are at first view inconsistent with the results obtained by the APase activity studies. However, Live/Dead staining demonstrated a significant higher amount of cells exhibiting damaged cell envelopes at pH 4.5 and 6 (~45% and ~50%, respectively), compared to the sample incubated at pH 3 (~10%) (Fig. 3.9). The increased cytoplasmic membrane permeability of some cells may lead to an enhanced release of phosphorylated organic compounds which serve as substrates for the archaeal APase.

Although a significant release of inorganic phosphates from the cells was demonstrated at pH 3, we observed, considering the error bars, no differences between the uranium-treated and untreated cell samples. This finding excludes the formation of uranyl phosphate mineral phases at this pH, which is in accordance to spectroscopic studies of the uranium complexes produced by *S. acidocaldarius* at pH 1.5 and 3 [133]. The absence of U(VI) biomineralization might be explained by the lower release of orthophosphate and/or a general inhibition of the mineral formation at highly acidic conditions. The latter assumption is supported by a recent

study demonstrating that uranyl phosphate minerals are rather unstable at acidic pH values [86].

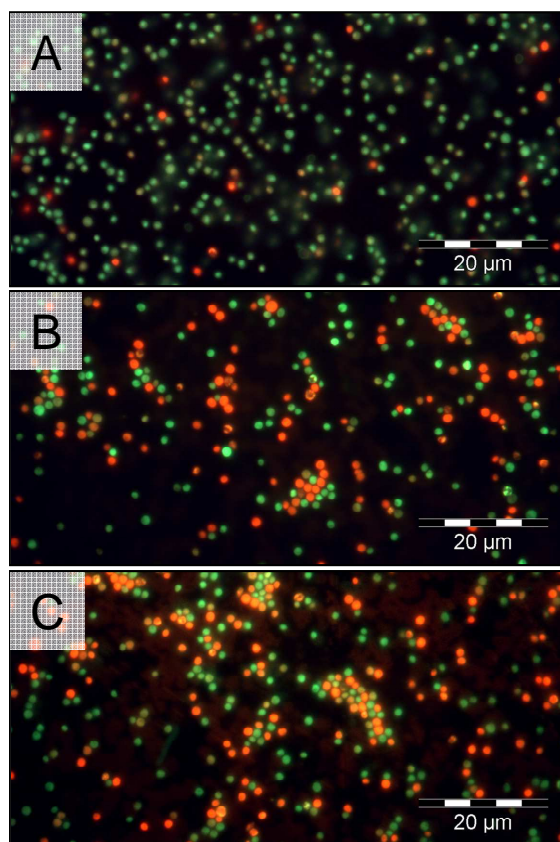


Figure 3.9. Microscopic pictures of *S. acidocaldarius* stained with the Live/Dead Kit after the treatment with uranium at pH 3 (A), pH 4.5 (B) and pH 6 (C) for 48 hours. Pictures were taken at 1000-fold magnification in fluorescence mode using a fluorescence mirror unit (U-MSWB; Olympus Optical Co. GmbH, Hamburg, Germany) with excitation wavelengths between 420 and 460 nm. For the differentiation of live and dead cells a mixture of two stains was used. Green fluorescence is caused by SYTO 9, a stain which generally labels all cells in a population. In contrast, the red fluorescent stain, propidium iodide, penetrates only cells with damaged cell membranes, causing a reduction in the SYTO 9 fluorescence when both dyes are present.

In contrast to that, the uranium-treated and untreated samples incubated at pH 4.5 and pH 6 differed significantly from each other. Phosphate concentration in the supernatant of the uranium-treated sample incubated at pH 4.5 was reduced to more than 80% compared to the control sample. In the sample incubated at pH 6 the difference in phosphate concentration was about 65%. This removal of phosphate from the supernatant was assigned to the precipitation of inorganic uranyl phosphate complexes in both samples. The reason for the lower removal of phosphate from the uranium-treated samples at pH 6, compared to that at pH 4.5, is most likely due to lower uranium concentration used at this pH.

Our findings demonstrate that inorganic phosphate, responsible for the uranium complexation at moderate pH values (pH 4.5 and 6), is released by the cells of *S. acidocaldarius*, as a

consequence of both, increased cytoplasmic membrane permeability and the APase activity of the strain.

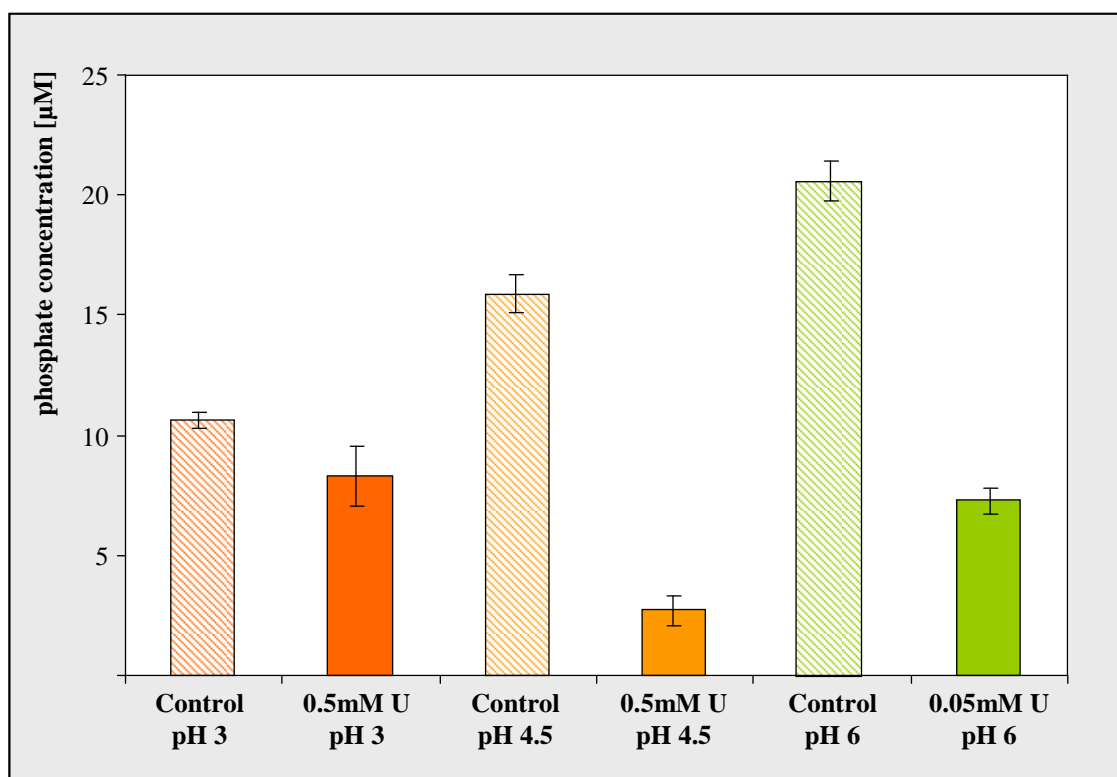


Figure 3.10 Amount of orthophosphate released by the cells of *S. acidocaldarius* into the supernatant after an incubation of 48 hours in dependency on pH and the presence of uranium.

Microscopic Analyses

The formed uranyl phosphate minerals were localized by using light microscopy. As evident from the results presented in Figure 3.11, the mineral phases formed after 48 hours exhibit a needle-like structure with a length of up to 2 μm (Fig. 3.11-A). In addition, they show a green luminescence after excitation with ultraviolet light (Fig. 3.11-a), as it is well-known for autunite and other secondary uranium minerals [219]. In parallel samples, which were stored after the treatments with uranium for a longer time at 4 °C, a further mineralization of U(VI) was observed. As shown in Figures 3.11-B and 3.11-b, after two weeks bigger uranyl minerals with more complex morphology, consisting of several needle-like crystals, started to appear. The formed minerals continued to grow and after six months the single crystals exhibited a length of up to 10 μm (Fig. 3.11-C and c).

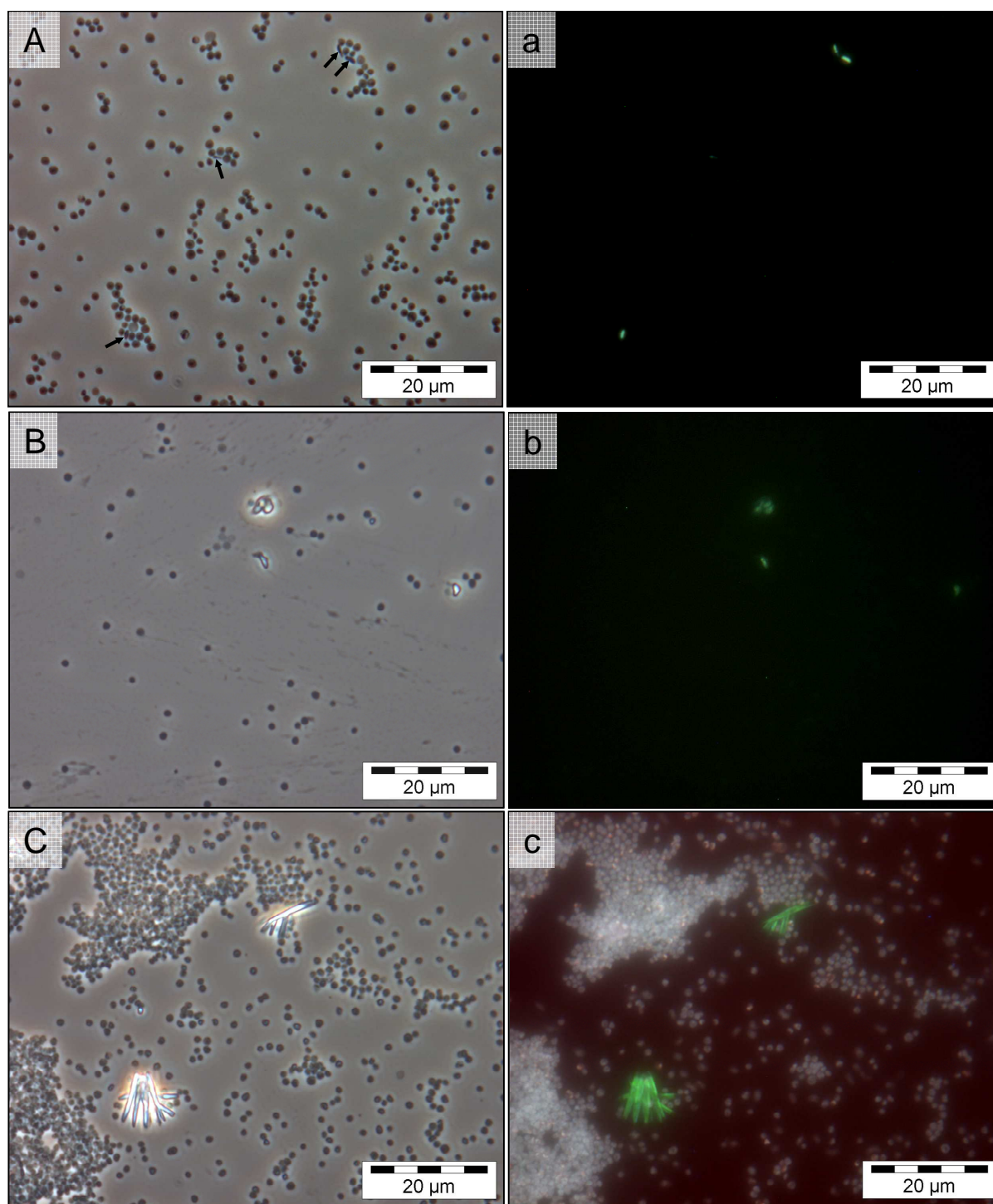


Figure 3.11. Light microscopic pictures of the uranyl phosphate mineral phases formed by the cells of *S. acidocaldarius* at moderate acidic conditions after an incubation for 48 hours (A and a), two weeks (B and b) and six months (C and c). All pictures were taken at 1000-fold magnification in phase contrast mode (A, B and C) and in fluorescence mode using a filter unit with excitation wavelengths between 360 and 370 nm (a, b and c).

In order to improve uranium detection in the samples incubated with U(VI) for 48 hours we additionally performed TEM analyses coupled with EDX. By using this method we observed in the sample treated at pH 4.5 contrasting electron-dense uranium accumulates, which were

localized intracellularly, associated with the cytoplasmic membrane (Fig. 3.12-A). These deposits probably represent a part of the formed organic uranium complexes and contained only low amounts of uranium. Therefore, these deposits were exclusively detected in the parallel TEM samples, which were not contrasted with lead citrate (Fig. 3.12-A).

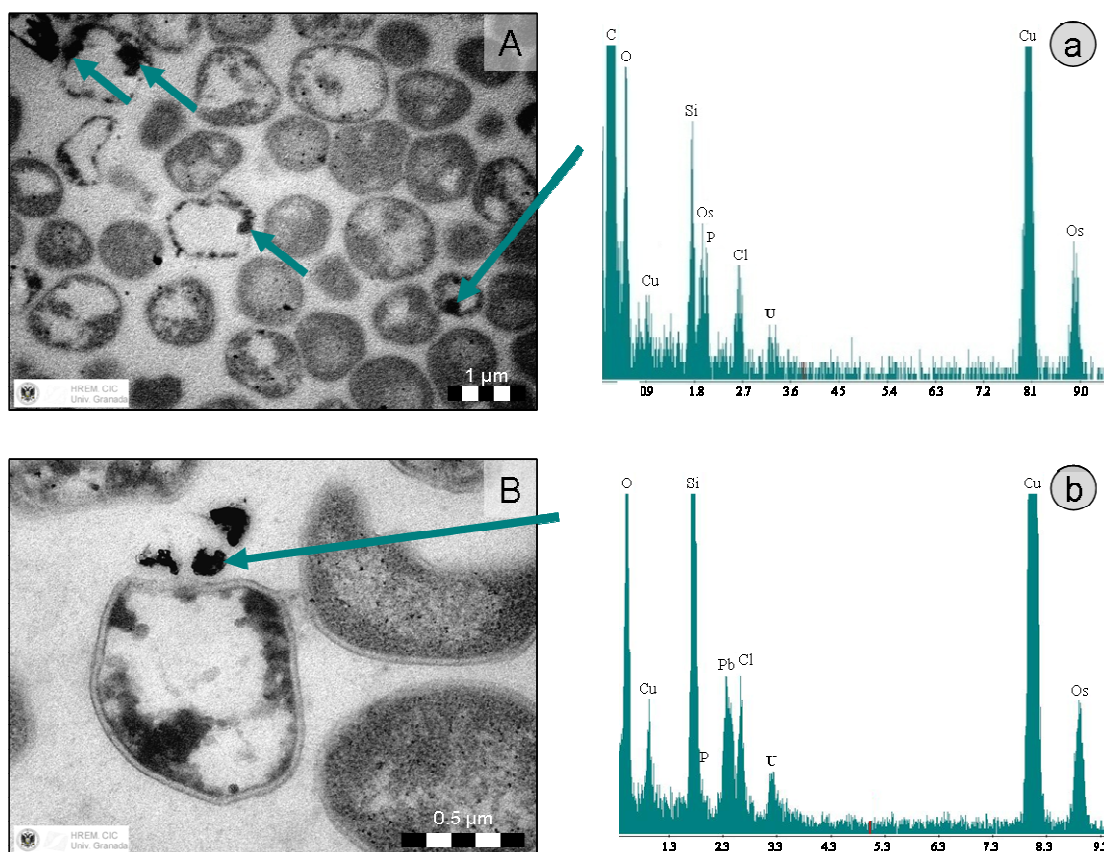


Figure 3.12. TEM micrographs of ultra-thin sections of *S. acidocaldarius* incubated with 0.5 mM U(VI) at pH 4.5 for 48 hours. Uranium accumulates were located at the inner surface of the cytoplasmic membrane (A) as well as in extracellular accumulates (B). EDX-spectra of selected uranium accumulates, marked with arrowheads, were recorded to confirm the presence of uranium (a and b).

As evident from the presented EDX spectrum (Fig. 7a), the most likely organic complexes consist besides of uranium (U) of phosphorous (P) and oxygen (O). The peaks for C, Cu, Os, Pb and Cl are a result from the TEM sample preparation and the copper grid used to support the ultra-thin cell sections. The presence of Si results from the oil in the diffusion pump of the column of the used TEM system. Such intracellular uranium deposits were exclusively detected in apparently empty cells. This indicates that the formation of these uranium deposits is a consequence of the increased cytoplasmic membrane permeability due to the cell death. Overall such uranium deposits were detected in five to ten percent of the cells.

We did also observe some extracellular uranium-containing complexes most likely representing the inorganic mineral phases (Fig. 3.12-B). As evident from the corresponding

EDX spectrum they contain high amounts of uranium (U), and as in the case of the organic complexes, phosphorous (P) and oxygen (O) (Fig. 3.12-b).

Hence, TEM studies revealed that the increased binding of this radionuclide which was observed after longer incubations of 48 hours at the studied moderate pH of 4.5 is primarily based on an uncontrolled uranium uptake by the damaged archaeal cells, which exhibit an increased permeability of the cytoplasmic membrane, and consequent intracellular U(VI) binding by functional groups, provided by the cytoplasmic membrane and other cellular structures. In addition, and to a much lesser extent, the extracellular precipitation of inorganic uranyl phosphate minerals contributed to the increased U(VI) binding after 48 hours.

As already suggested within the bioaccumulation results, we did not observe uranium deposits at the S-layer which is the only cell wall component in the studied archaeon. This is in contrast to bacteria which have a thick peptidoglycan layer (in the case of Gram-positive bacteria) or a complex multi-layered cell wall (in the case of Gram-negative bacteria) both rich in uranium binding ligands, which may protect the bacterial cells from the toxicity of uranium [150]. It was approved that the basic function of the S-layer of *S. acidocaldarius* is to keep the cell shape at extreme conditions such as high temperatures (about 70 °C) and acidity (pH about 2) [220, 221] but as demonstrated by TEM obviously not to bind metals.

Unfortunately, our efforts to localize uranium by TEM in the sample incubated at pH 6 failed most likely due to ten-times lower uranium concentration used, compared to that used for the sample incubated at pH 4.5. The formation of uranium minerals in the sample incubated at pH 6 was, however, clearly demonstrated by light microscopy.

CONCLUSIONS

Results obtained in this study allow to conclude that at moderate acidic conditions, typical for environments polluted with uranium, U(VI) can be immobilized by thermoacidophilic archaeal strains of the species *S. acidocaldarius* which are indigenous in heavy metal-polluted environments. At pH 4.5, U(VI) is bound to organic phosphate groups, which are also involved in the U(VI) complexation at lower pH values. In addition, the unusual cell wall structure of *S. acidocaldarius* which in contrast to bacteria consists only of a proteinaceous S-layer, allowed the spectroscopic detection and the determination of the structural parameters of U(VI) complexes formed by the carboxylic groups. After longer incubations at these non-optimal for the archaeal strain conditions an increased cytoplasmic

membrane permeability was observed, which results in an uptake of U(VI) into the cells and a subsequent binding by functional groups of the intracellular structures. TEM also revealed extracellular uranium accumulates which might have inorganic origin. However, the spectroscopic data clearly demonstrated that the studied archaeal cells bind the main part of U(VI) *via* organic functional groups. This result is in contrast to the previously studied interactions of acidophilic bacteria with U(VI), where the binding occurs in a pH-independent way, e.g. only organic phosphate groups participate in the complexation process at pH 2 and at pH 4.5 as well. Moreover, the described process differs also from the observed precipitation of U(VI) mainly in inorganic phosphate phases by all neutrophilic bacteria, at this pH. In the case of *S. acidocaldarius* this function seems to be limited at pH 4.5, maybe due to the non-optimal temperature conditions and/or the fact that this archaeon contains less polyphosphate bodies which are the source of the enzymatically-produced orthophosphate implicated in the process of biomineralization. Therefore, the results of the present study suggest that the mechanisms of interaction and detoxification of U(VI) by the cells of the studied here archaeal strain *S. acidocaldarius* differ significantly from both acidophilic and non-acidophilic bacteria. At pH 6, however, uranyl phosphate mineral phases were, as in the case of most bacteria, the only uranium complexes found after the treatment of the cells with U(VI) for 48 hours. This can most likely be explained by the lower amount of uranium in the solution along with the higher release of orthophosphate from the cells.

Chapter IV

Complexation of uranium by S-layer and cell ghosts of *Sulfolobus acidocaldarius*.

T. Reitz, M. L. Merroun, A. Rossberg, A. Barkleit,
R. Steudtner, and S. Selenska-Pobell

ABSTRACT

U(VI) binding by two cell envelope fractions of *S. acidocaldarius*, both maintaining the shape of the cells, was investigated by using time-resolved laser-induced fluorescence spectroscopy and X-ray absorption spectroscopy, combined with biological methods. The first fraction, refereed as “SlaA-layer ghosts”, consisted of the outermost proteinaceous surface layer of *S. acidocaldarius* called “SlaA-layer”. The second fraction, refereed as “cell envelope ghosts”, consisted of cytoplasmic membrane and another inserted in it S-layer protein, called “SlaB”, anchoring the SlaA. We demonstrate that at highly acidic conditions (pH 1.5 and 3), covering the physiological optimum of the archaeal strain, the “SlaA-layer ghosts” do not bind U(VI), while the “cell envelope ghosts” bind U(VI) *via* organic phosphate groups similarly to whole cells. Hence, at acidic conditions the outermost SlaA-layer does not provide protective functions against U(VI) to the cells of this acidophilic archaeon.

In contrast to the whole cells, the U(VI) binding mode of the cell envelope ghosts at moderate acidic pH (pH 4.5 and 6) is not significantly changed. At these pH values a complexation of U(VI) by the SlaA-layer ghosts *via* its carboxylic groups is stimulated. At these unfavourable for *S. acidocaldarius* conditions the fraction of the extremely stable SlaA-layer ghosts is strongly increased due to the death of a considerable part of the cells. The latter indicates that in moderate acidic environments the “SlaA-layer ghost” structures may influence migration of U(VI).

Keywords: *Sulfolobus acidocaldarius*, S-layer, Cell envelope ghosts, Interactions with U(VI), X-ray absorption spectroscopy, Time-resolved laser-induced fluorescence spectroscopy

INTRODUCTION

Highly ordered and self-assembling proteinaceous surface layers (S-layers) are widespread structures of the prokaryotic cell envelopes [220-224]. In Gram-positive bacteria they are usually anchored to the peptidoglycan and in Gram-negative mostly to their outer membrane [91, 224, 225]. In many archaea, as in the case of the studied in the present work acidothermophilic crenarchaeon *Sulfolobus acidocaldarius*, S-layers represent the only cell wall component and provide mechanical, osmotic and possibly thermal stabilization of the cells, crucial for their survival in harsh environmental conditions [220-222, 226]. Despite their occurrence in a wide range of prokaryotes, no uniform function was attributed to the known up to date S-layers. For many bacteria, in contrast to most archaea, S-layers are not essential for their survival and can be even lost in laboratory. Their maintenance on the cell surface in natural conditions can be, however, connected with various important environmental functions, such as a barrier for cell-lytic enzymes [223] and shields against predators [227]. S-layers support the invasive process of various pathogenic bacteria *via* their protection against humoral immune defence of the infected organisms [228] and play important role as a virulence factor [223]. In *Bacillaceae* S-layers serve as adhesion sites for cell-associated exoenzymes [91] or as metal [93, 229-231] and even radionuclide binding surfaces [150, 231]. For the latter case an interesting protection mechanism against U(VI) toxicity was postulated, which is based on the high uranium binding capacity of the S-layer of the uranium waste pile isolate *Bacillus sphaericus* JG-A12 [150]. The authors of the latter study demonstrated that after the saturation with uranium the S-layer was discarded from the cell surface and replaced by newly-synthesized S-layer lattices which continue to bind the radionuclide [150].

It was published that the S-layers of most bacteria living at moderate conditions possess tetragonal (p4) or oblique (p2) lattices regularity, while the S-layer lattices of extremophilic archaea usually exhibit p6- or p3-symmetry [220] and as a rule they are much more stable [226]. Their function as an exoskeleton structure, which gives the archaeal cells defined and invariable shape at various harsh conditions was recently postulated [221]. The possible function of archaeal S-layers against toxic metals and radionuclides was not yet studied.

The cells of the studied archaeal strain are covered with a detergent-resistant proteinaceous S-layer, called SlaA-layer [81]. The outermost SlaA-layer possesses p3-symmetry and is fasten to the archaeal cells *via* another, integrated into the cytoplasmic membrane, anchoring protein [90], recently called SlaB [81]. The SlaA-layer is very stable against high temperature, proteases, and detergents. Therefore standard purification procedures result in the isolation of

empty SlaA-layer ghosts with the shape of the cells [232, 233]. These ghosts can be only mechanically (e.g. *via* sonication) disrupted in monolayer sheets, which are comparable to those yielded usually from bacteria without mechanical disintegration. Due to the extreme stability of the SlaA-layer such empty ghosts of *S. acidocaldarius* may also be present in natural systems.

In this study the interactions were investigated of U(VI) with purified SlaA-layer ghosts and with cell envelope ghosts of *S. acidocaldarius*, consisting of cytoplasmic membrane covered with SlaB- and SlaA-protein layers. The comparison of the obtained results with those about the recently published interactions of whole cells of *S. acidocaldarius* with uranium [133, 164] allow to clearly differentiate the role of the SlaA-layer in the bioaccumulation of this radionuclide.

MATERIALS AND METHODS

Preparation of the SlaA-layer ghosts and the cell envelope ghosts

S. acidocaldarius (strain DSM 639) was purchased from the German Collection of Microorganisms and Cell Cultures - “Deutsche Sammlung für Mikroorganismen und Zellkulturen” (DSMZ, Braunschweig, Germany) and cultivated at pH 2.7 and 70 °C in a large-scale fermentation system (Pilot System, Applikon Biotechnology Inc., Foster City, CA, USA) equipped with a 70 L bioreactor, a bio-controller (Model ADI 1010), and a control unit (ADI 1075) with three pneumatic pumps (acid, base, and antifoam), stirrer controller, and rotameters. The automatic control of pH, temperature and dissolved oxygen during the fermentation process resulted in an efficient growth of the strain, which assured high yields of cell envelope structures. After reaching the end of the logarithmic growth phase ($OD_{600} \sim 0.9$), the archaeal cells were harvested by using a continuous flow centrifuge (10000 g, 15 min) (CARR® ViaFuge® Pilot 9010, Kendro, Newtown, CT, USA). For cell lysis, the biomass was suspended in 10 mM HEPES buffer (pH 7), containing 2 mM EDTA and 0.15% SDS, and stirred for one hour at room temperature, according to Michel and co-workers [201]. After the addition of 4 mM $MgCl_2$, released DNA was digested by DNase I. Preparation of the SlaA-layer ghosts was performed in the following way: To achieve complete removal of the cytoplasmic membrane and the additionally anchored in it SlaB protein, the cell lysate was treated with 2% SDS and stirred overnight. After a centrifugation of the suspension (40000 g, 30 min), the lower dark part of the resulting pellet

was discarded, whereas the upper white part was suspended in HEPES buffer (pH 7) containing 2 mM EDTA and 2% SDS and incubated for 60 min at 60 °C. This washing procedure with hot SDS was performed one more time. After that the suspension was centrifuged and the upper part of the resulting pellet, consisting of the purified outermost S-layer sacculi, i.e. SlaA-layer ghosts, was suspended in distilled water (pH ~6.4). SDS was removed from the SlaA-layer ghosts by eight wash steps with distilled water. In order to obtain “cell envelope ghosts”, i.e. empty cell sheaths, consisting of the cytoplasmic membrane covered by the SlaB and SlaA-layers, an aliquot of the thick mucilaginous suspension, obtained after a shorter cell lysis (20 min), was directly centrifuged for 30 min at 40000 g without any further SDS treatment. After that the upper beige layer was selectively suspended and washed five times with distilled water. Both cell envelope fractions were stored at 4 °C and microscopically checked for microbial contamination before use.

SDS-PAGE analysis of the SlaA-layer and the cell envelope ghosts

The protein content of both cell envelope fractions (SlaA-layer ghosts and cell envelope ghosts) was analysed by using denaturing sodium dodecyl sulfate polyacrylamide gel electrophoresis (SDS-PAGE) according to Laemmli [131] in a Mini-PROTEAN® II electrophoresis cell system (Bio-Rad Laboratories, Munich, Germany). For complete solubilisation, the SlaA-layer and the cell envelope ghosts were initially incubated in sodium carbonate buffer (20 mM, pH 10) for 20 min at 45 °C according to Grogan and co-workers [232] and subsequently heated (95 °C) for 5 min in SDS sample buffer [131]. The proteins were separated on a 10% separation gel. Because of the low content of basic amino acids (0.3 mol% arginine, 0.3 mol% histidine and 2.2 mol% lysine) [220] the common Coomassie Brilliant Blue dye is unsuitable to stain the S-layer protein of *S. acidocaldarius*. To increase sensitivity we stained the SDS gel with colloidal Coomassie Brilliant Blue G-250 [234].

SlaA-layer stability assay

The pH stability of the isolated SlaA-layer ghosts was studied in two buffer systems, in order to cover a pH range from pH 1 to 12 - Sørensen's citrate buffer (0.1 M citric acid, 0.2 M NaOH; pH adjusted with 0.1 M HCl) and Theorell-Stenhagen-buffer (33 mM citric acid, 33 mM phosphoric acid, 57 mM boric acid, 34.4 mM NaOH; pH adjusted with 0.1 M HCl). 200 µg each of the purified SlaA-layer ghosts were suspended in 2 ml of the buffer solutions. The tested pH ranges were pH 1 to 4 for Sørensen's citrate buffer and pH 2 to 12 for the Theorell-Stenhagen-buffer (step size in both cases was 0.5). The suspensions were incubated

for 48 hours on a rotary shaker at room temperature and afterwards absorption spectra of all samples were recorded in the range from 245 to 400 nm using a UV/Vis spectrometer (TIDAS 100, J&M Analytik AG, Esslingen, Germany) with the accompanying software TidasDAQ. The integration time was set to 250 ms and 20 single spectra were accumulated for each sample. Background was recorded by measuring a buffer solution without SlaA-layer protein and automatically subtracted from the spectra of all samples. For comparison, untreated SlaA-layer ghosts suspended in distilled water and SlaA-monomers were measured as well. The latter were produced by a dissociation of the SlaA-layer ghosts at 60 °C in 0.1 M phosphate buffer (pH 9) [201].

Biochemical analyses of the SlaA-layer ghosts

Potentiometric titration experiments were carried out under inert gas (N₂) atmosphere at 25 °C. About 75 mg SlaA-layer ghosts were suspended in carbonate-free deionised water, supplemented with sodium perchlorate to assure an ionic strength of 0.1 M. The suspension was initially acidified with carbonate-free HClO₄ to a starting pH of about 2.7 and subsequently titrated with carbonate-free 10 mM NaOH (Titrisol, Merck, Darmstadt, Germany). The pH was continuously measured with a BlueLine 16 pH electrode (Schott, Mainz, Germany). The dynamic titration procedure was performed with an automatic titrator (TitroLine alpha plus, Schott, Mainz, Germany), monitored by the accompanied software (TitriSoft 2.11, Schott, Mainz, Germany), and analysed with the Software Hyperquad2006 [235].

The amount of phosphate groups of the SlaA-protein was quantified by colorimetric measurements, according to [140]. Phosphate was released from the SlaA-layer ghosts by alkaline hydrolysis. 100 µl 2 M NaOH were added to 100 µl SlaA-layer ghost suspension, containing about 4.5 mg SlaA-protein, and subsequently incubated at 100 °C for 15 min. The reaction was stopped by the addition of 100 µl 4.7 M HCl. After cooling down to room temperature, 100 µl phosphate reagent [140] was added to the samples. After that, they were incubated for 20 min at room temperature and subsequently the absorption of the formed complex was measured at 660 nm. In addition, the total amount of phosphorous in the SlaA-layer ghost fraction was measured using inductively-coupled-plasma mass-spectroscopy (ICP-MS) according to Merroun and co-workers [150].

Treatments with U(VI)

Parallel portions of the SlaA-layer ghosts and cell envelope ghosts were rinsed twice with 0.1 M NaClO₄ at pH 1.5, 3, 4.5, and 6, respectively, and after that suspended in the respective NaClO₄ solution. The pH of the suspensions was checked and if necessary adjusted to the desired values. After the complete removal of the washing solution, uranyl nitrate diluted in 0.1 M NaClO₄ with the corresponding pH was added. The final concentration of the SlaA-protein in the samples was 0.5 mg/mL and that of uranium was $5 \cdot 10^{-4}$ M, beside at pH 6, where it was reduced to $5 \cdot 10^{-5}$ M to prevent the formation and precipitation of poorly soluble uranyl hydroxide species. Samples were incubated at room temperature for 48 hours on a rotary shaker. Subsequently, the SlaA-layer ghosts were removed from the solutions by centrifugation (30000 g, 30 min) and the unbound uranium in the supernatant was measured by ICP-MS using an Elan 9000 system (Perkin Elmer, Waltham, MA, USA). Control reactions without SlaA-layer ghosts were treated in the same way to exclude abiotic uranium removal from the solution, due to precipitation and/or chemical sorption at the used test vials. The amount of accumulated uranium was normalized to the dry biomass, which was determined by weighting parallel samples after drying for 48 hours at 70 °C. Isolated cell ghosts were treated analogically.

Time-Resolved Laser-induced Fluorescence Spectroscopy (TRLFS)

After the contact with U(VI) for 48 hours the SlaA-layer ghosts as well as the cell envelope ghosts were washed twice with 0.1 M NaClO₄ at pH 1.5, 3, 4.5, and 6, respectively, and subsequently suspended in the corresponding washing solution. Room temperature measurements of the suspensions were conducted in a quartz micro cuvette by using a Nd-YAG laser system (Spectra Physics, Santa Clara, CA, USA) [187] with an intensity of 0.3 mJ. The central wavelength of the spectrograph was set to 520 nm and the gate time of the ICCD camera was between 30 and 50 μs (complete detection system: HORIBA Jobin Yvon GmbH, Darmstadt, Germany). For time-resolved measurements a digital delay generator (DG535, Stanford Research Systems, Sunnyvale, CA, USA) was used. The number of laser pulses for excitation (30 to 70) was adjusted depending on the amount of uranium in the samples. Before each series of measurements the background signal was measured 2 ms after the laser pulse and automatically subtracted from the spectra.

For luminescence measurements at cryogenic conditions, 3 ml each of the SlaA-layer ghosts suspensions were filled into plastic cuvettes, subsequently sealed with parafilm and placed horizontally in a freezer (-20 °C) over night. Immediately before measurement, the frozen

sample was removed from the cuvette and transferred in a specifically designed sample holder (metal block with one hole to insert the sample and three windows for laser irradiation). Temperature of the measuring system was decreased to 153 K using a cryostat (RDK 10-320) with an ultra-pump station (PT50 KIT/DN 40 KF), a compression unit (RW2) and a low temperature controller LTC60 (complete system: Oerlikon Leybold, Dresden, Germany). A Nd-YAG laser system (Inlite II, Continuum Electro-Optics Inc., Santa Clara, CA, USA), providing a wavelength of 266 nm, was used for the luminescence excitation in the samples. The central wavelength of the spectrograph was 515 nm and spectra were recorded between 429 and 600 nm using an ICCD-camera (model 7467-0008, Princeton Instruments, Trenton, NJ, USA) with a gate width of 2 μ s.

The spectrographs of both systems were calibrated using a mercury lamp with known emission lines. 101 U(VI) luminescence spectra (each calculated by averaging three single measurements) were recorded after defined delay times. Deconvolution of the emission spectra and luminescence lifetime calculations were performed using Origin 7.5 (OriginLab Corporation, Northampton, MA, USA) including the PeakFit module 4.0.

X-ray Absorption Spectroscopy (XAS)

For XAS measurements, about 50 mg of the SlaA-layer ghosts were treated with U(VI) for 48 hours. After the contact with U(VI) the SlaA-layer ghosts were washed twice with 0.1 M NaClO₄ at pH 4.5 and 6, respectively. Subsequently they were dried for three days at 35 °C in a vacuum oven (VT 6025, Heraeus-Instruments Vacutherm, Hanau, Germany). After that the samples were powdered and mounted on Kapton tape. Six layers of sample-covered tape were stuck on the top of each other and subsequently shrink-wrapped. The XAS measurements were performed at the Rossendorf Beamline (ROBL) at the European Synchrotron Radiation Facility (ESRF), Grenoble, France [134]. Samples were measured at room temperature in fluorescence mode using a Si(111) double-crystal monochromator and a 13-element germanium fluorescence detector. The energy was calibrated by measuring the yttrium *K*-edge transmission spectrum of a Y foil and defining the first inflection point as 17038 eV. Six U *L*_{III}-edge fluorescence spectra of each cell sample were recorded and averaged. Subsequently dead-time correction was applied. For XANES analysis the pre-edge background was subtracted and the absorption coefficient was normalized to equal intensity at 17230 eV so that all spectra could be plotted on the same scale. XANES spectra of two reference solutions, one of U(VI) and another one of U(IV), each at a concentration of

$4 \cdot 10^{-2}$ M in 1 M HClO_4 , were recorded as well. The stock solution of the U(VI) was obtained by dissolving sodium diuranate in 7 M HClO_4 . Part of this solution was reduced electrochemically to U(IV) at a mercury pool cathode and reduction was confirmed by UV/Vis spectroscopy. The EXAFS oscillations were isolated from the raw, averaged data by removal of the pre-edge background, approximated by a first-order polynomial, followed by μ_0 -removal *via* spline fitting techniques and normalization using a Victoreen function. The ionization energy for the U L_{III} -electron, E_0 , was arbitrarily defined as 17185 eV for all averaged spectra. The EXAFS spectra were analysed according to standard procedures using the program EXAFSPAK [135]. The theoretical scattering phases and amplitude functions were calculated from a structural model of uranyl triacetate *via* the software FEFF8.2 [136]. During the fitting procedure, the coordination number (N) of the U- O_{ax} single scattering (SS) path was held constant at two. N of the U- O_{ax} multiple scattering (MS) path was also fixed at a value of two and the radial distance (R) as well as the Debye-Waller (σ^2) factor were linked twice to those of the U- O_{ax} SS path. The second shell of carbon atoms (U- C_2) was fitted with the SS path as well as the MS paths, U- C_2 - C_1 and U- C_1 - C_2 - C_1 . During the fitting procedure, the coordination numbers of these two MS paths were linked twice and once to that of the U- C_2 SS path, respectively. The radial distance of both MS paths was linked to that of the U- C_2 SS path. The amplitude reduction factor was held constant at 1.0 for FEFF8.2 calculations and EXAFS fits. The shift in threshold energy, ΔE_0 , was varied as a global parameter in the fits.

RESULTS AND DISCUSSION

Properties of the purified SlaA-layer ghosts and the cell envelope ghosts

Both isolated cell envelope fractions of *S. acidocaldarius* were checked microscopically for the presence of non-lysed cells or other contaminations. As evident from the light microscopic pictures of the two cell envelope fractions shown in Figure 4.1, no intact cells were present in the purified SlaA-layer ghost and cell envelope ghost fractions. The ghosts of both fractions had a translucent appearance, indicating that they were free of cellular compounds and they both possessed the shape and the size of the whole cells, perceptibly due to the presence of the outermost SlaA-layer, obviously responsible for the shape and mechanical stability of the cells of the studied organism (Fig. 4.1).

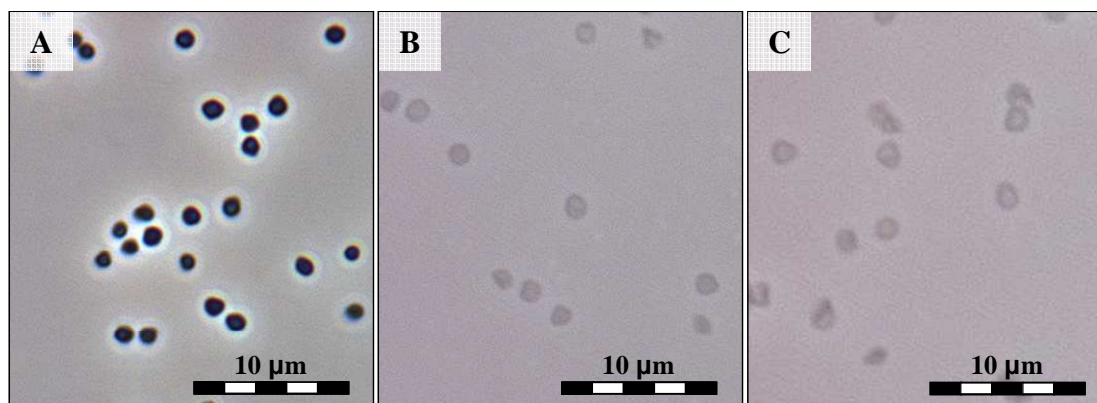


Figure 4.1. Light microscopic pictures of the *S. acidocaldarius* cells (A), of the isolated SlaA-layer ghosts (B), and of the cell envelope ghosts (C). Pictures were taken at 1000-fold magnification in phase contrast mode.

The protein composition of both cell envelope fractions was checked by using denaturing SDS-PAGE. As shown in Figure 4.2, only one band was observed in the lane corresponding to the purified SlaA-layer ghosts (Fig. 4.2, lane 1). This band represents the denatured SlaA-protein monomers which form the highly arranged protein lattice of the SlaA-layer. The molecular mass of about 150 kDa is well in line with those obtained in former studies [188, 201], as well as with the molecular weight, calculated from the primary structure of the SlaA-protein [220, 222].

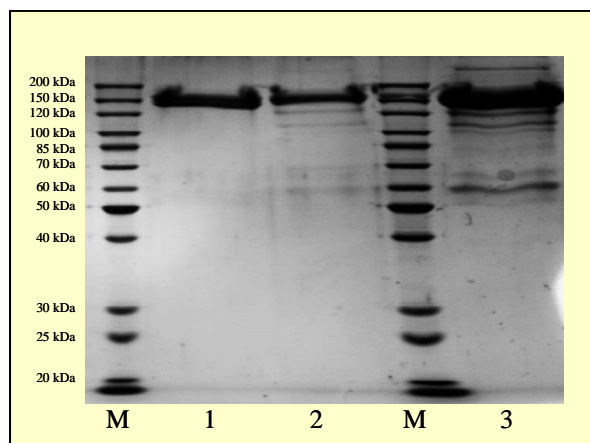


Figure 4.2. SDS-PAGE protein gel stained with colloidal Coomassie Brilliant Blue G-250. 1) 15 µg of the SlaA-layer ghosts; 2) 10 µg of the cell envelope ghosts; 3) 30 µg of the cell envelope ghosts; M) protein marker - Pageruler™ SM0661 (Fermentas GmbH, Sankt Leon-Rot, Germany)

As anticipated, the same protein band was observed in the sample prepared from the cell envelope ghosts (Fig. 4.2, lanes 2 and 3). In addition, several further protein bands were present in the cell envelope ghost fraction. The most prominent of these additional bands has a molecular mass of about 60 kDa which corresponds to that of the SlaB protein [90]

anchoring the SlaA-protein to the cytoplasmic membrane. The rest of the protein bands most likely represent integral membrane proteins or proteins attached to the cytoplasmic membrane. The pH stability of the SlaA-layer was studied, because the maintenance of the proteinaceous layer of the SlaA-layer ghosts in polymeric form during the U(VI) sorption experiments is of importance for drawing correct conclusions to natural systems. Dissociation into SlaA-protein monomers may lead to complexation of the added U(VI) at functional groups which are masked in the polymeric form. As we used an incubation time of 48 hours for the U(VI) sorption experiments, stability of the SlaA-layer was checked after incubations of 48 hours at different pH conditions. UV/Vis spectroscopy demonstrated that the SlaA-layer ghosts were stable at all acidic conditions (down to pH 1) as well as at neutral and slightly basic pH conditions up to pH of 8 (Fig. 4.3).

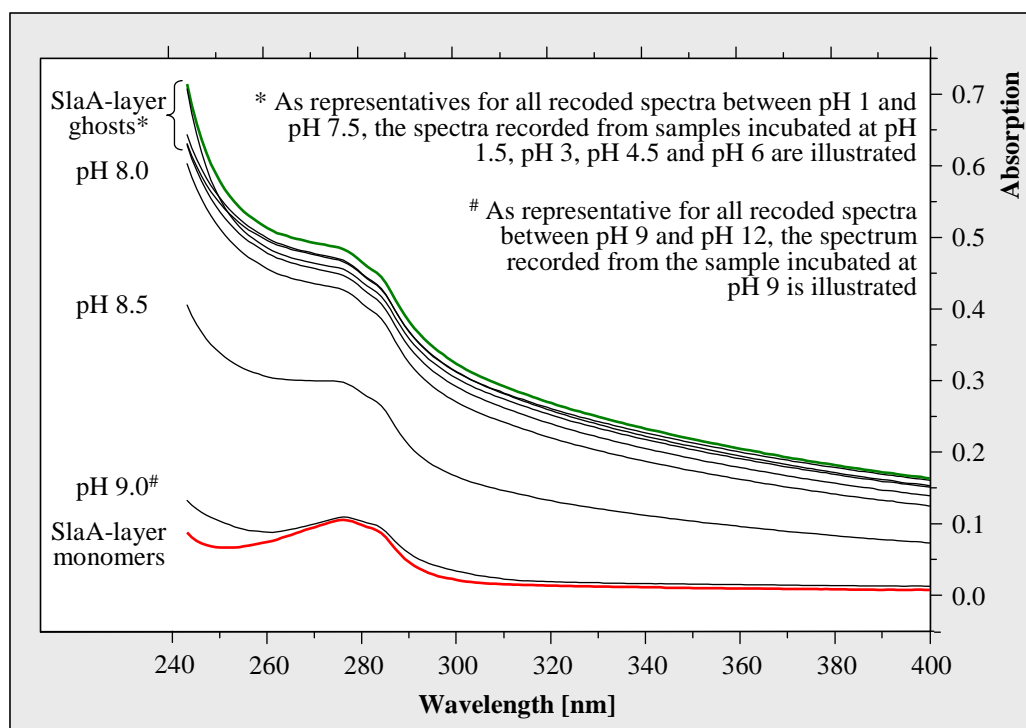


Figure 4.3. UV/Vis spectra recorded from the SlaA-layer ghosts after incubations at different pH values for 48 h at room temperature. The preservation of the polymeric structure is exemplary shown by the samples incubated at pH 1.5, 3, 4.5 and 6 together with an untreated SlaA-layer ghosts sample solved in water (green spectrum). The SlaA-monomer control sample (red spectrum) was obtained by incubation of the SlaA-layer ghosts at 60 °C in 0.1 M phosphate buffer (pH 9) according to Michel and co-workers [201].

The spectra recorded from these samples correspond very well to that recorded from native SlaA-layer ghosts, suspended in distilled water. As evident from the results presented in Figure 4.3, the spectra of the native SlaA-layer ghosts as well as those recorded after incubations at pH 1.5, 3, 4.5, and 6 shows an absorption maximum at around 277 nm and a

light diffusion at lower wavelengths. At pH 8.5 the SlaA-layer ghost polymers started to dissociate into monomers, which is indicated by a reduction of this light diffusion effect. At pH 9 and above the SlaA-layer ghosts are dissociated into SlaA-protein monomers, which exhibit exclusively the peak at 277 nm (Fig. 4.3). Consistently, the spectra recorded from these samples (pH 9 to pH 12) show a high similarity to that of SlaA-protein monomers, which were produced from polymers by an incubation at 60 °C in 0.1 M phosphate buffer (pH 9) according to Michel and co-workers [201]. An extension of the incubation time from 48 to 60 hours did not change the results regarding the stability of the SlaA-layer ghosts (not shown). These findings indicate that the SlaA-layer ghosts are stable at the experimental conditions at which their capability to interact with U(VI) was studied, namely room temperature, pH range from 1.5 to 6, and incubation time of 48 hours.

The results of the potentiometric titration measurements are presented in Figure 4.4. Dynamic titration, starting at the acidic pH, ensured that the native, polymeric form of the SlaA-layer ghosts was preserved, at least in the most relevant pH range (pH 1 to 6), which was used in the U(VI) sorption experiments. The best fit of the titration data was obtained using a three-site model. The presence of ionisable groups with pK_a values of (4.78 ± 0.08) , (6.31 ± 0.04) and (8.03 ± 0.09) and corresponding concentrations of (6.83 ± 0.66) , (11.8 ± 0.2) , and (5.74 ± 0.48) mol/mol_{SlaA-protein}, was demonstrated.

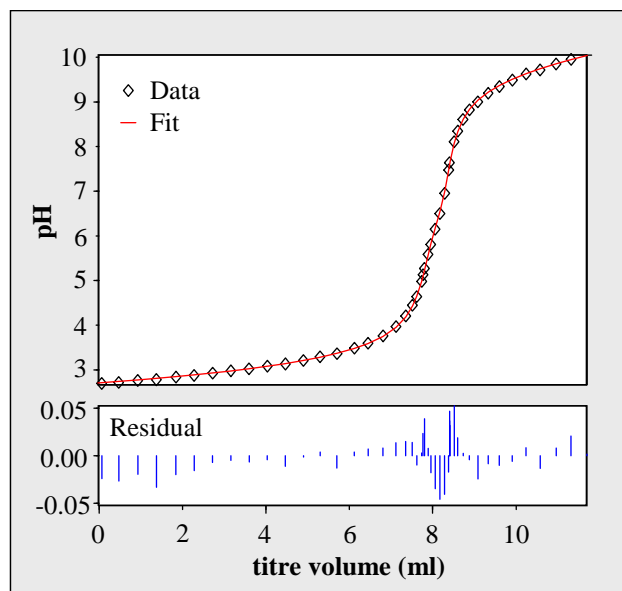


Figure 4.4. Titration results recorded from the proteinaceous SlaA-layer ghosts of *S. acidocaldarius* in the range from pH 2.6 to pH 10.1. The best fit, calculated by using the software “Hyperquad” (continuous line) and the corresponding residual (bottom) are shown, as well.

With respect to the pH range used for the uranium sorption studies, the functional groups represented by the first pK_a value of 4.78 ± 0.08 might be partly involved in the U(VI) complexation at pH 4.5 and, in particular, at pH 6. This pK_a value can be assigned to carboxylic groups of aspartic and glutamic acid residues [163, 236]. According to the primary structure of the mature S-layer protein [220], 18 aspartic acid residues and 27 glutamic acid residues provide a total number of 45 binding-capable, carboxylic groups per mol of SlaA-protein. However, the potentiometric titration data suggest, that only 15% of these groups are available in the native form of the SlaA-layer ghosts polymers.

The functional groups represented by the pK_a of 6.31 play only a minor role in the U(VI) complexation at the studied conditions. The pK_a can be attributed to the imidazole ring of histidine [236]. The third pK_a of (8.03 ± 0.09) most likely concerns amino groups [236] or possibly hydroxyl groups [205] which are, however, not relevant at the pH conditions during the U(VI) sorption experiments.

The presence of phosphate groups which may provide binding sites for uranium and other heavy metals [150] was checked by colorimetric measurements as well as by phosphorous determination using ICP-MS. Both methods clearly demonstrated the absence of phosphate groups in the SlaA-layer ghost fraction, which is in agreement with previous studies [222] and thus verified the high purity of the SlaA-layer ghosts.

U(VI) sorption by the SlaA-layer and the cell envelope ghosts

As demonstrated in Figure 4.5 the uranium binding capacities of the two cell envelope fractions differed significantly. No removal of uranium was observed by the purified SlaA-layer ghosts from the solutions at pH 1.5 and pH 3. This indicates that the U(VI) complexation in this case was very low and below the detection limit of the technique. Small amounts of U(VI) were bound by the SlaA-layer ghosts at pH 4.5 (2.1 ± 0.6 mg/g_{protein}) and pH 6 (5.5 ± 1.1 mg/g_{protein}). These values correspond to a binding capacity of (1.3 ± 0.4) and (3.5 ± 0.7) mol of uranium per mol of SlaA-protein at pH 4.5 and 6, respectively. With respect to the total amount of binding capable carboxylate groups (6.83 ± 0.66) mol/mol_{SlaA-protein}, determined by titration studies, only about the half of these available functional groups were involved in the U(VI) complexation at pH 6, although all of them should exist in their deprotonated form. The latter can be explained by unfavourable placement of some of the carboxylic groups in spaces of the highly ordered lattice of the SlaA-layer ghosts which are inaccessible for the relatively big uranium atoms. The significantly lower amount of U(VI) bound at pH 4.5 can be attributed to the high pK_a value of the carboxylic groups of the

aspartic and glutamic acid residues of the SlaA-layer protein. Hence, not all carboxylic groups of the SlaA-protein in the SlaA-layer ghosts are deprotonated at this pH and/or accessible to U(VI), i.e. capable to bind it.

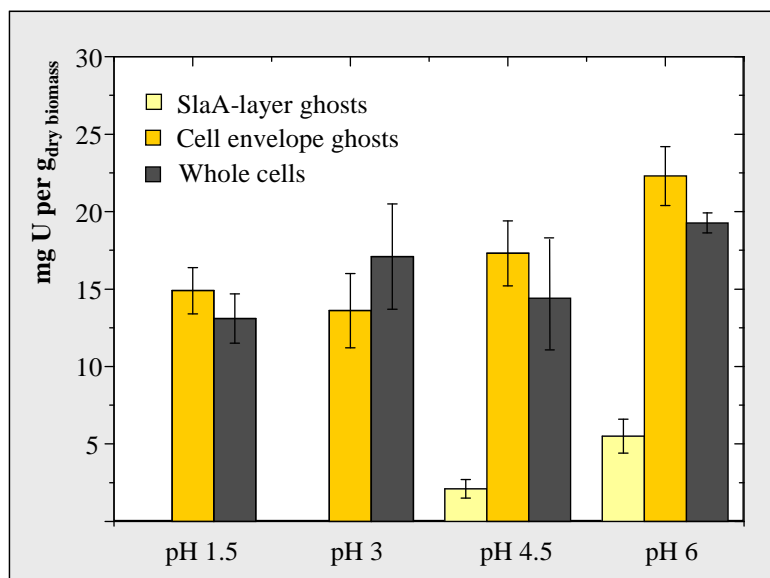


Figure 4.5. U(VI) binding capacities of the SlaA-layer ghosts, the cell envelope ghosts and whole cells of *S. acidocaldarius* at different pH values (biomass concentration was 0.5 ± 0.05 mg). Incubation time was 48 hours for the SlaA-layer ghosts and the cell envelope ghosts and one hour for the living cells.

In contrast to the SlaA-layer ghosts, the cell envelope ghosts bind significantly higher amounts of U(VI). After 48 hours of incubation at pH 1.5, 3, 4.5 and 6 the bound uranium per gram dry biomass of cell envelope ghosts was (14.9 ± 1.5) mg, (13.6 ± 2.4) mg, (17.3 ± 2.1) mg, and (22.3 ± 1.9) mg, respectively. These values correspond well to the binding capacity of U(VI) by whole cells of *S. acidocaldarius* at corresponding experimental conditions (Fig. 4.5, Chapter II and III).

The comparison of the binding capacities of the SlaA-layer ghosts, cell envelope ghosts and whole cells of *S. acidocaldarius* demonstrates that at acidic conditions which are optimal for the studied acidophilic archaeal strain no complexation of U(VI) occurs by its outermost proteinaceous SlaA-layer. At pH 4.5 and 6 the SlaA-layer ghosts bind about 15% and 25% of the total amount of U(VI) complexed by the whole cells, respectively. As shown in Figure 4.5, the uranium binding capability of the cell envelope ghosts was comparable to those of the whole cells. These findings indicate that the main part of U(VI) is complexed by *S. acidocaldarius* at functional groups of the cytoplasmic membrane and/or those of associated with it proteins.

TRLFS studies on the U(VI) complexes formed at the SlaA-layer and the cell envelope ghosts

As already demonstrated by the sorption studies, no U(VI) was bound by the SlaA-layer ghosts of *S. acidocaldarius* at highly acidic conditions (pH 1.5 and 3). In line with this finding we could only obtain very weak luminescence spectra featuring main emission bands around 489, 510, and 532 nm (not shown) which were assigned to traces of the free uranyl ion in the solution (Table 4.1), caused by a desorption of weakly bound to the SlaA-layer uranium and/or an insufficient washing procedure.

In contrast to that, the luminescence intensity of the uranium complexes formed at pH 1.5 and 3 by the cell envelope ghost fraction of the studied archaeon was much higher (Fig. 4.6) which is in agreement with the higher amount of uranium bound by this fraction. As evident from the peak fitting results presented in Table 4.1, the corresponding luminescence emission maxima of these two samples were shifted to the red with about 9 nm compared to those of the free uranyl ion. The emission bands correspond well to those of U(VI) complexed at phosphate groups of organic compounds, such as sugar phosphates [158], phospholipids [161], phosphorylated nucleosides [159], and lipopolysaccharides [163] (Table 4.1).

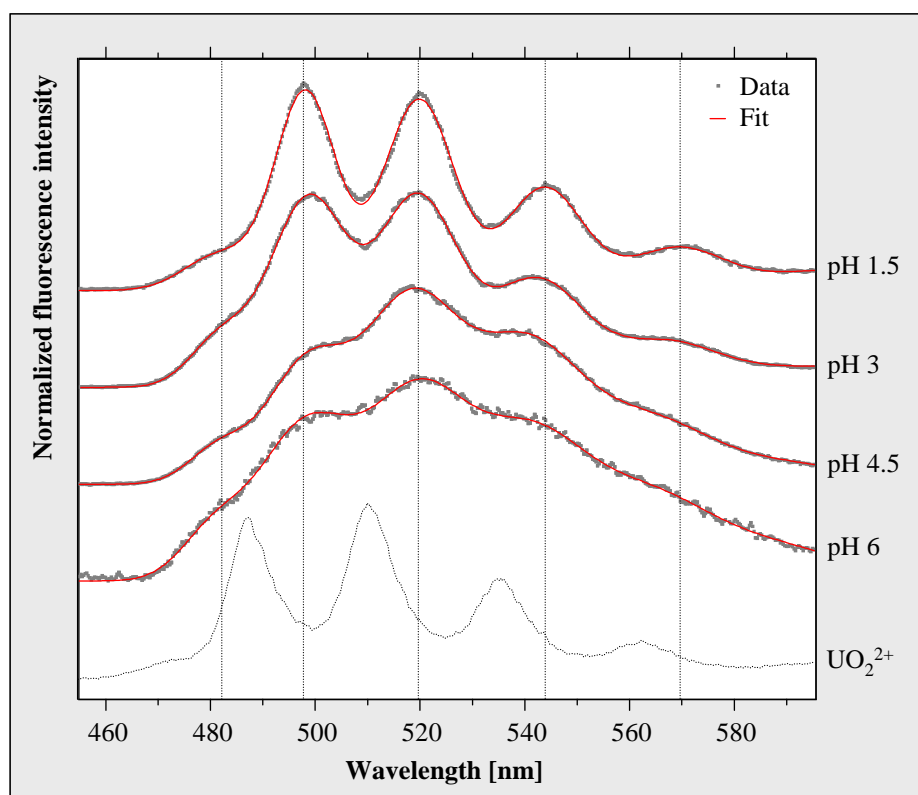


Figure 4.6. Luminescence spectra of the U(VI) complexes formed at the cell envelope ghosts of *S. acidocaldarius* at room temperature at pH 1.5, 3, 4.5, and 6 as well as that of the free uranyl ion. For a better comparison the position of the calculated peak maxima of the sample incubated at pH 1.5 are pointed out by dotted lines.

Table 4.1. Luminescence emission maxima of the U(VI) complexes formed by the cell envelope ghosts and the SlaA-layer ghosts of *S. acidocaldarius* as well as those of the uranium complexes formed by whole cells of the strain and selected uranyl model complexes.

Sample	Emission peak below 470 nm		Main luminescence emission maxima ^a		Reference
Uranyl ion					
UO ₂ ²⁺ (pH1.5)	488.9	510.5	534.0		This work
Cell envelope ghosts					
Uranyl complexes formed at pH 1.5	498.1	519.7	543.8		This work
Uranyl complexes formed at pH 3	498.7	519.6	542.5		This work
Uranyl complexes formed at pH 4.5	498.3	519.0	541.1		This work
Uranyl complexes formed at pH 6	497.8	519.3	541.0		This work
Uranyl phosphoryl complexes					
UO ₂ -fructose(6)phosphate	497.1	519.0	543.3		[158]
UO ₂ -DMGP	497.4	519.3	542.4		[161]
UO ₂ -AMP	497.0	519.0	542.0		[159]
R-O-PO ₃ -UO ₂	498.1	519.6	542.9		[163]
Whole Cells (Chapter II/III)					
Uranyl complexes formed at pH 1.5	498.3	520.3	543.6		[133]
Uranyl complexes formed at pH 3	498.7	520.2	543.6		[133]
Uranyl complexes formed at pH 4.5	499.2	520.0	542.7		[164]
Uranyl complexes formed at pH 6	502.6	523.1	545.4		Chapter III
Uranyl carbonate mineral					
Bayleyite	506.9	527.6	551.4		[237]
SlaA-layer ghosts					
Uranyl complexes formed at pH 4.5 (153 K)	463.8	492.9	513.7	536.2	This work
Uranyl complexes formed at pH 6 (153 K)	462.4	494.7	514.4	535.9	This work
Uranyl carboxylate complexes					
Uranyl acetate	462.9	494.6	514.3	535.9	[166]
Uranyl acetate (253 K)	463.7	495.3	515.2	537.5	^b
(R-COO) ₂ -UO ₂	466.0	498.1	518.0	539.0	[167]
Uranyl hydrolytic species					
(UO ₂) ₂ (OH) ₂ ²⁺	498.3	519.7	543.4		[238]
(UO ₂) ₃ (OH) ₅ ⁺	496	514	535		[239]

^a Error of emission bands is ± 0.5 nm

^b Götz, Christian (personal communication)

The luminescence spectra recorded from the cell envelope ghost fraction incubated with U(VI) at higher pH values (pH 4.5 and 6) exhibit less-separated peaks (Fig. 4.6). Nevertheless, peak fitting results showed highly similar luminescence emission maxima

compared to those found at pH of 1.5 and 3 (Table 4.1). This indicates that at the four pH values studied (1.5, 3, 4.5, and 6) the added U(VI) was complexed in an analogous way. The emission maxima of the U(VI) complexes obtained from the four samples are very similar to those formed by the whole cells of *S. acidocaldarius* at highly acidic conditions (pH 1.5 and 3) [133], at which U(VI) was complexed solely *via* organic phosphate groups, and also to those formed by the whole cells at the moderate acidic pH of 4.5, at which U(VI) was complexed mainly *via* phosphate groups of organic origin (Table 4.1) [164]. On the basis of this finding we propose that the organic phosphate groups play a significant role in the complexation of U(VI) by the cell envelope ghosts not only at pH values of 1.5 and 3 but also at pH 4.5 and 6. However, it is important to mention that the luminescence emission of organic uranyl phosphate complexes is much stronger than that of uranyl carboxylate complexes, and for this reason the formation of the latter complexes at pH of 4.5 and 6 may be underestimated by using TRLFS.

In addition to the position of the emission maxima, the decay of the luminescence was used to distinguish the uranyl species present in the samples of the treated cell envelope ghosts (Table 4.2). In each of the two samples treated with uranium at pH 1.5 and 3 time-resolved studies revealed three different luminescence lifetimes - one of about 3 μ s, a second one of about 25 μ s, and a third one of about 100 μ s (Table 4.2).

Table 4.2. Luminescence lifetimes calculated from room temperature TRLF spectroscopic measurements of the U(VI) complexes formed at the cell envelope ghosts of *S. acidocaldarius* at different pH values.

	pH 1.5	pH 3	pH 4.5	pH 6
Lifetime 1 (τ_1)	$2.61 \pm 0.25 \mu\text{s}$	$3.06 \pm 0.25 \mu\text{s}$	$2.81 \pm 0.28 \mu\text{s}$	2.81^a
Lifetime 2 (τ_2)	$25.7 \pm 1.6 \mu\text{s}$	$23.0 \pm 1.9 \mu\text{s}$	$24.5 \pm 2.1 \mu\text{s}$	$22.8 \pm 3.3 \mu\text{s}$
Lifetime 3 (τ_3)	$103 \pm 6 \mu\text{s}$	$97.3 \pm 5.1 \mu\text{s}$	$92.1 \pm 8.9 \mu\text{s}$	$108 \pm 13 \mu\text{s}$
Lifetime 4 (τ_4)			$9.15 \pm 1.35 \mu\text{s}$	$12.1 \pm 1.8 \mu\text{s}$

^a Lifetime was fixed during the fitting procedure

This suggests that the same three luminescent uranium species were formed in these two samples. Fitting procedures of the recorded spectra after a delay time of 30 μ s (excluding the short-living species) and after a delay time of 200 μ s (including exclusively the spectra of the long-living species) resulted in identical positions of the main emission bands, within the margin of error (± 0.5 nm). This indicates that the three uranyl species formed at pH 1.5 and 3 share a high structural similarity. The two shorter lifetimes of about 3 μ s and 25 μ s are well in line with those of uranyl complexes formed by whole cells of *S. acidocaldarius* at the same pH values of 1.5 and 3, in which organic phosphate groups are implicated [133]. The third

luminescence lifetime of about 100 μs was, however, not observed in the mentioned study performed with whole cells. One possible explanation for this long lifetime could be that the luminescence signal represents a uranyl complex formed at a binding site, specifically accessible in the cell envelope ghost sample, e.g. at the inner site of the cytoplasmic membrane, which in the whole cells is inaccessible for U(VI). Moreover it is also possible, that some uranyl ions could be captured in the bag-looking ghosts and as a result the ratio of U(VI) to phosphate groups could be increased inside the ghosts that can influence the structure of the additionally formed uranium complexes as well. On the basis of the above mentioned consistency of the main emission bands of this third uranyl species to those of the already described two ones, we suggest that U(VI) in it is complexed *via* organic phosphate groups as well. The different lifetimes of the three uranyl phosphate complexes can be explained on one hand by the various origins of the organic phosphate groups which can be supplied by different types of biomolecules of the cell envelope ghosts, such as phospholipids, phosphorylated peptides, or lipopolysaccharides. On the other hand, diverse complexes containing different number of phosphate groups coordinated to U(VI) can also exhibit different luminescence lifetimes [161, 163].

The described three uranyl phosphate species were formed also in the cell envelope ghosts sample treated with U(VI) at pH 4.5 (Table 4.2). Moreover, an additional U(VI) species characterized by a luminescence lifetime of $(9.45 \pm 1.35) \mu\text{s}$ was found in this sample. This lifetime is similar to that $(10.8 \pm 1.4) \mu\text{s}$ calculated recently for the uranyl carboxylate complexes formed by whole cells of *S. acidocaldarius* [164]. In addition, a similar lifetime of $(7.3 \pm 1.4) \mu\text{s}$ was obtained for the uranyl glutamic acid complexes, formed at phosphate-free peptidoglycan predominantly at pH 4.5 (Table 4.1) [167].

In the case of the cell envelope ghosts sample incubated at pH 6, four lifetimes, three, corresponding to the uranyl phosphate species and one for the uranyl carboxylate species, were found as well. In this case, however, the shortest lifetime (τ_1) had to be fixed during the fitting procedure most likely due to a very low amount of the short-living species in this sample.

Hence, the low separation of the absorption peaks in the TRLF spectra of the samples treated at pH 4.5 and 6 in comparison to those of the spectra measured from the samples incubated at highly acidic conditions (pH 1.5 and 3), might be caused by the overlapping luminescence of uranyl phosphate and uranyl carboxylate species. However, another explanation for the shape of the recorded spectra could be the formation of aquatic uranyl hydroxide complexes. The

latter, highly luminescent complexes are usually formed at moderate acidic pH, possibly after desorption of weakly bound to the cell envelope ghosts uranium into the washing solution. In particular, the hydrolytic species $(\text{UO}_2)_3(\text{OH})_5^+$ and $(\text{UO}_2)_2(\text{OH})_2^{2+}$ are formed at the studied pH values (Table 1), according to a calculation with the speciation code EQ3/6 using uranyl(VI) hydrolysis formation constants of Guillaumont and co-workers [75]. The presence of these hydrolytic species would lead to an overlapping of different luminescence emission bands (Table 4.1) and therefore could also explain the low separation of the absorption peaks in the TRLF spectra at pH 4.5 and 6. The luminescence lifetimes of these hydrolytic species had been determined to be about 23 μs ($(\text{UO}_2)_3(\text{OH})_5^+$) and about 9.5 μs ($(\text{UO}_2)_2(\text{OH})_2^{2+}$) [238, 239]. Hence, they agree very well to two of the lifetimes (τ_2 and τ_4) determined for the U(VI)/cell envelope ghosts complexes and can therefore not be distinguished from them.

The TRLFS results of the uranium complexes formed by the cell envelope ghosts of *S. acidocaldarius* demonstrate that at highly acidic conditions (pH 1.5 and 3) U(VI) is predominately bound *via* organic phosphate groups. With increasing the pH to 4.5 and 6, the carboxylic groups of the cell envelope proteins may also play a role in the uranium binding.

As mentioned above, we were also able to demonstrate uranium binding by the SlaA-layer ghost fraction at moderate acidic conditions (pH 4.5 and 6) (Fig. 4.5). On the basis of the performed titration analyses (Fig. 4.3) this might be attributed to the increased part of deprotonated carboxylic groups in the SlaA-protein at these two pH values. However, we were not able to confirm this assumption by performing TRLF spectroscopy measurements at room temperature. Both samples exhibit, in general, low luminescence properties and the recorded spectra did not allow to detect any protein-bound U(VI) complexes (not shown).

In order to reduce dynamic quenching effects and therewith to increase the sensitivity of this spectroscopic method we performed the TRLF measurements of U(VI)/SlaA-layer ghost complexes formed at pH 4.5 and 6 at cryogenic conditions (153 K). As evident from the spectra presented in Figure 4.7 there are three clearly distinguishable luminescence emission maxima and in both cases (pH 4.5 and 6) they were slightly shifted to the red in a way similar to those found for uranyl acetate, measured at room temperature as well as at lower temperature (Table 4.1). In addition, a small but distinct peak located at about 463 nm was found in both samples which is also considered as indicative for uranyl carboxylate complexes (Table 4.1). The U(VI) luminescence decay of the two uranium-treated SlaA-layer ghost samples was fitted with a bi-exponential and tri-exponential decay function, respectively. From the SlaA-layer ghost sample incubated at pH 4.5, luminescence lifetimes of $(23.7 \pm 1.3) \mu\text{s}$ and of $(234 \pm 15) \mu\text{s}$ were calculated (Table 4.3).

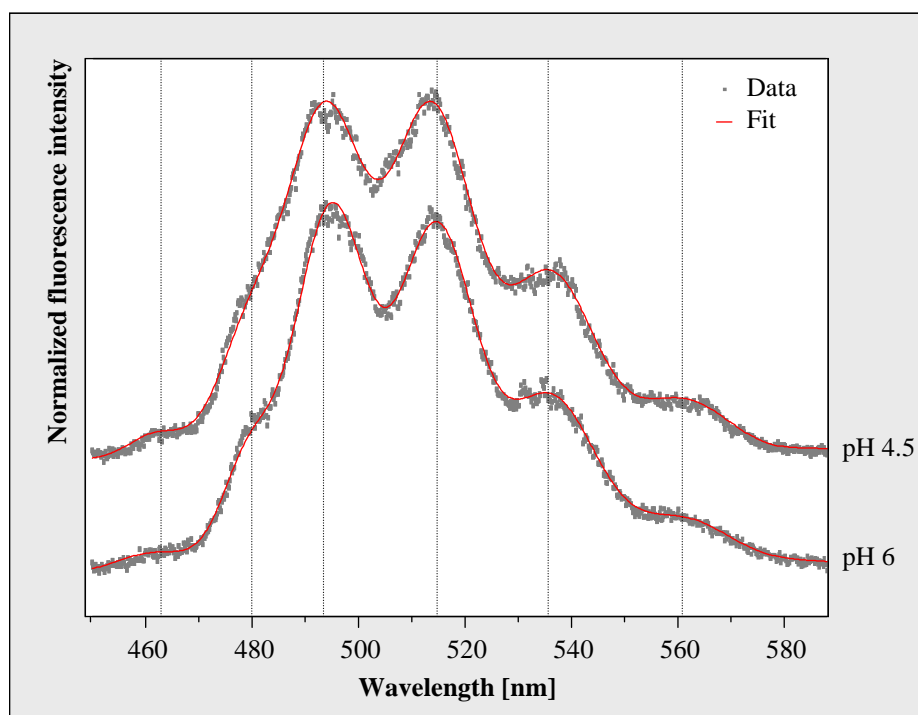


Figure 4.7. Luminescence spectra recorded at low temperature (153 K) of the uranium complexes formed by the SlaA-layer ghosts of *S. acidocaldarius* at pH 4.5 and 6. For a better comparison the position of the calculated peak maxima of the sample incubated at pH 4.5 are pointed out by dotted lines.

The lifetime of $(23.7 \pm 1.3) \mu\text{s}$ is attributed to the formed organic uranyl carboxylate complexes, which was confirmed by a lifetime fit of the data between 460 and 466 nm, a region of the spectrum which is exclusively influenced by the luminescence of the first emission band. A corresponding lifetime of $(23.0 \pm 2.4) \mu\text{s}$ was also calculated from the SlaA-layer ghosts sample incubated at pH 6, indicating the formation of identical uranyl carboxylate complexes. It is important to stress that some aquatic uranyl carbonate complexes, which might be formed in the solution at this pH, also can generate an emission band between 660 and 665 nm. However, significantly longer luminescence lifetimes of 800 to 1000 μs were described for these aquatic uranyl carbonate complexes at cryogenic conditions in the literature [240, 241]. Moreover the presence of the latter complexes is excluded at the lower pH of 4.5 at which, according to calculations with EQ3/6, no aquatic uranyl carbonate complexes are formed (Table 1). The extremely long lifetimes of $(234 \pm 15) \mu\text{s}$ and $(141 \pm 6) \mu\text{s}$ found in the samples treated at pH 4.5 and 6, respectively, were attributed to one or a mixture of uranyl hydrolytic species, as the emission maxima after longer delay times are shifted to higher wavelength towards the positions of the uranyl hydrolytic species. Moreover, long luminescence lifetimes of more than 100 μs were recently described for aquatic U(VI) hydroxide species by using cryo-TRLFS [240].

Table 4.3. Luminescence lifetimes calculated from low temperature TRLF spectroscopic measurements of the U(VI) complexes formed at the SlaA-layer ghosts of *S. acidocaldarius* at different pH values.

	pH 4.5 (153 K)	pH 6 (153 K)
Lifetime 1 (τ_1)	$23.7 \pm 1.3 \mu\text{s}$	$23.0 \pm 2.4 \mu\text{s}$
Lifetime 2 (τ_2)	$234 \pm 15 \mu\text{s}$	
Lifetime 3 (τ_3)		$4.21 \pm 0.44 \mu\text{s}$
Lifetime 4 (τ_4)		$141 \pm 6 \mu\text{s}$

In addition, one more luminescence lifetime of $(4.21 \pm 0.44) \mu\text{s}$ was calculated from the sample incubated at pH 6, which could result from both, another aquatic uranyl complex in the solution or from an additional U(VI)/SlaA-protein complex formed at these conditions at which, as demonstrated by the titration experiments, more carboxylic groups of the SlaA-protein are deprotonated. The results demonstrated that the use of cryogenic techniques opens up new possibilities to investigate the U(VI) complexation by organic ligands of the microbial cell surfaces.

XAS studies

In order to obtain information regarding the molecular structure of the uranyl carboxylate complexes which were formed at pH 4.5 and 6 by the SlaA-layer ghosts, we performed X-ray absorption spectroscopy. X-ray absorption spectra can be divided into four sections: The pre-edge, the X-ray Absorption Near Edge Structure (XANES), the Near Edge X-ray Absorption Fine Structure (NEXAFS) and the Extended X-ray Absorption Fine Structure (EXAFS). The XANES region ($\pm 10 \text{ eV}$ around the absorption edge) provides information about the oxidation state of uranium. The samples were measured as dried powder to avoid uncontrolled biochemical processes, which can influence the fate of uranium in the samples during their transportation to the beamline. The sample preparation is based on soft desiccation, which does not influence the structural parameters of the formed uranium complexes, as it was demonstrated by Merroun and co-workers [162]. As shown in Figure 4.8, the absorption edge, i.e. white line, of the X-ray absorption spectra of both samples is located at $\sim 17166 \text{ eV}$ and therewith corresponds well to the edge position of the U(VI) reference solution. In addition, a peak located at 17188 eV , arising from the multiple scattering contribution of the two axial oxygen atoms of U(VI) [137], was observed in both spectra (Fig. 4.8, dashed line). These findings clearly demonstrate that uranium is present in both samples as U(VI).

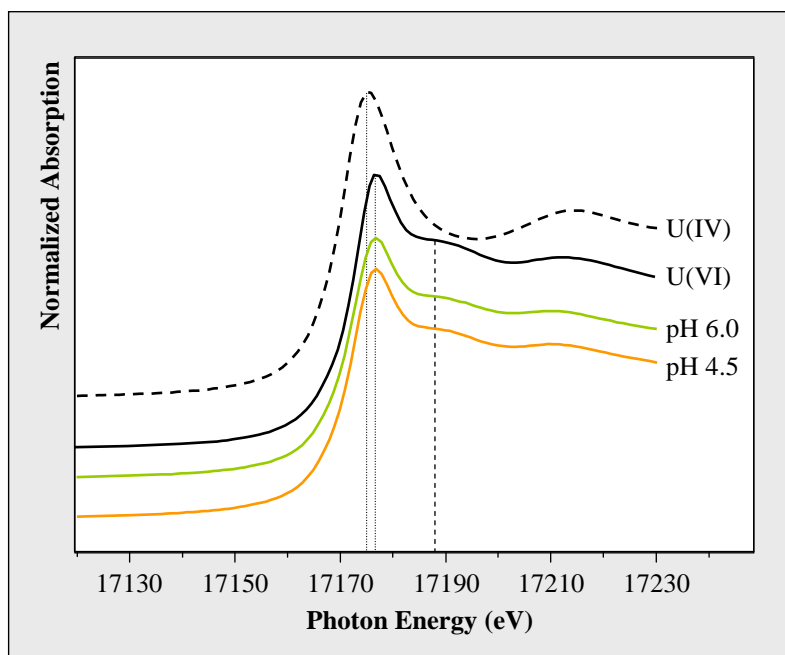


Figure 4.8. Uranium L_{III} -edge X-ray absorption spectra recorded from the uranium complexes formed at the SlaA-layer ghosts of *S. acidocaldarius* at pH 4.5 and 6 together with those of two reference solutions, one of U(VI) and another one of U(IV). For comparison, the positions of the white line of U(IV) and U(VI) are illustrated by dotted lines. The position of the absorption peak (~ 17188 eV), which represents the multiple scattering path of the axial oxygen atoms of U(VI) is marked by a dashed line.

The NEXAFS (10-50 eV above the edge) and EXAFS (from 50 eV above the absorption edge) regions comprise information about the local environment of the uranium atoms and therewith about the molecular structure of the formed complexes. The isolated U L_{III} -edge k^3 -weighted EXAFS spectra and their corresponding Fourier Transforms (FT) are shown in Figure 4.9. Quantitative fitting of the spectra was performed by using the theoretical phase and amplitude functions calculated with the FEFF8.2 code from a structural model of uranyl triacetate. The best calculated fits for both samples are also shown in Figure 4.9 and the corresponding structural parameters are summarized in Table 4.4.

As already suggested by the results of the TRLFS studies, the EXAFS spectra recorded from both samples strongly resemble to each other, which confirms the formation of highly similar uranium complexes at both investigated pH values. In addition, the EXAFS spectra are well in line with that of uranyl triacetate and even almost identical with the recently recorded EXAFS spectrum of an aquatic 1:2 U(VI)/succinate complex [171] indicating that similar U(VI) complexes were formed at the archaeal S-layer. The most prominent peak of both FTs located at $R + \Delta \sim 1.3$ Å is assigned to the single backscattering mode (U-O_{ax}) of the two axial oxygen atoms of U(VI). The multiple scattering path (U-O_{ax}-U-O_{ax}) of this axial oxygen shell is also quite important for the fitting of uranyl EXAFS spectra and have an intensity maximum in the FT at $R + \Delta \sim 2.9$ Å. The second peak of both FTs is attributed to the

scattering contribution of the oxygen atoms in the equatorial plane. Fitting results of both investigated samples revealed four to five equatorial oxygen atoms at a radial distance of 2.42 to 2.44 Å. In addition, a shell (U-C₁) containing two to three carbon atoms was fitted at a radial distance of 2.90 Å. This distance is typical for the U-C shell of U(VI) complexed by the two oxygen atoms of a carboxylate group in a bidentate binding mode. A corresponding complexation mode was already suggested by the EXAFS studies of the uranium complexes formed by whole cells of *S. acidocaldarius* at pH 4.5 [164]. However, the EXAFS spectra, obtained from whole cells, were rather complex and strongly dominated by U(VI), monodentately bound to organic phosphate groups. Hence, a proper determination of the structural parameters of the U(VI) complexes formed at carboxylate groups was impossible in these samples. The formation of comparable complexes, possessing a bidentate coordination of uranium by carbon atoms was also demonstrated in studies with bacterial cells and their S-layer proteins [150].

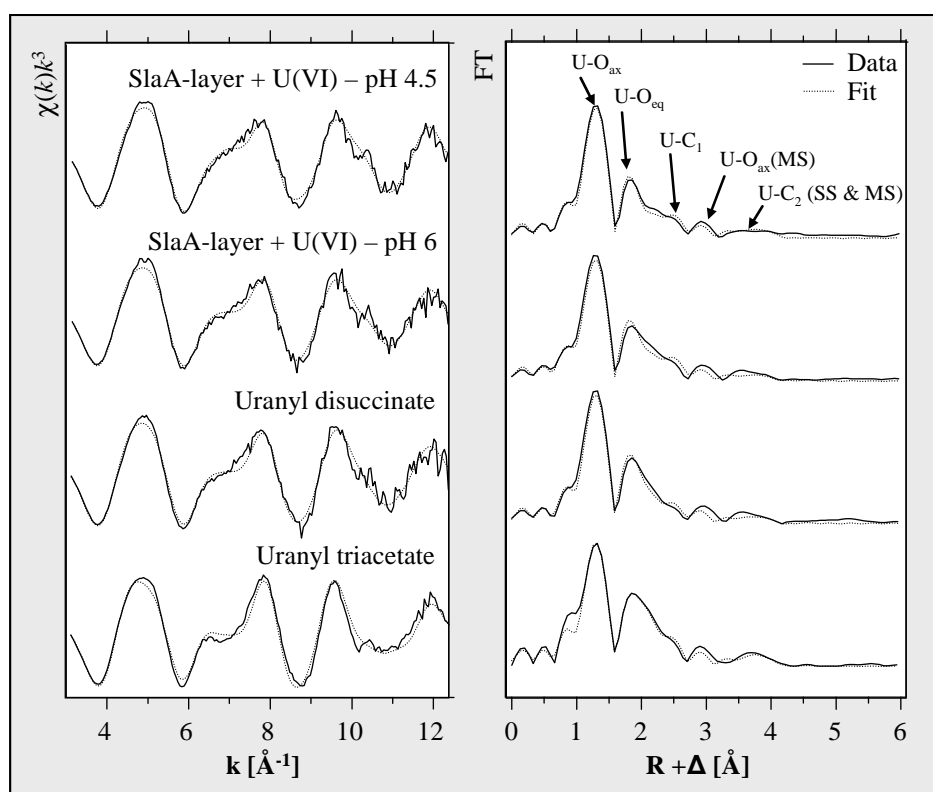


Figure 4.9. Uranium L_{III} -edge k^3 -weighted EXAFS spectra (left) and the corresponding Fourier transforms (right), along with the best shell fits, of the uranium complexes formed at the SlaA-layer ghosts of *S. acidocaldarius* at pH 4.5 and pH 6 as well as those of the two model compounds uranyl disuccinate [171] and uranyl triacetate.

Table 4.4. Structural parameters of the uranium complexes formed at the SlaA-layer ghosts of *S. acidocaldarius* at pH 4.5 and 6, as well as those of the model compounds uranyl disuccinate [171] and uranyl triacetate.

Sample	Shell	N ^a	R (Å) ^b	σ ² (Å ²) ^c	ΔE ₀ (eV)
pH 4.5	U-O _{ax}	2.0 ^d	1.77(1)	0.0021(1)	2.9(4)
	U-O _{ax} (MS)	2.0 ^d	3.54 ^e	0.0042 ^e	
	U-O _{eq}	5.0(4)	2.42(1)	0.014(1)	
	U-C ₁	2.8(2)	2.90(1)	0.0038 ^d	
	U-C ₂	2.8 ^f	4.37(1)	0.0038 ^d	
pH 6	U-O _{ax}	2.0 ^d	1.77(1)	0.0020(1)	3.4(5)
	U-O _{ax} (MS)	2.0 ^d	3.54 ^e	0.0040 ^e	
	U-O _{eq}	4.4(5)	2.44(1)	0.011(1)	
	U-C ₁	2.6(3)	2.90(1)	0.0038 ^d	
	U-C ₂	2.6 ^f	4.36(1)	0.0038 ^d	
Uranyl disuccinate	U-O _{ax}	2.0 ^d	1.77(1)	0.0021(1)	3.5(5)
	U-O _{ax} (MS)	2.0 ^d	3.54 ^e	0.0042 ^e	
	U-O _{eq}	4.4(5)	2.44(1)	0.009(1)	
	U-C ₁	2.3(3)	2.90(1)	0.0038 ^d	
	U-C ₂	2.3 ^f	4.37(2)	0.0038 ^d	
Uranyl triacetate	U-O _{ax}	2.0 ^d	1.78(1)	0.0022(1)	4.9(4)
	U-O _{ax} (MS)	2.0 ^d	3.56 ^e	0.0044 ^e	
	U-O _{eq}	4.8(3)	2.47(1)	0.0064(6)	
	U-C ₁	3.1(3)	2.89(1)	0.0038 ^d	
	U-C ₂	3.1 ^f	4.38(1)	0.0038(1)	

Standard deviations as estimated by EXAFSPAK are given in parenthesis

^a Errors in coordination numbers are ± 25%

^b Errors in distance are ± 0.02 Å

^c Debye-Waller factor

^d Parameter fixed for calculation

^e Radial distance (R) and Debye-Waller factor (σ²) linked twice to R and σ² of the of the U-O_{ax} path

^f Coordination number (N) linked to the N of U-C₁ path

A second shell of carbon atoms (U-C₂) assigned to the C-atom bearing the carboxylic group was detected at radial distances of 4.37 Å and 4.36 Å in the samples incubated at pH 4.5 and 6, respectively. As mentioned above, the obtained structural parameters of both samples are well in line with respect to the calculated errors. The only differences which can be discussed were observed in the U-O_{eq} shell. At pH 6 a radial distance of 2.44 Å and a Debye-Waller factor of 0.011 Å² were calculated for this shell and agree very well to the structural parameters calculated for the recently investigated uranyl disuccinate complex (Table 4.4). As pointed out by the authors of the latter study, the uranyl ion is bound bidentately in this complex to two carboxylic groups and additionally exhibits two fully hydrated equatorial oxygen atoms. This structure was also proposed to be the most probable one for the 1:2 uranyl acetate complex by using Infrared and Raman spectroscopy [242]. The calculated structural parameters of the U(VI)/SlaA-layer ghosts sample incubated at pH 6 (R = 2.44 Å, σ² = 0.011 Å²) can thus be explained by a split U-O_{eq} shell comprising four equatorial oxygen atoms which are bidentately bound to carbon (published characteristic distance ~2.47 Å,

[168]) and one or two equatorial oxygen atoms which exists in their hydrated form (published characteristic distance 2.41 - 2.42 Å [209, 243]).

In contrast to that, the lower radial distance (2.42 Å) along with the higher Debye-Waller factor (0.014 Å^2) calculated for the U-O_{eq} shell of the U(VI) complexes formed at pH 4.5 suggest that U(VI) is predominantly bound to only one carboxylate group. This assumption is supported by highly similar structural data ($R = 2.42 \text{ Å}$, $\sigma^2 = 0.012 \text{ Å}^2$) obtained for the U-O_{eq} shell of uranyl monoacetate [171]. However, the high coordination number calculated for the U-C₁ shell is not in agreement with this complexation model. This implicates, probably, another complexation mode of uranyl, unknown behind the bidentate binding mode, to the carboxylate groups of the SlaA-protein at pH 4.5. Infrared and Raman spectroscopic studies of uranyl acetate complexes [244] revealed that U(VI) can be bound to carboxylate groups in a bidentate, and additionally in a pseudo-bridging complexation mode. The U-O_{eq} distance of such pseudo-bridged structures was estimated to be 2.35-2.40 Å [245] and could therewith explain both, the lower radial distance and the higher Debye-Waller factor of the U-O_{eq} shell. The XAS studies demonstrate that U(VI) forms inner-sphere complexes at the carboxylate groups of the SlaA-layer ghosts at the studied moderate acidic conditions, predominantly in a bidentate binding mode. According to the structural parameters, the existence of 1:2 uranyl carboxylate complexes was demonstrated in the sample incubated at pH 6. Besides these complexes, the formation of additional uranyl carboxylate complexes was proposed for the sample incubated at pH 4.5.

CONCLUSIONS

In this study, the complexation of U(VI) by two different cell envelope fractions of *S. acidocaldarius*, refereed as “SlaA-layer ghosts” and “cell envelope ghosts” was investigated. The comparison of the binding capacity of the two cell envelope fractions clearly revealed that the major part of the complexed U(VI) is bound to functional groups of the cytoplasmic membrane. At highly acidic conditions (pH 1.5 and 3) uranium was only complexed by the cell envelope ghosts, whereas no complexation by the purified SlaA-layer ghosts was observed. By using TRLFS we demonstrated that organic phosphate groups are responsible for the U(VI) complexation by the cell envelope ghosts. These results demonstrate that the proteinaceous SlaA-layer of *S. acidocaldarius* does not play a protective role against uranium at highly acidic conditions which correspond to the physiological

optimum of the strain. With increasing the pH to 4.5 and 6 the carboxylic groups of the proteins from the cell envelope ghosts increasingly contribute in the uranium binding.

The SlaA-layer ghosts complex U(VI) only at pH 4.5 and 6. At these pH values the carboxylic groups of the SlaA-layer are partly (pH 4.5) or completely (pH 6) deprotonated, that enables the formation of uranyl carboxylate complexes. The XAS studies revealed that the complexation mode of the uranyl complexes formed at the SlaA-layer ghosts corresponds well to that of uranyl disuccinate. Thus at moderate acidic conditions, the migration of uranium may be influenced by the outermost SlaA-layer. Moreover, the extremely stable fraction of the SlaA-layer ghosts produced at these unfavourable for the strain conditions can influence uranium behaviour by itself as well.

Chapter V

Formation of magnetic gold nanoparticles using the SlaA-layer of *Sulfolobus acidocaldarius* as a template.

Thomas Reitz, Thomas Herrmannsdörfer, Mohamed L. Merroun,
Andrea Geissler and Sonja Selenska-Pobell

Published in extract in:

Magnetic Au Nanoparticles on Archaeal S-Layer Ghosts as Templates.

Sonja Selenska-Pobell, Thomas Reitz, Rico Schönemann, Thomas Herrmannsdörfer,
Mohamed Merroun, Andrea Geißler, Juan Bartolomé, Fernando Bartolomé, Luis Miguel
García, Fabrice Wilhelm and Andrei Rogalev

Nanomaterials and Nanotechnology, ISSN: 1847-9804, InTech

ABSTRACT

Gold nanoparticles were produced by using the S-layer ghosts of the acidothermophilic crenarchaeon *Sulfolobus acidocaldarius* as a template. TEM analyses demonstrated that the size of the nanoparticles was about 2 to 3.5 nm. EDX analysis revealed that the nanoparticles were associated with the surface layer lattice probably, *via* the thiol groups, which are characteristic for the SlaA-protein. We suggest that the pores of the SlaA-layer lattice most likely function as a barrier around the single nanoparticles and prevent further crystal growth. XPS analysis clearly demonstrated that the clusters consisted mainly of Au(0). Most interesting feature of the formed gold nanoparticles is their magnetic behaviour. As demonstrated by SQUID magnetometry, the studied gold nanoparticles possess a magnetic moment of order $0.1 \mu_B/\text{Au atom}$. This is the first study demonstrating the formation of magnetic gold nanoparticles on a not-modified, natural biotemplate, in a clean and environmental friendly way.

INTRODUCTION

During the last decade, the production, characterization and application of nano-sized particles of noble metals have become a fast developing topic of modern science and technology. These particles are an effective bridge between bulk materials and atomic structures and very perspective for the development of future key technologies. Whereas bulk material usually exhibits constant physical properties regardless of its size, due to the low number of metal atoms at the surface compared to the number of atoms in the bulk, the properties of nanoparticles are often unusual and dependent on their size and shape. These variable characteristics of metal particles with a size reduced down to the nanoscale, is based on an electron redistribution caused by surface- and quantum-size effects [246]. These effects, in turn, result from the increase of the relative amount of metal atoms at the particle surface and the reduction of the spatial electronic motion to small regions of space in one, two, or three dimensions of these surface-localized atoms. With regard to these effects, the catalytic, optical and magnetic properties of nano-scaled particles can be changed by a variation of their size and shape [247-250]. Nano-sized noble-metal particles have become a subject of intense research and were used for catalysis [247, 251, 252], biomedicine [253, 254], as optical bio- and chemosensors [255-258], and for environmental remediation [259]. They can be formed by chemical procedures, but also by using biological substrates. The latter mentioned, organic substrates are advantageous, as they provide a non-toxic and therefore environmentally friendly matrix for nanofabrication procedures. Suitable templates for the formation of noble-metal nanoparticles and nanoclusters are regularly arranged biomolecules, like DNA [260, 261] or self-assembling chaperonins [262], and virus particles [263, 264]. Moreover, paracrystalline surface layer (S-layer) proteins, which are found at the cell surface of many prokaryotic microorganisms, were also used to produce gold, platinum, and palladium nanoparticles [94, 248, 265-269] or even regularly distributed gold nanoclusters [233]. Recent studies demonstrated that a size reduction of noble-metal particles down to the nanoscale can evoke magnetisms in these intrinsically non-magnetic elements [248, 270, 271]. The S-layer protein of the bacterial strain *Bacillus sphaericus* JG-A12 was used as biological matrix for the formation of magnetic Pd and Pt nanoparticles, which had a size of about 1 nm. [248]. In contrast to that, no magnetism was observed, studying gold nanoparticles formed at the mentioned S-layer protein. Magnetic gold nanoparticles were, up to date, exclusively synthesized chemically, stabilized by polymers [272, 273] or Fe₃O₄ nanoparticles [274]. In addition, some studies derivatized the gold nanoparticles by thiol groups to induce ferromagnetism [275-277], based on the method, first described by Brust

and co-workers [278]. The thiol groups were shown to interact strongly with a gold surface and induce significant charge redistribution [246], in particular, the generation of extra electron holes in the 5*d* band of the gold atoms located at the surface which were caused by a charge transfer to the sulphur atoms of the thiol group [277]. Assuming an important role of thiol groups for magnetization of gold, the absence of these groups in the S-layer protein of *B. sphaericus* JG-A12 likely explain the formation of non-magnetic gold nanoparticles. Diluweit and co-workers introduced thiol-groups into a S-layer protein of another *Bacillus sphaericus* strain and found out that thiol groups stimulate gold nanoparticle formation [94]. However, they did not measure magnetic properties of the formed nanoparticles.

In this work, the S-layer protein, called “SlaA”, of the acidothermophilic crenarchaeon *Sulfolobus acidocaldarius* was used as a matrix for the formation and stabilization of gold nanoparticles. The rationale for choosing this S-layer protein was the indigenous presence of two sulphur-containing cystein residues per monomer. These residues provide thiol groups, usually not present in bacterial S-layer proteins, which might, on the one hand stimulate Au nanoparticle formation and, on the other hand influence the properties of the formed gold nanoparticles.

MATERIAL AND METHODS

Gold nanoparticles preparation

SlaA-layer ghosts of *Sulfolobus acidocaldarius* (strain DSM 639) were prepared from fresh grown cells as described in Chapter IV. For metallization the SlaA-layer ghosts were initially incubated in gold(III) solution (HAuCl₄, pH ~2.5) and shaken at room temperature for 24 hours in the dark. All experiments were performed in clean and sterile Greiner centrifugation tubes. Necessary glassware was rigorously cleaned in “aqua regia” before use. The used gold tetrachloride concentrations were 3 mM and 0.3 mM and those of the SlaA-layer ghosts 0.1, 0.25, 0.5, and 1 mg/mL. After the first step of incubation, the not-deposited Au(III) was removed by centrifugation and subsequent washing procedures of the SlaA-layer pellet with triple-distilled water. The amount of gold removed from the solution by the SlaA-layer ghosts at different Au(III) and S-layer concentrations was calculated after determination of the unbound gold present in the supernatant by using inductively-coupled-plasma mass-spectrometry (ICP-MS). For each single approach, a reference sample (gold solution without SlaA-layer ghosts) was prepared, shaken, and

measured analogically. Gold reduction was performed by using boron hydride dimethylamine (DMAB) in a concentration of 22 mM. Immediately after the addition of DMAB, the solutions were centrifuged (9000 g, 20 min) and the obtained pellets were dried under vacuum at 35 °C.

Transmission-electron microscopy (TEM) and Energy Dispersive X-ray spectroscopy (EDX)

For TEM sample preparation, gold nanoparticle-containing SlaA-layer ghosts were dried, subsequently dehydrated with ethanol, sonicated and deposited on a carbon-coated copper grid. TEM observations were made using a high resolution Philips CM 200 transmission electron microscope at an acceleration voltage of 200 kV. EDX analysis, which provides elemental information, were performed at the same voltage using a spot size of 70 Å and a live counting time of 200 s. TEM studies were performed at the “Centro de Instrumentación Científica” of the University of Granada (Spain).

X-ray Photoelectron Spectroscopy (XPS)

XPS enables to determine the binding energies of atoms and thus to characterize the bonding states. Nanoparticle-containing SlaA-layer ghosts were prepared as described before. Instead of drying under vacuum, the obtained pellet was suspended in triple-distilled water. Two times about 10 µL of the S-layer suspension was applied and subsequently dried up on Si-wafer. XPS measurements were performed using a scanning auger electron spectrometer (Microlab 310F, Fisons, Ipswich, UK) with field-emission cathode and hemispherical sector analyser with accessory XPS-unit (Al/Mg - X-ray tube). The X-ray spot had a size of about 2 x 3 mm. Measurements were conducted in CAE mode using a pass energy of 10 eV. The 1s peak of carbon (284.6 eV) was used for energy calibration.

Magnetization measurements

Magnetization measurements were performed using a Superconducting QUantum Interference Device (SQUID) magnetometer. This method allows for measuring the total magnetic moment of a sample, including all atomic and molecular magnetic contributions. A small part of the prepared cell pellets was fixed in a specially designed sample holder. During the measurement, the magnetic field was held constant ($B_0 = 2$ T) in the superconducting magnetic field coil while the sample was consistently moved through a pick-up coil system of the flux transformer connected to the SQUID. Magnetization data were taken at temperatures

$1.8\text{ K} \leq T \leq 300\text{ K}$ using a liquid-He cooled variable-temperature insert installed in the commercial SQUID-magnetometer setup (MPMS, Quantum Design, Inc., San Diego, USA). In order to scale the measured magnetic moments on the amount of substance, the weight of the sample was determined. For calculating the magnetic moment arising from each single gold atom, the proportion of gold in the sample was additionally calculated on the basis of the ICP-MS results.

RESULTS AND DISCUSSION

Au(III) complexation

The calculated amounts of Au(III) associated with the SlaA-layer in dependency on the concentration of gold in the solution, as well as on that of the SlaA-layer ghosts in the sample, are presented in Figure 5.1.

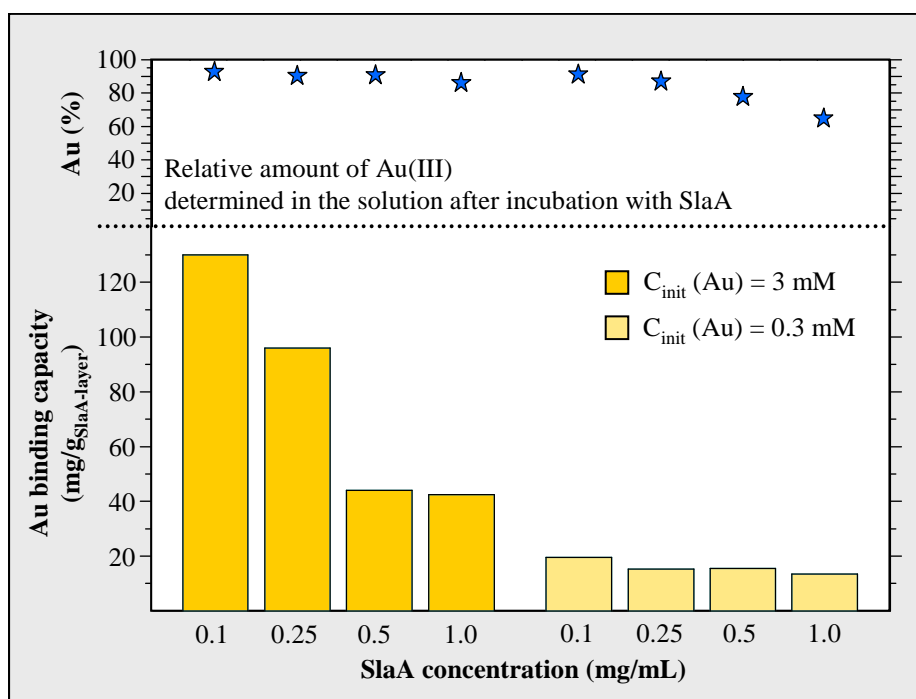


Figure 5.1. Amount of Au(III) associated with the SlaA-layer ghosts in dependency on the initial gold- and S-layer concentration after incubation for 24 hours (bottom). In the upper part of the figure the corresponding relative amount of remaining Au(III) in the solution is plotted.

The underlying mechanism for the complexation of Au(III) is not yet clear. A covalent binding of Au(III) to functional groups of the SlaA-protein, might be excluded, as these groups are present in their protonated form at the studied pH conditions. However, a link between gold and sulphur atoms at a comparably low pH of 3 has been suggested by previous

investigations on Au(III) sorption on seaweed waste [279]. In this case the proposed mechanism for Au binding involves a reduction of gold by surface components of the biosorbent, followed by the retention of the ionic Au(I) species at the sulphur-containing sites. A similar mechanism might underlie the gold deposition at the SlaA-layer.

As evident from Figure 5.1, the removal of gold from the solution strongly depends on both parameters, the initial gold concentration and the SlaA-layer ghost concentration. A reduction of the concentration of the SlaA-layer ghosts in the sample resulted in a more efficient gold complexation. The reason for this is the aggregation of the SlaA-layer ghosts at increased concentrations, limiting the surface and therewith the deposition sites. At the lower gold concentration (0.3 mM) the removal of Au(III) from the solution by the SlaA-layer ghosts was significantly reduced. This finding is on the first view rather incomprehensible, as a large amount (70 to 90%) of the Au(III) was still available in the solutions after the incubation (Figure 5.1, top). The most plausible explanation for this is that the gold cations were caught in the SlaA-layer sacculi and kept within them by weakly, non-covalent interactions. Assuming that, the amount of gold associated with the SlaA-layer sacculi strongly depends on the initial Au(III) concentration, as this parameter predominantly determines the number of gold atoms which diffuse into the SlaA-layer sacculi and could be entrapped within. To what extent the amount of initially complexed Au(III) is relevant for the generation of magnetic properties in the formed nanoparticles is not yet examined. However, a corresponding correlation is conceivable due to the fact that we observed no magnetic properties in a sample with a lower gold/S-layer proportion (35 mg/g_{SlaA-layer}). For the production of magnetic gold nanoparticles, initial gold- and SlaA-layer ghost- concentrations of 3 mM and 0.1 mg/mL, respectively, were shown to be suitable. We also checked whether the pH of the gold solution has an influence on the initial Au(III) complexation and, as a consequence of this, possibly on the magnetic behaviour of the formed gold nanoparticles. However, we do not observe any significant differences in both parameters, using H₂AuCl₄ solutions at pH values between pH 2.5 and 7.5 (not shown).

Gold reduction

After the initial retention of Au(III) within the SlaA-layer ghosts and the removal of the unbound gold, the noble-metal in the sample was chemically reduced to its metallic form by DMAB. Immediately after the addition of the electron donor DMAB, the colour of the SlaA-layer suspension changed from pale yellow to pale purple. This observation confirmed the formation of gold nanoparticles and is based on oscillation changes of the conduction

band electrons (surface Plasmon oscillations) [280]. The colour of gold nanoparticles in transparent solution depends on the shape and the size of gold nanoparticles, because these parameters determine the surface plasmon resonance frequencies as well as the width of the plasmon absorption band [281].

Characterization of the gold nanoparticles

The formed gold nanoparticles were visualized by TEM coupled with EDX. Gold nanoparticles were distributed rather irregularly at the S-layer lattice and did not reveal a regular pattern (Fig. 5.2).

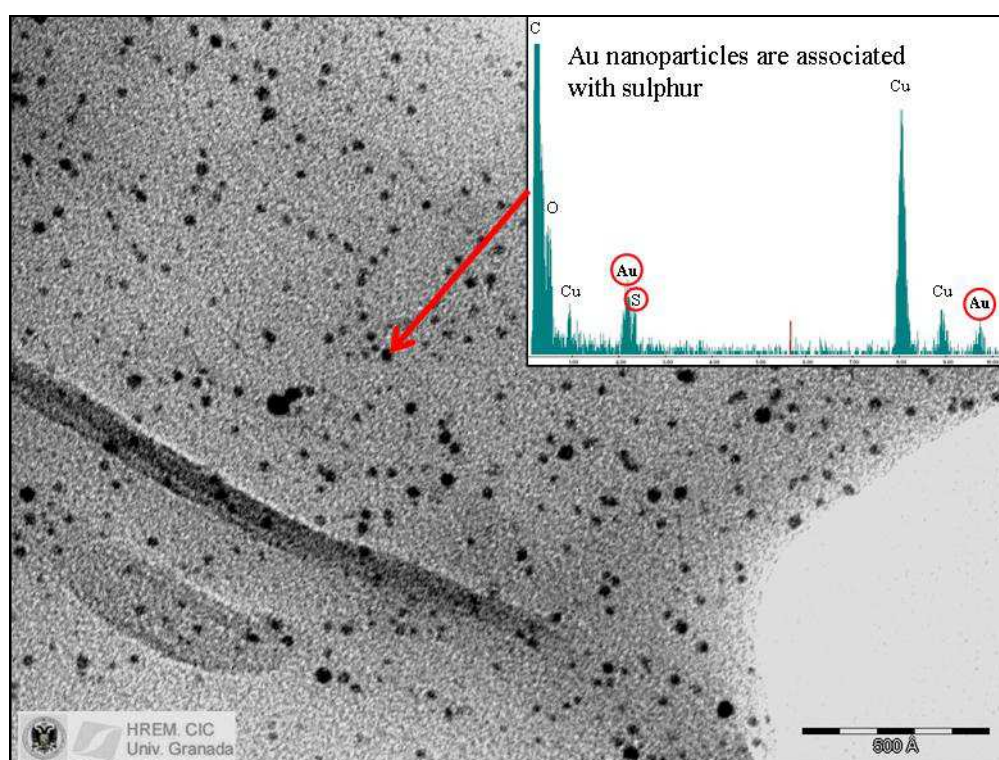


Figure 5.2. Transmission electron micrograph and a representative EDX spectrum of gold nanoparticles formed at the SlaA-layer of *S. acidocaldarius*.

This finding is in agreement with the observation made by Mark and co-workers who investigated the formation of self-assembled, ordered arrays of gold nanoparticles using the S-layer of *S. acidocaldarius* [233]. In contrast to our approach, the authors of the latter study used another strategy for Au nanocluster formation: S-layer-coated TEM grids were floated for 30 min with pre-synthesized, citrate-capped gold nanoparticles with a size of about 5 nm. However, as mentioned above, an irregular distribution of gold nanoparticles was observed, very similar to the results of our nanocluster formation procedure.

The recorded EDX spectra exhibit energy peaks which are specific for gold, as well as for carbon, oxygen, sulphur and copper (Fig. 5.2). The carbon as well as the copper peak arises from the carbon-coated copper grid supporting the TEM sample. The elements oxygen and sulphur are structural components of the SlaA-protein. The large sulphur peak suggests that the gold nanoparticles are associated with the SlaA-protein ghosts *via* the sulphhydryl group of the protein. The size of the formed particles varied between 1.8 and 4 nm, whereby most particles exhibit diameters between 2 and 3.5 nm (Figure 5.3, bottom).

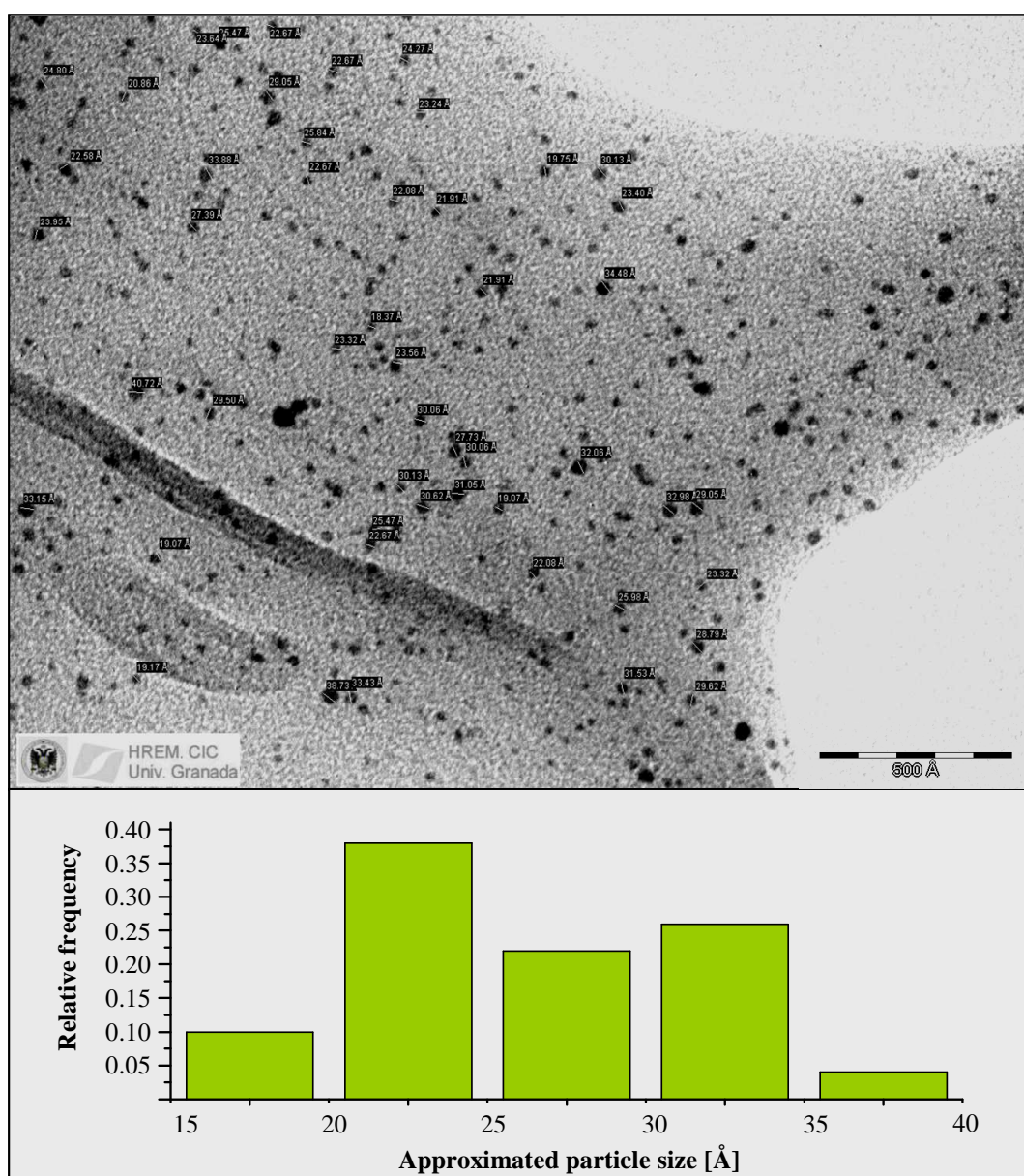


Figure 5.3. Approximated size of the gold nanoparticles formed at the SlaA-layer of *S. acidocaldarius*, determined by transmission electron microscopic analysis.

X-ray Photoelectron Spectroscopy (XPS) was used to differentiate the part of metallic gold from the amount of Au(III) in the samples. The spectrum shows a rather low signal of the gold double-peak, due to the low amount of gold associated with the SlaA-layer (Figure 5.4). With regard to the position of the 1s peak of carbon the measured signal was shifted about 4 eV to higher binding energies.

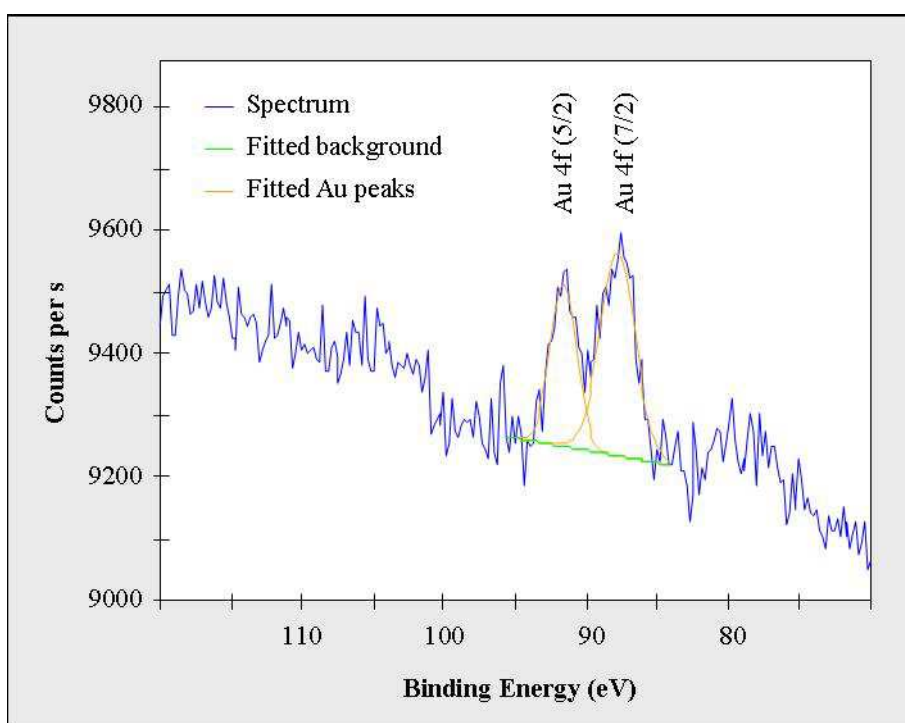


Figure 5.4. X-ray photoelectron spectrum measured from the gold nanoparticles formed at the SlaA-layer of *S. acidocaldarius*.

Nevertheless, the position of the Au 4f (7/2)-peak around 84 eV (~88 eV in Figure 5.4) clearly demonstrates that most of the gold is present in the samples in its metallic form: position of Au 4f (7/2) according to the literature [282]: 84.0 eV (metallic); 85.9 eV (in Au₂O₃). This finding differs significantly from the partial reduction of Au(III) to Au(0) found in gold nanoparticles formed at the S-layer protein lattice of the bacterial strain *Bacillus sphaericus* JG-A12 [266]. The authors of the latter study demonstrated that only about 40% of the gold in the samples existed in a form of Au(0). The zero-valent oxidation state of gold additionally supports the assumption that the gold-thiol linkage does not have the characteristics of gold sulphide and suggest another complexation mode.

Magnetic properties of the gold nanoparticles

Magnetic properties of the formed nanoparticles were investigated by using SQUID magnetometry - a very sensitive method, which is able to measure extremely weak magnetic fields as well as small magnetic moments.

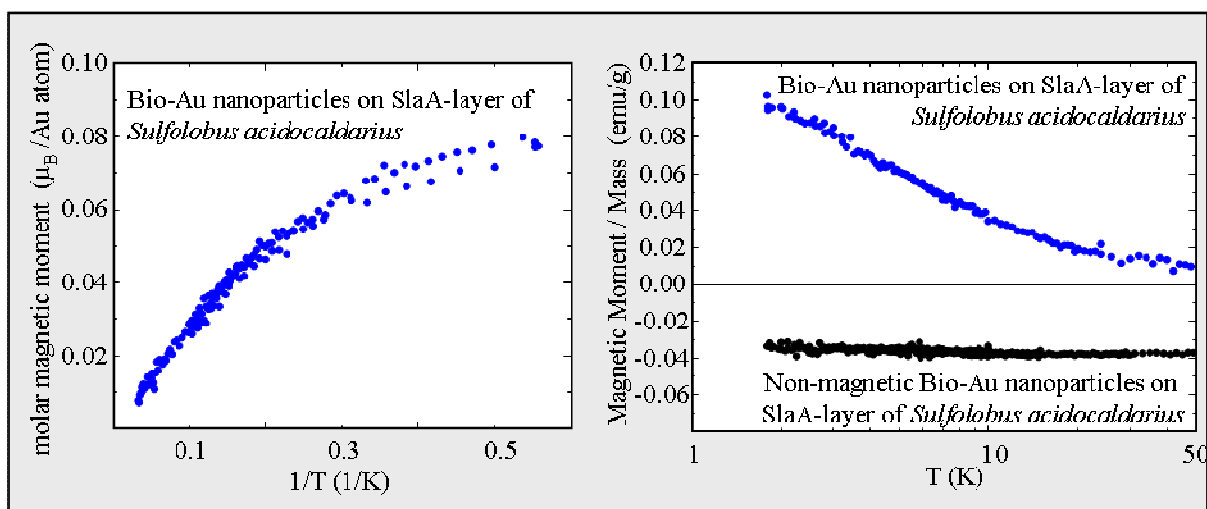


Figure 5.5. Magnetic moments of the gold nanoparticles formed at the SlaA-layer of *S. acidocaldarius*, scaled to one gold atom (left) and to the total weight (right). In addition, the SQUID spectrum obtained from a non-magnetic reference sample, differing from the magnetic sample by a significant lower amount of gold, is presented.

The results presented in Figure 5.5 demonstrate that the studied gold nanoparticles are paramagnetic and possess a magnetic moment of about $0.1 \mu_B$ per gold atom. Interestingly, no magnetic properties were observed in a reference sample, differing from the magnetic sample by a significantly lower Au(III) deposition ($\sim 30\%$ of that, calculated for the magnetic sample). Comparable results, demonstrating the absence of magnetism, also arose from gold nanoparticles formed on the S-layer of the above mentioned *B. sphaericus* S-layer, which possesses no sulphur.

As a control, all samples were checked for iron impurities, which could skew magnetic results. The amount of iron determined by ICP-MS was in each sample below the detection limit confirming that the measured signals arise from the gold nanoparticles. However, we observed no magnetic properties in a reference sample, differing from the magnetic sample by a significant lower amount of gold ($35 \text{ mg/g}_{\text{SlaA-layer}}$), initially associated with the SlaA-biopolymer (Figure 5.5). The amount of gold initially bound by the SlaA-layer likely influences the size of the later formed gold nanoparticles and as a consequence of this plays a decisive role for the occurrence of magnetic properties. In addition, no magnetic properties were observed in gold nanoparticles formed on the already mentioned S-layer protein of

B. sphaericus JG-A12, which does not possess cysteine residues, and therefore without thiol groups (not shown). We suggest that the described magnetic properties of the gold nanoparticles formed at the SlaA-layer lattice most likely depends on both, the presence of thiol groups and the size of the formed nanoparticles, which in turn can be tuned by varying the initial gold- and SlaA-layer concentration. According to the literature, these so-called size and ligand effects determine the structure and number of holes in the *d*-electron band [271], which in turn influences the magnetic behaviour of the formed gold nanoparticles.

CONCLUSIONS

In this study we demonstrated that the SlaA-layer ghosts of *S. acidocaldarius* are a good macromolecular template for formation of magnetic gold nanoparticles. Within this process the thiol groups provided by the SlaA-protein, are most likely essential for both, the initial deposition of gold within the SlaA-layer ghosts and the evocation of the gold magnetism. Moreover, the results strongly suggest an influence of the nanoparticle size on the occurrence of gold magnetism.

Outlook

The results obtained in the studies performed in the frame of this thesis demonstrate some unique and new aspects of microbial interactions with uranium and gold.

It was shown, that the investigated bacterial isolate *Paenibacillus* sp. JG-TB8 has a high capability to immobilize uranium in oxygenated, moderate acidic soils *via* mineralization of this radionuclide, caused by enzymatically released orthophosphate. However, the phosphatase activity, which is responsible for the latter process, is suppressed under anaerobic conditions. We demonstrated some aeration-dependent differences in the protein expression pattern of the strain. In further studies, the phosphatase protein of this strain could be identified by two-dimensional protein gel electrophoresis, sequenced and finally over-expressed to enhance U(VI) immobilization. Further research might also investigate the reasons for the absence of phosphatase activity under anaerobic conditions. For drawing conclusions on the impact of this strain in the uranium mining waste pile “Haberland”, it would also be interesting to investigate whether the strain is present mainly in oxic or anoxic soil compartments of the Haberlandhalde. This can be investigated *via* a direct quantification of the strain using strain-specific probes or by using real-time PCR with strain-specific primer sets. Moreover, another possibility is to monitor the presence of populations of this strain in contaminated soils under aerobic and anaerobic conditions within microcosm-scale studies.

The second microbial strain studied in this work, the thermoacidophilic crenarchaeon *S. acidocaldarius*, is for some reasons more relevant to radioactive wastes, and even to future repositories, although we demonstrated that this strain immobilizes U(VI) less effective than the studied *Paenibacillus* sp. JG-TB8 and other bacteria. Nevertheless, one of the reasons for the relevance of *S. acidocaldarius* is its intrinsic property to preferentially grow at low pH values. Moreover, we demonstrated within this thesis that moderate temperatures do not completely suppress the enzyme activity of *S. acidocaldarius*. These properties allow metabolic active *S. acidocaldarius* populations in uranium wastes and radionuclide-contaminated waters that usually exhibit moderate temperatures and a moderate or even highly acidic pH. As it is evident from the results within this thesis, *S. acidocaldarius* is able to interact with U(VI) at these conditions, e.g. at moderate acidic pH the strain immobilizes U(VI) *via* biomineralization. However, the results raised questions which need further investigation. Future studies may address the reasons for the absence of U(VI) biomineralization at pH 3, although the highest phosphatase activity was detected at this pH.

In order to determine whether the low amount of degradable organic polyphosphate, described for *S. acidocaldarius*, or the dissolution chemistry of uranyl phosphate minerals inhibits mineral formation, an organic phosphate source should be added to the U/archaea system. Depending on whether biomineralization occurred in this case or not, the low amount of polyphosphate or the uranium chemistry hinders microbial U(VI) biomineralization. In the case that the amount of polyphosphates limits the mineralization, the strain in combination with organic phosphate sources (e.g. glycerol-3-phosphate) may be used as a biological “tool” for uranium immobilization in contaminated sites. The potential of this strain could, for example, be studied by performing column experiments. *S. acidocaldarius* and a phosphate source may be added to contaminated soils or sludge and after certain times the amount of leachable uranium could be determined.

Another interesting aspect of *S. acidocaldarius* is its thermophilic nature, which could be used to provide information about microbial interactions with actinides at elevated temperatures, which are relevant to nuclear waste repositories, because it is predicted that the temperature close to the repositories will be significantly higher than the ambient temperature. In case of an accidentally release of radioactive waste material it could be transported into and subsequently with the groundwater. As the chemical behaviour as well as the thermodynamics of complexation reactions of radionuclides at elevated temperatures differs from those at moderate temperatures the interactions of actinides with various organic and inorganic ligands at elevated temperatures must be known. For studying the impact of microorganisms on uranium mobility at elevated temperatures, future studies could focus on exactly this topic, using *S. acidocaldarius* as a model organism. From the results presented in this thesis, one can expect that the phosphatase activity of the strain is significantly higher than that measured at room temperature. This might result in a very efficient U(VI) biomineralization, at least at moderate acidic conditions.

Other topics for future studies are based on the unique properties of the archaeal SlaA-layer. As demonstrated in this work, the SlaA-layer ghosts are very stable against acidity and detergents. Besides that, they are also resistant against high temperatures and decomposition enzymes, i.e. proteases. Moreover the SlaA-layer represents a highly-ordered, biological and, thus, non-toxic structural matrix which can be used for a multiplicity of applications in biotechnology. Although the applicability for uranium complexation is limited due to the low amount of U(VI) binding ligands, we demonstrate that Au ions interact with the SlaA-layer, which can be used to produce gold nanoclusters with interesting properties. However, there

are still open questions regarding the underlying mechanisms for the initial Au deposition and the evocation of magnetic properties which are topics of on-going research. Moreover, future studies might focus on the production of better applicable Au nanoclusters, i.e. the production of highly ordered nanoclusters with a more consistent particle size. This might be achieved by dissolving the SlaA-layer ghosts and subsequently reassemble them on different supporting material to obtain equally SlaA-coated surfaces.

Literature

1. Ahearne, J.F.: Radioactive waste: The size of the problem. *Physics Today*, 1997. **50**(6): p. 24-29.
2. Hagen, M. and A.T. Jakubick: Returning the WISMUT Legacy to Productive Use, 2006, Springer: Heidelberg. p. 11-26.
3. <http://www.wismut.de/> (19.01.2011).
4. Diehl, P.: Altstandorte des Uranbergbaus in Sachsen, 2003.
5. Choppin, G.R. and B.E. Stout: Actinide behavior in Natural-Waters. *Science of the Total Environment*, 1989. **83**(3): p. 203-216.
6. Markich, S.J.: Uranium speciation and bioavailability in aquatic systems: an overview. *Scientific World Journal*, 2002. **2**: p. 707-29.
7. Fields, M.W., T.F. Yan, S.K. Rhee, S.L. Carroll, P.M. Jardine, D.B. Watson, C.S. Criddle, and J.Z. Zhou: Impacts on microbial communities and cultivable isolates from groundwater contaminated with high levels of nitric acid-uranium waste. *FEMS Microbiology Ecology*, 2005. **53**(3): p. 417-428.
8. Geissler, A. and S. Selenska-Pobell: Addition of U(VI) to a uranium mining waste sample and resulting changes in the indigenous bacterial community. *Geobiology*, 2005. **3**: p. 275-285.
9. Suzuki, Y., S.D. Kelly, K.A. Kemner, and J.F. Banfield: Microbial populations stimulated for hexavalent uranium reduction in uranium mine sediment. *Applied and Environmental Microbiology*, 2003. **69**(3): p. 1337-1346.
10. Radeva, G. and S. Selenska-Pobell: Bacterial diversity in water samples from uranium wastes as demonstrated by 16S rDNA and ribosomal intergenic spacer amplification retrievals. *Canadian Journal of Microbiology*, 2005. **51**(11): p. 910-923.
11. North, N.N., S.L. Dollhopf, L. Petrie, J.D. Istok, D.L. Balkwill, and J.E. Kostka: Change in bacterial community structure during in situ biostimulation of subsurface sediment cocontaminated with uranium and nitrate. *Applied and Environmental Microbiology*, 2004. **70**(8): p. 4911-4920.
12. Anderson, R.T., H.A. Vronis, I. Ortiz-Bernad, C.T. Resch, P.E. Long, R. Dayvault, K. Karp, S. Marutzky, D.R. Metzler, A. Peacock, D.C. White, M. Lowe, and D.R. Lovley: Stimulating the in situ activity of *Geobacter* species to remove uranium from the groundwater of a uranium-contaminated aquifer. *Applied and Environmental Microbiology*, 2003. **69**(10): p. 5884-5891.
13. Akob, D.M., H.J. Mills, and J.E. Kostka: Metabolically active microbial communities in uranium-contaminated subsurface sediments. *FEMS Microbiology Ecology*, 2007. **59**(1): p. 95-107.
14. Bencheikh-Latmani, R., J.O. Leckie, and J.R. Bargar: Fate of uranyl in a quaternary system composed of uranyl, citrate, goethite, and *Pseudomonas fluorescens*. *Environmental Science & Technology*, 2003. **37**(16): p. 3555-3559.
15. Ohnuki, T., T. Yoshida, T. Ozaki, M. Samadfam, N. Kozai, K. Yubuta, T. Mitsugashira, T. Kasama, and A.J. Francis: Interactions of uranium with bacteria and kaolinite clay. *Chemical Geology*, 2005. **220**(3-4): p. 237-243.
16. Walker, S.G., C.A. Flemming, F.G. Ferris, T.J. Beveridge, and G.W. Bailey: Physicochemical interaction of *Escherichia coli* cell envelopes and *Bacillus subtilis* cell walls with two clays and ability of the composite to immobilize heavy metals from solution. *Applied and Environmental Microbiology*, 1989. **55**(11): p. 2976-84.

17. Mullen, M.D., D.C. Wolf, F.G. Ferris, T.J. Beveridge, C.A. Flemming, and G.W. Bailey: Bacterial Sorption of Heavy-Metals. *Applied and Environmental Microbiology*, 1989. **55**(12): p. 3143-3149.
18. Volesky, B.: Sorption and Biosorption. 2003, Montreal, Canada: BV Sorbex, Inc.
19. Lloyd, J.R. and L.E. Macaskie: Biochemical basis of microbe-metal interactions. In *Interactions of Microorganisms with Radionuclides* (eds Keith-Roach, M.J. and F.R. Livens). 2002, Elsevier Sciences Ltd, Oxford, UK, p. 313-342.
20. Huber, G. and K.O. Stetter: *Sulfolobus metallicus*, sp-nov, a novel strictly chemolithoautotrophic thermophilic archaeal species of metal-mobilizers. *Systematic and Applied Microbiology*, 1991. **14**(4): p. 372-378.
21. Huber, G., C. Spinnler, A. Gambacorta, and K.O. Stetter: *Metallosphaera sedula* gen-nov and sp-nov represents a new genus of aerobic, metal-mobilizing, thermoacidophilic archaeobacteria. *Systematic and Applied Microbiology*, 1989. **12**(1): p. 38-47.
22. DiSpirito, A.A. and O.H. Tuovinen: Uranous ion oxidation and carbon-dioxidefixation by thiobacillus-ferrooxidans. *Archives of Microbiology*, 1982. **133**(1): p. 28-32.
23. Beller, H.R.: Anaerobic, nitrate-dependent oxidation of U(IV) oxide minerals by the chemolithoautotrophic bacterium *Thiobacillus denitrificans*. *Applied and Environmental Microbiology*, 2005. **71**(4): p. 2170-2174.
24. Suzuki, Y., S.D. Kelly, K.M. Kemner, and J.F. Banfield: Direct microbial reduction and subsequent preservation of uranium in natural near-surface sediment. *Applied and Environmental Microbiology*, 2005. **71**(4): p. 1790-1797.
25. Liu, C.X., Y.A. Gorby, J.M. Zachara, J.K. Fredrickson, and C.F. Brown: Reduction kinetics of Fe(III), Co(III), U(VI) Cr(VI) and Tc(VII) in cultures of dissimilatory metal-reducing bacteria. *Biotechnology and Bioengineering*, 2002. **80**(6): p. 637-649.
26. Lovley, D.R., S.J. Giovannoni, D.C. White, J.E. Champine, E.J.P. Phillips, Y.A. Gorby, and S. Goodwin: *Geobacter metallireducens* gen-nov sp-nov, a microorganism capable of coupling the complete oxidation of organic-compounds to the reduction of iron and other metals. *Archives of Microbiology*, 1993. **159**(4): p. 336-344.
27. Suzuki, Y., S.D. Kelly, K.M. Kemner, and J.F. Banfield: Enzymatic U(VI) reduction by *Desulfosporosinus* species. *Radiochimica Acta*, 2004. **92**(1): p. 11-16.
28. Wade, R. and T.J. DiChristina: Isolation of U(VI) reduction-deficient mutants of *Shewanella putrefaciens*. *FEMS Microbiology Letters*, 2000. **184**(2): p. 143-148.
29. Wu, W.M., J. Carley, T. Gentry, M.A. Ginder-Vogel, M. Fienen, T. Mehlhorn, H. Yan, S. Carroll, M.N. Pace, J. Nyman, J. Luo, M.E. Gentile, M.W. Fields, R.F. Hickey, B. Gu, D. Watson, O.A. Cirpka, J. Zhou, S. Fendorf, P.K. Kitanidis, P.M. Jardine, and C.S. Criddle: Pilot-scale in situ bioremediation of uranium in a highly contaminated aquifer. 2. Reduction of u(VI) and geochemical control of u(VI) bioavailability. *Environmental Science & Technology*, 2006. **40**(12): p. 3986-95.
30. Lovley, D.R., E.J.P. Phillips, Y.A. Gorby, and E.R. Landa: Microbial reduction of uranium. *Nature*, 1991. **350**: p. 413-416.
31. Kashefi, K. and D.R. Lovley: Reduction of Fe(III), Mn(IV), and toxic metals at 100°C by *Pyrobaculum islandicum*. *Applied and Environmental Microbiology*, 2000. **66**(3): p. 1050-1056.
32. Dassa, E., M. Cahu, B. Desjoyaux-Cherel, and P.L. Boquet: The acid phosphatase with optimum pH of 2.5 of *Escherichia coli*. Physiological and Biochemical study. *Journal of Biological Chemistry*, 1982. **257**(12): p. 6669-76.

33. Kurosawa, N., K. Fukuda, Y.H. Itoh, and T. Horiuchi: Partial purification and characterization of thermostable acid phosphatase from thermoacidophilic archaeon *Sulfolobus acidocaldarius*. *Current Microbiology*, 2000. **40**(1): p. 57-60.
34. Porschen, R.K. and E.H. Spaulding: Phosphatase activity of anaerobic organisms. *Applied Microbiology*, 1974. **27**(4): p. 744-7.
35. Allard, B., H. Boren, C. Pettersson, and G. Zhang: Degradation of humic substances by UV irradiation. *Environment International*, 1994. **20**(1): p. 97-101.
36. Sutton, R. and G. Sposito: Molecular structure in soil humic substances: The new view. *Environmental Science & Technology*, 2005. **39**(23): p. 9009-9015.
37. Lenhart, J.J., S.E. Cabaniss, P. MacCarthy, and B.D. Honeyman: Uranium(VI) complexation with citric, humic and fulvic acids. *Radiochimica Acta*, 2000. **88**(6): p. 345-353.
38. Lenhart, J.J. and B.D. Honeyman: Uranium(VI) sorption to hematite in the presence of humic acid. *Geochimica et Cosmochimica Acta*, 1999. **63**(19-20): p. 2891-2901.
39. Sachs, S., V. Brendler, and G. Geipel: Uranium(VI) complexation by humic acid under neutral pH conditions studied by laser-induced fluorescence spectroscopy. *Radiochimica Acta*, 2007. **95**(2): p. 103-110.
40. Schmeide, K., S. Sachs, M. Bubner, T. Reich, K.H. Heise, and G. Bernhard: Interaction of uranium(VI) with various modified and unmodified natural and synthetic humic substances studied by EXAFS and FTIR spectroscopy. *Inorganica Chimica Acta*, 2003. **351**: p. 133-140.
41. Shanbhag, P.M. and G.R. Choppin: Binding of uranyl by humic-acid. *Journal of Inorganic & Nuclear Chemistry*, 1981. **43**(12): p. 3369-3372.
42. Wei, M., J.L. Liao, N. Liu, D. Zhang, H.J. Kang, Y.Y. Yang, Y. Yang, and J.N. Jin: Interaction between uranium and humic acid (I): Adsorption behaviors of U(VI) in soil humic acids. *Nuclear Science and Techniques*, 2007. **18**(5): p. 287-293.
43. Li, W.C., D.M. Victor, and C.L. Chakrabarti: Effect of pH and uranium concentration on interaction of uranium(vi) and uranium(iv) with organic-ligands in aqueous-solutions. *Analytical Chemistry*, 1980. **52**(3): p. 520-523.
44. Lovley, D.R., J.L. Fraga, E.L. Blunt-Harris, L.A. Hayes, E.J.P. Phillips, and J.D. Coates: Humic substances as a mediator for microbially catalyzed metal reduction. *Acta Hydrochimica et Hydrobiologica*, 1998. **26**(3): p. 152-157.
45. Fredrickson, J.K., H.M. Kostandarites, S.W. Li, A.E. Plymale, and M.J. Daly: Reduction of Fe(III), Cr(VI), U(VI), and Tc(VII) by *Deinococcus radiodurans* R1. *Applied and Environmental Microbiology*, 2000. **66**(5): p. 2006-11.
46. Neilands, J.B.: Siderophores: structure and function of microbial iron transport compounds. *Journal of Biological Chemistry*, 1995. **270**(45): p. 26723-6.
47. Frazier, S.W., R. Kretzschmar, and S.M. Kraemer: Bacterial siderophores promote dissolution of UO₂ under reducing conditions. *Environmental Science & Technology*, 2005. **39**(15): p. 5709-5715.
48. Kalinowski, B.E., A. Oskarsson, Y. Albinsson, J. Arlinger, A. Odegaard-Jensen, T. Andlid, and K. Pedersen: Microbial leaching of uranium and other trace elements from shale mine tailings at Ranstad. *Geoderma*, 2004. **122**(2-4): p. 177-194.
49. Suzuki, Y. and J.F. Banfield: Geomicrobiology of uranium. *Reviews in Mineralogy and Geochemistry*, 1999: p. 393-432.
50. Johnson, D.B.: Biodiversity and interactions of acidophiles: Key to understanding and optimizing microbial processing of ores and concentrates. *Transactions of Nonferrous Metals Society of China*, 2008. **18**(6): p. 1367-1373.
51. Schippers, A.: Microorganisms involved in bioleaching and nucleic acid-based molecular methods for their identification and quantification, In *Microbial processing*

- of metal sulfides* (eds Donati E.R. and W. Sand). 2007, Springer-Verlag GmbH, Berlin: Heidelberg. p. 3-33.
52. Gadd, G.M.: Microbial interactions with metals/radionuclides: the basis of bioremediation, In *Interactions of Microorganisms with Radionuclides* (eds Keith-Roach, M.J. and F.R. Livens). 2002, Elsevier Sciences Ltd, Oxford, UK, pp. p. 179-203.
 53. Gadd, G.M.: Microbial influence on metal mobility and application for bioremediation. *Geoderma*, 2004. **122**(2-4): p. 109-119.
 54. Lloyd, J.R. and J.C. Renshaw: Bioremediation of radioactive waste: radionuclide-microbe interactions in laboratory and field-scale studies. *Current Opinion in Biotechnology*, 2005. **16**(3): p. 254-260.
 55. Whicker, F.W., T.G. Hinton, M.M. MacDonell, J.E. Pinder, 3rd, and L.J. Habegger: Environment. Avoiding destructive remediation at DOE sites. *Science*, 2004. **303**(5664): p. 1615-6.
 56. Appukuttan, D., A.S. Rao, and S.K. Apte: Engineering of *Deinococcus radiodurans* R1 for bioprecipitation of uranium from dilute nuclear waste. *Applied and Environmental Microbiology*, 2006. **72**(12): p. 7873-7878.
 57. Volesky, B.: Biosorption and me. *Water Research*, 2007. **41**(18): p. 4017-4029.
 58. Gadd, G.M.: Biosorption: critical review of scientific rationale, environmental importance and significance for pollution treatment. *Journal of Chemical Technology and Biotechnology*, 2009. **84**(1): p. 13-28.
 59. Macaskie, L.E.: An immobilized cell bioprocess for the removal of heavy-metals from aqueous flows. *Journal of Chemical Technology and Biotechnology*, 1990. **49**(4): p. 357-379.
 60. Cox, M.M. and J.R. Battista: *Deinococcus radiodurans* - the consummate survivor. *Nature Reviews Microbiology*, 2005. **3**(11): p. 882-92.
 61. Ruggiero, C.E., H. Boukhalfa, J.H. Forsythe, J.G. Lack, L.E. Hersman, and M.P. Neu: Actinide and metal toxicity to prospective bioremediation bacteria. *Environmental Microbiology*, 2005. **7**(1): p. 88-97.
 62. Gu, B.H., W.M. Wu, M.A. Ginder-Vogel, H. Yan, M.W. Fields, J. Zhou, S. Fendorf, C.S. Criddle, and P.M. Jardine: Bioreduction of uranium in a contaminated soil column. *Environmental Science & Technology*, 2005. **39**(13): p. 4841-4847.
 63. Xu, M.Y., W.M. Wu, L.Y. Wu, Z.L. He, J.D. Van Nostrand, Y. Deng, J. Luo, J. Carley, M. Ginder-Vogel, T.J. Gentry, B.H. Gu, D. Watson, P.M. Jardine, T.L. Marsh, J.M. Tiedje, T. Hazen, C.S. Criddle, and J.Z. Zhou: Responses of microbial community functional structures to pilot-scale uranium in situ bioremediation. *ISME Journal*, 2010. **4**(8): p. 1060-1070.
 64. Chang, Y.J., P.E. Long, R. Geyer, A.D. Peacock, C.T. Resch, K. Sublette, S. Pfiffner, A. Smithgall, R.T. Anderson, H.A. Vrionis, J.R. Stephen, R. Dayvault, I. Ortiz-Bernad, D.R. Lovley, and D.C. White: Microbial incorporation of C-13-labeled acetate at the field scale: Detection of microbes responsible for reduction of U(VI). *Environmental Science & Technology*, 2005. **39**(23): p. 9039-9048.
 65. Shelobolina, E.S., K. O'Neill, K.T. Finneran, L.A. Hayes, and D.R. Lovley: Potential for in situ bioremediation of a low-pH, high-nitrate uranium-contaminated groundwater. *Soil & Sediment Contamination*, 2003. **12**(6): p. 865-884.
 66. Nannipieri, P., L. Giagnoni, L. Landi, and G. Renella: Role of phosphatase enzymes in soil. In *Phosphorus in Action: Biological processes in soil phosphorus cycling* (eds Bünemann, E.K., A. Oberson, E. Frossard), 2011, Springer Verlag Berlin: Heidelberg. **100**: p. 215-243.

67. Macaskie, L.E., K.M. Bonthron, and D.A. Rouch: Phosphatase-mediated heavy metal accumulation by a *Citrobacter* sp. and related enterobacteria. *FEMS Microbiology Letters*, 1994. **121**(2): p. 141-6.
68. Satta, G., G. Grazi, P.E. Varaldo, and R. Fontana: Detection of bacterial phosphatase-activity by means of an original and simple test. *Journal of Clinical Pathology*, 1979. **32**(4): p. 391-395.
69. Powers, L.G., H.J. Mills, A.V. Palumbo, C. Zhang, K. Delaney, and P.A. Sobecky: Introduction of a plasmid-encoded phoA gene for constitutive overproduction of alkaline phosphatase in three subsurface *Pseudomonas* isolates. *FEMS Microbiology Ecology*, 2002. **41**(2): p. 115-23.
70. Beazley, M.J., R.J. Martinez, P.A. Sobecky, S.M. Webb, and M. Taillefert: Uranium Biomineralization as a result of bacterial phosphatase activity: insights from bacterial isolates from a contaminated subsurface. *Environmental Science & Technology*, 2007. **41**: p. 5701-5707.
71. Choppin, G.R.: Actinide speciation in the environment. *Journal of Radioanalytical and Nuclear Chemistry*, 2007. **273**(3): p. 695-703.
72. Mattigod, S.V.: Validation of Geochemical Equilibrium Models, In Chemical equilibrium and reaction models (eds Löppert, R.H, A.P. Schwab, S. Goldberg. 1995, Madison, WI, USA. SSSA special publication number 42: p. 201-218.
73. Wolery, T.: EQ3/6: A Software Package for Geochemical Modelling of Aqueous Systems: Package Overview and Installation Guide., 1992: Lawrence Livermore National Laboratory.
74. Grenthe, I., J. Fuger, R.J.M. Konings, R.J. Lemire, B. Muller, C.N. Cregu, and H. Wanner: Chemical thermodynamics of uranium. *OECD publications*, 1992: p. 1-715.
75. Guillaumont, R., T. Fanghänel, J. Fuger, I. Grenthe, V. Neck, D.A. Palmer, and M.H. Rand: Update on the chemical thermodynamics of uranium, neptunium, plutonium, americium and technetium, 2003, Issy-les-Moulineaux: ELSEVIER.
76. Brock, T.D., K.M. Brock, R.T. Belly, and R.L. Weiss: *Sulfolobus* - A new genus of sulfur-oxidizing bacteria living at low ph and high temperature. *Archiv für Mikrobiologie*, 1972. **84**(1): p. 54-68.
77. Reitz, T. *Einfluss von Uran auf die Archaea-Diversität in Bodenproben aus der Haberlandhalde*. 2006. TU Dresden.
78. Geissler, A., M. Merroun, G. Geipel, H. Reuther, and S. Selenska-Pobell: Biogeochemical changes induced in uranium mining waste pile samples by uranyl nitrate treatments under anaerobic conditions. *Geobiology*, 2009. **7**(3): p. 282-294.
79. Kletzin, A.: General Characteristics and Important Modell Organisms, 2007, ASM Press: Herndon. p. 14-92.
80. Kandler, O. and H. König: Cell wall polymers in Archaea (Archaeobacteria). *Cellular and Molecular Life Sciences*, 1998. **54**(4): p. 305-308.
81. Veith, A., A. Klingl, B. Zolghadr, K. Lauber, R. Mentele, F. Lottspeich, R. Rachel, S.V. Albers, and A. Kletzin: *Acidianus*, *Sulfolobus* and *Metallosphaera* surface layers: structure, composition and gene expression. *Molecular Microbiology*, 2009. **73**(1): p. 58-72.
82. Merroun, M., C. Hennig, A. Rossberg, G. Geipel, T. Reich, and S. Selenska-Pobell: Molecular and atomic analysis of uranium complexes formed by three eco-types of *Acidithiobacillus ferrooxidans*. *Biochemical Society Transactions*, 2002. **30**(4): p. 669-672.
83. Merroun, M., M. Nedelkova, A. Rossberg, C. Hennig, and S. Selenska-Pobell: Interaction mechanisms of bacterial strains isolated from extreme habitats with uranium. *Radiochimica Acta*, 2006. **94**: p. 723-729.

84. Nedelkova, M., M.L. Merroun, A. Rossberg, C. Hennig, and S. Selenska-Pobell: Microbacterium isolates from the vicinity of a radioactive waste depository and their interactions with uranium. *FEMS Microbiology Ecology*, 2007. **59**: p. 694-705.
85. Albers, S.V., Z. Szabo, and A.J.M. Driessen: Protein secretion in the Archaea: multiple paths towards a unique cell surface. *Nature Reviews Microbiology*, 2006. **4**(7): p. 537-547.
86. Wellmann, D.M., K.M. Gunderson, J.P. Icenhower, and S.W. Forrester: Dissolution kinetics of synthetic and natural meta-autunite minerals under acidic conditions. *Geochemistry Geophysics Geosystems*, 2007. **8**(11): p. 1-16.
87. Selenska-Pobell, S. and M.L. Merroun: Accumulation of heavy metals by microorganisms: biomineralisation and nanocluster formation, In *Prokaryotic Cell Wall Compounds: Structure and Biochemistry* (eds König, H., H. Claus, A. Varma), 2010, Springer Verlag: Heidelberg. p. 483-500.
88. Martinez, R.J., M.J. Beazley, M. Taillefert, A.K. Arakaki, J. Skolnick, and P.A. Sobecky: Aerobic uranium (VI) bioprecipitation by metal-resistant bacteria isolated from radionuclide- and metal-contaminated subsurface soils. *Environmental Microbiology*, 2007. **9**(12): p. 3122-3133.
89. Renninger, N., R. Knopp, H. Nitsche, D.S. Clark, and J.D. Keasling: Uranyl precipitation by *Pseudomonas aeruginosa* via controlled polyphosphate metabolism. *Applied and Environmental Microbiology*, 2004. **70**(12): p. 7404-7412.
90. Grogan, D.W.: Organization and interactions of cell envelope proteins of the extreme thermoacidophile *Sulfolobus acidocaldarius*. *Canadian Journal of Microbiology*, 1996. **42**(11): p. 1163-1171.
91. Sara, M. and U.B. Sleytr: S-layer proteins. *Journal of Bacteriology*, 2000. **182**(4): p. 859-868.
92. Ilk, N., E.M. Egelseer, J. Ferner-Ortner, S. Kupcu, D. Pum, B. Schuster, and U.B. Sleytr: Surfaces functionalized with self-assembling S-layer fusion proteins for nanobiotechnological applications. *Colloids and Surfaces a-Physicochemical and Engineering Aspects*, 2008. **321**(1-3): p. 163-167.
93. Sleytr, U.B., C. Huber, N. Ilk, D. Pum, B. Schuster, and E.M. Egelseer: S-layers as a tool kit for nanobiotechnological applications. *FEMS Microbiology Letters*, 2007. **267**(2): p. 131-44.
94. Dieluweit, S., D. Pum, and U.B. Sleytr: Formation of a gold superlattice on an S-layer with square lattice symmetry. *Supramolecular Science*, 1998. **5**(1-2): p. 15-19.
95. Murphy, W.M. and E.L. Shock: Environmental aqueous geochemistry of actinides. 1999, *Reviews in Mineralogy and Geochemistry*, **38**(1): 221-253.
96. Baik, M.H., S.P. Hyun, W.J. Cho, and P.S. Hahn: Contribution of minerals to the sorption of U(VI) on granite. *Radiochimica Acta*, 2004. **92**(9-11): p. 663-669.
97. Barnett, M.O., P.M. Jardine, S.C. Brooks, and H.M. Selim: Adsorption and transport of uranium(VI) in subsurface media. *Soil Science Society of America Journal*, 2000. **64**(3): p. 908-917.
98. Pedersen, K.: Microorganisms and their influence on radionuclide migration in igneous rock environments. *Journal of Nuclear and Radiochemical Sciences*, 2005. **6**(1): p. 11-15.
99. Renshaw, J.C., J.R. Lloyd, and F.R. Livens: Microbial interactions with actinides and long-lived fission products. *Comptes Rendus Chimie*, 2007. **10**(10-11): p. 1067-1077.
100. Merroun, M.L. and S. Selenska-Pobell: Bacterial interactions with uranium: an environmental perspective. *Journal of Contaminant Hydrology*, 2008. **102**(3-4): p. 285-95.

101. Nakajima, A. and T. Tsuruta: Competitive biosorption of thorium and uranium by *Micrococcus luteus*. *Journal of Radioanalytical and Nuclear Chemistry*, 2004. **260**(1): p. 13-18.
102. Sar, P. and S.F. D'Souza: Biosorptive uranium uptake by a *Pseudomonas* strain: characterization and equilibrium studies. *Journal of Chemical Technology and Biotechnology*, 2001. **76**(12): p. 1286-1294.
103. Macaskie, L.E., R.M. Empson, A.K. Cheetham, C.P. Grey, and A.J. Skarnulis: Uranium bioaccumulation by a citrobacter sp as a result of enzymatically mediated growth of polycrystalline HUO_2PO_4 . *Science*, 1992. **257**(5071): p. 782-784.
104. Wall, J.D. and L.R. Krumholz: Uranium reduction. *Annual Review of Microbiology*, 2006. **60**: p. 149-166.
105. Brim, H., S.C. McFarlan, J.K. Fredrickson, K.W. Minton, M. Zhai, L.P. Wackett, and M.J. Daly: Engineering *Deinococcus radiodurans* for metal remediation in radioactive mixed waste environments. *Nature Biotechnology*, 2000. **18**(1): p. 85-90.
106. Istok, J.D., J.M. Senko, L.R. Krumholz, D. Watson, M.A. Bogle, A. Peacock, Y.J. Chang, and D.C. White: In situ bioreduction of technetium and uranium in a nitrate-contaminated aquifer. *Environmental Science & Technology*, 2004. **38**(2): p. 468-75.
107. Selenska-Pobell, S.: Diversity and activity of bacteria in uranium waste piles, In *Interactions of Microorganisms with Radionuclides* (eds Keith-Roach, M.J. and F.R. Livens). 2002, Elsevier Sciences Ltd, Oxford, UK, p. 225-254.
108. Selenska-Pobell, S., G. Kampf, K. Flemming, G. Radeva, and G. Satchanska: Bacterial diversity in soil samples from two uranium waste piles as determined by rep-APD, RISA and 16S rDNA retrieval. *Antonie Van Leeuwenhoek*, 2001. **79**(2): p. 149-161.
109. Hengstmann, U., K.J. Chin, P.H. Janssen, and W. Liesack: Comparative phylogenetic assignment of environmental sequences of genes encoding 16S rRNA and numerically abundant culturable bacteria from an anoxic rice paddy soil. *Applied and Environmental Microbiology*, 1999. **65**(11): p. 5050-8.
110. Elo, S., L. Maunuksela, M. Salkinoja-Salonen, A. Smolander, and K. Haahtela: Humus bacteria of Norway spruce stands: plant growth promoting properties and birch, red fescue and alder colonizing capacity. *FEMS Microbiology Ecology*, 2000. **31**(2): p. 143-152.
111. Ash, C., F.G. Priest, and M.D. Collins: Molecular identification of rRNA group 3 bacilli (Ash, Farrow, Wallbanks and Collins) using a PCR probe test. Proposal for the creation of a new genus *Paenibacillus*. *Antonie Van Leeuwenhoek*, 1993. **64**(3-4): p. 253-60.
112. Garrity, G.M., T.G. Lilburn, J.R. Cole, S.H. Harrison, J. Euzaby, and B.J. Tindall: Taxonomic Outline of the Bacteria and Archaea, Release 7.7, in *Part 9 - The Bacteria: Phylum "Firmicutes": Class "Bacilli"* 2007. p. 333-398.
113. Shida, O., H. Takagi, K. Kadowaki, L.K. Nakamura, and K. Komagata: Transfer of *Bacillus alginolyticus*, *Bacillus chondroitinus*, *Bacillus curdlanolyticus*, *Bacillus glucanolyticus*, *Bacillus kobensis*, and *Bacillus thiaminolyticus* to the genus *Paenibacillus* and emended description of the genus *Paenibacillus*. *International Journal of Systematic and Evolutionary Microbiology*, 1997. **47**(2): p. 289-98.
114. Elo, S., I. Suominen, P. Kampfer, J. Juhanaja, M. Salkinoja-Salonen, and K. Haahtela: *Paenibacillus borealis* sp. nov., a nitrogen-fixing species isolated from spruce forest humus in Finland. *International Journal of Systematic and Evolutionary Microbiology*, 2001. **51**: p. 535-545.
115. Iida, K.I., Y. Ueda, Y. Kawamura, T. Ezaki, A. Takade, S. Yoshida, and K. Amako: *Paenibacillus motobuensis* sp. nov., isolated from a composting machine utilizing soil

- from Motobu-town, Okinawa, Japan. *International Journal of Systematic and Evolutionary Microbiology*, 2005. **55**: p. 1811-1816.
116. Kim, D.S., C.Y. Bae, J.J. Jeon, S.J. Chun, H.W. Oh, S.G. Hong, K.S. Baek, E.Y. Moon, and K.S. Bae: *Paenibacillus elgii* sp. nov., with broad antimicrobial activity. *International Journal of Systematic and Evolutionary Microbiology*, 2004. **54**(Pt 6): p. 2031-5.
117. Ma, Y.C. and S.F. Chen: *Paenibacillus forsythiae* sp nov., a nitrogen-fixing species isolated from rhizosphere soil of Forsythia mira. *International Journal of Systematic and Evolutionary Microbiology*, 2008. **58**: p. 319-323.
118. Takeda, M., Y. Kamagata, S. Shinmaru, T. Nishiyama, and J. Koizumi: *Paenibacillus koleovorans* sp. nov., able to grow on the sheath of *Sphaerotilus natans*. *International Journal of Systematic and Evolutionary Microbiology*, 2002. **52**(Pt 5): p. 1597-601.
119. Yoon, J.H., H.M. Oh, B.D. Yoon, K.H. Kang, and Y.H. Park: *Paenibacillus kribbensis* sp nov and *Paenibacillus terrae* sp nov., biofloculants for efficient harvesting of algal cells. *International Journal of Systematic and Evolutionary Microbiology*, 2003. **53**: p. 295-301.
120. Yoon, J.H., D.K. Yim, J.S. Lee, K.S. Shin, H.H. Sato, S.T. Lee, Y.K. Park, and Y.H. Park: *Paenibacillus campinasensis* sp. nov., a cyclodextrin-producing bacterium isolated in Brazil. *International Journal of Systematic and Evolutionary Microbiology*, 1998. **48 Pt 3**: p. 833-7.
121. Atlas, R.M.: Handbook of Microbiological Media. 3rd ed. ed2004, Boca Raton: CRC Press.
122. Lane, D.J.: 16S/23S rRNA Sequencing, 1991, Wiley & Sons: West Sussex, UK. p. 113-175.
123. Brosius, J., M.L. Palmer, P.J. Kennedy, and H.F. Noller: Complete nucleotide sequence of a 16S ribosomal RNA gene from *Escherichia coli*. *Proceedings of the National Academy of Sciences of the United States of America*, 1978. **75**(10): p. 4801-5.
124. Don, R.H., P.T. Cox, B.J. Wainwright, K. Baker, and J.S. Mattick: 'Touchdown' PCR to circumvent spurious priming during gene amplification. *Nucleic Acids Research*, 1991. **19**(14): p. 4008.
125. Sanger, F., S. Nicklen, and A.R. Coulson: DNA sequencing with chain-terminating inhibitors. *Proceedings of the National Academy of Sciences of the United States of America*, 1977. **74**(12): p. 5463-5467.
126. Muyzer, G., E.C. Dewaal, and A.G. Uitterlinden: Profiling of complex microbial-populations by denaturing gradient gel-electrophoresis analysis of polymerase chain reaction-amplified genes-coding for 16s ribosomal-rna. *Applied and Environmental Microbiology*, 1993. **59**(3): p. 695-700.
127. Altschul, S.F., T.L. Madden, A.A. Schaffer, J.H. Zhang, Z. Zhang, W. Miller, and D.J. Lipman: Gapped BLAST and PSI-BLAST: a new generation of protein database search programs. *Nucleic Acids Research*, 1997. **25**(17): p. 3389-3402.
128. Thompson, J.D., D.G. Higgins, and T.J. Gibson: CLUSTAL W: improving the sensitivity of progressive multiple sequence alignment through sequence weighting, position-specific gap penalties and weight matrix choice. *Nucleic Acids Research*, 1994. **22**(22): p. 4673-80.
129. Saitou, N. and M. Nei: The neighbor-joining method: a new method for reconstructing phylogenetic trees. *Molecular Biology and Evolution*, 1987. **4**(4): p. 406-25.
130. Felsenstein, J.: PHYLIP: Phylogenetic Inference Package version 3.5c., 1993.

131. Laemmli, U.K.: Cleavage of structural proteins during assembly of head of bacteriophage-T4. *Nature*, 1970. **227**(5259): p. 680-&.
132. Poole, R.K., H.D. Williams, J.A. Downie, and F. Gibson: Mutations affecting the cytochrome-d-containing oxidase complex of *Escherichia coli* K12 - identification and mapping of a 4th locus, Cydd. *Journal of General Microbiology*, 1989. **135**: p. 1865-1874.
133. Reitz, T., M.L. Merroun, A. Rossberg, and S. Selenska-Pobell: Interactions of *Sulfolobus acidocaldarius* with uranium. *Radiochimica Acta*, 2010. **98**(5): p. 249-257.
134. Matz, W., N. Schell, G. Bernhard, F. Prokert, T. Reich, J. Claußner, W. Oehme, R. Schlenk, S. Dienel, H. Funke, F. Eichhorn, M. Betzl, D. Pröhl, U. Strauch, G. Hüttig, H. Krug, W. Neumann, V. Brendler, P. Reichel, M.A. Denecke, and H. Nitsche: ROBL - a CRG Beamline for Radiochemistry and Materials Research at the ESRF. *Journal of Synchrotron Radiation*, 1999. **6**: p. 1076-1085.
135. George, G.N. and I.J. Pickering: A Suite of Computer Programs for Analysis of X-ray Absorption Spectra. 2000.
136. Ankudinov, A.L., B. Ravel, J.J. Rehr, and S.D. Conradson: Real-space multiple-scattering calculation and interpretation of x-ray-absorption near-edge structure. *Physical Review B*, 1998. **58**(12): p. 7565-7576.
137. Hudson, E.A., P.G. Allen, L.J. Terminello, M.A. Denecke, and T. Reich: Polarized x-ray-absorption spectroscopy of the uranyl ion: Comparison of experiment and theory. *Physical Review B*, 1996. **54**(1): p. 156-165.
138. Reynolds, E.S.: The use of lead citrate at high ph as an electron-opaque stain in electron microscopy. *The Journal of Cell Biology*, 1963. **17**: p. 208-212.
139. Buss, J.E. and J.T. Stull: Measurement of chemical phosphate in proteins. *Methods in Enzymology*, 1983. **99**: p. 7-14.
140. Ekman, P. and O. Jäger: Quantification of subnanomolar amounts of phosphate bound to seryl and threonyl residues in phosphoproteins using alkaline hydrolysis and malachite green. *Analytical Biochemistry*, 1993. **214**: p. 138-141.
141. Shida, O., H. Takagi, K. Kadowaki, L.K. Nakamura, and K. Komagata: Emended description of *Paenibacillus amylolyticus* and description of *Paenibacillus illinoisensis* sp nov and *Paenibacillus chibensis* sp nov. *International Journal of Systematic and Evolutionary Microbiology*, 1997. **47**(2): p. 299-306.
142. Tzeneva, V.A., Y.G. Li, A.D.M. Felske, W.M. de Vos, A.D.L. Akkermans, E.E. Vaughan, and H. Smidt: Development and application of a selective PCR-denaturing gradient gel electrophoresis approach to detect a recently cultivated *Bacillus* group predominant in soil. *Applied and Environmental Microbiology*, 2004. **70**(10): p. 5801-5809.
143. Deuerling, E., A. Mogk, C. Richter, M. Purucker, and W. Schumann: The ftsH gene of *Bacillus subtilis* is involved in major cellular processes such as sporulation, stress adaptation and secretion. *Molecular Microbiology*, 1997. **23**(5): p. 921-33.
144. Nakano, M.M., Y.P. Dailly, P. Zuber, and D.P. Clark: Characterization of anaerobic fermentative growth of *Bacillus subtilis*: identification of fermentation end products and genes required for growth. *Journal of Bacteriology*, 1997. **179**(21): p. 6749-55.
145. Marino, M., T. Hoffmann, R. Schmid, H. Mobitz, and D. Jahn: Changes in protein synthesis during the adaptation of *Bacillus subtilis* to anaerobic growth conditions. *Microbiology*, 2000. **146** (Pt 1): p. 97-105.
146. Nakano, M.M. and P. Zuber: Anaerobic growth of a "strict aerobe" (*Bacillus subtilis*). *Annual Review of Microbiology*, 1998. **52**: p. 165-190.

147. Chun, S.C., R.W. Schneider, and I.M. Chung: Determination of carbon source utilization of *Bacillus* and *Pythium* species by Biolog (R) microplate assay. *Journal of Microbiology*, 2003. **41**(3): p. 252-258.
148. Luckevich, M.D. and T.J. Beveridge: Characterization of a dynamic S layer on *Bacillus thuringiensis*. *Journal of Bacteriology*, 1989. **171**(12): p. 6656-67.
149. Pena, G., J. Miranda-Rios, G. de la Riva, L. Pardo-Lopez, M. Soberon, and A. Bravo: A *Bacillus thuringiensis* S-layer protein involved in toxicity against *Epilachna varivestis* (Coleoptera: Coccinellidae). *Applied and Environmental Microbiology*, 2006. **72**(1): p. 353-60.
150. Merroun, M.L., J. Raff, A. Rossberg, C. Hennig, T. Reich, and S. Selenska-Pobell: Complexation of uranium by cells and S-layer sheets of *Bacillus sphaericus* JG-A12. *Applied and Environmental Microbiology*, 2005. **71**(9): p. 5532-5543.
151. Wu, W.M., J. Carley, M. Fienen, T. Mehlhorn, K. Lowe, J. Nyman, J. Luo, M.E. Gentile, R. Rajan, D. Wagner, R.F. Hickey, B. Gu, D. Watson, O.A. Cirpka, P.K. Kitanidis, P.M. Jardine, and C.S. Criddle: Pilot-scale in situ bioremediation of uranium in a highly contaminated aquifer. 1. Conditioning of a treatment zone. *Environmental Science & Technology*, 2006. **40**(12): p. 3978-85.
152. Ferris, F.G. and T.J. Beveridge: Site specificity of metallic ion binding in *Escherichia coli* K-12 lipopolysaccharide. *Canadian Journal of Microbiology*, 1986. **32**(1): p. 52-55.
153. Reitz, T., M.L. Merroun, and S. Selenska-Pobell: Interactions of *Paenibacillus* sp. and *Sulfolobus acidocaldarius* strains with U(VI), In *Uranium, Mining and Hydrogeology*, (eds Merkel, B.J. and A. Hasche-Berger). 2008, Springer-Verlag: Heidelberg. p. 703-710.
154. Panak, P.J., R. Knopp, C.H. Booth, and H. Nitsche: Spectroscopic studies on the interaction of U(VI) with *Bacillus sphaericus*. *Radiochimica Acta*, 2002. **90**: p. 779-783.
155. Fowle, D.A., J.B. Fein, and A.M. Martin: Experimental study of uranyl adsorption onto *Bacillus subtilis*. *Environmental Science & Technology*, 2000. **34**: p. 3737-3741.
156. Malekzadeh, F., A.M. Latifi, M. Shahamat, M. Levin, and R.R. Colwell: Effects of selected physical and chemical parameters on uranium uptake by the bacterium *Chryseomonas* MGF-48. *World Journal of Microbiology & Biotechnology*, 2002. **18**(7): p. 599-602.
157. Bäuerlein, E.: Biomineralization of unicellular organisms: An unusual membrane biochemistry for the production of inorganic nano- and microstructures. *Angewandte Chemie*, 2003. **42**(6): p. 614-641.
158. Koban, A., G. Geipel, A. Rossberg, and G. Bernhard: Uranium(VI) complexes with sugar phosphates in aqueous solution. *Radiochimica Acta*, 2004. **92**(12): p. 903-908.
159. Merroun, M.L., G. Geipel, R. Nicolai, K.-H. Heise, and S. Selenska-Pobell: Complexation of uranium (VI) by three eco-types of *Acidithiobacillus ferrooxidans* studied using time-resolved laser-induced fluorescence spectroscopy and infrared spectroscopy. *Biometals*, 2003. **16**: p. 331-339.
160. Koban, A. and G. Bernhard: Complexation of uranium(VI) with glycerol 1-phosphate. *Polyhedron*, 2004. **23**(10): p. 1793-1797.
161. Koban, A. and G. Bernhard: Uranium(VI) complexes with phospholipid model compounds – A laser spectroscopic study. *Journal of Inorganic Biochemistry*, 2007. **101**(5): p. 750-757.
162. Merroun, M., C. Hennig, A. Rossberg, T. Reich, and S. Selenska-Pobell: Characterization of U(VI)-*Acidithiobacillus ferrooxidans* complexes using EXAFS,

- transmission electron microscopy, and energy-dispersive X-ray analysis. *Radiochimica Acta*, 2003. **91**(10): p. 583-591.
163. Barkleit, A., H. Moll, and G. Bernhard: Interaction of uranium(VI) with lipopolysaccharide. *Dalton Transactions*, 2008(21): p. 2879-2886.
164. Reitz, T., M.L. Merroun, A. Rossberg, R. Steudtner, and S. Selenska-Pobell: Bioaccumulation of U(VI) by *Sulfolobus acidocaldarius* at moderate acidic conditions. *Radiochimica Acta*, 2011.
165. Geipel, G., G. Bernhard, M. Rutsch, V. Brendler, and H. Nitsche: Spectroscopic properties of uranium(VI) minerals studied by time-resolved laser-induced fluorescence spectroscopy (TRLFS). *Radiochimica Acta*, 2000. **88**(9-11): p. 757-762.
166. Vogel, M., A. Günther, A. Rossberg, B. Li, G. Bernhard, and J. Raff: Biosorption of U(VI) by the green algae *Chlorella vulgaris* in dependence of pH value and cell activity. *Science of the Total Environment*, 2010.
167. Barkleit, A., H. Moll, and G. Bernhard: Complexation of uranium(VI) with peptidoglycan. *Dalton Trans*, 2009(27): p. 5379-85.
168. Denecke, M.A., T. Reich, M. Bubner, S. Pompe, K.H. Heise, H. Nitsche, P.G. Allen, J.J. Bucher, N.M. Edelstein, and D.K. Shuh: Determination of structural parameters of uranyl ions complexed with organic acids using EXAFS. *Journal of Alloys and Compounds*, 1998. **271**: p. 123-127.
169. Hennig, C., P.J. Panak, T. Reich, A. Rossberg, J. Raff, S. Selenska-Pobell, W. Matz, J.J. Bucher, G. Bernhard, and H. Nitsche: EXAFS investigation of uranium(VI) complexes formed at *Bacillus cereus* and *Bacillus sphaericus* surfaces. *Radiochimica Acta*, 2001. **89**(10): p. 625.
170. Boswell, C.D., R.E. Dick, and L.E. Macaskie: The effect of heavy metals and other environmental conditions on the anaerobic phosphate metabolism of *Acinetobacter johnsonii*. *Microbiology-Uk*, 1999. **145**: p. 1711-1720.
171. Lucks, C., A. Roßberg, A. Scheinost: Combined UV-vis and EXAFS study on the complex formation of uranium(VI) with several carboxylic acids, *in preparation*.
172. Viamajala, S., V. Sivaswamy, M.I. Boyanov, B.M. Peyton, R. Gerlach, W.A. Apel, R.K. Sani, A. Dohnalkova, K.M. Kemner, and T. Borch: Multiple mechanisms of uranium immobilization by *Cellulomonas* sp strain ES6. *Biotechnology and Bioengineering*, 2011. **108**(2): p. 264-276.
173. Beazley, M.J., R.J. Martinez, P.A. Sobecky, S.M. Webb, and M. Taillefert: Nonreductive Biomineralization of uranium(VI) phosphate via microbial phosphatase activity in anaerobic conditions. *Geomicrobiology Journal*, 2009. **26**(7): p. 431-441.
174. Merroun, M.L., M. Nedelkova, J.J. Ojeda, T. Reitz, J.M. Arias, M. Romero-Gonzales, and S. Selenska-Pobell: Bioprecipitation of uranium by natural bacterial isolates: a combined potentiometric titration, TEM and X-ray absorption spectroscopy study. *in Journal of Hazardous Materials*, submitted.
175. Goel, R., T. Mino, H. Satoh, and T. Matsuo: Enzyme activities under anaerobic and aerobic conditions inactivated sludge sequencing batch reactor. *Water Research*, 1998. **32**(7): p. 2081-2088.
176. Macaskie, L.E., B.C. Jeong, and M.R. Tolley: Enzymatically accelerated biomineralization of heavy-metals - application to the removal of americium and plutonium from aqueous flows. *FEMS Microbiology Reviews*, 1994. **14**(4): p. 351-367.
177. Lloyd, J.R.: Microbial reduction of metals and radionuclides. *FEMS Microbiology Reviews*, 2003. **27**(2-3): p. 411-425.

178. Francis, A.J., J.B. Gillow, C.J. Dodge, R. Harris, T.J. Beveridge, and H.W. Papenguth: Uranium association with halophilic and non-halophilic bacteria and archaea. *Radiochimica Acta*, 2004. **92**(8): p. 481-488.
179. Suzuki, Y. and J.F. Banfield: Resistance to, and accumulation of, uranium by bacteria from a uranium-contaminated site. *Geomicrobiology Journal*, 2004. **21**(2): p. 113-121.
180. Eichler, J.: Facing extremes: archaeal surface-layer (glyco)proteins. *Microbiology*, 2003. **149**: p. 3347-3351.
181. Groudev, S.N. and V.I. Groudeva: Microbial Communities in four Industrial Copper Dump Leaching Operations in Bulgaria. *FEMS Microbiology Reviews*, 1993. **11**(1-3): p. 261-268.
182. Marsh, R.M. and P.R. Norris: The isolation of some thermophilic, autotrophic, iron- and sulphur-oxidizing bacteria. *FEMS Microbiology Letters*, 1983. **17**: p. 311-315.
183. Lindström, E.B., S. Wold, N. Kettaneh-Wold, and S. Sääf: Optimization of pyrite bioleaching using *Sulfolobus acidocaldarius*. *Applied Microbiology and Biotechnology*, 1993. **38**: p. 702-707.
184. Hjort, K. and R. Bernander: Changes in cell size and DNA content in *Sulfolobus* cultures during dilution and temperature shift experiments. *Journal of Bacteriology*, 1999. **181**(18): p. 5669-5675.
185. Allen, M.B.: Studies with *Cyanidium caldarium*, an anomalously pigmented chlorophyte. *Archiv für Mikrobiologie*, 1959. **32**: p. 270-277.
186. Makarov, E.S. and V.I. Ivanov: Crystal structure of meta-autunite, $\text{Ca}(\text{UO}_2)_2(\text{PO}_4)_2 \cdot 6\text{H}_2\text{O}$. *Doklady Akad. Nauk SSSR*, 1960. **132**: p. 673-676.
187. Geipel, G., A. Brachmann, V. Brendler, G. Bernhard, and H. Nitsche: Uranium(VI) sulfate complexation studied by time-resolved laser-induced fluorescence spectroscopy (TRLFS). *Radiochimica Acta*, 1996. **75**: p. 199-204.
188. Grogan, D.W.: Phenotypic characterization of the archaeobacterial genus *Sulfolobus* - comparison of 5 wild-type strains. *Journal of Bacteriology*, 1989. **171**(12): p. 6710-6719.
189. Miller, K.W., S.S. Risanico, and J.B. Risatti: Differential tolerance of *Sulfolobus* strains to transition metals. *FEMS Microbiology Ecology*, 1992. **93**: p. 69-74.
190. Irving, H.M.N.H. and R.J.P. Williams: Order of stability of metal complexes. *Nature*, 1948. **162**: p. 746-747.
191. Boutamine, S., Z. Hank, M. Meklati, and O. Benali-Baitich: Alpha-benzoinomix: extractin agent for uranium(VI) tungsten(VI), molybdenum(VI) and some transition metals of the iron family. *Journal of Radioanalytical and Nuclear Chemistry*, 1994. **185**(2): p. 347-353.
192. Merroun, M. and S. Selenska-Pobell: Interactions of three eco-types of *Acidithiobacillus ferrooxidans* with U(VI). *BioMetals*, 2001. **14**: p. 171-179.
193. Remonsellez, F., A. Orell, and C.A. Jerez: Copper tolerance of the thermoacidophilic archaeon *Sulfolobus metallicus*: possible role of polyphosphate metabolism. *Microbiology*, 2006. **152**: p. 59-66.
194. Alvarez, S. and C.A. Jerez: Copper Ions stimulate polyphosphate degradation and phosphate efflux in *Acidithiobacillus ferrooxidans*. *Applied and Environmental Microbiology*, 2004. **70**(9): p. 5177-5182.
195. Keasling, J.D.: Regulation of intracellular toxic metals and other cations by hydrolysis of polyphosphate. *Annals of the New York Academy of Sciences*, 1997. **829**(1): p. 242-249.

196. Hu, M.Z.C., J.M. Norman, B.D. Faison, and M.E. Reeves: Biosorption of uranium by *Pseudomonas aeruginosa* strain CSU: Characterization and comparison studies. *Biotechnology and Bioengineering*, 1996. **51**(2): p. 237-247.
197. Bonhoure, I., S. Meca, V. Marti, J. De Pablo, and J.L. Cortina: A new time-resolved laser-induced fluorescence spectrometry (TRLFS) data acquisition procedure applied to the uranyl-phosphate system. *Radiochimica Acta*, 2007. **95**(3): p. 165-172.
198. Panak, P.J., S. Selenska-Pobell, S. Kutschke, G. Geipel, G. Bernhard, and H. Nitsche: Complexation of U(VI) with cells of *thiobacillus* and *thiomonas cuprina* of different geological origin. *Radiochimica Acta*, 1999. **84**: p. 183-190.
199. Jroundi, F., M.L. Merroun, J.M. Arias, A. Rossberg, S. Selenska-Pobell, and M.T. Gonzalez-Munoz: Spectroscopic and microscopic characterization of uranium biomineralization in *Myxococcus xanthus*. *Geomicrobiology Journal*, 2007. **24**(5): p. 441-449.
200. Kelly, S.D., K.M. Kemner, J.B. Fein, D.A. Fowler, M.I. Boyanov, B.A. Bunker, and N. Yee: X-ray absorption fine structure determination of pH- dependent U-bacterial cell wall interactions. *Geochimica et Cosmochimica Acta*, 2002. **66**(22): p. 3855-3871.
201. Michel, H., D.C. Neugebauer, and D. Oesterhelt: The 2-d crystalline cell wall of *Sulfolobus acidocaldarius*: Structure, solubilization, and reassembly. *Electron microscopy at molecular dimensions*, 1980: p. 27-35.
202. Arcos, D., F. Grandia, C. Domenech, A.M. Fernandez, M.V. Villar, A. Muurinen, T. Carlsson, P. Sellin, and P. Hernan: Long-term geochemical evolution of the near field repository: Insights from reactive transport modelling and experimental evidences. *Journal of Contaminant Hydrology*, 2008. **102**: p. 196-209.
203. Horhoianu, G., D. Ionescu, and G. Olteanu: Three-dimensional thermal-mechanical modelling of a spent nuclear fuel repository located in granite rock. *Environmental Aspects of Legacy Material Management*, 2004: p. 89-90.
204. Michalowicz, A., K. Provost, S. Laruelle, A. Mimouni, and G. Vlaic: F-test in EXAFS fitting of structural models. *Journal of Synchrotron Radiation*, 1999. **6**(Pt 3): p. 233-5.
205. Fein, J.B., C.J. Daughney, N. Yee, and B.P. Dave: A chemical equilibrium model for metal adsorption onto bacterial surfaces. *Geochimica et Cosmochimica Acta*, 1998. **61**(16): p. 3319-3328.
206. Denecke, M.A., T. Reich, S. Pompe, M. Bubner, K.-H. Heise, H. Nitsche, P.G. Allen, J.J. Bucher, N.M. Edelstein, and D.K. Shuh: Differentiating between monodentate and bidentate carboxylic ligands coordinated to uranyl ions using EXAFS. *Journal de Physique IV France*, 1997. **7**: p. 637-638.
207. Rossberg, A., K.U. Ulrich, S. Weiss, S. Tsushima, T. Hiemstra, and A.C. Scheinost: Identification of uranyl surface complexes on ferrihydrite: Advanced EXAFS data analysis and CD-MUSIC modeling. *Environmental Science & Technology*, 2009. **43**(5): p. 1400-6.
208. Rossberg, A. and A.C. Scheinost: Three-dimensional modeling of EXAFS spectral mixtures by combining Monte Carlo simulations and target transformation factor analysis. *Analytical and Bioanalytical Chemistry*, 2005. **383**(1): p. 56-66.
209. Thompson, H.A., G.E.J. Brown, and G.A. Parks: XAFS spectroscopic study of uranyl coordination in solids and aqueous solution. *American Mineralogist*, 1997. **82**: p. 483-496.
210. Le Gal, J.M., M. Manfait, and T. Theophanides: Applications of FTIR spectroscopy in structural studies of cells and bacteria. *Journal of Molecular Structure*, 1991. **242**: p. 397-407.

211. Naumann, D., G. Barnickel, H. Bradaczek, H. Labischinski, and P. Giesbrecht: Infrared Spectroscopy, a Tool for Probing Bacterial Peptidoglycan. *European Journal of Biochemistry*, 1982. **125**: p. 505-515.
212. Jiang, W., A. Saxena, B. Song, B.B. Ward, T.J. Beveridge, and C.B. Myneni: Elucidation of functional groups on gram-positive and gram-negative bacterial surfaces using infrared spectroscopy. *Langmuir*, 2004. **20**: p. 11433-11442.
213. Filip, Z., S. Herrmann, and J. Kubat: FT-IR spectroscopic characteristics of differently cultivated *Bacillus subtilis*. *Microbiological Research*, 2004. **159**: p. 257-262.
214. Guibal, E., C. Roulph, and P. Le Cloirec: Infrared spectroscopic study of uranyl biosorption by fungal biomass and materials of biological origin. *Environmental Science & Technology*, 1995. **29**: p. 2496-2503.
215. Günzler, H. and H.-U. Gremlich: IR Spectroscopy: An Introduction 2002, Weinheim, Germany: Wiley-VCH.
216. Müller, K., H. Foerstendorf, S. Tsushima, V. Brendler, and G. Bernhard: Direct spectroscopic characterization of aqueous actinyl(vi) species: a comparative study of Np and U. *Journal of Physical Chemistry A*, 2009. **113**: p. 6626-6632.
217. Cejka, J.: Infrared spectroscopy of the uranyl minerals, In: *Uranium - Mineralogy, Geochemistry and the Environment. Reviews in Mineralogy* (eds Burns, P.C. and R. Finch), 1999. **38**: p. 521-622.
218. Hollander, V.P.: Acid Phosphatases, 1971, Elsevier: Amsterdam. p. 449-498.
219. Gorobets, B.S. and Sidorenko, G.A.: Luminescence of Secondary Uranium Minerals at Low-Temperatures. *Atomnaya Energiya*, 1974. **36**(1): p. 6-13.
220. Claus, H., E. Akca, T. Debaerdemaeker, C. Evrard, J.P. Declercq, J.R. Harris, B. Schlott, and H. König: Molecular organization of selected prokaryotic S-layer proteins. *Canadian Journal of Microbiology*, 2005. **51**(9): p. 731-743.
221. Engelhardt, H.: Are S-layers exoskeletons? The basic function of protein surface layers revisited. *Journal of Structural Biology*, 2007. **160**(2): p. 115-24.
222. König, H., R. Rachel, and H. Claus: Proteinaceous Surface Layers of Archaea, 2007, ASM Press: Herndon. p. 315-353.
223. Messner, P., C. Schäffer, E.M. Egelseer, and U.B. Sleytr: Occurrence, Structure, Chemistry, Genetics, Morphogenesis, and Functions of S-layers. In *Prokaryotic Cell Wall Compounds: Structure and Biochemistry* (eds. König, H., H. Claus, A. Varma) 2010, Springer Verlag: Heidelberg. p. 53-109.
224. Sleytr, U.B. and T.J. Beveridge: Bacterial S-layers. *Trends in Microbiology*, 1999. **7**: p. 253-260.
225. Beveridge, T.J. and L.L. Graham: Surface Layers of Bacteria. *Microbiological Reviews*, 1991. **55**(4): p. 684-705.
226. Engelhardt, H.: Mechanism of osmoprotection by archaeal S-layers: a theoretical study. *Journal of Structural Biology*, 2007. **160**(2): p. 190-9.
227. Koval, S.F.: Predation on bacteria possessing S-layers., 1993, Plenum Press: New York. p. 85-92.
228. Mesnage, S., E. Tosi-Couture, M. Mock, P. Gounon, and A. Fouet: Molecular characterization of the *Bacillus anthracis* main S-layer component: evidence that it is the major cell-associated antigen. *Molecular Microbiology*, 1997. **23**(6): p. 1147-55.
229. Fahmy, K., M. Merroun, K. Pollmann, J. Raff, O. Savchuk, C. Hennig, and S. Selenska-Pobell: Secondary structure and Pd(II) coordination in S-layer proteins from *Bacillus sphaericus* studied by infrared and X-ray absorption spectroscopy. *Biophysical Journal*, 2006. **91**(3): p. 996-1007.

230. Pollmann, K., J. Raff, M. Merroun, K. Fahmy, and S. Selenska-Pobell: Metal binding by bacteria from uranium mining waste piles and its technological applications. *Biotechnology Advances*, 2006. **24**(1): p. 58-68.
231. Raff, J., U. Soltmann, S. Matys, S. Selenska-Pobell, H. Bottcher, and W. Pompe: Biosorption of uranium and copper by biocers. *Chemistry of Materials*, 2003. **15**(1): p. 240-244.
232. Grogan, D.W.: Isolation and fractionation of cell envelope from the extreme thermoacidophile *Sulfolobus acidocaldarius*. *Journal of Microbiological Methods*, 1996. **26**(1-2): p. 35-43.
233. Mark, S.S., M. Bergkvist, X. Yang, L.M. Teixeira, P. Bhatnagar, E.R. Angert, and C.A. Batt: Bionanofabrication of metallic and semiconductor nanoparticle arrays using S-layer protein lattices with different lateral spacings and geometries. *Langmuir*, 2006. **22**(8): p. 3763-3774.
234. Neuhoff, V., N. Arold, D. Taube, and W. Ehrhardt: Improved staining of proteins in polyacrylamide gels including isoelectric-focusing gels with clear background at nanogram sensitivity using coomassie brilliant blue G-250 and R-250. *Electrophoresis*, 1988. **9**(6): p. 255-262.
235. Gans, P., A. Sabatini, and A. Vacca: Investigation of equilibria in solution. Determination of equilibrium constants with the HYPERQUAD suite of programs. *Talanta*, 1996. **43**(10): p. 1739-1753.
236. Thurlkill, R.L., G.R. Grimsley, J.M. Scholtz, and C.N. Pace: pK values of the ionizable groups of proteins. *Protein Science*, 2006. **15**(5): p. 1214-1218.
237. Amayri, S., T. Reich, T. Arnold, G. Geipel, and G. Bernhard: Spectroscopic characterization of alkaline earth uranyl carbonates. *Journal of Solid State Chemistry*, 2005. **178**(2): p. 567-577.
238. Eliet, V., G. Bidoglio, N. Omenetto, L. Parma, and I. Grenthe: Characterization of hydroxide complexes of uranium(VI) by time-resolved fluorescence spectroscopy. *Journal of the Chemical Society-Faraday Transactions*, 1995. **91**(15): p. 2275-2285.
239. Moulin, C., I. Laszak, V. Moulin, and C. Tondre: Time-resolved laser-induced fluorescence as a unique tool for low-level uranium speciation. *Applied Spectroscopy*, 1998. **52**(4): p. 528-535.
240. Steudtner, R., T. Arnold, G. Geipel, and G. Bernhard: Fluorescence spectroscopic study on complexation of uranium(VI) by glucose – a comparison of room and low temperature measurements. *Journal of Radioanalytical and Nuclear Chemistry*, 2010.
241. Wang, Z.M., J.M. Zachara, W. Yantasee, P.L. Gassman, C.X. Liu, and A.G. Joly: Cryogenic laser induced fluorescence characterization of U(VI) in hanford vadose zone pore waters. *Environmental Science & Technology*, 2004. **38**(21): p. 5591-5597.
242. Kakihana, M., T. Nagumo, M. Okamoto, and H. Kakihana: Coordination structures for uranyl carboxylate complexes in aqueous-solution studied by IR and C-13 NMR-Spectra. *Journal of Physical Chemistry*, 1987. **91**(24): p. 6128-6136.
243. Vallet, V., U. Wahlgren, B. Schimmelpfennig, H. Moll, Z. Szabo, and I. Grenthe: Solvent effects on uranium(VI) fluoride and hydroxide complexes studied by EXAFS and quantum chemistry. *Inorganic Chemistry*, 2001. **40**(14): p. 3516-3525.
244. Quiles, F. and A. Burneau: Infrared and Raman spectroscopic study of uranyl complexes: hydroxide and acetate derivatives in aqueous solution. *Vibrational Spectroscopy*, 1998. **18**: p. 61-75.
245. Mosselmans, J.F., E. Bailey, and P. Schofield: A study of uranium speciation in acetate solutions at temperatures from 25 to 250 degrees C. *Journal of Synchrotron Radiation*, 2001. **8**: p. 660-662.

246. Zhang, P. and T.K. Sham: X-ray studies of the structure and electronic behavior of alkanethiolate-capped gold nanoparticles: The interplay of size and surface effects. *Physical Review Letters*, 2003. **90**(24): p. -.
247. Creamer, N.J., I.P. Mikheenko, P. Yong, K. Deplanche, D. Sanyahumbi, J. Wood, K. Pollmann, M. Merroun, S. Selenska-Pobell, and L.E. Macaskie: Novel supported Pd hydrogenation bionanocatalyst for hybrid homogeneous/heterogeneous catalysis. *Catalysis Today*, 2007. **128**: p. 80-87.
248. Herrmannsdorfer, T., A.D. Bianchi, T.P. Papageorgiou, F. Pobell, J. Wosnitza, K. Pollmann, M. Merroun, J. Raff, and S. Selenska-Pobell: Magnetic properties of transition-metal nanoclusters on a biological substrate. *Journal of Magnetism and Magnetic Materials*, 2007. **310**(2): p. E821-E823.
249. König, R., A. Schindler, and T. Herrmannsdorfer: Superconductivity of compacted platinum powder at very low temperatures. *Physical Review Letters*, 1999. **82**(22): p. 4528-4531.
250. Zhu, S.L. and W. Zhou: Optical properties and immunoassay applications of noble metal nanoparticles. *Journal of Nanomaterials*, 2010: Article ID 562035.
251. Narayanan, R.: Recent advances in noble metal nanocatalysts for suzuki and heck cross-coupling reactions. *Molecules*, 2010. **15**(4): p. 2124-2138.
252. Haruta, M.: When Gold is not noble: Catalysis by nanoparticles. *The Chemical Record*, 2003. **3**(2): p. 75-87.
253. Cai, W., T. Gao, H. Hong, and J. Sun: Applications of gold nanoparticles in cancer nanotechnology. *Nanotechnology, Science and Applications* 2008. **1**: p. 17-32.
254. Huang, X.H., P.K. Jain, I.H. El-Sayed, and M.A. El-Sayed: Gold nanoparticles: interesting optical properties and recent applications in cancer diagnostic and therapy. *Nanomedicine*, 2007. **2**(5): p. 681-693.
255. Haes, A.J., S.L. Zou, G.C. Schatz, and R.P. Van Duyne: A nanoscale optical biosensor: The long range distance dependence of the localized surface plasmon resonance of noble metal nanoparticles. *Journal of Physical Chemistry B*, 2004. **108**(1): p. 109-116.
256. Lee, K.S. and M.A. El-Sayed: Gold and silver nanoparticles in sensing and imaging: Sensitivity of plasmon response to size, shape, and metal composition. *Journal of Physical Chemistry B*, 2006. **110**(39): p. 19220-19225.
257. Kim, M.H., S. Kim, H.H. Jang, S. Yi, S.H. Seo, and M.S. Han: A gold nanoparticle-based colorimetric sensing ensemble for the colorimetric detection of cyanide ions in aqueous solution. *Tetrahedron Letters*, 2010. **51**(36): p. 4712-4716.
258. Kim, Y.J., R.C. Johnson, and J.T. Hupp: Gold nanoparticle-based sensing of "spectroscopically silent" heavy metal ions. *Nano Letters*, 2001. **1**(4): p. 165-167.
259. Pradeep, T. and Anshup: Noble metal nanoparticles for water purification: A critical review. *Thin Solid Films*, 2009. **517**(24): p. 6441-6478.
260. Le, J.D., Y. Pinto, N.C. Seeman, K. Musier-Forsyth, T.A. Taton, and R.A. Kiehl: DNA-templated self-assembly of metallic nanocomponent arrays on a surface. *Nano Letters*, 2004. **4**(12): p. 2343-2347.
261. Maeda, Y., H. Tabata, and T. Kawei: Two-dimensional assembly of gold nanoparticles with a DNA network template. *Applied Physics Letters*, 2001. **79**(8): p. 1181-1183.
262. McMillan, R.A., C.D. Paavola, J. Howard, S.L. Chan, N.J. Zaluzec, and J.D. Trent: Ordered nanoparticle arrays formed on engineered chaperonin protein templates. *Nature Materials*, 2002. **1**(4): p. 247-52.
263. Radloff, C., R.A. Vaia, J. Brunton, G.T. Bouwer, and V.K. Ward: Metal nanoshell assembly on a virus bioscaffold. *Nano Letters*, 2005. **5**(6): p. 1187-91.

-
264. Royston, E.S., A.D. Brown, M.T. Harris, and J.N. Culver: Preparation of silica stabilized Tobacco mosaic virus templates for the production of metal and layered nanoparticles. *Journal of Colloid and Interface Science*, 2009. **332**(2): p. 402-7.
265. Hall, S.R., W. Shenton, H. Engelhardt, and S. Mann: Site-specific organization of gold nanoparticles by biomolecular templating. *Chemphyschem*, 2001. **2**(3): p. 184-186.
266. Merroun, M., A. Rossberg, C. Hennig, A.C. Scheinost, and S. Selenska-Pobell: Spectroscopic characterization of gold nanoparticles formed by cells and S-layer protein of *Bacillus sphaericus* JG-A12. *Materials Science & Engineering C-Biomimetic and Supramolecular Systems*, 2007. **27**(1): p. 188-192.
267. Bergkvist, M., S.S. Mark, X. Yang, E.R. Angert, and C.A. Batt: Bionanofabrication of ordered nanoparticle arrays: Effect of particle properties and adsorption conditions. *Journal of Physical Chemistry B*, 2004. **108**(24): p. 8241-8248.
268. Wahl, R., M. Mertig, J. Raff, S. Selenska-Pobell, and W. Pompe: Electron-beam induced formation of highly ordered palladium and platinum nanoparticle arrays on the S layer of *Bacillus sphaericus* NCTC 9602. *Advanced Materials*, 2001. **13**(10): p. 736-740.
269. Pompe, W., M. Mertig, R. Kirsch, R. Wahl, L.C. Ciacchi, J. Richter, R. Seidel, and H. Vinzelberg: Formation of metallic nanostructures on biomolecular templates. *Zeitschrift für Metallkunde*, 1999. **90**(12): p. 1085-1091.
270. Pereiro, M., D. Baldomir, and J.E. Arias: Unexpected magnetism of small silver clusters. *Physical Review A*, 2007. **75**(6): 063204.
271. Yamamoto, Y., T. Miura, Y. Nakae, T. Teranishi, M. Miyake, and H. Hori: Magnetic properties of the noble metal nanoparticles protected by polymer. *Physica B-Condensed Matter*, 2003. **329**: p. 1183-1184.
272. Hori, H., Y. Yamamoto, T. Iwamoto, T. Miura, T. Teranishi, and M. Miyake: Diameter dependence of ferromagnetic spin moment in Au nanocrystals. *Physical Review B*, 2004. **69**(17): p. -.
273. Yamamoto, Y., T. Miura, M. Suzuki, N. Kawamura, H. Miyagawa, T. Nakamura, K. Kobayashi, T. Teranishi, and H. Hori: Direct observation of ferromagnetic spin polarization in gold nanoparticles. *Physical Review Letters*, 2004. **93**(11): p. -.
274. Banerjee, S., S.O. Raja, M. Sardar, N. Gayathri, B. Ghosh, and A. Dasgupta: How old nanoparticle acquires magnetism? - Formation of large orbital moment at the nterface. *Materials Science*, 2010:0912.3319v2.
275. Crespo, P., R. Litran, T.C. Rojas, M. Multigner, J.M. de la Fuente, J.C. Sanchez-Lopez, M.A. Garcia, A. Hernando, S. Penades, and A. Fernandez: Permanent magnetism, magnetic anisotropy, and hysteresis of thiol-capped gold nanoparticles. *Physical Review Letters*, 2004. **93**(8): p. 087204.
276. de la Venta, J., V. Bouzas, A. Pucci, M.A. Laguna-Marco, D. Haskel, S.G.E. te Velthuis, A. Hoffmann, J. Lal, M. Bleuel, G. Ruggeri, C.D. Fernandez, and M.A. Garcia: X-ray Magnetic Circular Dichroism and Small Angle Neutron Scattering Studies of Thiol Capped Gold Nanoparticles. *Journal of Nanoscience and Nanotechnology*, 2009. **9**(11): p. 6434-6438.
277. Garitaonandia, J.S., E. Goikolea, M. Insausti, M. Suzuki, N. Kawamura, H. Osawa, I.G. del Muro, K. Suzuki, J.D. Cashion, C. Gorria, F. Plazaola, and T. Rojo: Thiol-capped ferromagnetic Au nanoparticles investigated by Au L-3 x-ray absorption spectroscopy. *Journal of Applied Physics*, 2009. **105**(7): p. -.
278. Brust, M., M. Walker, D. Bethell, D.J. Schiffrin, and R. Whyman: Synthesis of thiol-derivatized gold nanoparticles in a 2-phase liquid-liquid system. *Journal of the Chemical Society-Chemical Communications*, 1994(7): p. 801-802.

- 279. Romero-Gonzalez, M.E., C.J. Williams, P.H.E. Gardiner, S.J. Gurman, and S. Habesh: Spectroscopic studies of the biosorption of gold(III) by dealginated seaweed waste. *Environmental Science & Technology*, 2003. **37**(18): p. 4163-4169.
- 280. Mulvaney, P.: Surface plasmon spectroscopy of nanosized metal particles. *Langmuir*, 1996. **12**(3): p. 788-800.
- 281. El-Brolossy, T.A., T. Abdallah, M.B. Mohamed, S. Abdallah, K. Easawi, S. Negm, and H. Talaat: Shape and size dependence of the surface plasmon resonance of gold nanoparticles studied by photoacoustic technique. *European Physical Journal Special Topics*, 2008. **153**: p. 361-364.
- 282. Juodkazis, K., J. Juodkazyte, V. Jasulaitiene, A. Lukinskas, and B. Sebekas: XPS studies on the gold oxide surface layer formation. *Electrochemistry Communications*, 2000. **2**(7): p.

Danksagung

Diese Arbeit wurde am Institut für Radiochemie des Helmholtz-Zentrums Dresden-Rossendorf angefertigt.

Mein herzlicher Dank gilt Frau Dr. Sonja Selenska-Pobell für die intensive Betreuung dieser Promotionsarbeit. Sie hat diese Arbeit ins Leben gerufen, die Fragestellungen formuliert und die Forschung im Rahmen dieser Arbeit maßgeblich geformt. Außerdem möchte ich ihr für ihre ansteckende Begeisterung und ihren großen Ideenreichtum danken, womit sie mir immer zu einer positiven und kreativen Arbeitsatmosphäre verholfen hat. Letztlich möchte ich Ihr für das kritische Lesen meiner Arbeit ganz herzlich danken.

Mein Dank gilt Herrn Prof. Dr. Michael Schlömann für seine stets kritische Auseinandersetzung mit den Ergebnissen sowie seinen kreativen Anregungen für weitere Untersuchungen.

Außerdem möchte ich Herrn Prof. Dr. Gert Bernhard danken. Zum einen für seinen Einsatz für die Bereitstellung meiner Promotionsstelle und zum anderen für sein stetiges Interesse an der Arbeit und die Bereitschaft zur Begutachtung dieser Arbeit.

Dr. Maria Romero-González möchte ich für Ihr wissenschaftliches Interesse an meiner Arbeit danken und die damit einhergehende Bereitschaft, ein zusätzliches Fachgutachten über diese Doktorarbeit anzufertigen.

Außerdem danke ich allen Mitarbeitern, Doktoranden, Diplomanden, Praktikanten und Gastwissenschaftlern des Instituts für Radiochemie, die auf wissenschaftlicher, menschlicher oder emotionaler Ebene zur Anfertigung dieser Arbeit beigetragen haben.

Hervorzuheben, und damit mit einem speziellem Dankeschön versehen sind dabei:

Herr Dr. Mohamed L. Merroun, der mir vom ersten bis zum letzten Tag mit Rat und Tat zur Seite stand. Neben der wissenschaftlichen Betreuung danke ich ihm für sein stetiges Bemühen um meine fachliche Entwicklung heranzutreiben. Außerdem gelang es ihm, seine Begeisterung für die Verwendung moderner, spektroskopischer Techniken zur Untersuchung biologischer Systeme auf mich zu übertragen.

صديقي جزىلا شكرا

Herr Dr. Andre Rossberg, der sich Tage- und Nächtelang mit der Messung von XAS Spektren sowie mit der Korrektur meiner EXAFS Auswertungen und hoch-signifikanten F-Tests beschäftigte.

Herr Dr. Thomas Herrmannsdörfer, der gemeinsam mit seinem Team den äußerst spannenden Magnetismus der gebildeten Gold-Nanopartikel entdeckte und damit entscheidenden Einfluss auf den letztendlich sehr langen Titel meiner Arbeit ausübte.

Ein besonderer Dank geht außerdem an (zufällige, wertungsfreie! Reihenfolge):

Monika Dudek, Dr. Andrea Geissler, Dr. Astrid Barkleit, Bo Li, Dr. Harald Foerstendorf, Dr. Robin Steudtner, Tobias Günther, Ulrike Weinert, Dr. Sabine Kutschke, Katrin Flemming, Claudia Joseph, Christan Götz, Manja Vogel, Annette Rumpel, Ursula Schaefer, Sylvia Gürtler, Aline Ritter, Falk Lehmann, Franziska Lederer, Katrin Flemming, Velina Bachvarova, Dr. Johannes Raff, Dr. Katrin Pollmann, Dr. Gerhard Geipel, Andre Marquard, Nico Müller, Robert Münch, Tilo Zachmann, Kay Großmann, Ulrike Jankowski, Dr. Galina Radeva, Fernando Morcillo, Sabrina Hedrich, Anne Heller, Genia Grambole, Carola Eckardt, Dr. Helfried Reuther, Andrea Scholz

- meine Praktikanten: Antje Gehrmann, Kristin Harnisch, Kristin Schmidt, Peter Sebald
- das Team des Sekretariats: Claudia Kirmes und Jenny Kovacs
- das Team der Werkstatt: Dirk Falkenberg, Bernd Hiller, Steffen Henke
- die IT-Spezialistin Manuela Eilzer
- die Mitarbeiter der ROssendorf BeamLine an der ESRF
- die Mitarbeiter der Universität Granada (Abteilung Mikrobiologie) und Maria del Mar.
- meinen PC (der jetzt hoffentlich in Rente gehen darf!)

Abschließend danke ich meiner Familie und meinen Freunden für die Unterstützung während der gesamten Promotionszeit sowie die zuletzt zahlreichen Tritte in den Hintern die ich benötigte, um diese Arbeit abzugeben.

Ein ganz spezieller Dank gilt der- oder demjenigen, die/den ich in dieser Danksagung vergessen habe. Sie/Er möge es mir verzeihen. Als Entschuldigung lade ich die männlichen „Opfer“ auf ein Bier, die weiblichen auf einen Wein, und die weiblichen Singles auf einen Kinobesuch ein!

Versicherung

Hiermit versichere ich, dass ich die vorliegende Arbeit ohne unzulässige Hilfe Dritter und ohne Benutzung anderer als der angegebenen Hilfsmittel angefertigt habe; die aus fremden Quellen direkt oder indirekt übernommenen Gedanken sind als solche kenntlich gemacht. Bei der Auswahl und Auswertung des Materials sowie bei der Herstellung des Manuskripts habe ich Unterstützungsleistungen von folgenden Personen erhalten:

Dr. Sonja Selenska-Pobell
Dr. Mohamed L. Merroun
Dr. Andre Rossberg
Dr. Robin Steudtner
Dr. Thomas Herrmannsdörfer
Dr. Harald Foerstendorf
Dr. Andrea Geissler
Dr. Astrid Barkleit
Bo Li

Weitere Personen waren an der Abfassung der vorliegenden Arbeit nicht beteiligt. Die Hilfe eines Promotionsberaters habe ich nicht in Anspruch genommen. Weitere Personen haben von mir keine geldwerten Leistungen für Arbeiten erhalten, die nicht als solche kenntlich gemacht worden sind.

Die Arbeit wurde bisher weder im Inland noch im Ausland in gleicher oder ähnlicher Form einer anderen Prüfungsbehörde vorgelegt.